

DEVELOPMENT OF FUNCTIONALIZED ALGINATE-BASED HYDROGELS TO REDUCE FIBROSIS IN THE TRANSPLANTATION OF MICROENCAPSULATED CELLS

THÈSE N° 8949 (2018)

PRÉSENTÉE LE 9 NOVEMBRE 2018

À LA FACULTÉ DES SCIENCES DE BASE

LABORATOIRE DE SYNTHÈSE ET PRODUITS NATURELS

PROGRAMME DOCTORAL EN CHIMIE ET GÉNIE CHIMIQUE

ÉCOLE POLYTECHNIQUE FÉDÉRALE DE LAUSANNE

POUR L'OBTENTION DU GRADE DE DOCTEUR ÈS SCIENCES

PAR

Francois Rémi Pierre NOVERRAZ

acceptée sur proposition du jury:

Dr A.-S. Chauvin, présidente du jury

Prof. S. Gerber, directrice de thèse

Dr S. Lablanche, rapporteuse

Prof. G. Borchard, rapporteur

Prof. M. Lutolf, rapporteur



ÉCOLE POLYTECHNIQUE
FÉDÉRALE DE LAUSANNE

Suisse
2018

Acknowledgement

I had the great pleasure to meet and work with many wonderful people during the time of my doctoral studies and I would like to thank them for their support and contribution at any scale to this thesis.

Foremost, I am profoundly grateful to Prof. Sandrine Gerber-Lemaire who gave me the opportunity to work in her research group with the ideal environment for the achievement of a doctoral thesis. Her dedication, support and guidance helped me enormously for the whole the time of the research and writing of this thesis.

I would like to thank Dr. Christine Wandrey for her precious knowledge and support. Her pertinent suggestions and advices were a valuable help for my work.

My sincere thanks to the members of the jury, Prof. Borchard Gerrit, Dr. Lablanche Sandrine and Prof. Lutolf Matthias, for taking the time to examine and review the manuscript of my thesis. I also thank Dr. Chauvin Anne-Sophie for chairing the jury and her kindness as a lab neighbor.

I wish to express my gratitude to our collaborators from the group of “Cultures cellulaires et transplantations” of Geneva University Hospitals (HUG): Prof. Léo Bühler for his cheerfulness and deep knowledge of medicine, Dr. Carmen Gonelle-Gispert, Dr. Elisa Montanari and Joël Pimenta without whom the realization of this thesis would not have been possible. Their time, patience and their expertise and feedbacks allowed productive collaboration between the chemical and medical points of view.

I also would like to thank our partners at the “Commissariat à l'énergie atomique et aux énergies alternatives” (CEA): Frédéric Bottausci, Emily Tubbs and Roxane Crouigneau for the interesting meetings mind opening toward new technology.

I would like to give many thanks to all the personal of the ISIC's Mass Spectrometry facility at EPFL: Dr. Menin Laure, Sepulveda Francisco and especially Daniel Ortiz who gave me invaluable help with my work and spent his time to work out solution to problems I brought him.

My thanks also to the personal of the Nuclear Magnetic Resonance (NMR) service of EPFL: Miéville Pascal, and Bornet Aurelien who both were very helpful and did not hesitate to take some of their precious time to analyze and explain in detail their fascinating work.

Naturally, I thank Dr. Solène Passemard who welcomed me warmly in the lab. Her expertise, motivation and enthusiasm unquestionably helped me for the whole time she was around. It was a pleasure to work and enjoy the conferences trips with her.

All the present and formers members of the Group for Functionalized Biomaterials, Jeremy for his “funny” jokes, Lucmuc a.k.a lucalg for her nice company during the conferences and road-trips, Raphaël for his interesting “facts” and incomparable taste for food and Laura who despite having just started her thesis already brought a nice magical touch to the lab. Also our special guess Delphine who always brought her smile and good mood for the time she spent in our lab.

I warmly thank them for the good time we spend together in and out of the lab, the discussions, debates and laughs we had together.

For the first two years of my thesis it was a pleasure to work at the BCH building with the past and present members of the Zhu, Cramer and Waser's group. In particular Antonin (that's my boy!!), Dylanister the gamer, magic Raph and salsa-Nicolas with whom we've witnessed the birth and death of the baby foot era. Cyril, Mathias, Alexandre and Balázs for the interesting conversations we had. Bastien and Remis to whom I wish the best for their thesis. Danilegende, Sophie, Frank, Erwann, Guillaume, Marion, Bastian, Coralie, Benoît and Jack, for the all the "aperos" and their cheerfulness at any time.

I would like to thanks also all passing person; master students and apprentice in the group: Yannick "the biker", Mayoutz "the federator", Antony "the cosplayer", Florence "the machine", Denis "week-needle", Claire "ping-pong", Camille, and Alexandra for bringing their good energies/vibes/moods during their internships in our lab.

I am also very grateful to the helpful team of BCH and CH "magasin": Annelise, Gladys, Benjamin, Jacques and Marie who always answered my requests and the nicest way with smile.

Finally I would like to thank my family for their support and generosity along all my academic course.

Abstract

Nowadays, the development of cell therapy relies mainly on the advances made toward cell microencapsulation which allows to evade the need for immunosuppression during cell transplantation. Among the materials considered for cell encapsulation, hydrogels distinguish themselves by their exceptional properties. Due to its gelling properties in contact with divalent cations, the biopolymer sodium alginate (Na-alg), has been widely studied for the microencapsulation and transplantation of cells. However, several drawbacks, notably defects in permselectivity and a poor durability in vivo are limiting the translation of alginate-based hydrogels in clinical applications. In addition, the transplantation of cells without immunosuppressive treatment exposes the cells to adverse host responses such as inflammation and fibrosis. At this time, several approaches have been considered for the development of an ideal material for cell encapsulation; however many challenges still remain to be overcome in this domain. Hence, the present research project is focused on the further development of hydrogels in order to improve their properties toward cell encapsulation.

The first part of this research focused on the development of new types of one-component hybrid alginate-based hydrogels. These hydrogels combine the gelling properties of Na-alg with covalent crosslinking within the same polymeric structure. In order to do so, a new synthetic approach was developed allowing the functionalization on the hydroxyl position of alginate with heterobifunctional poly(ethylene glycol) (PEG) linkers through carbamate bond. This allowed to maintain the carboxyl moieties available for the formation of electrostatic interactions. Two types of one-component hybrid hydrogel were developed with this method adding either thiols or lipoyl moieties on alginate leading to an improvement of mechanical properties while preserving a good biocompatibility.

Yet, transplantation of encapsulated cells in a foreign host body have to face immune response, in particular inflammation and pericapsular fibrosis overgrowth (PFO) which ultimately leads to necrosis of the encapsulated cells and loss of graft functionality. Therefore, the second part of this research project focuses on tuning the composition of the polymeric components of the hydrogels with anti-inflammatory agents which would reduce PFO in vivo. Different anti-inflammatory agents were considered for this purpose. The best candidate (ketoprofen) was then PEGylated via either ester or amide bonds and grafted on the backbone of alginate to ensure a controlled release at the site of transplantation. By analyzing the fibrotic tissue around the microspheres, it was observed that the incorporation of ketoprofen in the structure of the hydrogel significantly reduced PFO 30 days after transplantation.

In summary, Na-alg was functionalized with a new synthetic methodology allowing the incorporation of either functionalities reinforcing the mechanical resistance of the hydrogel or anti-inflammatory compounds improving the biocompatibility of the graft.

Keywords: Alginate, cell microencapsulation, cell therapy, controlled release, functionalization, microspheres, hydrogel.

Résumé

De nos jours, le développement de thérapies cellulaires repose essentiellement sur l'avancement des technologies liées à l'encapsulation cellulaire. Cette approche permet la transplantation cellulaire sans avoir recours à des traitements immunosuppresseurs. Parmi les matériaux considérés pour l'encapsulation cellulaire, les hydrogels se démarquent par leurs propriétés exceptionnelles. Compte tenu de sa faculté de gélification en contact avec des cations divalents, le biopolymère alginate de sodium (Na-alg), a été largement étudié pour la microencapsulation et transplantation de cellules. Cependant, plusieurs limitations, en particulier des défauts de perméabilité sélective et le manque de durabilité *in vivo*, ont fortement ralenti son développement dans des applications cliniques. De plus, la transplantation cellulaire sans traitement immunosuppresseur doit faire face aux réponses adverses du corps telles que l'inflammation et la fibrose. Actuellement, plusieurs approches ont été considérées afin de développer le matériel idéal pour l'encapsulation cellulaire; toutefois de grand progrès restent à faire dans ce domaine pour permettre le succès d'applications cliniques. Par conséquent, ce travail de recherche est focalisé sur le développement des hydrogels afin d'améliorer leurs propriétés en relation avec l'encapsulation cellulaire.

Dans un premier temps, ce travail de recherche s'est concentré sur le développement de nouveaux hydrogels hybrides à un seul composant dérivant de l'alginate. Ce type d'hydrogels combine les propriétés de gélification de Na-alg avec des liaisons covalentes dans une même structure polymérique. A cet effet, une nouvelle voie de synthèse a été développée permettant la fonctionnalisation des groupements hydroxyle de l'alginate avec des poly(éthylène glycol) (PEG) hétérobifonctionnels via une liaison carbamate. Cette approche permet de garder les groupements carboxyle de l'alginate disponibles pour la formation d'interactions électrostatiques. Deux types d'hydrogel ont été développés de cette manière, en ajoutant des groupements thiols ou lipoyl sur l'alginate résultant dans les deux cas de figures en une amélioration des propriétés mécaniques tout en préservant une bonne biocompatibilité.

Cependant, la transplantation cellulaire est confrontée aux réponses immunitaires du receveur telles que l'inflammation et la prolifération de fibrose pericapsulaire (PFP) qui provoque à terme la nécrose des cellules encapsulées et donc la perte de fonctionnalité de la greffe. Par conséquent, la deuxième partie de ce travail de recherche s'est focalisée sur la modification de la composition des composés polymériques de l'hydrogel avec des agents anti-inflammatoires capable de réduire la PFP *in vivo*. Plusieurs anti-inflammatoires ont été considérés à cet effet. Le meilleur candidat (ketoprofène) a été PEGylé via une liaison ester ou une liaison amide puis lié sur la structure de l'alginate pour assurer sont relargage contrôlé localisé sur le site de transplantation. L'analyse des tissus fibreux autour des microsphères a permis de démontrer l'effet positif de l'incorporation du kétoprofène dans la structure de l'hydrogel en observant une réduction significative de la PFP 30 jours après la greffe.

En résumé, l'alginate a été fonctionnalisé à l'aide d'une nouvelle voie de synthèse permettant l'incorporation de fonctionnalités renforçant les propriétés mécaniques de l'hydrogel ou de composés anti-inflammatoires améliorant la biocompatibilité de la greffe.

Mots-Clés : Alginate, fonctionnalisation, hydrogel, microsphères, microencapsulation cellulaire, relargage, thérapie cellulaire.

Abbreviations

Alg	Alginate
Ar	Aromatic
Atm	Atmosphere
aq.	Aqueous
Boc/Boc₂O	Di-tert-butyl dicarbonate
calcd.	Calculated
CDI	Carbodiimidazole
COL1A1	Alpha-1 type I collagen
DAMPs	danger-associated molecular patterns
DCC	N,N'-dicyclohexylcarbodiimide
DCM	Dichloromethane
DIPEA	N,N-Diisopropylethylamin
DMAP	4-dimethylaminopyridine
DMEM	Dulbecco's Modified Eagle's Medium
DMF	N,N-Dimethylformamide
DMSO	Dimethyl sulfoxide
DMAP	4-Dimethylaminopyridine
DOSY	Diffusion ordered spectroscopy
DTT	Dithiothreitol
EDCI	1-Ethyl-3-(3-dimethylaminopropyl)carbodiimide
equiv	Equivalent
ESI-MS	Electrospray ionization-mass spectrometry
EtOAc	Ethyl acetate
EtOH	Ethanol
FAP-α	Fibroblast Activation Protein- α
FCC	Flash column chromatography
FDA	Food and Drug Administration
g	Gram
HATU	1-[Bis(dimethylamino)methylene]-1H-1,2,3-triazolo[4,5-b]pyridinium 3-oxide hexafluorophosphate
HBSS	Hank's Balanced Salt Solution
HOBt	Hydroxybenzotriazole
hr	Hour
HRMS	High resolution mass spectrometry
LiHMDS	LithiumHexamethyldisilazide
MeOH	Methanol
MOPS	3-(N-morpholino)propanesulfonic acid
MS	Microspheres
MSCs	Mesenchymal stem cells
MsOH	Methanesulfonic acid
MMP-1	Matrix metalloproteinase-1
MOPS	3-(Nmorpholino)propanesulfonic acid
Na-alg	Sodium alginate

NEt₃	Triethylamine
NMR	Nuclear Magnetic Resonance
PAMPs	pathogen-associated molecular patterns
PE	Petroleum ether
PEG	Poly(ethylene glycol)
PFO	Pericapsular fibrosis overgrowth
ppm	Parts per million
rt	Room temperature
RT-PCR	Real-time reverse transcription PCR
sat.	Saturated
TBA	Tetrabutyl ammonium
TBAB	Tetra-n-butylammonium bromide
TBDMS	Tributyldimethylsilyl
TBTU	O-(Benzotriazol-1-yl)-N,N,N',N'-tetramethyluronium tetrafluoroborate
TGFβ₁	Transforming growth factor
TFA	Trifluoroacetic acid
TFAA	Trifluoroacetic anhydride
THF	Tetrahydrofuran
TLC	Thin layer chromatography
TsCl	Tosyl chloride
wt	weight
α-SMA	α-smooth muscle actin

TABLE OF CONTENTS

1	Introduction.....	1
1.1	Diabetes and therapy.....	1
1.2	Cell therapy.....	3
1.3	Microencapsulation.....	3
1.3.1	Cell microencapsulation.....	4
1.4	Hydrogels.....	5
1.4.1	Physical hydrogel.....	5
1.4.2	Chemical hydrogel.....	7
1.4.3	Hybrid hydrogels.....	8
1.5	Microencapsulation Techniques.....	10
1.6	Properties of hydrogels for cell microencapsulation.....	11
1.6.1	Mechanical resistance.....	11
1.6.2	Permeability.....	12
1.7	Properties of biological components.....	13
1.7.1	Source of cells.....	13
1.7.2	Site of transplantation.....	13
1.7.3	Biocompatibility.....	14
2	Thesis objectives.....	19
2.1	Inhibition of pericapsular fibrotic overgrowth.....	19
2.1.1	Inhibitors of fibroblast activation protein- α	19
2.1.2	Nonsteroidal anti-inflammatory drugs.....	20
3	Results and Discussion.....	23
3.1	Synthesis of anti-fibrotic derivatives.....	23
3.1.1	Derivatives of FAP- α inhibitors.....	24
3.1.2	Curcumin derivatives.....	28
3.1.3	Ketoprofen derivatives.....	30
3.2	Anti-fibrotic activity and biocompatibility.....	32
3.3	Alginate derivatives for the engineering of hydrogels.....	34
3.3.1	Alginate-PEG-(triazole)-SH.....	35
3.3.2	Alg-PEG-SH and Alg-PEG-LA derivatives containing linear PEGs.....	39
3.4	Conjugation of anti-inflammatory compounds to alginate-based hydrogels.....	44
3.4.1	Conjugation through disulfide cluster formation.....	44
3.5	Grafting of PEGylated ketoprofen on alginate.....	46

3.5.1	Quantification of the anti-fibrotic effect	51
3.5.2	Biocompatibility with encapsulated material	53
3.5.3	Mechanical resistance	56
3.6	Three components system	56
4	Conclusion	61
5	Experimental section.....	65
5.1	Materials and methods.....	65
5.2	Tetra(ethylene glycol) derivatives.....	66
5.3	Derivatization of lipoic acid with tetra(ethylene glycol) derivatives	71
5.4	FAP-alpha inhibitor block 1	81
5.5	FAP-alpha inhibitor block 2	85
5.6	Curcumin derivatives.....	97
5.7	ketoprofen derivatives	111
5.8	Preparation of PEG-KET and grafting on Alginate.....	124
5.9	Synthesis of alginate-lipoic acid.....	134
5.10	Microspheres formation.....	138
5.11	Determination of the degree of grafting	139
5.12	Quantitative analysis by UHPLC-ESI-HRMS	140
5.13	Transplantation of microspheres in mice.....	141
5.14	Histological analysis.....	142
5.15	Quantification of pericapsular fibrotic overgrowth.....	142
5.16	Real-Time RT-PCR.....	142
5.17	Insulin secretion test.....	143
6	Annexes.....	145
7	References.....	149
8	Curriculum vitae	167

1 INTRODUCTION

1.1 DIABETES AND THERAPY

Diabetes is a disease characterized by the inability of the metabolism to regulate blood sugar levels. The level of sugar, more specifically glucose, in the blood is controlled by cellular intake which relies on several mechanisms such as the insulin transduction pathway. Insulin is a hormone produced in the pancreas often described as the “key” that opens the cells to glucose which makes it an essential element for the blood sugar levels regulation.^{1,2} Diabetic patients either lack of insulin or their cells are unresponsive to it. To differentiate those two cases, diabetes has been categorized into two types commonly called type 1 diabetes (T1D) and type 2 diabetes (T2D). The former referring to the alienation of the immune system leading to the destruction of the cells responsible for insulin production (beta cells) resulting in a lack of insulin in the whole metabolism. The second (T2D) refers to insulin insensitivity.³ In this case insulin is still produced but cells do not respond properly to it and cannot use the glucose present in the blood. Both types of diabetes have the same consequence which is an alteration of the insulin transduction pathway compromising the regulation of blood sugar level. Dysfunctional blood glucose control is the major factor causing many complications such as chronic kidney disease, lower limb amputation, retinopathy resulting in blindness, heart attack, strokes and nerve damage. These severe complications are life-threatening and therefore, constant regulation of blood sugar level is imperative for the well-being of diabetic patients.

The growing incidence of diabetes has become a major health concern in recent years. According to the World Health Organization (WHO), diabetes is the eighth leading cause of death worldwide. In 2012, 1.5 million deaths were related to diabetes. The number of people over 18 years old living with diabetes was estimated globally to 422 million in 2014. As illustrated in Figure 1.1, the incidence of diabetes has steadily increased over the last decades. This is due to several parameters such as the population growth, longer life expectancy, and the rise in prevalence of diabetes at each age. During the last 30 years the amount of people with diabetes has almost quadrupled and it has been estimated that 28% of this increase results from a rise in age specific prevalence.⁴

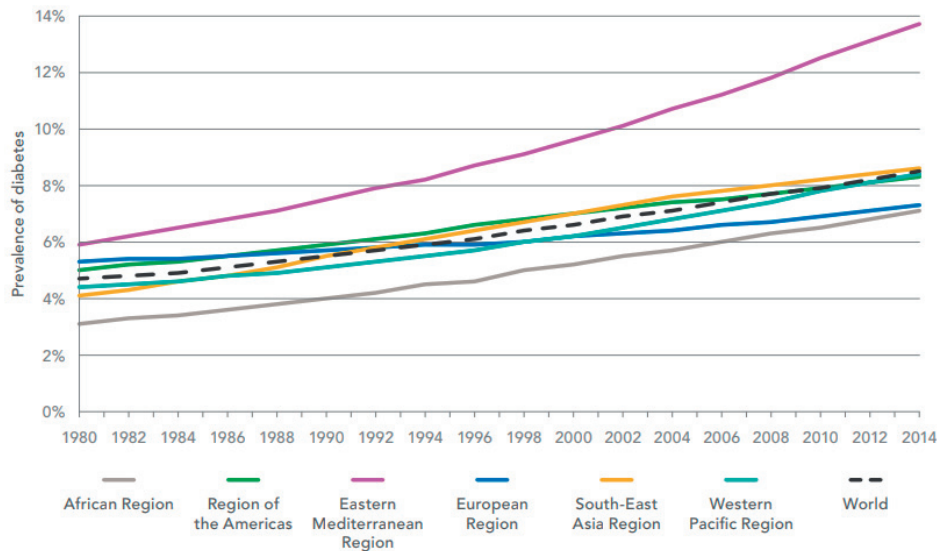


Figure 1.1 Trend in prevalence of diabetes, 1980-2014, by WHO region. Graphic taken from "Global Report on Diabetes; World Health Organization, 2016".⁴

Several therapeutic modalities are currently proposed to diabetic patients depending on the type of diabetes and the stage of the disease. Diet and exercise alone can be sufficient to regulate blood sugar level in the certain cases of T2D. In addition, T2D patients can receive medication to stimulate insulin release and enhance the sensitivity of body tissues to insulin. For patients with insulin-dependent diabetes (mainly T1D patients), the standard treatment relies on intense blood glucose monitoring and exogenous insulin supply. Given that insulin is degraded by the stomach enzymes, insulin cannot be given orally and it is usually administered under the skin using a syringe, or insulin pumps guided by glucose sensors. This therapy was initially developed by Dr. Frederick Banting in 1921 who was able to isolate insulin from a dog's pancreas for injection to a diabetic patient, resulting in the regulation of his blood sugar level.^{5,6} Since then, the biosynthesis of insulin was developed allowing the production of "human" insulin through genetic engineering. Nowadays, most insulins on the market originate from genetic engineering, thus avoiding animal sources.⁷ Even though insulin therapy tremendously improved the life condition of diabetic patients, it cannot fully prevent hypoglycemia insults and long-term side complications. In particular, insulin supply has to be adjusted to many parameters such as food intake (type and amount), the activity of the patient, his level of exercise and also his general state. For instance, stress can greatly influence the need for insulin. To overcome some of these limitations, insulin analogues were developed to achieve more reliable duration of therapeutic effect. The choice of insulin source is thus an important parameter that has to be closely controlled to insure the proper regulation of blood sugar level in diabetic patients.

A new paradigm regarding the treatment of insulin-dependent diabetes and several other diseases appeared with the discovery of cell therapy which was defined in 1993 by the Food and Drug Administration (FDA) as "the prevention, treatment, cure, diagnosis or mitigation of diseases or injuries in humans by the administration of autologous, allogeneic, or xenogeneic cells that have been manipulated or altered ex vivo".⁸

1.2 CELL THERAPY

Cell therapy involves the transplantation of living cellular material in a host body. The beneficial effect of such treatment relies on the ability of the transplanted living cells to produce a therapeutic effect through the sustained secretion of biomolecules such as cytokines, hormones, etc. or even to substitute cells which were dysfunctional or not initially present in the host.

The pioneering input for such strategy appeared back in 1931 when professor Paul Niehans directly administered fresh animal cells to several patients suffering from various health conditions; however, the success of this method was very mitigated at that time.^{9,10} Three decades later, in 1968, the first successful human transplantation of bone marrow in a 5 month old victim of lymphopenic immunological deficiency was reported.¹¹⁻¹³ Since then, the field of cell therapy has been intensively investigated as it holds great promise for several clinical applications, including the replacement of injured or dysfunctional cells, and the treatment of metabolic disorders, degenerative disorders, cancer and end-stage organ failure such as acute liver failure.^{14,15} Even though the vast potential of cell therapy brought the attention of a wide public, only a few translations to clinics have been achieved so far. One can mention the engineering of autologous hematopoietic stem cells for cancer immune therapy.¹⁶ Other successful approaches are related to the engraftment of manipulated epidermal cells for the treatment of severely burnt patients¹⁷ and the engraftment of cultured limbus containing stem cells for corneal therapy.¹⁸ While the use of stem cells in therapeutic products raises high expectations due to their potential for differentiation into a variety of cell types, several ethical and safety concerns hampered their development in clinical protocols.¹⁹⁻²³

Concerning the treatment of insulin-dependent diabetes, recent reports highlighted the beneficial effect of the transplantation of human pancreatic islets for patients suffering from incomplete glucose control despite exogenous insulin supply. For 44% of the recipients, optimal glycemic control was restored for over 3 years, thus significantly improving their quality of life.²⁴ However, the transplantation of human pancreatic islets, as well as other cell-based therapies, are limited by the shortage of suitable human donor cells. Moreover, the quality of cells harvested from human donors is highly variable, which greatly compromises the reproducibility of such treatments. Finally, in most cases, permanent immunosuppressive medication is needed to avoid the rejection of the transplant and these treatments cause detrimental effects to both the recipients and grafted cells.²⁵

To overcome these limitations, immunoprotection of effector cells by microencapsulation into three-dimensional semi-permeable hydrogels appears as an attractive alternative to maintain cell functionality without the need for immunosuppressive regimen.²⁶

1.3 MICROENCAPSULATION

Microencapsulation is a general term referring to a process in which gas, liquid, or solid are surrounded by a coating material forming so capsules in the micrometer range. Numerous applications relying on microencapsulation were developed for the immobilization of a large variety of components including food ingredients, drugs, cosmetics and construction materials. In parallel, several techniques became available to manufacture microcapsules with adjustable

properties depending on the targeted applications. The engineering of the coating material highly depends on the purpose of the encapsulation, which can vary from simple protection of the ingredients to their controlled release or even improvement of their properties. Each application calls for specific materials and encapsulation methods. The encapsulation of biologically active components (bioencapsulation) such as cells, tissues, enzymes, bacteria, or nucleic acids has also been widely investigated. The entrapment of living cells remains one of the most challenging processes as it imposes many constraints on both the hydrogel materials and the encapsulation technology to maintain cell viability and sustained metabolic functionality.

1.3.1 Cell microencapsulation

The microencapsulation of cells was initially proposed in 1933 by Bisceglie²⁷ who demonstrated the sustained metabolic activity of Langerhans islets over more than two weeks after immobilization into polymer-based hydrogels (section 1.4). The concept of "artificial cells" was proposed three decades later by Chang,²⁸ relying on the use of a semi permeable membrane to isolate encapsulated material from the immune system, creating immuno-protected transplantable cells. The main principle of such system is illustrated in Figure 1.2.

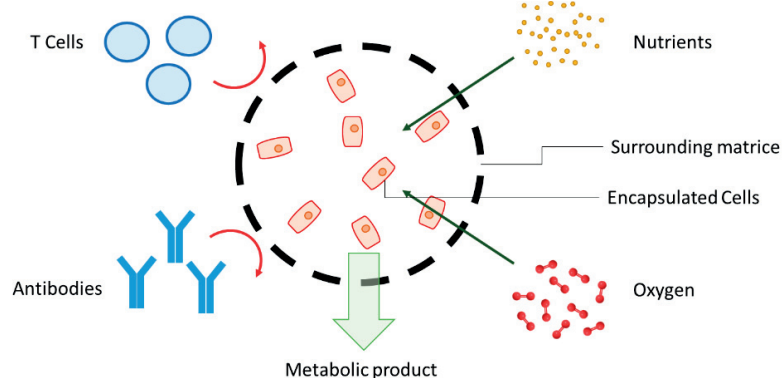


Figure 1.2 Principle of cell microencapsulation

In view of the different important roles that should be fulfilled by the surrounding matrix, the encapsulation materials should meet specific requirements. To protect the inner cells from mechanical stress and deteriorating environment, the material should exhibit an adequate resistance. Permeability of the membrane should allow the diffusion of nutrients, oxygen and cell metabolic products while preventing direct contact with host antibodies and immune cells. The benefit of this approach is not only to evade the need for immunosuppressive treatment but it also provides the opportunity for transplantation of xenogeneic cells which would ensure a more standardized and larger-sized source of cells.²⁹ Cell microencapsulation could in theory be applied to any transplantation therapy aiming at the on-demand supply of metabolites.³⁰ In the case of insulin-dependent diabetes, the transplantation of xenogeneic insulin-producing cells could overcome the lack of human donors³¹ and decrease or even avoid the recourse to permanent immunosuppressive medication.

The perspective of cell transplantation without immunosuppression would be a major breakthrough for patients suffering from severe diseases which already weakened their health conditions, such as liver failure,^{32–34} renal failure,^{35–37} cancer,³⁸ and diabetes mellitus.^{39–41}

Promising results in the field of microencapsulated cell therapies were reported, including xenotransplantation studies.⁴²

The generic term used for cell containing microcapsules is microspheres (MS) which refers to the shape and size of the material. Microspheres have also been called microbeads when addressing homogeneous hydrogel. If the hydrogel exhibits a heterogeneous three-dimensional network, or consists of microbeads surrounded by a membrane, the term microcapsule is most frequently used.

1.4 HYDROGELS

Following the pioneering work of Wichterle⁴³ on cross-linked poly(hydroxyethyl methacrylate) as an alternative to plastic in view of medical applications, hydrogels have been widely recognized as versatile biomaterials⁴⁴⁻⁴⁹ with outstanding characteristics for bioencapsulation⁵⁰⁻⁵³ due to their high water content. Composed of natural or synthetic polymer chains, hydrogels form three-dimensional matrices of various stiffness. Two main classes of hydrogels have been studied and are described as physical and chemical hydrogels. Physical hydrogel refers to polymeric network assembled through physical forces only such as electrostatic interactions, whereas chemical hydrogels refers to a network of polymers covalently linked through specific chemical binding reactions.

1.4.1 Physical hydrogel

The network of physical hydrogels is held by the interaction of junction domains present in the polymer. These junction domains can be sites for ionic bonding, hydrogen bonding or even hydrophobic interactions.⁵⁴⁻⁵⁶ This type of hydrogels rapidly became popular since they can be easily obtained in a one-step process without the need for cross-linking agents. Most of the physical hydrogels developed for bioencapsulation rely on ionic bonding between a polyelectrolyte and multivalent ions of opposite charges. Due to its advantageous gelling properties in contact with divalent cations (Ba^{2+} , Ca^{2+}), the natural polysaccharide sodium alginate (Na-alg, Figure 1.3) is by far the most widely used biomaterial for cell immobilization.

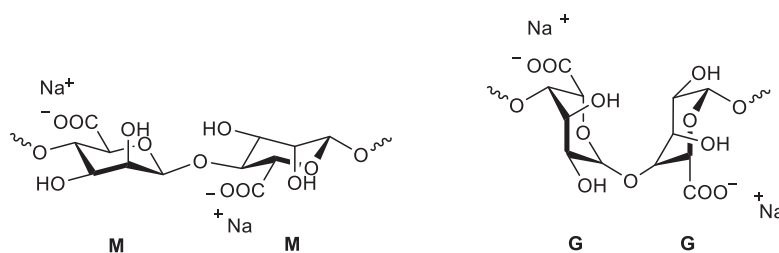


Figure 1.3 Sodium alginate structure; D-mannuronic acid (M) and L-guluronic acid (G) residues

Na-alg is composed of D-mannuronic (M) and L-guluronic acid (G) residues. The numerous charges present on its chemical structure confers to Na-alg the ability to interact with multivalent cations to form "ionotropic" hydrogel (Figure 1.4) or with polyelectrolyte displaying opposite charge (polycations) to form a polyelectrolyte complex (or simplex). Using divalent cation is the most straightforward method to form hydrogel from Na-alg.

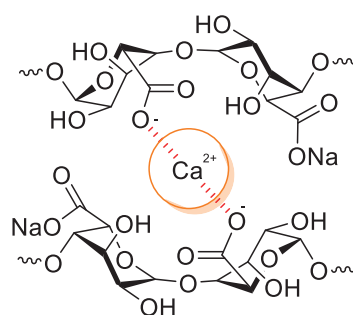


Figure 1.4 Junction domain of alginate with divalent cation Ca^{2+}

One of the easiest and most common way to form alginate-based hydrogels consists in dropping an aqueous solution of the polymer (Na-alg) into a solution containing divalent cations such as Ca^{2+} called a gelation bath. Under neutral conditions and at room temperature, Na-alg rapidly builds a rigid network by formation of ionic bonds between the GG sequences (junction domains) present in the biopolymers. Among the variety of cell microencapsulation applications reported with Na-alg, illustrative examples are listed in Table 1.

Table 1 – Selected alg-based physical hydrogels applied for cell microencapsulation. BMSC: Bone marrow mesenchymal stem cells; ADSC: Adipose-derived stem cells; CSP: Human mesenchymal progenitor cells from the subchondral bone marrow; WJMSC: Wharton's jelly mesenchymal stem cells; ARPE-19: Human retinal pigment epithelial cells.

Divalent ions	Cell type	Target
Ca^{2+}	BMSC Hepatocytes Pig islets ADSC CSP	Treatment of stress urinary incontinence ⁵⁷ Development of bio-artificial liver ⁵⁸ Impact of implantation sites on the biocompatibility ⁵⁹ Study of angiogenic and osteogenic potential of ADSC ^{60,61} Therapeutic approach for cartilage regeneration ⁶²
Ba^{2+}	Rat islets Neuroblastoma WJMSC	Study of islets function in vitro and in vivo ⁶³ Cryopreservation of neurospheres by encapsulation ⁶⁴ Optimized microencapsulation of MSC by vibrational nozzle ⁶⁵
$\text{Ba}^{2+}/\text{Ca}^{2+}$	Human islets ARPE-19	Viability and function after transplantation into diabetic mice ⁶⁶ In vitro study of encapsulated human retinal pigment epithelial cells ⁶⁷

Although the formation of hydrogels from Na-alg is a straightforward process, the properties of the resulting MS depend on several parameters including molar mass, configuration and constitution of the starting polymer as well as the preparation conditions (section 1.5). In particular, sequences of two L-guluronic residues display favorable conformation for ionic bonding while D-mannuronic residues do not contribute to ionotropic interactions but bring more flexibility to the resulting network. Different ratios of these residues can thus lead to drastic changes in the hydrogel properties.⁶⁸ In addition, one of the major drawbacks of alg-based physical hydrogels is their limited mechanical stability and their lack of durability for long-term applications. These hydrogels generally dissolve when chelators such as phosphate, lactate or citrate and non-gelling cations are present in the environment above a certain concentration.⁶⁹ Different methods have been investigated to overcome this limitation. Coating the MS with polycations such as poly(L-lysine) (PLL), poly(L-ornithine) or chitosan to form polyanion-polycation complexes on the surface of the MS have been suggested to reinforce the MS. However, even by adding a final layer of Na-alg to neutralize the excess of positive

charges, biocompatibility issues were reported with these systems primarily due to surface attachment of proteins (section 1.7.3). Polycation-containing hydrogels activate inflammatory cascades which leads, ultimately, to the death of the encapsulated cells.⁷⁰

1.4.2 Chemical hydrogel

The main advantage of chemical hydrogels rises from their resistance and long term durability. These properties arise from the matrix of chemical hydrogels which is based on the combination of cross-reactive functionalities through irreversible cross-links. Nevertheless, many parameters are required for the formation of these resistant covalent bonds since the process of hydrogel formation, when applied to bioencapsulation, should not compromise cell integrity and viability. Only mild conditions can be used with non-cytotoxic solvents and reagents which limit the choice to water soluble components and biocompatible cross-linkers.⁷¹ Moreover the aqueous solutions need to be buffered with the appropriate osmolality to provide viable environment for cells. Finally, the chemical reaction involved for the formation of the covalent network should not interfere with cell components or metabolic products. Several combinations of polymers with different binding methods responding to these requirements have been explored for cell encapsulation.

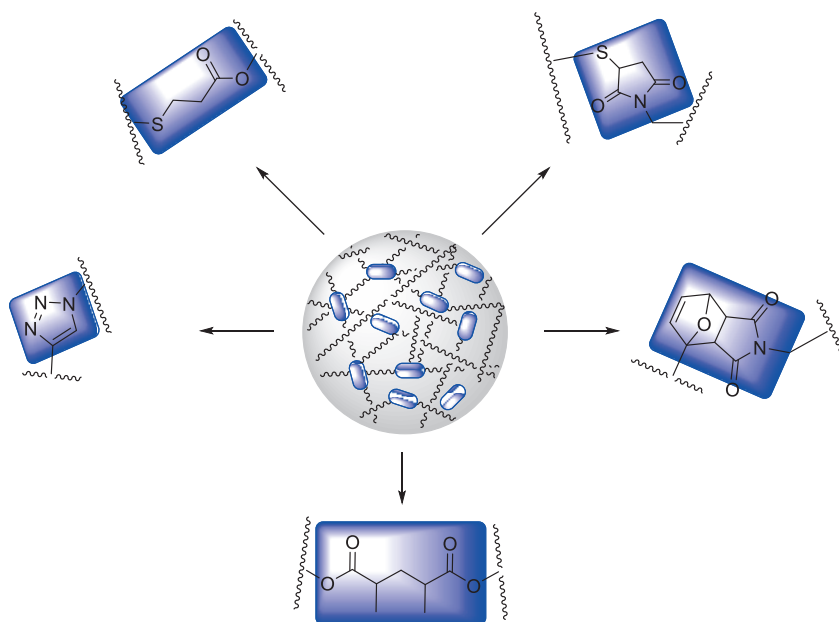


Figure 1.5: Examples of junction sites for the formation of chemical hydrogels. Clockwise from top left: thiol + acrylate (Michael addition)^{72,73}; thiol + maleimide (Michael addition)⁷⁴; furan + maleimide (diels alder)⁷⁵; 2x acrylate (Photopolymerization)^{74, 76}; azide + alkyne (Huisgen 1,3-dipolar azide-alkyne “click reaction”)⁷⁷.

Modified poly(ethylene glycol) (PEG) with various functional groups have been used for the preparation of chemical hydrogel to encapsulate different types of cells. Fibroblast and keratinocytes were successfully immobilized in MS resulting from thiol-ene reaction between PEG diacrylate and thiolated gelatin.^{72,73} Using combination of PEG derivatives containing maleimide reactive functionality and acrylate or maleimide moieties afforded hydrogel suitable for the encapsulation of C2C12 myoblast.⁷⁴ Photo-polymerization of fibrinogen-g-PEG acryloyl and PEG diacrylate provided hydrogels suitable for the encapsulation of BMSC.⁷⁶ Photo-polymerization of PEG diacrylate was also studied and led to the formation of MS usable

for the encapsulation Huh-7.5 cells.⁷⁸ Numerous examples using other chemical polymers such as chitosan, dextran, hyaluronic acid or poly(vinyl alcohol) with chemical modification allowing the formation of chemical hydrogels have been investigated.^{79–82} This panel of chemical hydrogels have demonstrated good properties for the encapsulation of various cell types.

Nevertheless, the slow kinetics of covalent bonds formation (in comparison with electrostatic interactions) can affect the shape of the resulting hydrogels and limit their applications. Generally, the rheological properties of the solution is also a parameter of great importance for the formation of chemical or physical hydrogels in the view of cell encapsulation.⁸³

1.4.3 Hybrid hydrogels

Combining the fast gelation of physical hydrogels with the high resistance of chemical hydrogels is the main purpose behind the development of hybrid hydrogels. Alginate based hybrid hydrogels have shown remarkable properties by merging the spontaneous formation of physical hydrogel in presence of divalent cations in combination with various covalent binding methods. One approach consists in the formation of multi-layer hydrogels such as alg-PLL-alg (APA)⁸⁴ which incorporate cross-linking between adjacent layers of the MS. For instance, phenyl azide moieties appended to poly-L-lysine create covalent bonds with alginate when irradiated with UVA in a cell compatible protocol. The resulting hybrid MS showed high stability in alkaline buffer (pH 12) compared with purely physical MS (three years instead of one min).

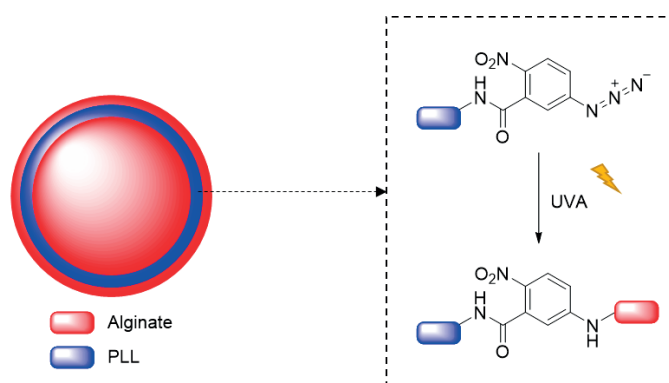


Figure 1.6: Representation of a multilayer alg-PLL-alg microsphere.

Another approach using methacrylate polymers and PLL demonstrated the formation of covalent binding in the core or on the surface of the MS depending on the molecular weight of the crosslinker used. For this purpose the reactive polyanion, poly(methacrylic acid, sodium salt-co-2-[methacryloyloxy]ethyl acetoacetate) was co-encapsulated in calcium alginate (Ca-alg) core followed by exposure to PLL of different size. The free amine groups of PLL reacted with the acetoacetate groups of the polyanion chain to form covalent bonds (enamine).⁸⁵ Approaches based on chemical cross-linking through complementary reactive groups attached to two oppositely charged polyelectrolytes were also investigated with promising results for cell microencapsulation.^{85,86} A two-component hydrogel composed of an interpenetrating polymer network of Ca-alg and covalently cross-linked vinyl sulfone-terminated multiarm poly(ethylene glycol) exhibited improved mechanical resistance compared to pure physical Ca-alg MS. HuH7 cells were encapsulated in this system and viable over two weeks.^{87–90} Another

two-component hydrogel was obtained from the mixture of Na-alg and Na-alg functionalized with cysteamine exhibiting again improved mechanical properties and good biocompatibility with the encapsulation of EDX cells over 30 days.⁹¹ (Figure 1.7)

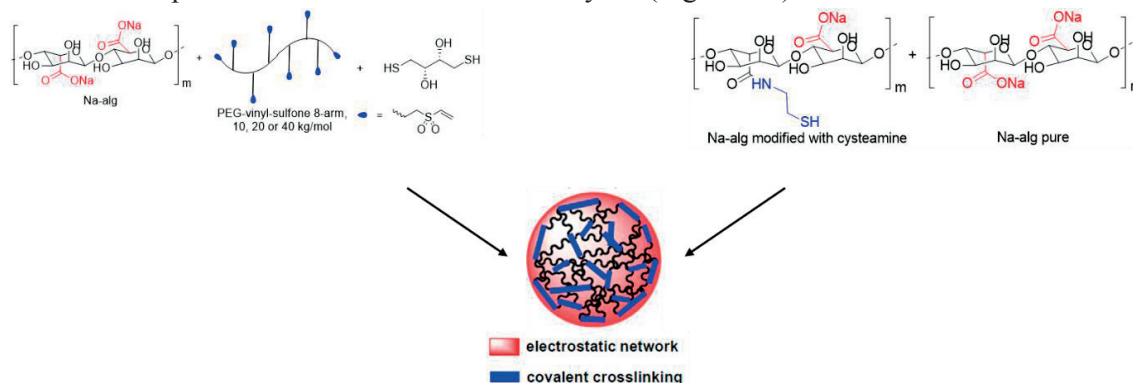


Figure 1.7 : Examples of alginate based hybrid hydrogels from multicomponents system.

Pushing further the improvement of hydrogels, one-component hydrogels with both physical and chemical binding sites present on the precursor polymer were developed. This method has the advantage to overcome the introduction of a second polymer which facilitate the process of hydrogel preparation (Figure 1.8).

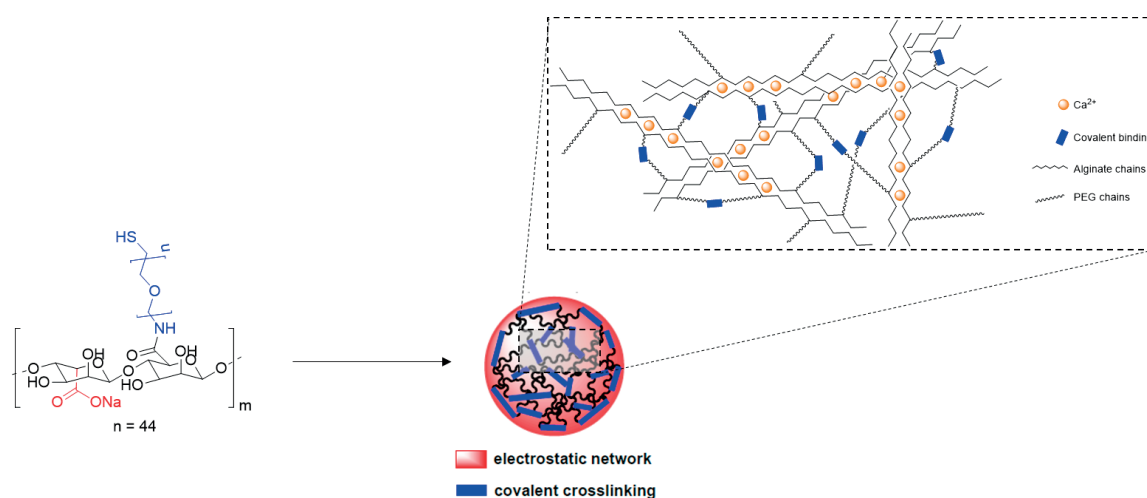


Figure 1.8: Example of an alginate based one-component hybrid hydrogel system with thiols moieties incorporated on the structure of alginate for the formation of covalent bonds through disulfide bridges.

The first reported application using this approach was the formation of Na-alg derivative with heterobifunctional thiol terminated PEG grafted on the carboxyl groups of alginate (Figure 1.8). The MS formed from this polymer exhibited improved mechanical properties combined with good biocompatibility with encapsulated material (Huh-7 cells).⁸⁷ Alternative one-component hydrogel systems imply the grafting of azide-terminated PEG chains to Na-alg for concomitant ionotropic interaction with Ca²⁺ and chemical ligation through Staudinger reaction of the azide moieties with phosphine-containing components present in the gelation bath.⁹² Human pancreatic islets were successfully encapsulated using such systems.⁹³

1.5 MICROENCAPSULATION TECHNIQUES

Various methods for the formation of MS have been developed to answer the needs of the numerous applications using this technology. The need for large scale production of robust core material can be achieved by a panel of technologies including pan coating, air suspension coating, emulsification or spray drying which have showed great advantages for industrial production of encapsulated materials.^{94–96} Nevertheless due to their rough conditions and broad size distribution these methods can hardly be adapted to cell encapsulation. Alternatively, softer methods such as droplets extrusion or microfluidics have been successfully used for the formation of cell-containing MS. Droplets extrusion is the most widely used method for cell encapsulation as it relies on a simple instrumental setup. It consists of dripping a cell-containing solution of polymer through a needle into a gelation bath to shape MS containing cells entrapped in their core. The main limitations of this straightforward method are the need for low viscosity initial polymer solution and the large diameter of the resulting MS ranging from 1.5 to 3 mm. The optimal size of MS used for cell encapsulation was estimated to range from 100 to 500 μm granting high surface-to-volume ratio which ensures good transport of nutrient and oxygen to the encapsulated cells.⁹⁷ In order to reduce the size of the beads while using droplet extrusion systems, different methods were developed. A simple instrumentation is the coaxial air-flow droplet generator.⁹⁸ The principle is to blow air with constant flow toward the end of the needle used for the extrusion to shape droplets ranging from 200 to 1000 μm at the needle outlet. Another approach consists of using a vibrating nozzle. The vibration breaks the droplets from the nozzle affording so uniform smalls MS.⁹⁹ Uniform beads in a good size range were also obtained by applying a high electrostatic field between the needle and the gelation bath. The size of the droplets can be tuned by controlling the electrostatic pulse.^{100–102} Finally a method called “jet breakage by rotating elements” can produce small sized MS with good homogeneity using kinetic force such as rotating nozzles, a rotating disk or a cutting wire.¹⁰³

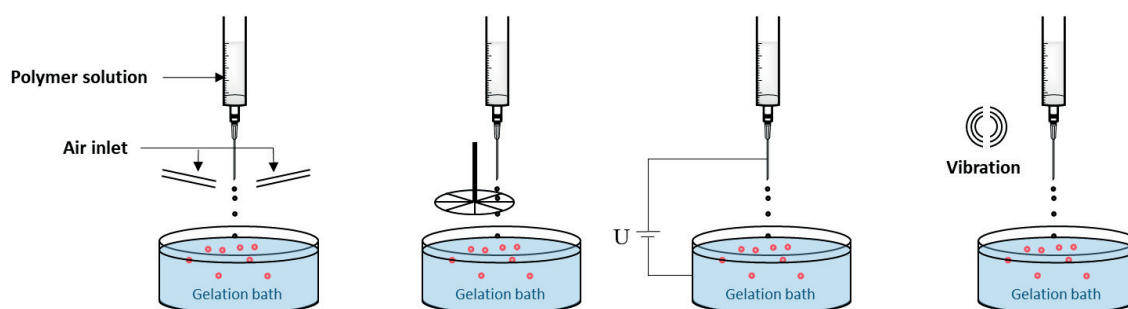


Figure 1.9 : Principle of droplets formation by (left to right): coaxial air-flow, rotating disk (jet cutting), electrostatic potential and vibrating nozzle

Recently promising results were reported using microfluidic technology for the encapsulation of living cells delivering MS with high homogeneity in size distribution.^{104–107} This technology produces MS from an aqueous precursor solution which is shaped to the desired droplet size with the help of an immiscible oil phase such as mineral oil, silicone oil, corn oil, hexadecane oil, or fluorinated oil.¹⁰⁸

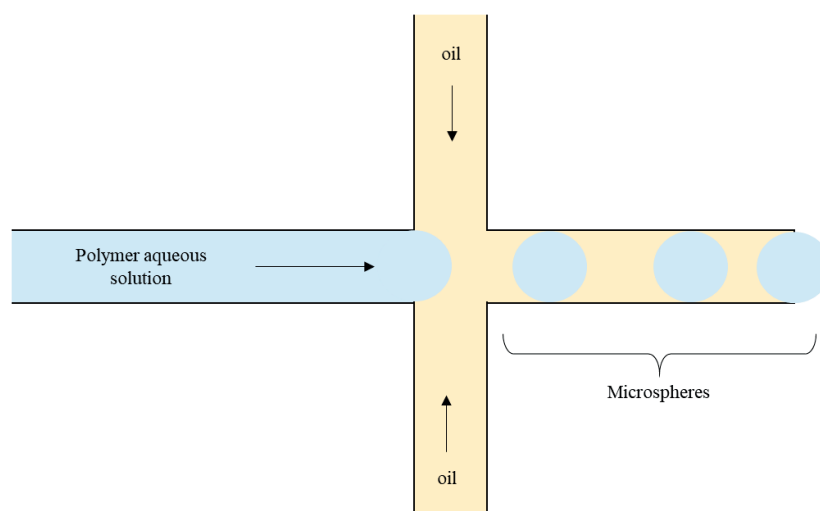


Figure 1.10: Principle of MS formation using microfluidics

The hydrogel network is then further internally crosslinked by ionic gelation or photopolymerization which showed good compatibility for cell microencapsulation.¹⁰⁹ This technology requires a sophisticated instrumental setup and a good control of the different parameters such as the pressure in the system, the viscosity of the solutions (oil and aqueous) and the design of the microfluidic chips (size and length of the channels). Nonetheless, droplets with very low polydispersity were obtained with microfluidics devices allowing the encapsulation of several types of cells.^{110–116} Moreover, single cell microencapsulation was achieved with this technology, which can be advantageous for various applications.^{117,118} Still, the production of a large amount of droplets by microfluidic systems within a short time scale, which is essential for clinical applications, remains a difficult task. The scaling up of such methods could however be a major breakthrough in the field of cell encapsulation.¹¹⁹

1.6 PROPERTIES OF HYDROGELS FOR CELL MICROENCAPSULATION

When intended for cell microencapsulation and transplantation, the hydrogel polymeric materials should display a panel of properties suitable to sustain long term cell viability and functionality. In particular, the immobilization matrix should protect the encapsulated cells from external mechanical stress and detrimental environment while ensuring the cross-diffusion of nutrients, oxygen, metabolic products and waste. Larger sized biomolecules (antibodies) and immune cells should not be able to cross the MS membrane. Below are presented the main parameters which play a crucial role in tuning the properties hydrogel materials.

1.6.1 Mechanical resistance

The mechanical resistance of MS is a determining factor for the long term viability of the encapsulated cells *in vivo*. Low resistance MS are subject to disintegration leading to a loss of immunoprotection resulting in graft failure. The importance of mechanical stability in cell encapsulation has been emphasized in recent years, giving rise to various methods for its evaluation.^{120–123} The main characteristics contributing to the protection of the encapsulated cells from the environmental constraints are the deformability (stiffness) and the resistance to fracture (toughness) of the hydrogel. The forces to which MS are exposed *in vivo* can vary a lot with respect to the transplantation site and the animal model but no study gives precise

information about the magnitude of these forces and the exact resistance requirements with respect to the model used.

Nonetheless, the importance of mechanical resistance has been recognized and several methods have been developed to assess the mechanical properties of MS. The attributes such as physical resistance and deformation under compression can be quantitatively measured by means of a Texture Analyser.^{124–126} The MS are set under a probe which applies defined compression while monitoring the resistance of the material. Both the breaking load and the mechanical resistance to defined compressions can be determined with this instrument. Either a layer of several MS or a single MS can be evaluated with such system. Furthermore, the stiffness of the capsules can be measured by including cycles of compressions and monitoring the evolution of the resistance through multi-compression cycles. Importantly, this measurement provides valuable information regarding the ability of MS for shape recovery under repetitive deformations.

Another method allowing qualitative evaluation of the hydrogel resistance consists in simply exposing the MS to a hypotonic solution such as water, leading to an increase of the osmotic pressure resulting in the swelling and potential disintegration of the MS.¹²⁷ Such an experiment provides valuable information on the swelling properties of the MS, which is mostly relevant with physical hydrogels upon ion exchange and resulting in loss of cell protection.

1.6.2 Permeability

One of the main purposes of cell encapsulation lies in the selective permeability of the hydrogel materials. More specifically, the hydrogel materials should block the contact of encapsulated cells with host immune cells and antibodies while allowing the diffusion of nutrients, oxygen and metabolic products. Even though the control of permselectivity is recognized as a crucial element in the field of cell encapsulation, different statements were reported concerning the optimal pore sizes to promote high performance of the encapsulated cells.^{128–131} On the one hand, one argues that the main role of the membrane is to protect encapsulated cells from direct contact with immune cells. If one considers only this role, a certain flexibility regarding the size of the pores is allowed as long as an inert polymer is used. On the other hand, a strict control of the pore size and the permeability may help reducing leakage of components to the outside of the capsule thus reducing immune reaction of the host. This last approach is mainly relevant in the case of xenotransplantation.¹²³

Measuring the permeability of hydrogels can be delicate and different methods have been developed for that purpose. The most important parameter describing the permeability regarding cell encapsulation is the molecular weight cut-off (MWCO) of the membrane. It represents the minimum size (molecular weight) of a compound excluded from the pores of the hydrogel. To measure MWCO, the common approach is the sized-based exclusion experiment which consists in measuring the diffusion of labeled compound such as dextran, pullulans or proteins of different sizes through the MS membrane. The observation of the diffusion can be achieved by different means such as the monitoring of fluorescent or radioactively tagged compounds.^{66,132–135} However, depending on the compound chosen to assess the MWCO the results has to be taken cautiously, as the size of polysaccharides for example cannot be directly compared to a protein of the same weight.¹³⁶ Another method used with success is the inverse size-exclusion chromatography (ISEC). In this method, solutes of various sizes are eluted through a column filled with MS, allowing to measure their partition between the mobile phase and the stagnant MS phase.¹³⁶ This technique can provide precise information on the pore size

and distribution but requires high volume of MS which can be challenging depending on the material and/or the method of production. The mesh size of the molecular network of the hydrogel can also be directly measured by cryo-scanning electron microscopy (cryo-SEM).¹³⁷ Although it provides an accurate direct measurement, one has to keep in mind that the hydrogel molecular network might drastically change during the freezing process.

1.7 PROPERTIES OF BIOLOGICAL COMPONENTS

To overcome the limitations of cell-based therapies, which mainly lie in the shortage of suitable cells for transplantation and the lack of long-term functionality of encapsulated cells, several parameters should be controlled, including the sources of cells, the site of transplantation and the biocompatibility toward the host.

1.7.1 Source of cells

As mentioned before, a major advantage of cell encapsulation lies in the possibility to use non-human cell sources in xenotransplantation protocols. This eventually leads to the question of the optimal alternative source of cells replacing human donors. One of the most contemplated source of cells for this purpose is porcine cells. This model has already shown good compatibility for islets transplantation.^{138,139} More precisely, the use of neonatal pigs islet-like cells (NICCs) has demonstrated great advantages for this application, since NICCs are easily purified, exhibits low levels of T-cell response and a high resistance to ischemia and inflammation.¹⁴⁰ Recent studies on NICCs led to the conclusion that islet clusters should be isolated from porcine during the first month of their life, and that the maturation of NICCs islets was optimal after 12 days of culture.¹⁴¹⁻¹⁴³ In addition, recent progress in genome editing technologies, such as CRISPR/Cas9, allowed to precisely remove or insert genes anywhere in the genome.¹⁴⁴ Genetically modified pigs were produced with numerous genetic modifications, allowing the removal of several porcine antigens (GalT/CMAH/b4GalNT2 triple gene KO) and incorporation of human genes regulating the immune response, the complement or the coagulation.¹⁴⁴ Furthermore, the risk of xenozoonosis, i.e. the transmission of porcine infectious agents to humans, such as porcine endogenous retroviruses (PERV), was successfully blocked using the Crisp technology.¹⁴⁵ Other source of transgenic islets cells were considered like the fish tilapia.^{146,147} Encouraging results were obtained with transplantation of encapsulated tilapia islets into mice in combination with immunosuppressive treatments, resulting in blood glucose level regulation for over 200 days.¹⁴⁸ However, considering the significant difference between human and tilapia insulins, the use of tilapia islets for diabetes cell therapy might be compromised. Due to close physiological similarities between pigs and humans and the possibility to inactivate PERV, pig species currently appear as the most promising xenogeneic cell source for the treatment of diabetes through islets xenotransplantation.¹⁴⁹

1.7.2 Site of transplantation

Several sites of transplantation have been considered for the deposition of encapsulated cells with good cell survival and functionality in different animals models.^{150,151} The optimal transplantation site needs to answer to several requirements such as sufficient vascularization to ensure the supply of oxygen and nutrients to the encapsulated cells, and good accessibility for the deposition and retrieval of the MS. The performance of different surgical sites was assessed by evaluating the survival of microencapsulated transplanted cells. A commonly used

site of transplantation showing an acceptable rate of success is the peritoneal cavity.^{59,152–154} This cavity has the main advantage of being very accessible for the deposition of MS and allows the transplantation of large amounts of material. Some studies however suggest that the vascularization/oxygenation in the peritoneal cavity is not optimal.⁵⁹ Also, MS floating in the cavity can make their recovery delicate. An alternative approach was developed with the surgical creation of an omental pouch as a site for the deposition of encapsulated islets. This method allowed better oxygenation and a good functionality of the encapsulated cells.^{155–157}

Transplantation under the kidney has also been studied and exhibited good results with islets transplantation.^{158,159} The access to this site is easy and the high vascularization allows good viability of the cellular material. Even though transplantation of free islets in immunosuppressed models at this site exhibits good results, the limited space under the kidney could be a serious limitation when considering the transplantation of microcapsules which requires bigger volume to reach insulin independence.

Subcutaneous locations are very accessible for transplantation and retrieval,¹⁶⁰ but display low blood supply. However, a study showed that the vascularization of these sites can be improved with prevascularization.¹⁶¹ Still, the physical constraints in these area are to be considered as a parameter affecting cell viability. The striated muscles also provide an easily accessible transplantation site with the advantage of being highly vascularized. Transplantation in mouse was done with good success taking profit of the high level of oxygen at this site. Nevertheless, transplantation in striated muscles has also been associated with strong fibrosis response.^{162,163} Finally, the portal vein is commonly used for islet transplantation providing efficient nutrition and blood supply. However, the risk of portal vein occlusion and the difficulty to retrieve MS from this site remain major limitations that have to be seriously considered in view of clinical applications.¹⁶⁴

1.7.3 Biocompatibility

Despite the recent progresses which were achieved over the last two decades in the engineering of polymeric hydrogels for cell immobilization and in the harvesting of cell batches with suitable quality for transplantation, the success of clinical applications based on microencapsulated cells remains hampered by host biocompatibility defects. While the physical and mechanical properties (resistance, stiffness, size, hydrophilicity) of the hydrogel MS can be modulated to promote viability and functionality of the encapsulated cells,¹⁶⁵ the host acceptance remains a major challenge.

Following the transplantation of encapsulated cells, the occurrence of pericapsular fibrotic overgrowth (PFO) is commonly observed, resulting in cell necrosis and ultimate loss of graft functionality.

As depicted in Figure 1.11, the formation of fibrotic tissue surrounding the transplanted MS compromises the supply of nutrients and oxygen as well as the excretion of metabolic

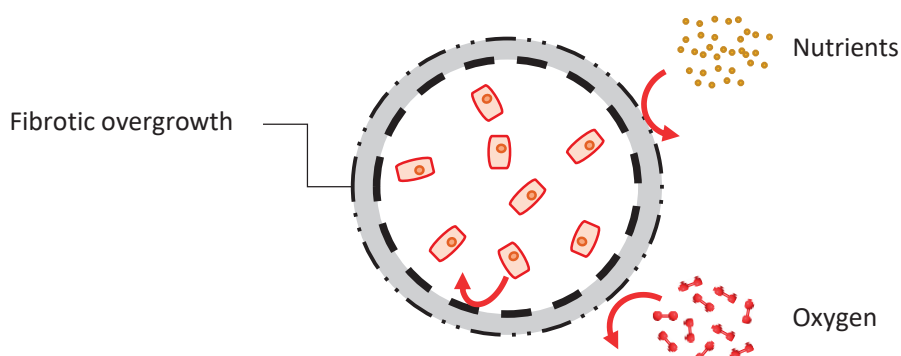


Figure 1.11 : Representation of pericapsular fibrotic overgrowth resulting in graft failure

products.^{30,166–169} Recently, the biocompatibility of the encapsulation materials has been the subject of intensive investigation to answer the needs of transplantation. In particular, several approaches were developed to enhance the long-term functionality of encapsulated living cells.¹⁷⁰

1.7.3.1 Mechanisms of inflammation

The inflammation occurring during the transplantation of MS follows complex patterns potentially involving numerous mechanisms.^{171–174} The processes of inflammation and fibrosis formation were described as three successive phases: the acute inflammation, the chronic inflammation and finally the long-lasting granulation tissue phase.¹⁷¹

The acute inflammation occurs directly after the transplantation of the microcapsules. This phase is defined by the attraction of granulocytic neutrophil cells in the area of transplantation. These cells carry chemotactic cytokines and chemokines which are small proteins stimulating the recruitment of specific surrounding cells. This immune response cannot be avoided, as the surgery needed for the transplantation is a natural trigger of the acute inflammation which is an essential protective response in injured tissues.¹⁷⁵ Nevertheless if these signals persist for several days, monocytes, macrophages and lymphocytes will accumulate in the area of inflammation. This progression of cell types present at the inflammation site is the turning point making the beginning of the chronic inflammation phase. Several factors have been associated with the prolongation of inflammatory signals occurring around the biomaterial after transplantation, leading to chronic inflammation.

The adsorption/desorption of proteins on the surface of the encapsulation material is a well-studied process that can be involved in the host inflammation response and highly depends on the nature of the material. The protein adsorption on the surface of the MS can trigger the inflammation mechanism in different ways. The adsorption of immunoglobulins (IgG, IgM and IgA) is the classical pathway leading to an immune response.¹⁷⁶ Another way is the adsorption of proteins and conformational change.^{177,178} It has been studied that the denaturation of protein C3 when adsorbed at the surface of biomaterials can lead to the activation of the complement cascade mechanism of inflammation. This is triggered by the products resulting from the denaturation of C3, which are strongly chemotactic for leukocytes involved in inflammatory

events.^{179–181} Nevertheless the adsorption mechanism is mainly observed when using charged hydrophobic surfaces. In the case of alginate hydrogels with very low hydrophobicity this process remains limited.¹⁷⁶

Another parameter susceptible to trigger and sustain the inflammation response is the release of pathogen-associated molecular patterns (PAMPs) and danger-associated molecular patterns (DAMPs) from the MS. The inflammation potential of these molecules were emphasized in two studies focusing on alginate-based hydrogels. The quality of the alginate material, in particular its purity is a key parameter for biocompatibility. In case of high concentration of PAMPs such as peptidoglycan, lipoteichoic acid, and flagellin which are recognized by Toll-like receptors (TLR2, 5, 8 and 9), the host immune response is activated.¹⁸² The release of DAMPs from encapsulated islets have been monitored by the quantification of HMGB1, DNA and uric acid which were shown to activate MyD88-TLR receptors.¹⁸³ In case inflammation signals are sustained in the same area, others cell types such as “vascularized fibrous tissue” fibroblasts and macrophages, foreign giant cells and polynuclear cells are recruited and the inflammation then turns to the long-lasting granulation tissue phase.¹⁸⁴

Several models were developed to assess the potential immune response toward encapsulation materials. One can mention the “whole blood model” which consists of placing empty hydrogels (without cell content) into human whole blood in presence of an anticoagulant (often lepirudin). This model covers many parameter involved in the early stage inflammation like the complement system, effector of coagulation (except for the thrombine inhibited when lepirudin is used) and fibrinolysis cascades. Leukocytes and platelets are also present in whole blood allowing the study of their behavior. Various types of MS have been analyzed using this model.^{185,186} These studies highlighted the fact that pure alginate MS were much less susceptible to provoke an inflammatory response whereas multilayer systems such as alginate-PLL-alginate, alginate-PLL, alginate-cellulose and sulfate-PMCG triggered the inflammation via different pathways involving adsorption mechanisms. Even though this method is an efficient non-invasive way to compare the inflammatory potential of many materials, one should keep in mind that the presence of cells in the MS would most likely change drastically the outcome.

While in vitro assays allow for the screening of many encapsulation materials without the recourse to animal models, the complexity of foreign body inflammation response cannot be fully reproduced in vitro.

1.7.3.2 Methodologies to reduce inflammation and fibrosis

In recent years, several approaches were investigated to reduce the inflammatory reaction to transplanted encapsulated cells. The formation of fibrotic tissue induced by the transplantation of MS can be triggered by the nature of the encapsulation material and of the cell content. It has been shown that the purity of the material used for the encapsulation such as alginate can significantly influence its biocompatibility.¹⁸² Moreover the cellular core of the capsules is highly susceptible to trigger the inflammation reaction given that cells are known to produce danger-associated molecular patterns identified as a source of inflammation reaction.¹⁸³ In particular, in the case of xenotransplantation, the cellular metabolites excreted from the MS are treated as foreign antigens by the host. The main reported approaches addressing PFO focus either on the modification of the MS surface, on the co-encapsulation of small molecular

modulators of the immune response, and/or on the modification of the cell content. A selection of the strategies recently developed is listed in Table 2.

Remarkable results were obtained with the co-encapsulation of mesenchymal stem cells (MSCs) which are able to produce small molecular modulators able to mitigate the immune response and therefore decrease PFO. Using Ba-alg MS, the co-encapsulation of hepatocellular carcinoma cells HuH7 with mesenchymal cells demonstrated significant reduction of PFO in vivo. The same method was used for the co-encapsulation of islets and exhibited not only reduction of fibrosis but also an improved survival and functionality of the allograft up to 50 days after treatment in diabetic mice.^{187,188} Another approach focusing on surface modification was achieved by coating the MS with chitosan which appeared to reduce protein absorption to the material surface¹⁸⁹ and lead to an extension of the life-time of encapsulated islets in mice and canine models.¹⁹⁰

A widely investigated approach addressing the issue of PFO focuses on the co-encapsulation of anti-inflammatory or immunosuppressive drugs with the effector cells. Several studies observed the enhancement of functionality of the encapsulated cells in relation with a reduction of fibrosis when small anti-inflammatory molecules were co-encapsulated.^{191–193} The screening of a panel of known anti-inflammatory drugs for co-encapsulation with rat islets highlighted the beneficial effect of curcumin to mitigate PFO and to maintain reduced blood glucose level over 60 days in mice model.¹⁹¹ A significant reduction of PFO was also observed with the co-encapsulation of ketoprofen in polyester MS in vivo.¹⁹⁴ However, the limitation of the co-encapsulation strategy lies in the *burst release effect* which reduces the time during which the drug effect can be expected. More efficient systems might be achieved by covalent drug conjugation to the polymeric material for improved release kinetics (section 2).

Table 2 : Strategies to reduce PFO in the transplantation of alginate-based MS; h: human; m: mouse; IP: intra-peritoneal; MSCs: mesenchymal stem cells; SC: sub-cutaneous; PFO: pericapsular overgrowth; PLO: poly(L-ornithine); PLA: poly(lactic acid)

Material	MS content	In vitro/ in vivo model	Outcome
Na-alg/Ba ²⁺	hMSCs : HUH7 (1:1)	C57BL/6 mice IP infusion	1.4 fold reduction of PFO ¹⁸⁷
	mMSCs / hHUH7 (2:1)	C57BL/6 mice SC injection	2 fold reduction of PFO ¹⁸⁷
		C57BL/6 mice SC injection	2.1 fold reduction of PFO ¹⁸⁷
	Stimulated mMSCs / m-islets (1:1)	C57BL/6 mice IP infusion	6 fold reduction of PFO 100% normoglycemic mice after 50 days ¹⁸⁸
Na-alg/Ba ²⁺	unstimulated mMSCs / m-islets (1:1)	C57BL/6 mice IP infusion	2.5 fold reduction of PFO 71% normoglycemic mice after 50 days ¹⁸⁸
	rat islets/curcumin 1 mg/mL	C57BL/6 mice IP infusion	reduced blood glucose level over 60 days

			no fibrosis on almost all capsules retrieved after 60 days ¹⁹¹
Na-alg/Ca ²⁺ cationic coating	Rat islets/pentoxifylline (PTX) 400 µg/mL	Co-culture of encapsulated islets with mice lymphocytes	burst release of PTX reduced attack of encapsulated islets by lymphocytes ¹⁹²
Na-alg/Ca ²⁺	Porcine islets MS coated with PEG-rapamycin layer	BALB/c mice IP infusion	reduced infiltration of fibrotic cells after 30 days no significant effect on blood glucose level ¹⁹³
alg/PLO/alg/Ca ²⁺	PLA loaded with ketoprofen	CD-1 mice IP infusion	75% of KET released during the 1st day no sign of inflammation after 63 days ¹⁹⁴
Na-alg/Ba ²⁺ chitosan coating	porcine islets	GalT KO mice	80% graft survival after 381 days 2 fold reduction of PFO ¹⁹⁰
	canine islets 3 transplantations	Pancreatectomized beagles	99% of capsules without PFO 231 days insulin independence ¹⁹⁰

The size and shape of the MS were also described as important parameters to influence the host immune response.¹⁹⁵ In recent study it was shown that larger beads (1.5 mm) exhibited less immune reaction and fibrosis than smaller beads made of different materials in rats and primate models.¹⁹⁶

2 THESIS OBJECTIVES

A large number of patients could benefit from progress in cell transplantation therapies if polymeric materials presenting optimal properties for cell microencapsulation could be produced. Maintaining the intrinsic favorable properties of alginate hydrogels but improving their physical properties, mechanical behavior and biocompatibility is at the heart of this work.

The main goal was to improve the longevity of encapsulated cells, in particular insulin producing cells, by reduction of PFO. Following the encouraging results observed with the co-encapsulation of small molecular modulators of the host immune response (section 1.7.3.2), an alternative approach based on the covalent conjugation of anti-inflammatory or anti-fibrotic compounds to the alginate backbone was developed. Controlled and sustained delivery of the active ingredient at the MS transplantation site is expected by hydrolysis of the covalent linkage *in vivo*.

The long term *in vivo* stability of the hydrogel MS was addressed in parallel and several alginate-based hybrid hydrogels were developed to form stable MS. In order to maintain the carboxylic groups of Na-alg available for ionic interactions, the modification of the hydroxyl groups of the alg backbone was investigated to introduce thiol- or 1,2-dithiolane-containing poly(ethylene) glycol derivatives. Concomitant fast ionotropic gelation and slow covalent crosslinking (disulfide bridge or disulfide cluster formation) was targeted during MS production.

Combining these two aspects was ultimately studied to produce functionalized hybrid alginate-based hydrogels for islets transplantation.

2.1 INHIBITION OF PERICAPSULAR FIBROTIC OVERGROWTH

The reduction of PFO might be achieved by inhibition of the inflammation cascade at different stages of the process. The most common inflammation modulators are the non steroidal anti-inflammatory drugs (NSAIDs), which inhibit enzymes involved in the early stage of the inflammation pathway. More specific small molecular effectors such as inhibitors of fibroblast activation protein- α (FAP- α) were also considered.

2.1.1 Inhibitors of fibroblast activation protein- α

Fibroblast activation protein- α (FAP- α) belongs to the post-proline dipeptidyl aminopeptidase family and shares high similarity with dipeptidyl peptidase IV (DPPIV).¹⁹⁷ Involved in the control of fibroblast growth or epithelial-mesenchymal interactions during development, tissue repair, and epithelial carcinogenesis, FAP- α plays a significant role during fibrosis formation. It is therefore reasonable to target the inhibition of this protein to prevent PFO. Several studies demonstrated that the selective inhibition of FAP- α protein can be achieved with small molecules containing the Gly-Pro sequence or analogues.¹⁹⁸ Moreover, it was previously demonstrated in the group¹⁹⁹ that cyano-Pro derivatives displayed effective FAP- α inhibition (Figure 2.1).²⁰⁰

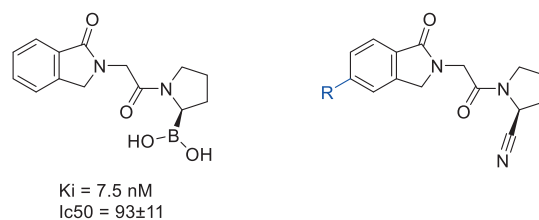


Figure 2.1 : Generic structure of FAP- α inhibitor (left) and derivative synthesized in the group (right)

These structures were thus selected for further modification in view of their covalent grafting to the alg backbone.

2.1.2 Nonsteroidal anti-inflammatory drugs

Non-steroidal anti-inflammatory drugs (NSAIDs) are among the most frequently used drugs by millions of people worldwide for their ability to relieve patients from pain, fever and inflammation.^{201,202} Curcumin and ketoprofen are both non-steroidal anti-inflammatory agents exhibiting therapeutic effects which are mostly associated with the inhibition of the proteins COX-1 and COX-2 involved in the early stage inflammation cascade.^{203–205}

The encapsulation of free curcumin and ketoprofen in alginate based hydrogels was already investigated and appeared to decrease PFO in mice.^{191,194} These two molecules were thus selected for covalent conjugation to the alg backbone and further local controlled delivery from the MS. Due to their remarkable therapeutic virtues, many natural and synthetic derivatives of curcumin (curcuminoids) have been developed and displayed similar anti-inflammatory characteristics.^{206,207} Derivatives of ketoprofen have also been synthesized showing good results as anti-inflammatory prodrugs with hydrolysable ester bonds.^{208–210}

While burst release of co-encapsulated free drugs results in short term action, we expected that slow release from covalent adducts would inhibit the early and subsequent stages of inflammation on an extended period of time which would drastically reduce fibrosis formation and improve the lifetime of the encapsulated cells. In the case of curcumin, the phenols groups were considered for derivatization to produce a doubly functionalized prodrug for the grafting to alginate. In the case of ketoprofen, the carboxylic function was used for the derivatization in order to prodrug candidates.

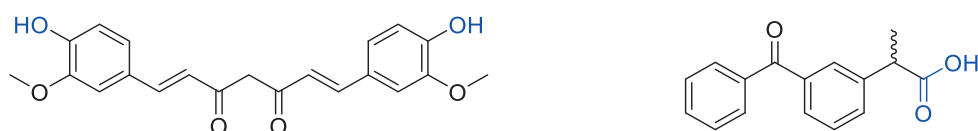


Figure 2.2 : Curcumin (left) and ketoprofen (right) chemical structures. The sites for derivatization are highlighted in blue

By combining improved stability and resistance rising from new alginate based hybrid hydrogels with the properties of inhibition of PFO provided through controlled release of anti-inflammatory/fibrotic compounds, the final objective of this research was to produce multifunctional alginate-based hydrogels for long-term cell therapy protocols.

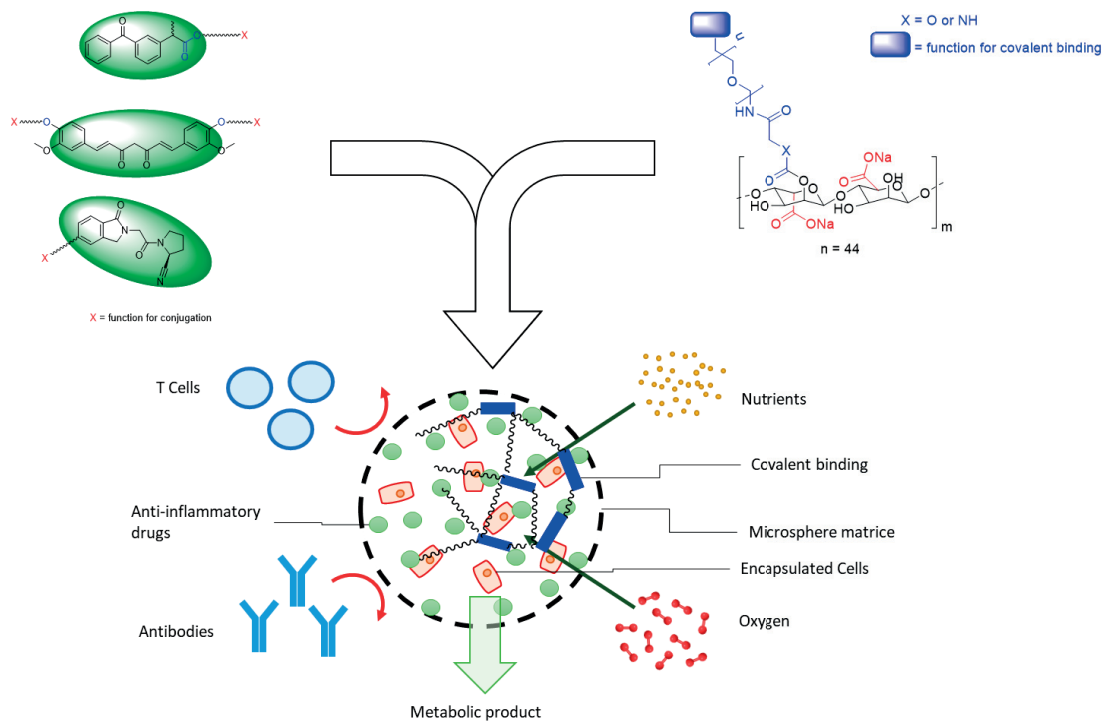


Figure 2.3 : Representation of new multifunctional hydrogels

3 RESULTS AND DISCUSSION

3.1 SYNTHESIS OF ANTI-FIBROTIC DERIVATIVES

One of the main limitation regarding transplantation of encapsulated cells is the formation of fibrotic tissues around the MS leading to the death of the encapsulated material. To address this issue, this work focused on covalent binding of anti-fibrotic small molecules (drugs) on the structure of hydrogels allowing a controlled release in vivo which would mitigate fibrosis formation over long term improving the life time and functionality of the encapsulated material.

The anti-fibrotic compounds considered for this work were thus chemically designed to display functionalities allowing covalent binding on the surface of the hydrogel either before or during the formation of the MS. For this purpose, polymers used for hydrogel formation were accordingly developed in parallel with the incorporation of new functionalities accessible for the integration of the drug derivatives (section 3.3). Since the formation of MS has to be performed in the presence of living cells, the reactions designed for the conjugation of the drugs at that stage have to be biorthogonal to avoid compromising cell viability. Hence the functionalities used for the formation of covalent binding during MS formation were maleimide, which can react with thiol groups through a 1,4-Michael addition, and lipoyl moieties that can produce clusters of disulfide bridges (Figure 3.1 left). In contrast, covalent binding of drugs on the polymer backbone before MS formation do not require specific biorthogonal conditions allowing more flexibility in the choice of the reaction used for this matter. Alkyne and amine moieties were thus synthetically added on the anti-fibrotic compounds for this purpose (Figure 3.1 right).

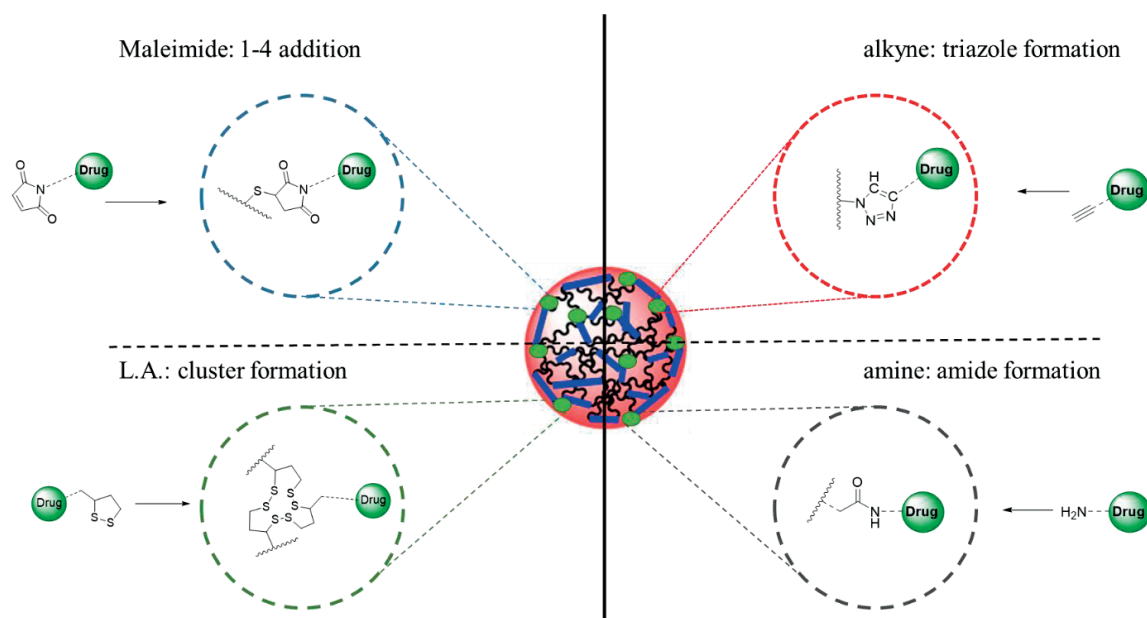


Figure 3.1 : Strategies for the grafting of anti-fibrotic compounds on microspheres

Three small molecules presenting a potential anti-fibrotic effect were thus derivatized to present the desired functionalities on their chemical structure: FAP- α inhibitors, Curcumin and Ketoprofen.

3.1.1 Derivatives of FAP- α inhibitors

The core of FAP- α inhibitor was modified with different moieties suitable for the formation of covalent bonds on the polymeric structure used for hydrogel formation. The structure responsible for the inhibition of FAP- α (Figure 3.2 right) was covalently linked through amide bond to maleimide, alkyne and two derivatives of lipoic acid (Figure 3.2 left).

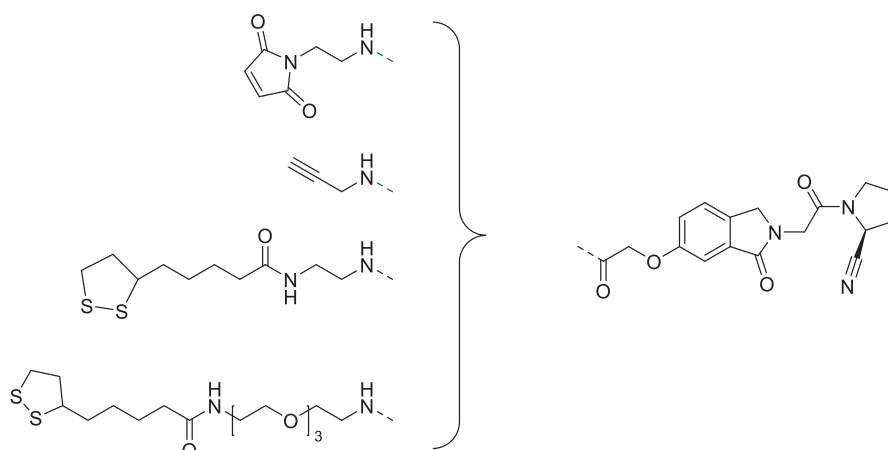
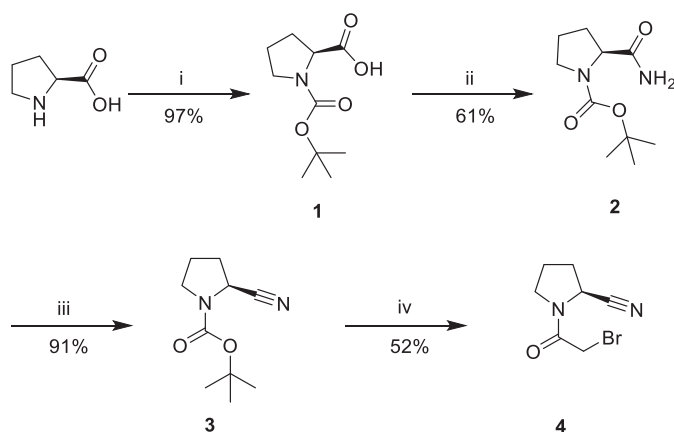


Figure 3.2 : Derivatization of FAP- α inhibitor

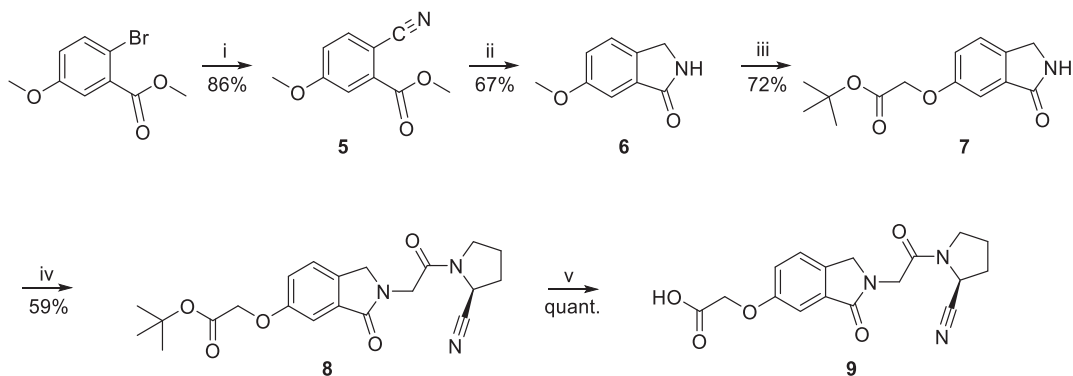
Based on a synthetic procedure previously developed in the Group for Functionalized Biomaterials,¹⁹⁹ the synthesis of the FAP- α inhibitor core started from L-proline which was converted into the activated cyano-pyrrolidine (**4**) derivative according to Scheme 1.

L-proline was first protected as a tert-butyl carbamate and then converted into amide using coupling agents (HOBt and EDCI) to yield (S)-tert-Butyl 2-carbamoylpyrrolidine-1-carboxylate (**2**). Dehydration in the presence of trifluoro acetic anhydride allowed formation of nitrile (**3**) in high yield. Treatment of **3** under reduced pressure with 2-bromoacetyl bromide resulted in one-pot deprotection/acylation of the amine moiety which to produce compound **4** in reasonable yield.



Scheme 1: Synthesis of the cyano-pyrrolidine block. Reagents and conditions: i- Boc_2O , Et_3N , DCM , 23°C , 16 hr; ii- HOBt , EDCI , NH_3 , THF , 23°C , 16 hr; iii- TFAA , Et_3N , DCM , 0°C to 23°C , 16 hr; iv- 2-bromoacetyl bromide, MeCN , reduced pressure, 23°C , 1 hr.

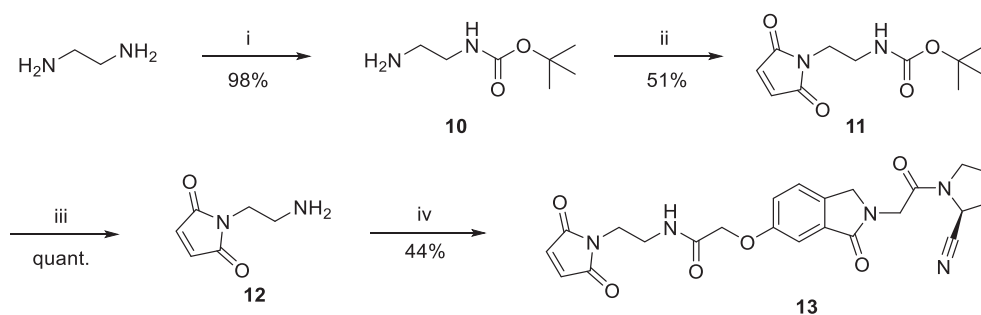
In parallel, the isoindolinone block (Scheme 2) was prepared from commercially available methyl 2-bromo-5-methoxy-benzoic acid. First, cyanation was achieved by successive treatment with CuCN and excess of KCN to afford intermediate **5** in 86% yield. The nitrile moiety was reduced in presence of Raney Ni under H_2 atmosphere which induced *in situ* cyclization to the isoindolinone derivative **6**. The methyl ether was then cleaved in presence of methionine and MsOH followed by O-alkylation with tert-butyl bromoacetate to produce carbamate **7** in 72% yield (2 steps). Deprotonation of the lactam moiety with LiHMDS , followed by N-alkylation in presence of compound **4** delivered the expected target derivative **8**. Cleavage of the *tert*-butyl ester under mild conditions provided the corresponding carboxylic acid in quantitative yield.



Scheme 2: Synthesis of FAP- α inhibitor free acid derivative. Reagents and conditions: i- 1) CuCN , DMF , 140°C , 30 min, 2) KCN , H_2O , 50°C , 1 hr; ii- Ni raney, H_2 , MeOH , 23°C , 16 hr; iii- 1) MsOH , methionine, 85°C , 16 hr, 2) *tert*-butyl bromoacetate, NaOH , TBAB , H_2O , DMF/DCM , 23°C , 16 hr; iv- LiHMDS , 0°C , **18**, THF , 23°C , 16 hr; v- SiO_2 , toluene, reflux, 60 min.

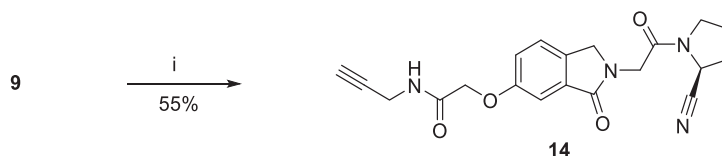
The intermediate **9**, presenting the FAP- α inhibitor core and a carboxyl group, was used as a building block for the introductions of the different functionalities considered for further conjugation to the hydrogel polymeric structure via amide formation. For the introduction of maleimide, a short linker was synthesized with an amine available for further coupling.

While the introduction of a tetra ethylene linker to maleimide was not met with success, a smaller spacer could be introduced (Scheme 3). Ethylenediamine was monoprotected in presence of Boc₂O and the remaining free amine reacted with maleic anhydride in presence of triethylamine. The resulting succinic acid was treated with sodium acetate at 65°C to produce the maleimide core in 51% yield. Quantitative cleavage of the tert-butyl carbamate in acidic medium afforded the maleimide derivative **12** which was coupled with **9** in the presence of TBTU.



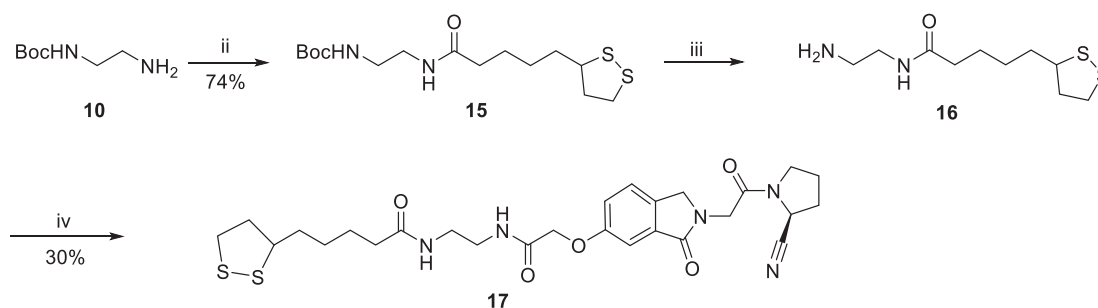
Scheme 3: Synthesis of maleimide derivative and conjugation to FAP- α inhibitor. i- Boc₂O, DCM, 16 hr; ii- 1) maleic anhydride, NEt₃, ethanol, 0°C, 4 hr, 2) Na acetate, acetic anhydride, 65°C, 30 min; iii- TFA, DCM, 0°C, 1 hr; iv- TBTU, DIPEA, **9**, THF, 23°C, 16 hr

The next derivative of FAP- α inhibitor was obtained through coupling with propargylamine to provide an alkyne moiety suitable for further “click reaction” with azide-containing substrates (Scheme 4).



Scheme 4 : Synthesis of FAP- α inhibitor alkyne derivative. i- HOBt, EDCI, DIPEA, propargylamine, 23°C, 12 hr.

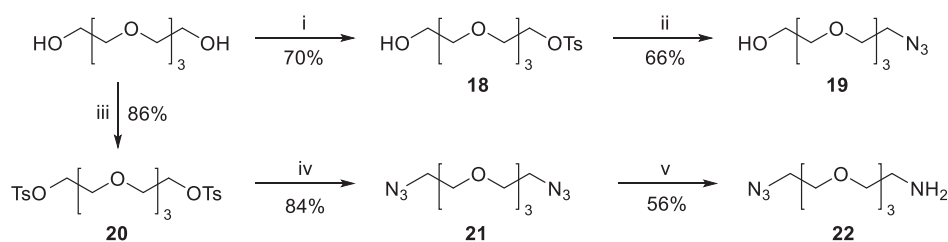
For the addition of a lipoic acid on the FAP- α inhibitor structure, N-Boc-ethylenediamine (**10**) was reacted with lipoic acid in presence of EDCI and HOBt to afford intermediate **15** in 75% yield. Acidic deprotection of the amine, followed by coupling with **9** provided an additional derivative of FAP- α presenting a lipoyl moiety for disulfide bridge cluster formation.



Scheme 5 : Conjugation of lipoic acid to FAP- α inhibitor. Reagents and conditions: i- *Boc*2O, 23°C, 12 hr; ii- lipoic acid, EDCI, HOBt, DIPEA, 23°C, 12 hr; iii- TFA, 0°C to 23°C 1.5 hr; iv- EDCI, HOBt, DIPEA, 9, 23°C, 16 hr.

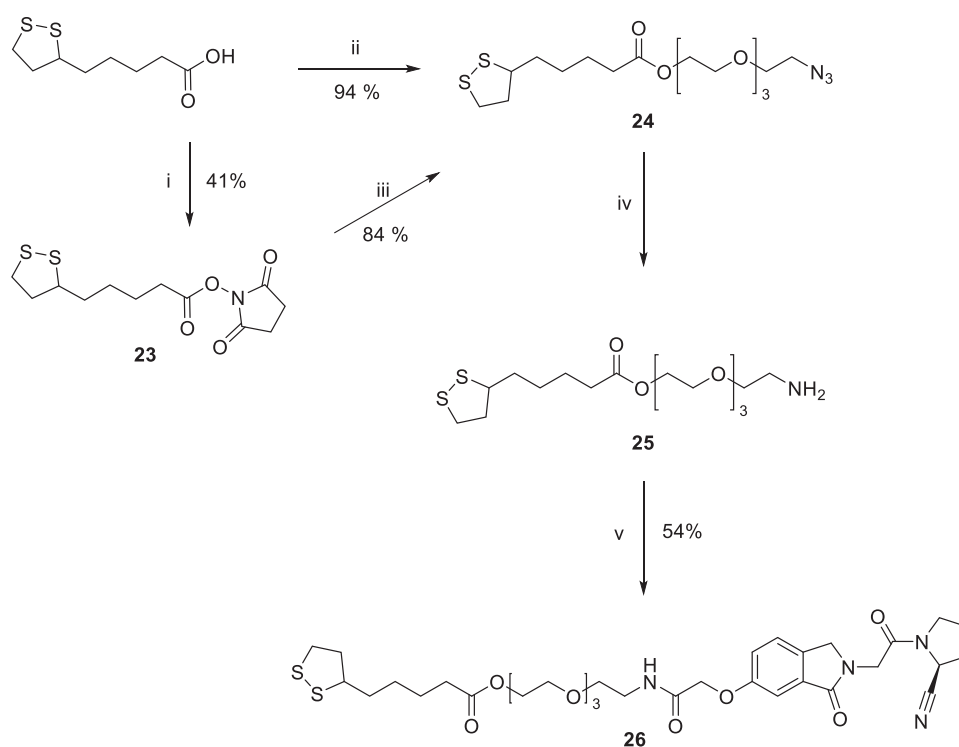
Subsequent experiments revealed a very low solubility of compound **17** in aqueous solutions which was a major limitation for further conjugation to the hydrogel structure during MS formation. Therefore, a hydrophilic spacer was introduced as depicted in Scheme 6.

Monotosylation of tetra(ethylene glycol) (TEG) was followed by the substitution of the tosyl group with sodium azide to afford intermediate **19** in good yield. Alternatively, TEG was subjected to ditosylation and substitution with sodium azide. The resulting diazide **21** was subjected to Staudinger reduction in biphasic medium to allow for mono-reduction and formation of derivative **22** in moderate yield.



Scheme 6: Synthesis of linkers derived from tetra(ethylene glycol). Reagents and conditions: i- NaOH, TsCl, 0°C to 23°C, 1 hr; ii- NaN_3 , 90°C, 7 hr; iii- TsCl, Et_3N , DMAP, 0°C to 23°C, 16 hr; iv- NaN_3 , 90°C, 16 hr; v- toluene, aq. HCl 5%, PPh_3 , 0°C to 23°C, 6 hr.

Lipoic acid was coupled to derivative **19**, either after activation in the form of N-hydroxysuccinimide (NHS) ester (**23**) or using HOBt/EDCI as coupling reagent. During the activation step, polymerization of the lipoyl moiety in the presence of NHS led to moderate yield of the activated intermediate. Better yield was obtained when performing direct esterification of lipoic acid. The azide was then reduced in presence of triphenylphosphine and HCl 5% to yield compound **25** which was kept in solution to avoid polymerization. Conjugation to FAP- α inhibitor **9** was achieved in the presence of TBTU/HOBt to provide the targeted derivative **26** in 54% yield.



Scheme 7 : Derivatization of FAP- α inhibitor with lipoic acid using TEG spacer. Reagents and conditions: i- NHS, DCC, 0°C to 23°C, 12 hr; ii- **19**, HOBT, EDCI, DIPEA, 23°C, 12 hr; iii- NEt_3 , 23°C, 12 hr; PPh₃, THF, aq. HCl 5%, 23°C, 17 hr.; v- TBTU, HOBT, DIPEA, **9**, 23°C, 16 hr.

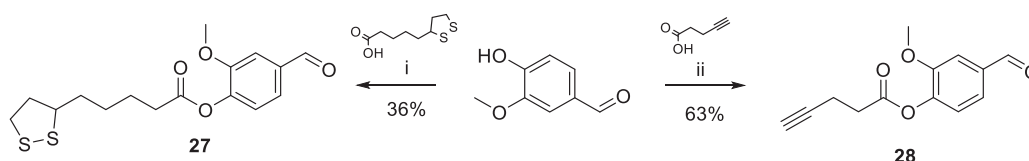
The investigation regarding conjugation of these FAP- α inhibitor derivatives on the structure of alginate-based hydrogels are not described here as they were not met with success and therefore discontinued.

3.1.2 Curcumin derivatives

Curcumin is known to exhibit several bioactivities including anti-inflammatory properties which have been associated with the inhibition of various inflammation pathways such as the protein COX-2.²⁰⁷ However, its potential is hindered by low solubility in aqueous media and rapid metabolism resulting in limited potency and poor absorption. Nevertheless, the potential of curcumin has been widely recognized and several derivatives (curcuminoids) have already been designed to address these limitations.^{211–213}

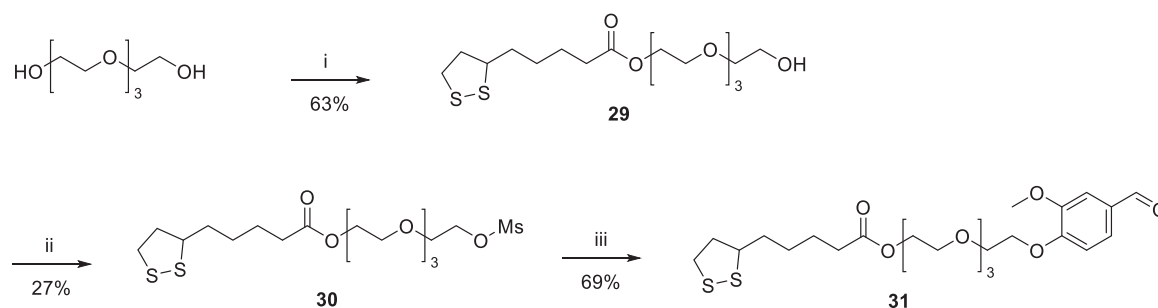
The initial attempts focusing on direct functionalization of the hydroxyl groups of curcumin by esterification were not met with success due to the formation of many side products, resulting in very low yield of the desired compounds. Therefore, an alternative strategy relying on the use of benzaldehyde derivatives such as vanillin as precursors for the formation of the 1,3-diketone moiety of curcumin was chosen.

The insertion of lipoyl and alkyne functions on vanillin was done by esterification on the hydroxyl group in presence of DMAP and DCC with lipoic acid and 4-pentynoic acid.



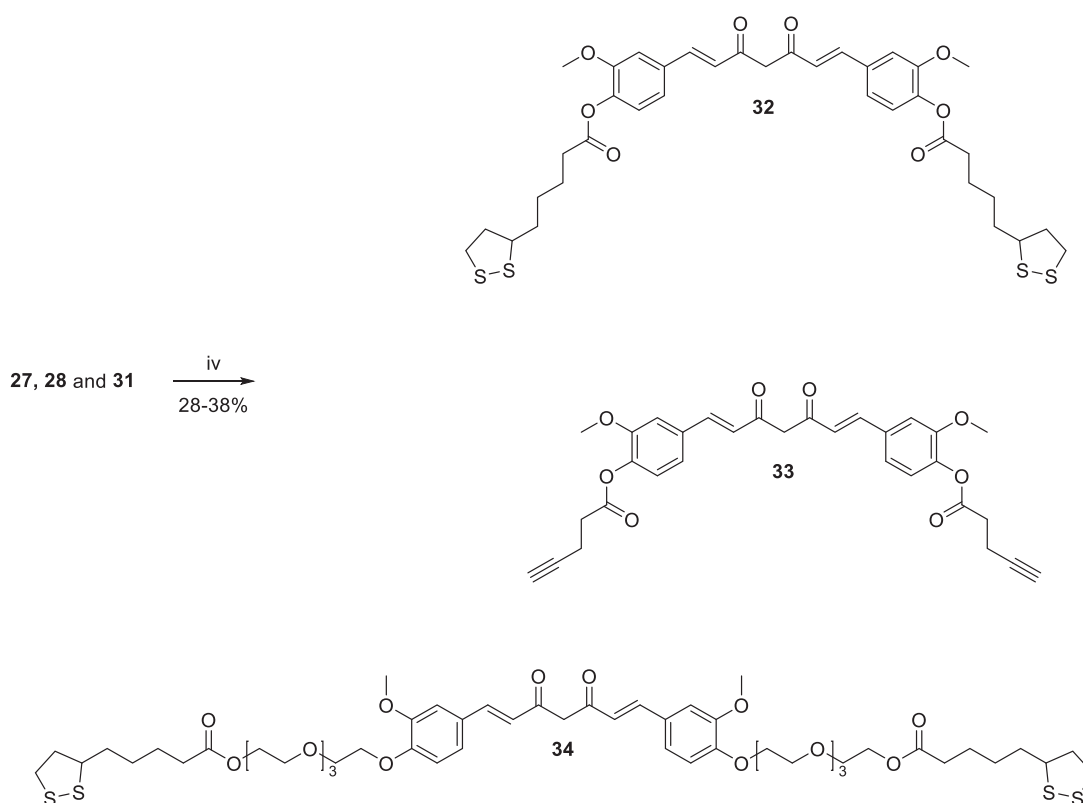
Scheme 8: Synthesis of vanillin derivatives. Reagents and conditions: *i*- DMAP, DCC, 23°C, 12 hr; *ii*- DMAP, DCC, 0°C to 23°C, 12 hr.

The introduction of a hydrophilic spacer was conducted by mono-esterification of TEG with lipoic acid, followed by activation of the remaining alcohol as a mesylate and nucleophilic substitution in the presence of vanillin. Only moderate yields were achieved throughout the sequence but the amount of material obtained was sufficient to perform the targeted conjugation assays.



Scheme 9: Synthesis of vanillin derivatives with TEG-L.A. linker. Reagents and conditions: *i*-lipoic acid, EDCI, DMAP, 10 hr; *ii*- MsCl, NEt₃, 0°C to 23°C 16 hr; *iii*- K₂CO₃, KI, 90°C, 12 hr.

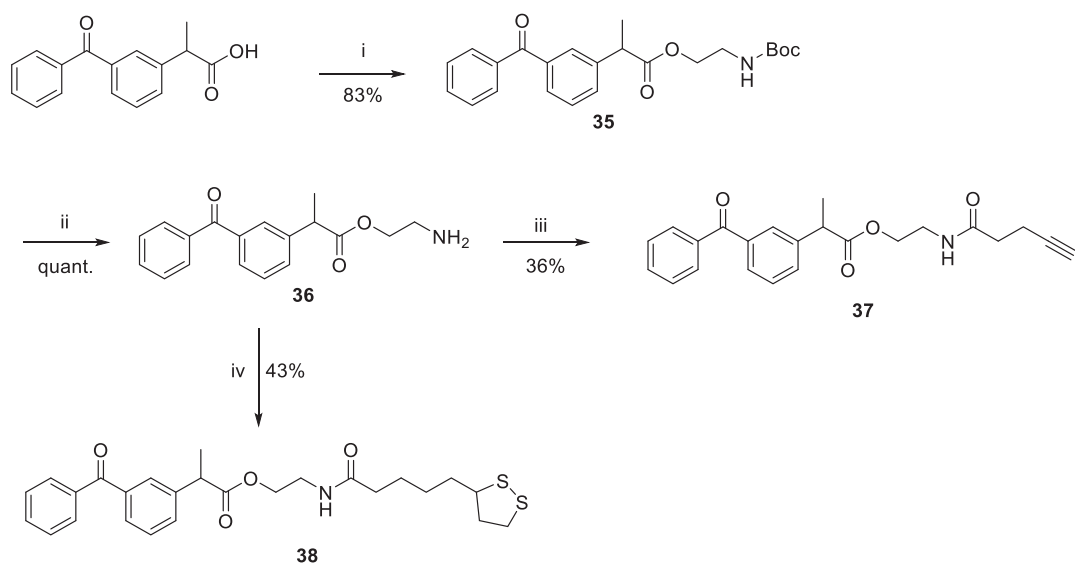
Two equivalents of the vanillin derivatives were then allowed to react in a double condensation reaction with acetylacetone in presence of boron oxide, tributyl borate n-butylamine affording the corresponding curcuminoids (**32**, **33** and **34**) in moderate yields (Scheme 10).



Scheme 10: Synthesis of curcuminoids. Reagents and conditions *i*- BO_3 , 2,4-pentanedione, 27 or 28 or 31, tributyl borate, *n*-butylamine, HCl (0.5 M) 80°C to 23°C , 3 hr.

3.1.3 Ketoprofen derivatives

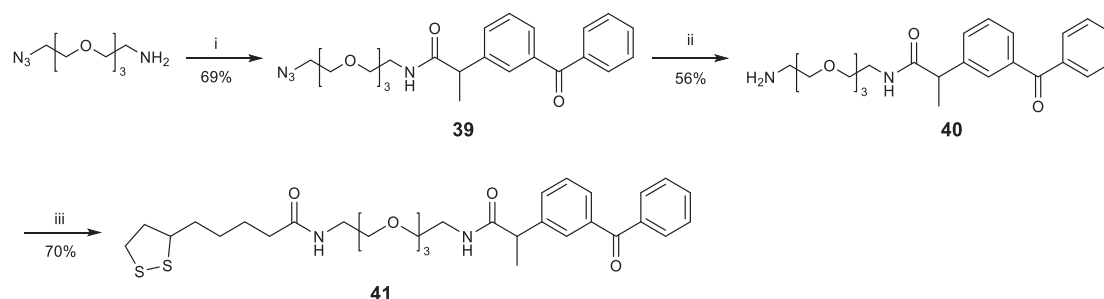
Ketoprofen is a widely used and studied nonsteroidal anti-inflammatory drug. As per curcumin, its anti-inflammatory propriety is associated with the inhibition of proteins COX-1 and COX-2.²⁰⁴ Derivatization of ketoprofen can easily be done using the reactivity of its carboxylic acid.



Scheme 11: Synthesis of ketoprofen derivatives. Reagents and conditions: *i*- *N*-Boc-ethanolamine, DMAP, DCC, 0°C to 23°C , 12 hr; *ii*- TFA, 23°C , 2 hr; *iii*- 4-pentynoic acid, HOBt, EDCI, DIPEA, 23°C , 12 hr; *iv*- lipoic acid, HOBt, EDCI, DIPEA, 23°C , 12 hr

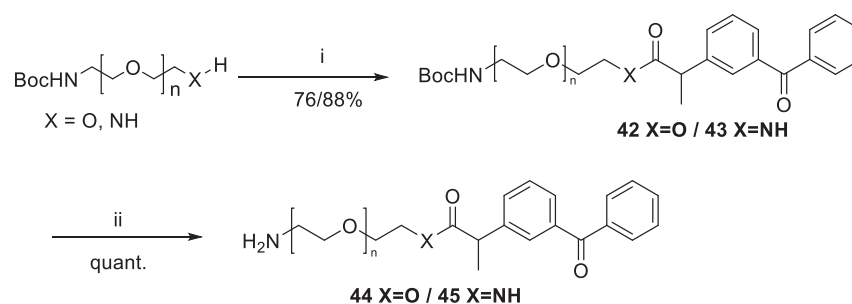
A small linker was introduced on the structure of ketoprofen by esterification with N-Boc-ethanolamine (**52**) in presence of DCC and DMAP yielding intermediate **35**. The amine was then deprotected in presence of trifluoroacetic acid and was allowed to react either with pentynoic acid or lipoic acid to afford the respective desired derivatives of ketoprofen in good yields (**37** and **38**).

To increase the solubility of the lipoyl containing derivative, ketoprofen was first coupled to TEG derivative (**22**), followed by Staudinger reduction of the terminal azide to provide intermediate **40** in 39% yield. The conjugation to lipoic acid through amide bond formation afforded KET-TEG-LA (**41**) in 70% yield.



Scheme 12: Synthesis of KET-TEG-LA. Reagents and conditions: *i*- ketoprofen, EDCI, HOBt, DIPEA, 23°C, 12 hr; *ii*- PPh₃, H₂O, 23°C, 12 hr; *iii*- lipoic acid, HOBt, EDCI, DIPEA, 23°C, 12 hr

The final strategy developed for the conjugation of ketoprofen to the backbone of alginate involved PEGylation of the drug for direct grafting on the hydroxyl groups of Na-alg. The PEGylation of ketoprofen was done starting from N-Boc mono-protected PEG2000 displaying either a free hydroxyl group or amine. The coupling on ketoprofen was achieved either by esterification on the hydroxyl or the formation of amide bond on the amine. The deprotection was done in acidic conditions yielding PEGylated ketoprofen with a free amine available for further conjugation on alginate backbone (section 3.4).



Scheme 13: Synthesis of PEGylated ketoprofen derivatives. Reagents and conditions: *i*- ketoprofen, [DCC, DMAP] or [HOBt, EDCI, DIPEA] 23°C, 12 hr; *ii*-HCl 4N, 23°C, 2 hr.

3.2 ANTI-FIBROTIC ACTIVITY AND BIOCOMPATIBILITY

The anti-fibrotic potential of the derivatives presented above was evaluated by quantification of different genes involved in fibrotic response, in myofibroblasts (collaboration with the group of Prof. Léo Bühler at the University Hospital in Geneva). Primary human fibroblasts were stimulated with the pro-fibrotic transforming growth factor beta 1 (TGF β 1) to differentiate into myofibroblasts, the effector cells of fibrosis. Only the derivatives of curcumin, ketoprofen and FAP-alpha inhibitor containing tetraethylene glycol (**26**, **34** and **41**) exhibited suitable solubility in aqueous media to perform this assay.

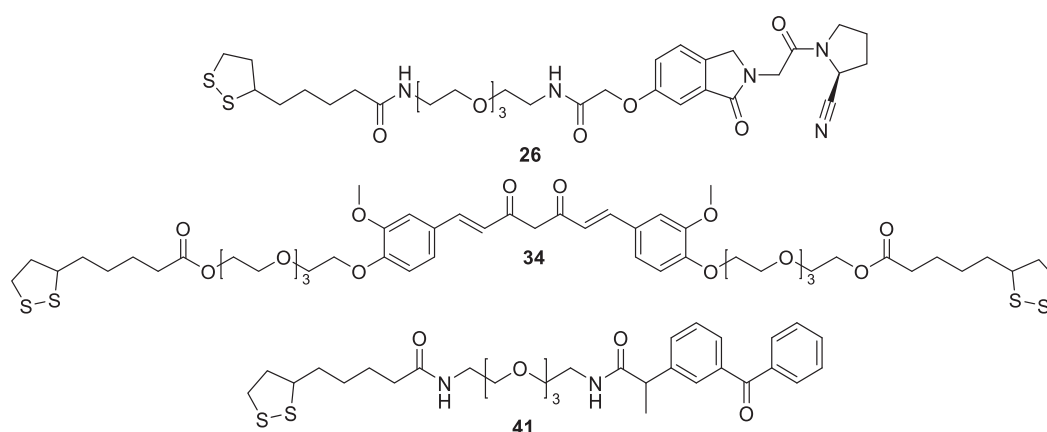


Figure 3.3: Structure of the drug derivatives used for the anti-fibrotic assay.

The mRNA expression of three genes was quantified by RT-PCR and normalized with respect to the expression of the gene RPL0 after incubation with different concentration of the anti-fibrotic derivatives for 24 hours. The expression of α -smooth muscle actin (α -SMA) which is a marker for myofibroblast highly increased in presence of TGF β 1. However, the two other monitored genes: alpha-1 type I collagen (COL1A1) and the matrix metalloproteinase-1 (MMP-1) remained unchanged.

Incubation with curcumin derivative at a concentration of 0.125, 0.25 and 0.5 mg/mL did not inhibit the expression of α -SMA which was only slightly reduced when incubated with a concentration of 1 mg/mL. COL1A1 expression was not affected but the expression of MMP1, which is an anti-fibrotic molecule, was notably reduced already with a concentration of 0.125 mg/mL. Hence the anti-fibrotic effect of the curcuminoid **34** was considered as not sufficient to expect a significant mitigation of fibrosis when covalently linked to the hydrogel.

On the other hand, good inhibition of α -SMA was observed when the primary human fibroblasts were incubated with the two other drugs derivatives. A concentration 0.5 mg/mL of compound **41** or 0.125 mg/mL of compound **26** was sufficient to observe significant inhibition of α -SMA. Moreover, a concentration of 0.5 mg/mL resulted in a small increased expression of MMP-1 associated with the inhibition of COL1A1 for both active compounds.

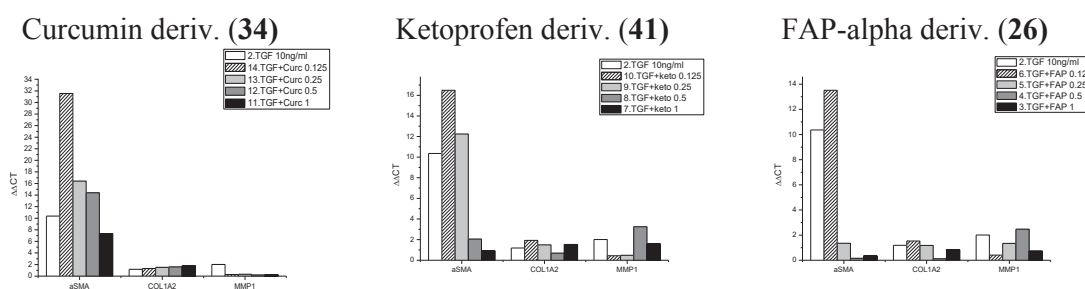


Figure 3.4: mRNA expressions of α -SMA, COL1A1 & MMP1 in presence of the drug derivatives 26, 34 and 41 ($n=3$).

The biocompatibility of these derivatives with encapsulated living material was confirmed monitoring the functionality of rats islets co-encapsulated in Ca-alg MS with the drug derivatives (26, 34 and 41). Islets and Na-alg solution (1000 IEq/mL of polymer solution) were mixed and extruded into a gelation bath containing CaCl_2 . The release of insulin from the resulting MS was then measured in different conditions (basal, stimulated in 16.7 mM glucose solution and stimulated with theophylline) and normalized with respect to the total amount of insulin (Figure 3.5). Non-encapsulated (free) islets were monitored as reference.

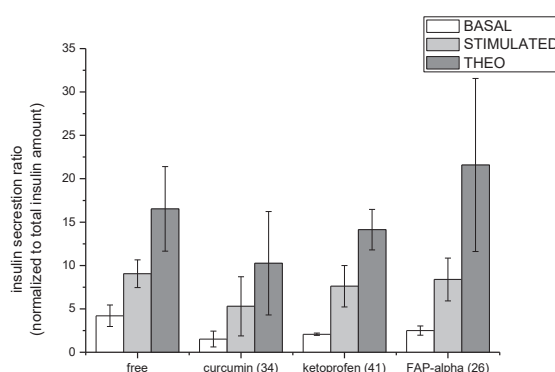


Figure 3.5: Insulin secretion of rats islet co-encapsulated in Ca-alg MS with compounds 26, 34 and 41 ($n=3$).

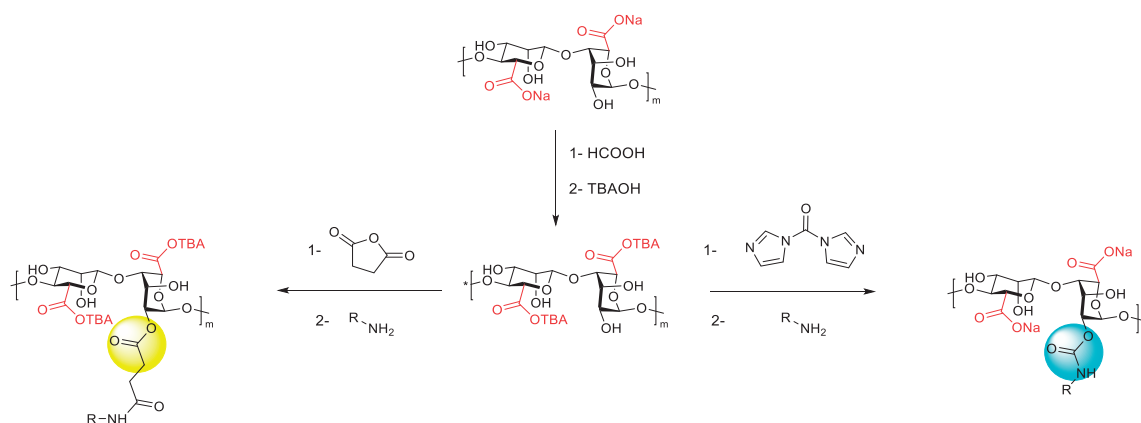
While when co-encapsulated with curcumin derivative (34) the functionality of the encapsulated islets was slightly reduced, the presence of the two other drug derivatives did not significantly affect islets functionality and thus their viability.

Among the three drug derivatives tested, FAP- α inhibitor derivative 26 and ketoprofen derivative 41 exhibited a superior anti-inflammatory potential. Nevertheless, the experiments focusing on the development of grafting methods of anti-fibrotic derivatives on the polymeric structure of the hydrogels (section 3.4) were performed predominantly on ketoprofen and curcumin derivatives which have the benefit of being already approved by the FDA and require less synthetical steps (better overall yield) when compared to the synthesis of FAP- α inhibitors derivatives.

3.3 ALGINATE DERIVATIVES FOR THE ENGINEERING OF HYDROGELS

As presented in section 1.4, Na-alg present excellent gelling properties in the presence of divalent cations and high cell compatibility. Na-alg thus appears as a perfect candidate for the development of new hybrid hydrogels. Hybrid hydrogels can either rise from a mixture of two polymers each bringing their contribution to the formation of physical and chemical interactions or by developing a polymeric structure possessing both properties. An interesting approach for the development of such system is thus the introduction of new functionalities capable to perform covalent crosslinking on the backbone of Na-alg. Different strategies were investigated to introduce new functionalities on the alginate backbone with the drive to produce one-component hybrid hydrogel presenting the ability to form rapid ionic interactions thanks to the properties of alginate and additional covalent bindings to reinforce the network. For this purpose, most existing strategies based their approach on the derivatization of the reactive carboxyl groups present on alginate.^{92,92,93,214–220} Although this approach allows direct derivatization of the polymer either via esterification or amide bond formation, each component added at this position prevents the carboxyl group to take part in the formation of physical hydrogel. In this scenario, high grafting degree (GD), representing the ratio of alginate units functionalized, is not practicable. To avoid this downside, alternative approaches were developed allowing selective derivatization of the hydroxyl groups present on the backbone of Na-alg which are not required for the formation of physical hydrogel. Consequently, functionalization at this position even with high GD should not affect the formation of physical hydrogel.

In our group, the first method allowing functionalization of the hydroxyl of alginate backbone in C3 and C2 positions of respectively the mannuronic and guluronic residues of alginate with the use of succinic anhydride was developed by Dr. F. Borcard. Na-alg was first converted into the corresponding tetrabutylammonium (TBA) salt to improve solubilization in organic solvents such as DMSO for further chemical transformations (Scheme 14). The hydroxyl groups of Na-alg were then allowed to react with succinic anhydride forming an ester bond and generating an easily accessible new carboxylic moiety available for further functionalization. The next step was amide bond formation in the presence of amine terminated heterobifunctional-PEG derivatives allowing the introduction of new reactive functionalities on the backbone of alginate available for covalent cross-binding.⁹¹ (Scheme 14 left)



Scheme 14 : Strategies developed for the functionalization of the hydroxyl moieties of Na-alg

Due to limitations arising from this method (see chapter 3.3.1), another approach was developed in our group, allowing the functionalization of the hydroxyl group of alginate using CDI chemistry. With this approach, hydroxyl groups are activated by the formation of imidazolide-alginate intermediate enabling the grafting of amine terminated heterobifunctional-PEG derivatives through a carbamate linkage.¹⁹⁷ (Scheme 14 right) The main advantage of this approach lies in the formation of a carbamate bond, more robust than ester bond formed when succinic anhydride was used to functionalized the hydroxyl group of alginate.

The evaluation of different hydrogels prepared by these two derivatization methods was done to define the optimal chemical composition in view of cell microencapsulation and potential for further incorporation of anti-fibrotic compounds (chapter 3.4). For this purpose, the mechanical properties of the resulting hydrogel along with their stability in different media were evaluated. The best candidates were finally evaluated for their biocompatibility *in vitro* and *in vivo*.

3.3.1 Alginate-PEG-(triazole)-SH

The first approach focused on the introduction of thiol moieties on Na-alg for the formation of disulfide bridge cross-linking during MS production. The thiol moieties were introduced on the alginate backbone via succinic anhydride chemistry followed by amide formation in the presence of heterobifunctional PEG 1000 and 2000 α -amine ω -thiol (PEG1000/2000-SH) (Figure 3.6). Depending of the reaction conditions, chemical modifications of Na-alg result in partial degradation of the polysaccharide backbone which affect the viscosity of the resulting polymeric solutions. Therefore, the formation of well-shaped MS requires to adjust the concentration of precursor solutions to reach viscosity range compatible with the extrusion setup used for MS production (50 to 600 mPa·s).

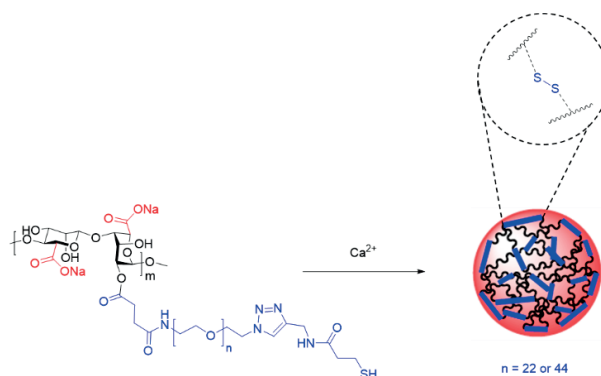


Figure 3.6 : Alg-PEG-SH derivative and hybrid hydrogel microsphere formation

First, the alginate derivative with thiol-terminated PEG 1000 (alg-PEG1000-SH) with a GD of 2.2% (determined by ¹H NMR) was evaluated. To produce the MS, solutions of the polymer (2 and 2.5 wt. %) in 3-(N-morpholino) propanesulfonic acid (MOPS) (10 mM, pH = 7.4) with a viscosity of respectively 191 and 310.5 mPa·s were extruded into a gelation bath containing CaCl₂ (100 mM).

Both polymer solutions led to the formation of MS which appeared to be much more opaque than MS formed from similar systems which do not contain a triazole moieties on the PEG grafting units (Figure 3.7).⁹¹

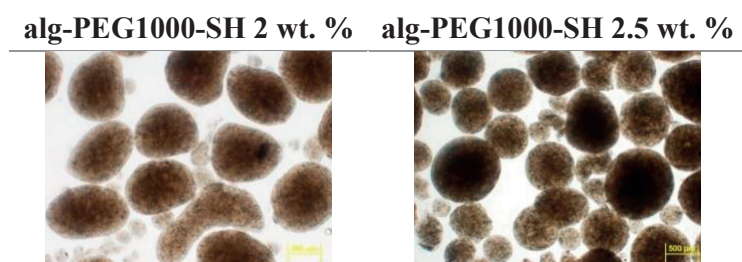


Figure 3.7: Microspheres produced from alg-PEG1000-SH (GD=2.2%)

The size of the MS measured at day 1 and day 7 following the extrusion revealed substantial shrinking of the MS over one week in the gelation bath (Table 3). This suggests that the density of the hydrogel matrix increases after MS formation due to the slow formation of the covalent bonds (disulfide bridges).

Table 3: Sizes of microspheres alg-PEG 1000 2.2% [μm] ($n=10$).

	Alg-PEG 1000 2%	Alg-PEG 1000 2.5%
Day 1	943.8 \pm 92.9	802.1 \pm 164.6
Day 7	464.8 \pm 44.6	451.1 \pm 68.2

The mechanical resistance properties of the MS were evaluated with a texture analyzer (Figure 3.9). The maximal resistance for one compression at 90% of the initial size reached 12.6 and 15.5 [N/mm^3] for the MS formed from respectively the solutions at 2 and 2.5 wt. % of the alg-PEG1000-SH derivative. For comparison, MS formed from unmodified Na-alg (3 wt%) displayed a mechanical resistance of 2.4 [N/mm^3]. In addition, the resistance response occurs early in the compression curve, which supports the idea that the hydrogel possesses a dense network. Repetitive compressions at 90% of the initial size (Figure 3.9 top right) shows that despite their high density, the MS present outstanding elastic properties. After 10 compressions, the shape recovery still exceeds 60%.

The stability of the hydrogel network was assessed by qualitative analysis of the resistance of the ionic and covalent interactions. The MS were placed either in tris(2-carboxyethyl) phosphine hydrochloride (TCEP) (0.5 M) to reduce disulfide bridges or in sodium citrate solutions (100 mM) which have the ability to replace the calcium ions and dissolve the physical hydrogel. The MS formed from alg-PEG1000-SH demonstrated good stability in TCEP but dissolved in sodium citrate. This observation was associated with the hypothesis that the amount of thiol grafted on alginate (GD = 2.2%) was not sufficient to maintain the network of the MS without ionotropic crosslinking; thus studies with alginate derivatives presenting higher GD were performed.

Alg-PEG 1000 and 2000 with respective GD of 6.7 and 5.7 % were produced. MS were formed from the extrusion of polymer solutions at different concentrations in MOPS (Figure 3.8). Due to the high viscosity and low homogeneity of alg-PEG2000-SH solutions, the extrusion protocol resulted in non-spherical massive pieces of hydrogel instead of round-shaped hydrogel (Figure 3.8).

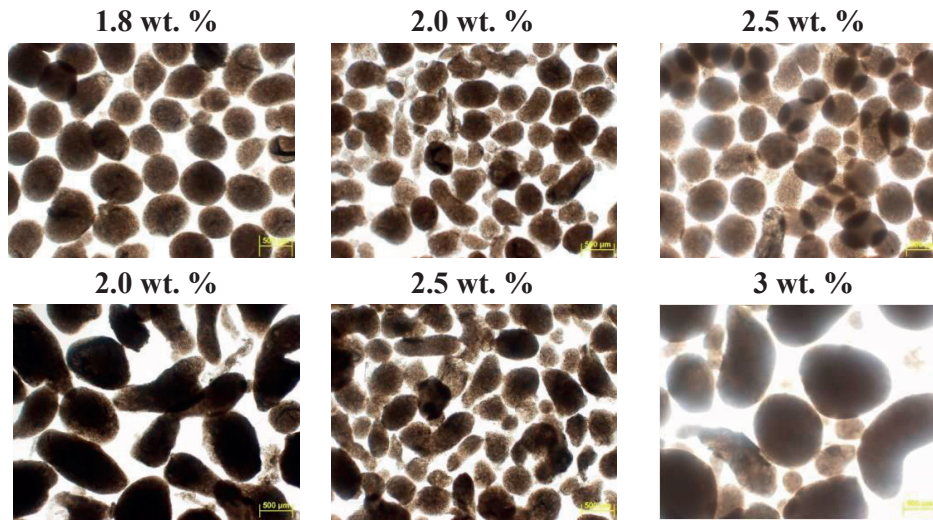


Figure 3.8: Microspheres formed from alg-PEG1000-SH 6.7% (top) and alg-PEG2000-SH 5.7% (bottom)

The opacity of both alg-PEG1000-SH and alg-PEG2000-SH MS indicate again a dense configuration of the hydrogel matrix. In addition, only alg-PEG2000-SH at 1.8 wt.% resulted in spherical shapes. The size of the MS measured 1 and 7 days after their formation (Table 4) were similar. The fact that these MS did not shrink (unlike to the ones with a lower GD) can be associated with a higher congestion of polymers within the hydrogel rising from the presence of additional PEGs chain due to the higher GD.

Table 4: Microspheres size [μm] and viscosity of alg-PEG1000-SH and alg-PEG2000-SH solutions ($n=10$).

	PEG 1000 1.8 wt. %	PEG 1000 2 wt. %	PEG 1000 2.5 wt. %	PEG 2000 2.5 wt. %
day 1	621.0 \pm 90.8	502.3 \pm 85.1	578.9 \pm 71.3	563.6 \pm 74.2
day 7	618.9 \pm 90.8	467.8 \pm 85.1	520.3 \pm 80.6	565.9 \pm 103.7
Viscosity	312.1 mPa·s	301.1 mPa·s	1839 mPa·s	959.9 mPa·s

Interestingly, the resistance of the MS was lower than the one measured for the MS with lower degree of grafting. It reached 6 [N/mm^3] for alg-PEG1000-SH and 4.4 [N/mm^3] for alg-PEG2000-SH. Both are still more resistant than pure Ca-alg hydrogel.

The measure of repetitive compressions revealed also larger decrease of the relative resistance over the cycles of compression. The MS are weakening after several compression to stabilize around 40 % of their initial resistance. No notable difference was observed between the alg-PEG1000-SH and alg-PEG2000-SH within the same concentration. Unfortunately, despite the higher grafting degree of heterobifunctional PEG thiol terminated, these MS were still unstable in sodium citrate solution.

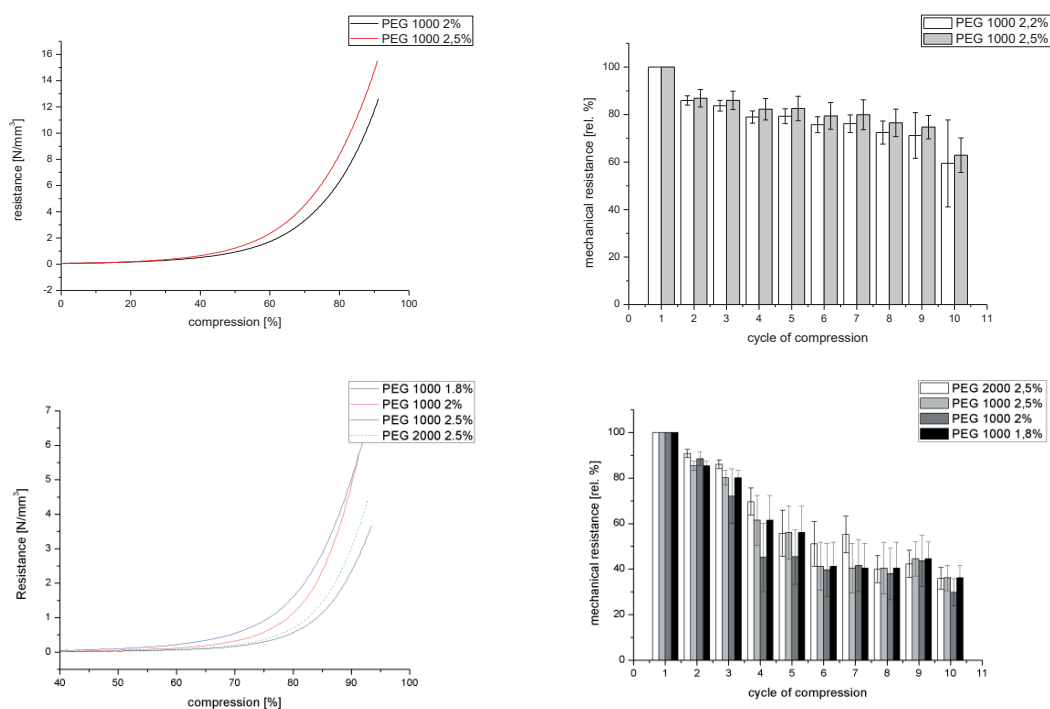


Figure 3.9: Mechanical resistance of microspheres prepared from Na-alg-PEG-SH. Low grafting degree (top); high grafting degree (bottom). Single compression to 90% of the initial size (left); repetitive compression (right) ($n=10$).

Finally, transplantation of MS produced from alg-PEG1000-SH (GD 6.7%; 1.8 wt.%) resulted in the dissolution of the hydrogel within 15 days. We hypothesized that the ester linkage used for the conjugation to the alginate backbone was labile in vivo. Further studies were thus performed on alginate derivatives presenting a carbamate linkage as grafting functionality (see Scheme 14, right).

Since MS of high opacity were only observed when formed with PEGylated alginate derivatives displaying 1,2,3-triazole moiety, it was envisaged that this chemical motif was responsible for this characteristic. A potential explanation of this observation is the formation of hydrogen bonds with the triazole moieties as illustrated in Figure 3.10 which could explain the formation of an opaque hydrogel structure.²²¹

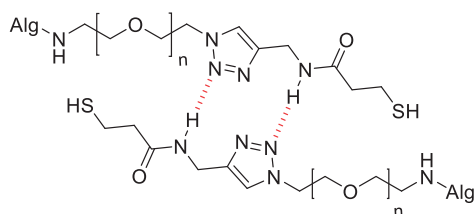


Figure 3.10: Hydrogen bonding between triazole groups present on PEG derivatives

Although these hydrogen bonding interactions may strengthen the hydrogel network, their formation is not well controlled and could already occur in the polymer solution, before contact with the gelation bath, resulting in non-homogeneous solutions and compromising the integrity of the resulting MS. Moreover, these interactions also reduce the flexibility of the PEG-SH

extremities, which may compromise the formation of the desired disulfide bridges. Most importantly, the main purpose of hybrid hydrogel which is to combine ionic and covalent binding is lost in this case. To avoid this scenario, alginate derivatives containing linear PEGs (exempt of triazole) were evaluated.

3.3.2 Alg-PEG-SH and Alg-PEG-LA derivatives containing linear PEGs

The next systems focused on alginate derivatives containing thiol or 1,2-dithiolane functionalities for the formation of simple disulfide bridges or disulfide clusters, respectively (Figure 3.11).^{222,223}

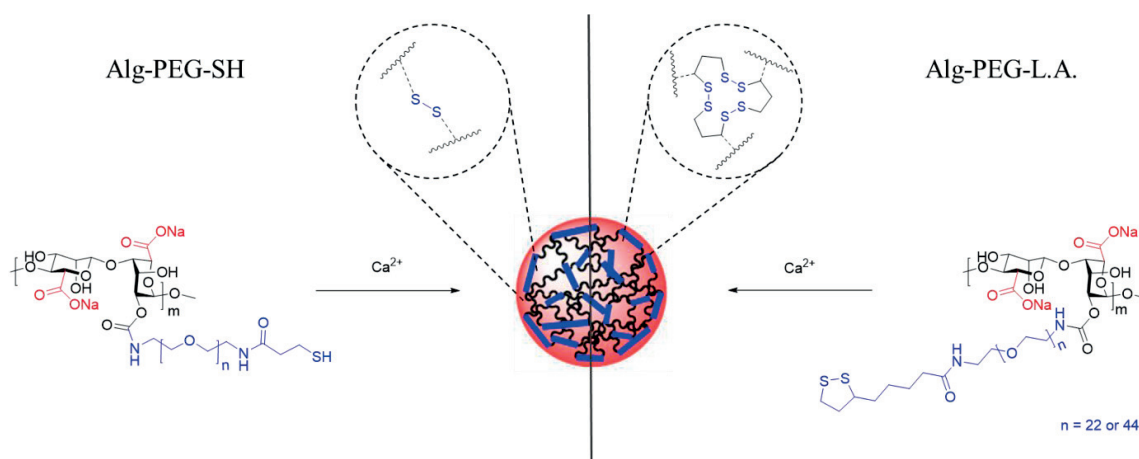


Figure 3.11: MS formation from alg-PEG-SH or alg-PEG-LA with carbamate grafting unit

The synthesis procedure depicted in Scheme 14 allowed the formation of alg-PEG1000-SH with several GD: 5.90%, 7.05%, 8.07% and 12.9%. MS were produced by extrusion of a 3 wt. % solution of the polymers (MOPS 10 mM, pH 7.4) into a gelation bath containing CaCl₂ (Figure 3.12). As expected, the opacity which was previously observed in the presence of triazole moieties, was largely reduced, supporting the hypothesis that hydrogen bonding interactions were responsible for this opacity.

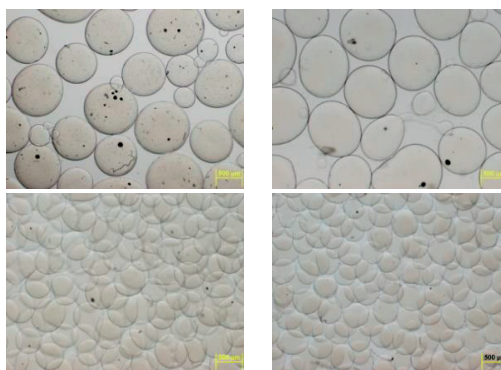


Figure 3.12: Microspheres from alg-PEG1000-SH 5.90% (top left) 7.05% (top right), 8.07% (bottom left), 12.9% (bottom right)

As the viscosity of the polymer solution decreased with the increase of the GD, we observed a clear dependence of the size and shape of the resulting MS on the value of the GD (Table 5). The shape and the size of the MS were highly dependent on the GD of the polymer. Interestingly, the size of these MS did not significantly evolve over 7 days in the gelation bath.

Table 5: Size of MS [μm] produced from alg-PEG1000-SH at day 1 and day 8 and viscosity of the polymer solution with respect to the degree of grafting ($n=10$).

Degree of grafting	5.9 %	7.05 %	8.07 %	12.9 %
Day 1	934.00 \pm 100.81	909.00 \pm 111.09	532.90 \pm 55.06	491.37 \pm 31.95
Day 8	913.07 \pm 105.56	940.89 \pm 122.89	540.50 \pm 46.42	468.47 \pm 34.32
Viscosity (3 w. %)	209.0 mPa·s	121.6 mPa·s	64.57 mPa·s	42.62 mPa·s

A drastic decrease of mechanical resistance and shape recovery was observed with the increase of grafting degree (annexes Figure 6.2). This singularity has been associated with a structural deformation of the hydrogel network caused by the increase of PEG chains within the hydrogel.

In light of the above, batches of alginate derivatives functionalized with thiol and lipoyl moieties through PEG1000 and 2000 spacers were prepared and evaluated (Table 6). The results concerning the synthesis and the evaluation of these polymers were published in “Synthesis Strategies to Extend the Variety of Alginate-Based Hybrid Hydrogels for Cell Microencapsulation” *Biomacromolecules* **2017**.¹⁹⁷

Table 6: Characteristics of alg-PEG derivatives wt. % in MOPS

Product	Viscosity (mPa·s)	Degree of grafting [%]
Alg-PEG1000-SH (3 wt. %)	209	5.2
Alg-PEG1000-LA (3 wt. %)	161	6.7
Alg-PEG2000-SH (4 wt. %)	53	13.0
Alg-PEG2000-LA (4 wt. %)	161	21.0
Na-alg (3 wt %)	245	-
Na-alg (4 wt %)	586	-

In view of the viscosity of the polymer solutions, the initial concentration was adjusted to produce well-shaped MS (3 wt. % for alg-PEG1000 derivatives and 4 wt. % for alg-PEG2000 derivatives). Two solutions of Na-alg (3 and 4 wt. %) were also characterized and used for the formation of Ca-alg MS, for comparison. Both alginate derivatives (thiol and 1,2-dithiolane) functionalized with the smaller PEG chain (PEG 1000) exhibited an increase of resistance when compressed at 90% of their initial size when compared to pure Ca-alg beads prepared from a 3 wt. %. Resistance values of 3 and 5 N/mm³ were measured for respectively alg-PEG1000-SH and alg-PEG1000-LA MS while Ca-alg MS was measured at 2.4 N/mm³. However, the alginate derivatives functionalized with longer PEG chain (PEG 2000) exhibited less resistance displaying only 1.2 and 2 N/mm³ for alg-PEG2000-SH and alg-PEG2000-LA MS, which is below the resistance of Ca-alg MS prepared from a 4 wt. % solution (2.6 N/mm³). Nevertheless, shape recovery performance upon repeated compression to 90% of the initial diameter exhibited great improvement with respect to Ca-alg MS for both length of PEG and both functionalities grafted on the alginate backbone (Figure 3.13).

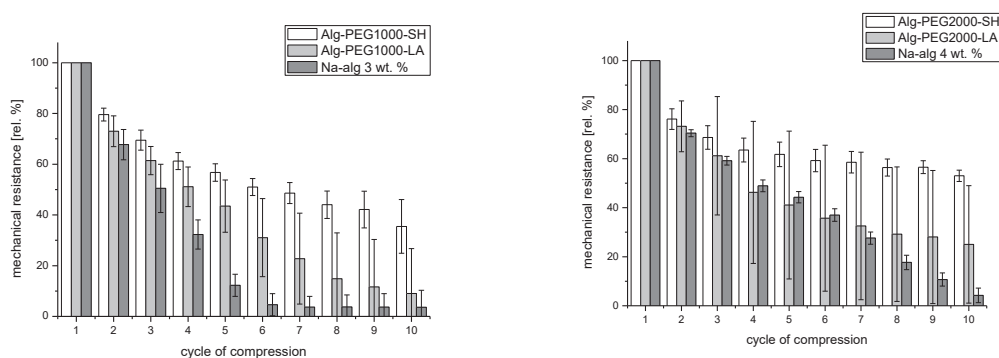


Figure 3.13: Shape recovery after 10 successive compressions to 90% of the initial diameter of alg-PEG1000-SH/LA, alg-PEG2000-SH/LA and Ca-alg MS ($n=10$).

When compared to Ca-alg MS, the improvement of the shape recovery performance was more pronounced for thiol-containing derivatives than for 1,2-dithiolane derivatives. While the elasticity seemed to be slightly enhanced in the presence of the longer PEG derivatives, we decided to investigate alg-PEG1000-SH/LA MS for cell microencapsulation, as their mechanical resistance was superior.

Mouse insulinoma cells MIN6 were used as model cells. The MIN6 cells were mixed in the polymers solution and extruded in a gelation bath containing CaCl_2 producing monodisperse MS with homogenous cell distribution. The MS were kept in cell culture medium for the subsequent analyses.

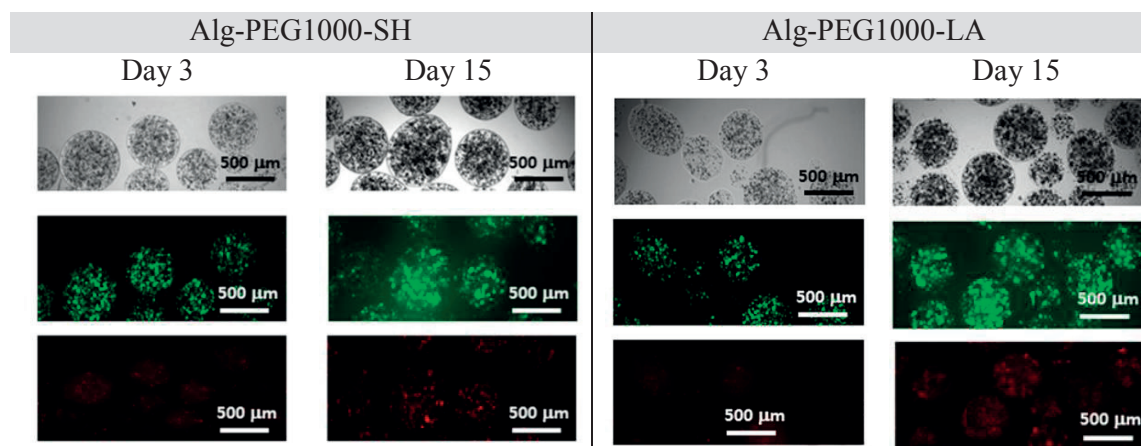


Figure 3.14: Microscopy image of MIN6 cells encapsulated in alg-PEG1000-SH and alg-PEG1000-LA at day 1 and day 15. Top panel: light microscopy, middle panel: staining of live cells with FDA (green), bottom panel: staining of dead cells with PI (red). “Reprinted (adapted) with permission from *Synthesis Strategies to Extend the Variety of Alginate-Based Hybrid Hydrogels for Cell Microencapsulation. Biomacromolecules*. Copyright 2017.”

Cell viability was assessed by fluorescein diacetate and propidium iodide (FDA/PI) staining according to the protocol established by Jones et al.²²⁴ 3, 10 and 15 days after encapsulation. While MIN6 cells viability at day 3 post-encapsulation was close to 100%, a decrease was observed after one week but stabilized around 70% viability from day 7 post-transplantation. This behavior is often observed for the encapsulation of cells in hydrogel matrices. After a decrease in viability over the first days post-encapsulation, a stabilization is then generally

observed as cells seem to adapt to their new environment on a longer time scale. Therefore, over this time period, the chemical composition of the hydrogels did not induce cytotoxicity.

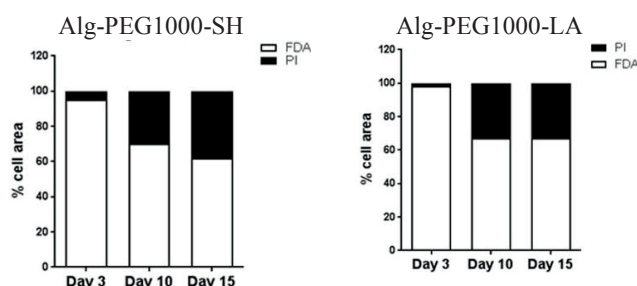


Figure 3.15: Quantification of viable and non-viable encapsulated MIN6 cells by FDI/PI staining at day 3, 10 and 15 expressed as % of the total cell area ($n = 6$). “Reprinted (adapted) with permission from Synthesis Strategies to Extend the Variety of Alginate-Based Hybrid Hydrogels for Cell Microencapsulation. Biomacromolecules. Copyright 2017.”

Interestingly, it was observed that the integrity of the MS depended on the nature of the chemical functionality used for covalent cross-linking. While alg-PEG1000-SH MS remained intact over 15 days, alg-PEG1000-LA MS showed some dissolution in vitro after 10 days (Figure 3.16). This was confirmed by observation under light-microscopy, which revealed out-diffusion of cells and translucent MS.

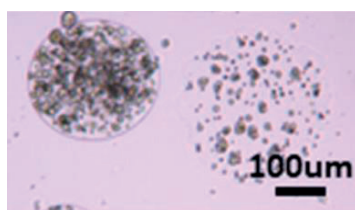


Figure 3.16: Light-microscopy image of MIN6 cells encapsulated in alg-PEG1000-LA at day 10. “Reprinted (adapted) with permission from Synthesis Strategies to Extend the Variety of Alginate-Based Hybrid Hydrogels for Cell Microencapsulation. Biomacromolecules. Copyright 2017.”

This observation indicates that disulfide cluster cross-linking is less stable in culture conditions than disulfide bridge cross-linking. Even though this characteristic is disadvantageous when considering cell encapsulation for long term cell therapy as it could lead to an acute rejection to the graft and hyper-immunization of the host which could impact on his chances for a subsequent transplants, some applications could benefit from the dissolution of the hydrogel and the research toward the development of alg-PEG-LA MS was continued.

To assess the compatibility of these polymers in vivo, cell free MS were transplanted into the peritoneal cavity of immune-competent mice and were retrieved after 30 days. Interestingly both hydrogels were stable and retrievable. Moreover, the MS exhibited no sign of fibrosis which indicate good biocompatibility of the material with the host.

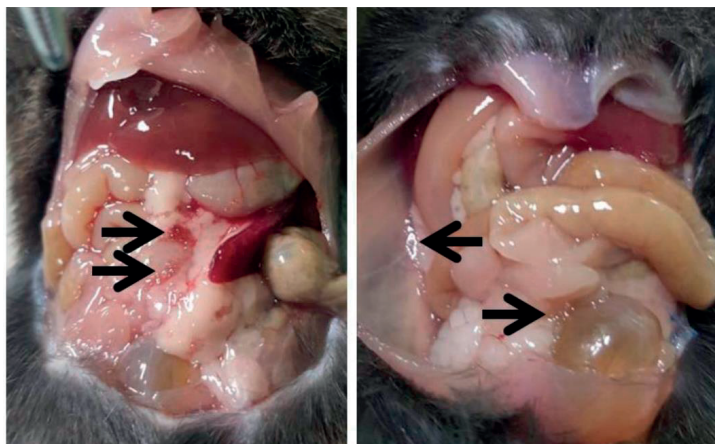


Figure 3.17: Macroscopic inspection at 30 days after intraperitoneal transplantation. Some MS are indicated by arrows. "Reprinted (adapted) with permission from Synthesis Strategies to Extend the Variety of Alginate-Based Hybrid Hydrogels for Cell Microencapsulation. Biomacromolecules. Copyright 2017."

In summary, new alginate derivatives were obtained by functionalization of the hydroxyl groups of Na-alg with heterobifunctional PEG derivatives through carbamate linkage. The MS obtained with these derivatives presented improved mechanical properties when compared to pure Ca-alg MS, in particular for shape recovery following multiple compressions. The nature of the functionality added on the biopolymer had a direct influence on the physical properties of the resulting MS, and also impacts their stability in different environments. The unexpected stability of alg-PEG-LA MS in the *in vivo* experiment may be due to the environment (pH and solutes) of the intraperitoneal site which provides suitable conditions for the stability of disulfide clusters whereas the encapsulation of MIN6 cells *in vitro* lead to dissolution of the same MS. A superior elasticity was observed for the derivatives with thiol moieties than with 1,2-dithiolane moieties. Moreover, MS displaying disulfide bridge covalent cross-linking present higher durability in culture medium than MS with disulfide clusters. Finally good biocompatibility was observed for both polymers with the encapsulated material and the host.

3.4 CONJUGATION OF ANTI-INFLAMMATORY COMPOUNDS TO ALGINATE-BASED HYDROGELS

Different strategies were considered for the grafting of the anti-inflammatory compounds on the backbone of alginate derivatives with respect to their structure. As exposed before, the strategies involving lipoyl and maleimide moieties were developed for the conjugation of the drugs during formation of the microspheres whereas alkyne and amine moieties were introduced on the drug structures in view of grafting on the alginate before hydrogel formation. To control the conjugation of the anti-fibrotic compounds during hydrogel formation, the following approaches focused on the derivatives displaying lipoyl moieties and alg-PEG-LA.

3.4.1 Conjugation through disulfide cluster formation

As depicted in Figure 3.18, the first approach involved the combination alginate derivatives and drug derivatives, both functionalized with 1,2-dithiolane moieties, during MS formation. Taking advantage of the fluorescent properties of curcuminoids, derivative **34** (see Scheme 10) was selected for the conjugation assay.

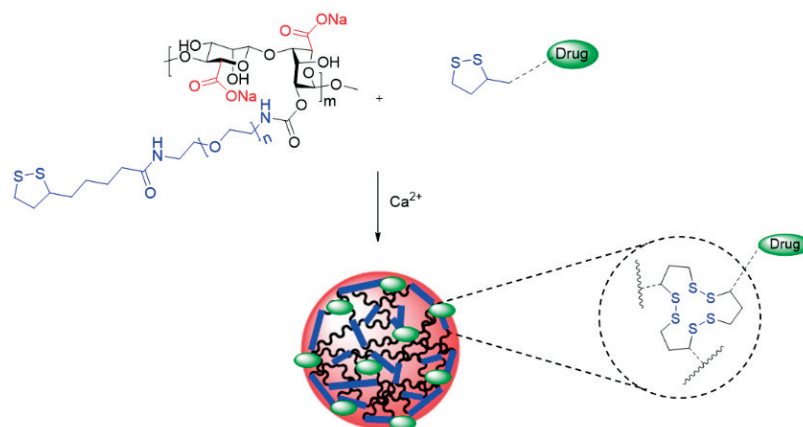


Figure 3.18: Conjugation of anti-inflammatory compounds displaying lipoyl moiety on the structure of hydrogel through formation of disulfide clusters.

To monitor the fluorescence of the curcuminoid core, the excitation and emission spectra of compound **34** in MOPS buffer were recorded at different concentrations on an *infinite 200 PRO* TECAN multiplate reader.

The excitation band of derivative **34** was remarkably wide and not very well-shaped. Nonetheless, the difference between the excitation and the emission bands was sufficient to allow monitoring by fluorescence. Moreover, optimization of the parameters allowed the detection of fluorescence at low concentration (around 4.56 nM) (Figure 3.19).

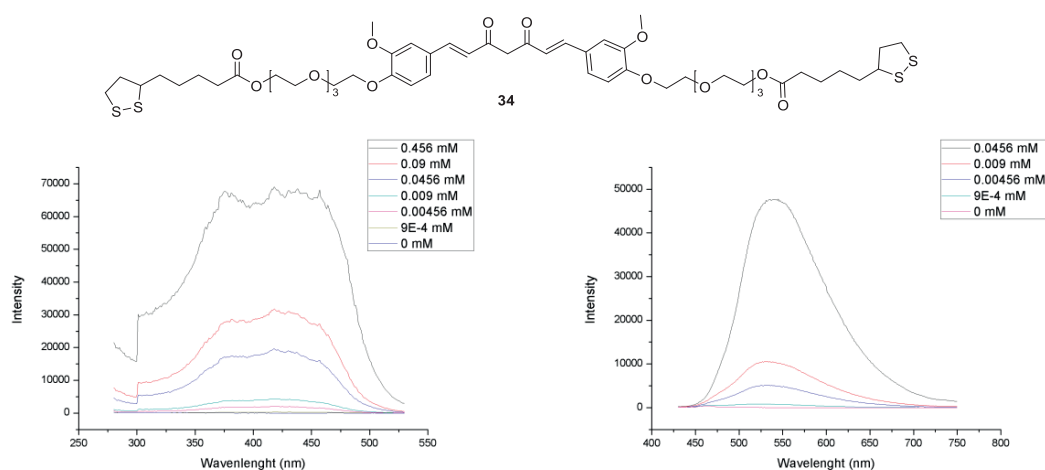


Figure 3.19: Excitation (left) and fluorescent emission (right) spectra of compound 34 for the indicated concentration in MOPS solution 10 mM.

MS were prepared by extruding a solution of alg-PEG2000-LA (4 wt. % in MOPS 10 mM) containing derivative 34 (1 mg/mL), into a gelation bath containing CaCl_2 . Since dithiothreitol (DTT) has been reported to favor disulfide cluster formation, the same experiment was repeated in the presence of DTT (0.5 eq. relative to the PEG chains). The same procedure was done in parallel with Na-alg (2 wt. %, without DTT).

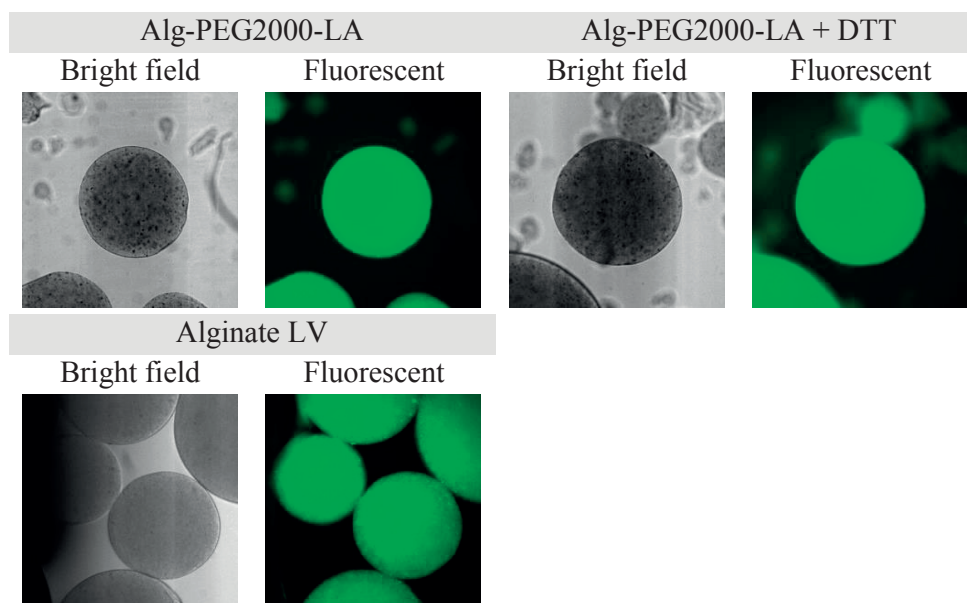


Figure 3.20: Microspheres prepared in presence of curcuminoid 34 under bright field and fluorescence microscopy: excitation CFP (436/12) emission YFP (500/20)

The MS exhibited a good morphology and were imaged by fluorescence microscopy on a LEICA DMI6000 B with CFP/YFP filters corresponding to the excitation and emission bands previously measured (Figure 3.20). All MS samples (1 mL of MS in 3 mL of MOPS solution) were monitored over a period of 25 days. At specific time points, both the supernatant and the MS were analyzed by fluorescence microscopy (Figure 3.21).

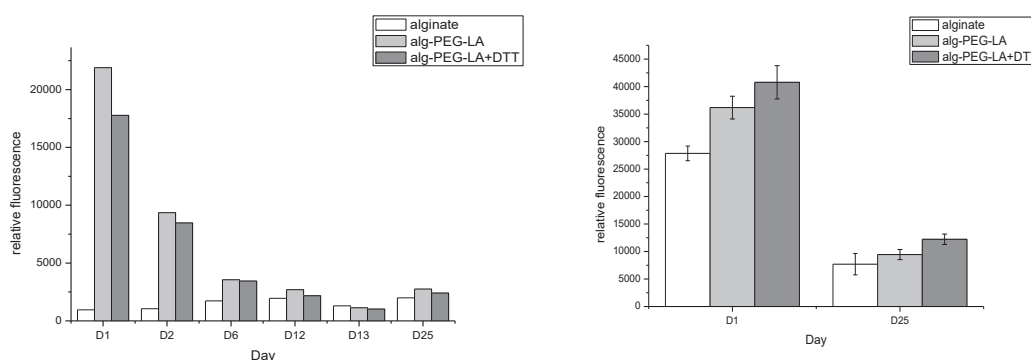


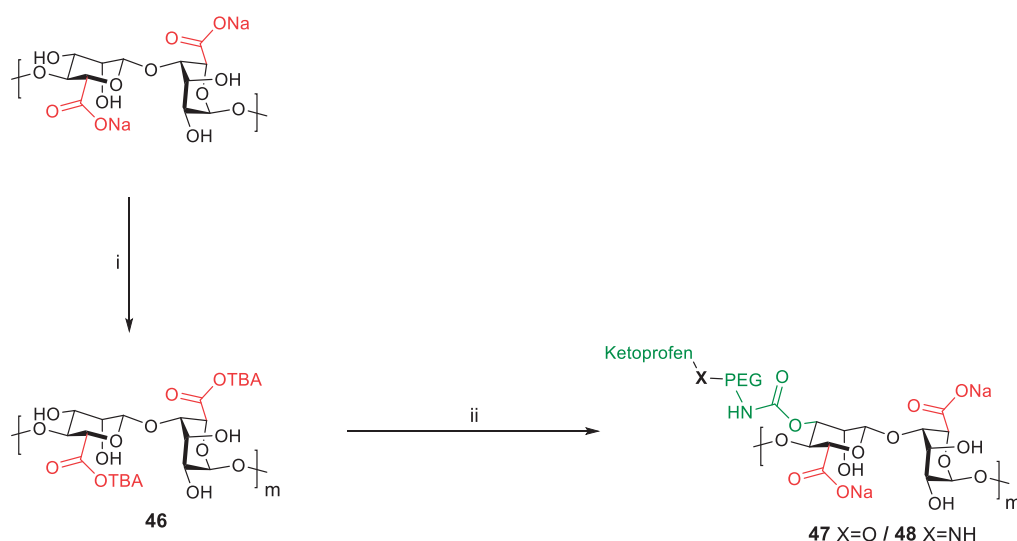
Figure 3.21: Fluorescence of the supernatant (left). Fluorescence of the microspheres (right).

As shown in Figure 3.21, the amount of curcuminoid released from alg-PEG2000-LA MS over the first two days was much higher than the release from Ca-alg MS. The presence of DTT during MS formation reduces slightly the release of compound **34**, which is an indication of the beneficial effect of DTT regarding the formation of disulfide clusters. Nevertheless, experiments reproduced with unmodified curcumin (without lipoyl moieties) exhibited similar release behaviors which does not support evidence of formation of disulfide clusters including the drug (annexes Figure 6.4). Moreover the measure of fluorescence of the microsphere by microscopy did not show a different behavior over the timespan of the experiment. Similar decrease of fluorescence was observed for all the MS over 25 days.

Since monitoring of the release of curcuminoid **34** by fluorescence did not provide direct evidence of the grafting of the drug on the structure of the hydrogel, subsequent investigations were focused on alternative strategies providing direct evidence of conjugation to the polymer prior the formation of the hydrogel.

3.5 GRAFTING OF PEGYLATED KETOPROFEN ON ALGINATE

The last conjugation approach focused on the grafting of PEGylated anti-inflammatory drugs (in particular, ketoprofen) to the alginate backbone prior to MS formation. Na-alg was first treated with formic acid to form the carboxylic acid which was then deprotonated in presence of TBAOH yielding TBA-alg (**46**). TBA-alg was then solubilized in DMSO, treated with 1,1'-carbodiimidazole (CDI) and reacted with either PEG-ester-KET (**44**) or PEG-amide-KET (**45**) to yield the corresponding functionalized alginate derivatives which were then purified by dialysis.



Scheme 15: Synthesis of alginate derivative with PEGylated ketoprofen (ester/amide). Reagents and conditions: i- HCOOH, TBAOH; ii-1) CDI, DMSO, 30 min, 2) 44 or 45, H₂O, 23°C, 2 hr.

The grafting degrees of alg-PEG-(ester/amide)-KET (**47** and **48**) were evaluated by deconvolution method of ¹H-NMR spectra. Different grafting degrees were obtained by varying the equivalence of the PEGylated ketoprofen. A GD of 7% was obtained with 0.1 eq. and a GD up to 20% with 0.2 eq. of the PEGylated drug. Direct confirmation of the covalent conjugation of PEGylated ketoprofen on the backbone of alginate was obtained by Diffusion Ordered Spectroscopy (DOSY) NMR. This method measures the relaxation time of the protons which is associated with the diffusion of the molecules. Since the diffusion itself depends on the sizes of the molecules, it is possible to differentiate the protons of molecules of different sizes. The characteristic peak of PEGylated ketoprofen (not grafted) and alg-PEG-KET were thus compared and exhibited different relaxation time confirming the covalent grafting of the PEGylated drug to the backbone of alginate (Figure 3.22). Moreover, DOSY experiment allowed the observation of the diffusion of the protons of alginate in correlation with the protons of PEG (annexes Figure 6.5).

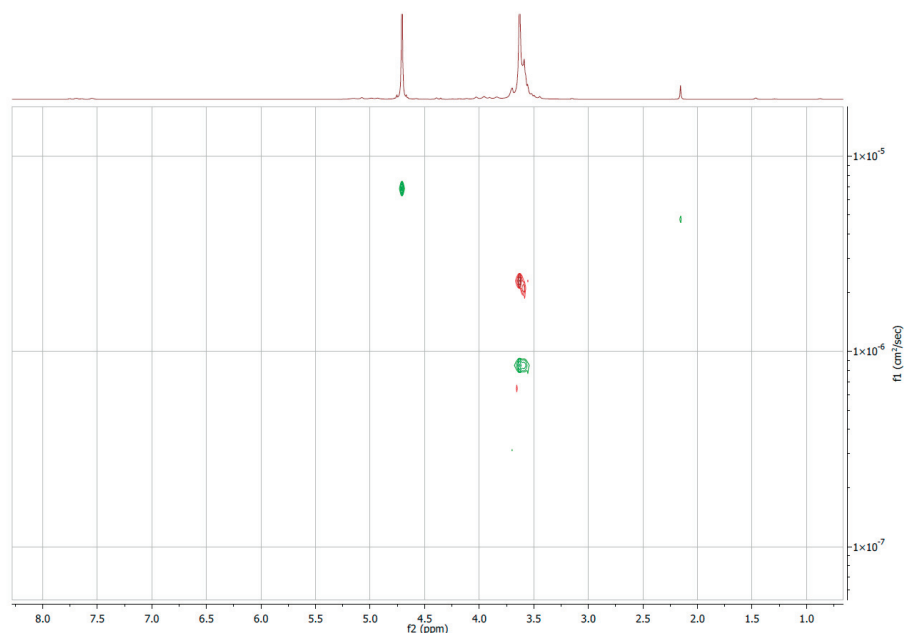


Figure 3.22: DOSY spectra of alg-PEG-KET (green) and un-grafted H_2N -PEG-KET (red).

MS were produced with the two polymers (**47** and **48**) by extruding 1 mL of 3 wt % solutions of alg-PEG-ester-KET (7% GD) and 1.2 mL of 2.5 wt % alg-PEG-amide-KET (7% GD) in MOPS, into a gelation bath containing $CaCl_2$, yielding MS with irregular morphology and wide size distribution (Figure 3.23).

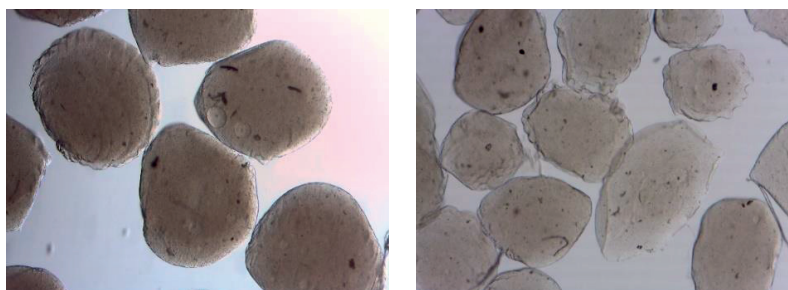


Figure 3.23: MS of alg-PEG-amide-ket (left) and alg-PEG-ester-ket (right)

To monitor the release of ketoprofen from the hydrogel, 1 mL of MS was placed in 3 mL gelation bath (MOPS, 100 mM $CaCl_2$) and aliquots of the supernatants were replaced at regular time points for 1 week (0.5, 1, 3, 6, 24, 48, 72, 96, 168 h). The amount of ketoprofen released was then quantified by LC-MS analysis of aliquots. The MS including ketoprofen through ester linkage (**47**) showed regular release of the drug during the time of the experiment whereas the release of ketoprofen linked through amide bonds was very slow with only traces of the drug detected in the supernatant over the time of the experiment (Figure 3.24). This observation emphasized the difference between the two types of bonds (amide and ester) used for the binding of ketoprofen, the ester bond being much more labile than amide in MOPS buffer.

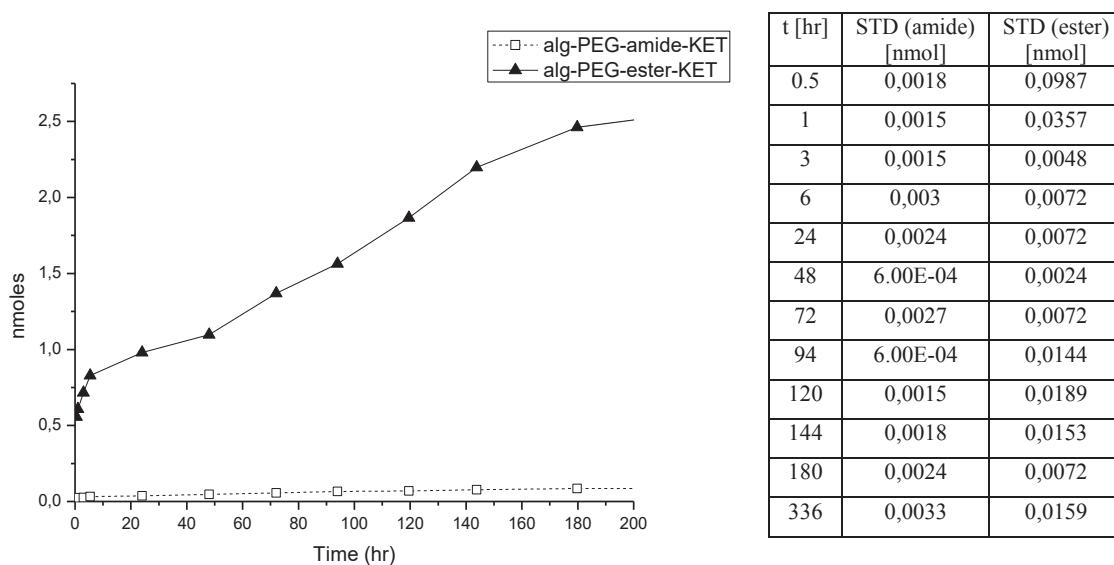


Figure 3.24: Cumulative release of ketoprofen from alginate-PEG-ester-KET and alginate-PEG-amide-KET microspheres at physiological pH (7.4) (n=3).

The production of MS with good morphology and size distribution was obtained by mixing Na-alg (1.5 wt. %) with the alginate derivatives (alg-PEG-ester-KET (**47**) or alg-PEG-amide-KET (**48**), both at 3.5 wt. %, with a GD of 20%) with weight:weight ratio of 2:1 before extrusion. For the sake of simplicity, the mixture of polymers are named **alg-A-KET** (for Na-alg:**47** / 2:1) and **alg-B-KET** (for Na-alg:**48** / 2:1) from this point forward. The extrusion of both mixture of polymers in a gelation bath containing CaCl₂ yielded monodisperse well-shaped MS. Using similar ratios, mouse insulinoma MIN6 cells were encapsulated by mixing the polymer solutions with the cells (3×10^6 cells/mL of polymer solution) before extrusion.

The corresponding results were published in: “Antifibrotic Effect of ketoprofen-Grafted Alginate Microcapsules in the Transplantation of Insulin Producing Cells” *Bioconjug. Chem.* **2018**.²²⁵

The MS obtained from the mixtures of polymers exhibited a good morphology with an average diameter between 500 and 600 μm . Homogeneous cell distribution was observed in both conditions. In parallel, MS from pure Na-alg were prepared with the same extrusion protocol, leading to similar characteristics (Figure 3.25).

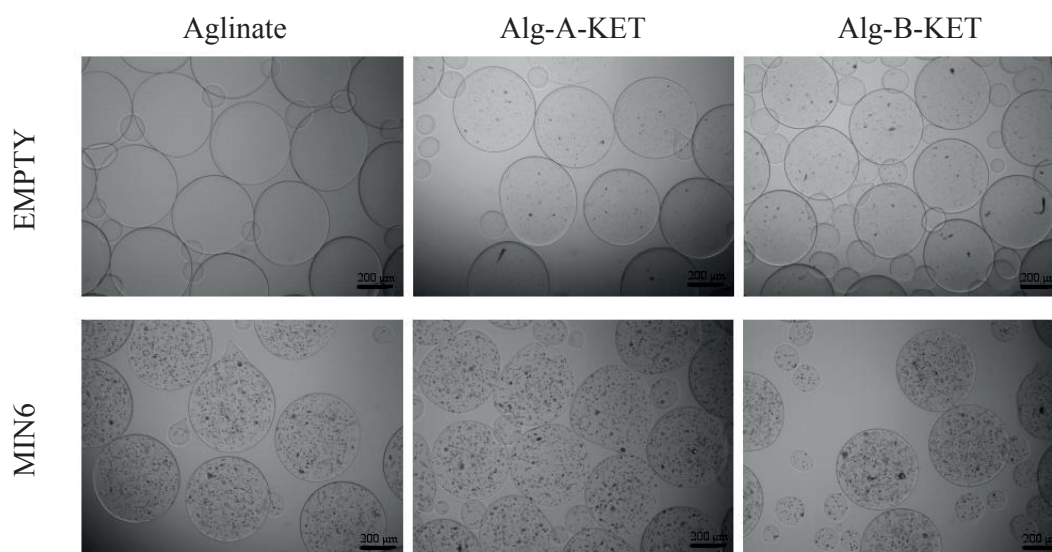


Figure 3.25: Empty microspheres (top) and MIN6 cells encapsulated (bottom) in alginate (left) alg-B-KET (middle) and alg-A-KET (right)

Since the drug release is known to be controlled by hydrolysis of the linkage to ketoprofen (ester or amide), the modification of the environment acidity is expected to influence the release rate of ketoprofen.²¹⁰ Therefore release of ketoprofen from the empty (cell-free) MS was studied in MOPS solution containing CaCl_2 (100 mM), adjusted to pH 3.0, 7.4, or 11. The amount of ketoprofen release was quantified by LC-MS analysis of the supernatant, which was withdrawn and replaced at regular time points over 2 weeks (0.5, 1, 3, 6, 24, 48, 72, 96, 168, and 336 h). At pH 7.4, MS incorporating ketoprofen through an ester linkage (alg-A-KET) showed regular release of the drug over 2 weeks, the covalent conjugation preventing burst effect within the first hours following microsphere formation. The rate of release was enhanced in basic conditions while acidic conditions slowed down the kinetics, which confirmed the hypothesis that hydrolysis controls the release rate of ketoprofen (Figure 3.26 left).²¹⁰ Under the same conditions, MS incorporating ketoprofen with an amide linkage (alg-B-KET) released only traces of the drug over 2 weeks (data not shown). The MS remained stable over 2 weeks under all pH conditions, showing the resistance of the electrostatic network toward a large range of pH. Since the release of ketoprofen over 14 days, was still monitored, one can expect the drug to have a long term anti-inflammatory impact around the MS when transplanted.

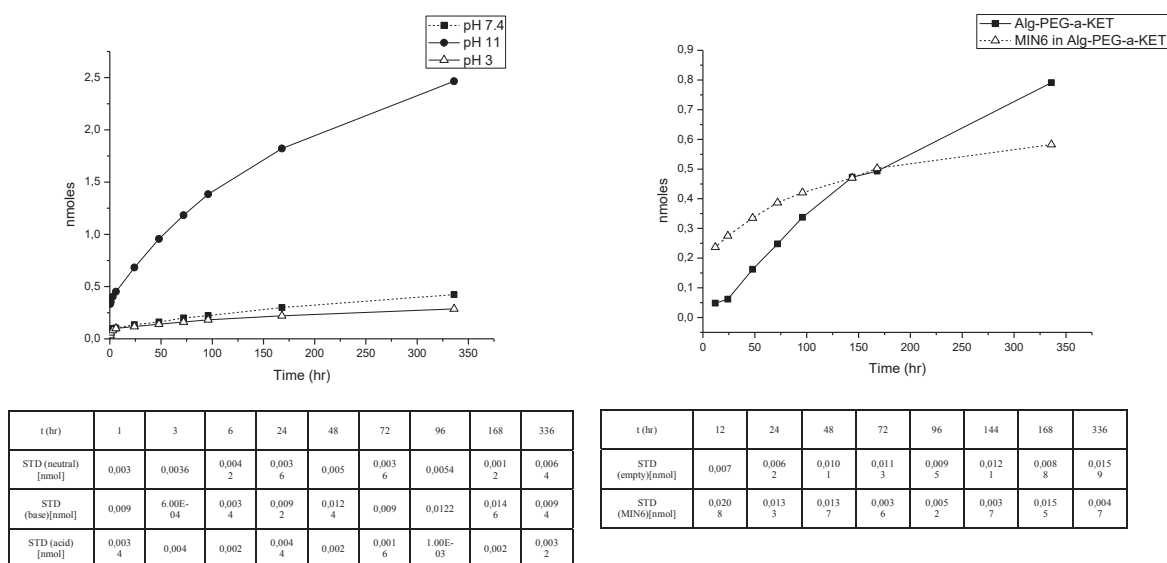


Figure 3.26: (left) *In vitro* cumulative ketoprofen release from alg-A-KET at the indicated pH value, under slow mechanical agitation ($n=3$). (right) ketoprofen release from microencapsulated MIN6 cells in alg-A-KET microspheres compared to empty alg-A-KET in the same conditions ($n=3$).

The release of ketoprofen in presence of MIN6 cells was then evaluated. 0.5 mL of MS containing cells were maintained in DMEM complete medium (1 mL) and aliquots of the medium (0.5 mL) were withdrawn and replaced with fresh culture medium over 2 weeks. As displayed on Figure 3.26 (right), the presence of MIN6 cells within the hydrogel induced faster release of the drug over the first 7 days. This observation might be due to the presence of hydrolytic enzymes of ester linkage in the encapsulated cells. Again, only traces of ketoprofen were observed in the supernatant of alg-B-KET MS for both conditions (data not shown). These data evidenced that the approach based on the covalent functionalization of hydrogel with drugs allows longer term release when compared to co-encapsulation strategy.¹⁹⁴

3.5.1 Quantification of the anti-fibrotic effect

In order to evaluate the anti-inflammatory potential of these hydrogels at the implantation site and its ability to mitigate pericapsular fibrotic overgrowth *in vitro*, empty and MIN6 cell containing MS of alg-A-KET, alg-B-KET and Ca-alg were transplanted into the peritoneal cavity of immune-competent mice and follow-up for a period of 30 days. Even though the release of ketoprofen from alg-B-KET was very low *in vitro*, the potential of this derivative toward mitigation of fibrosis formation was tested *in vivo* since the environment might induce ketoprofen release. After 30 days in the peritoneal cavity of the mice, the MS were retrieved and analyzed. Layers of fibrotic tissue of varying thickness were observed under light microscopy. A quantification of the cellular overgrowth revealed a lower amount of fibrotic tissue surrounding the empty MS containing ketoprofen; notably Alg-B-KET exhibited significant reduction of fibrosis (Figure 3.27). Interestingly, when observing the MS containing MIN6 cells, alg-A-KET exhibited significant decrease of fibrotic overgrowth compared to alg-B-KET which can be attributed to the higher release rate observed for ester bonds (Figure 3.24). A nonsignificant decrease of fibrosis was observed when compared to pure Na-alg. Similar results were observed with the analysis of MS retrieved at earlier time points (15 days) where

significant reduction of fibrotic tissue was observed around the ketoprofen-containing MS (Annexes, Figure 6.6).

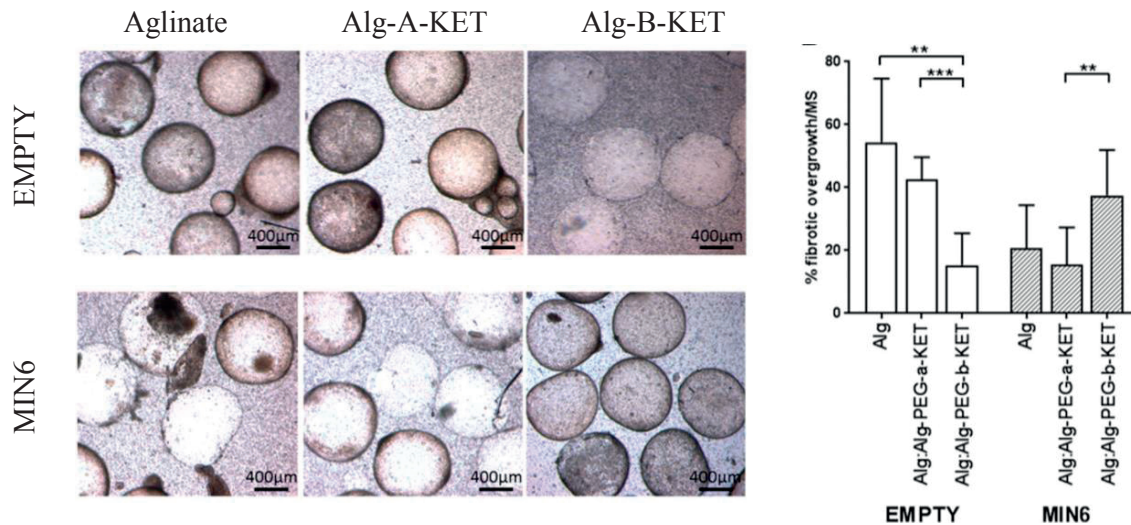


Figure 3.27 : (left) Bright-field microscopy images of MS retrieved from the peritoneum after 30 days of transplantation. Cell-free MS (upper panels) and with MIN6 cells (lower panels). (Right) Pericapsular fibrotic overgrowth quantified using ImageJ and expressed as a percentage of fibrotic overgrowth. Fibrotic overgrowth for cell-free MS (white bars) and for microspheres containing MIN6 cells (striped bars). All values are means \pm standard deviation (SD) of at least 5 MS. $**p < 0.01$, $***p < 0.001$. “Reprinted (adapted) with permission from Antifibrotic Effect of Ketoprofen-Grafted Alginate Microcapsules in the Transplantation of Insulin Producing Cells. *Bioconj. Chem.* Copyright 2018.”

The anti-fibrotic effect of ketoprofen-containing hydrogels was further evaluated by implanting the three types of MS under the kidney capsule and analysing of the collagen deposition by microscopy using Goldner’s Trichrome coloration after 4 weeks. The histological slice revealed fibrotic responses around the MS with fibrous collagen deposition (green) for all types of MS (Figure 3.28). The amount of collagen was quantified by computational imaging (Definiens software). Pure alginate empty MS did not induce an important fibrotic response, exhibiting a minimal pericapsular collagen deposition while a slightly higher amount of fibrotic tissue was observed in presence of alg-A-KET and alg-B-KET. On the other hand, pure Ca-alg MS containing MIN6 cells induced a strong fibrotic response with high collagen deposition. This observation is probably associated with the diffusion of DAMPs from the encapsulated cells triggering an inflammatory response from the foreign host body. This effect appeared to be significantly reduced around both ketoprofen-containing MS. Alg-A-KET exhibited the best results with less collagen deposition, which might again rise from the higher release rate of ketoprofen observed in vitro for this type of hydrogel.

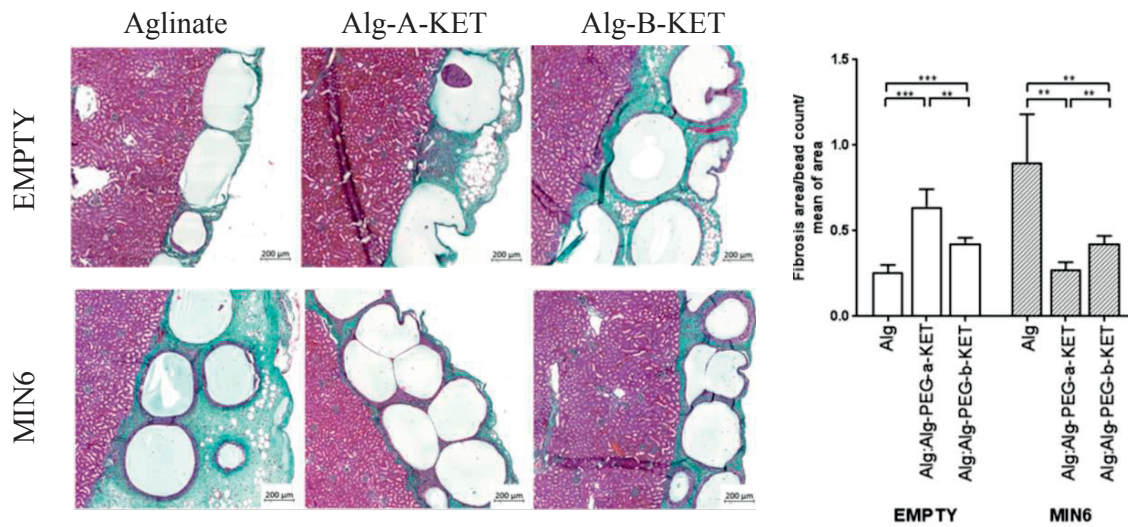


Figure 3.28: Quantification of collagen deposition around empty and MIN6 cells containing MS at 4 weeks after transplantation under the kidney capsule. (left) Sections of formalin-fixed and paraffin-embedded kidneys were colored with Goldner's Trichrome. cell-free MS (upper panels) and MS with MIN6 cells (lower panels). (right) Quantification of collagen deposition performed with Definiens software. Cell-free MS (white bars) and with MIN6 cells (striped bars). All values are means \pm standard deviation (SD) of 5 slides per condition. ** $p < 0.01$, *** $p < 0.001$. "Reprinted (adapted) with permission from Antifibrotic Effect of Ketoprofen-Grafted Alginate Microcapsules in the Transplantation of Insulin Producing Cells. *Bioconjug. Chem.* Copyright 2018."

The difference of fibrotic response which was observed between the peritoneal cavity and the kidney capsule might be explained by the higher vascularization of the environment located under the kidney capsule (see section 1.7.2). The significant anti-fibrotic effect, observed under the kidney capsule, due to the slow release of ketoprofen at the implantation site has the potential to improve the functionality of microencapsulated insulin producing cells as the high vascularization of this site of transplantation ensures efficient delivery of oxygen and nutrients to the cells.

3.5.2 Biocompatibility with encapsulated material

The viability of the encapsulated MIN6 cells was assessed at the end of both experiments (transplantation in the peritoneal cavity and under the kidney capsule) by insulin staining (Figure 3.29). Immunostaining allowed the detection of insulin in MIN6 cells for each condition after the transplantation, which confirmed the viability and good functionality of the encapsulated MIN6 cells 30 days after transplantation.

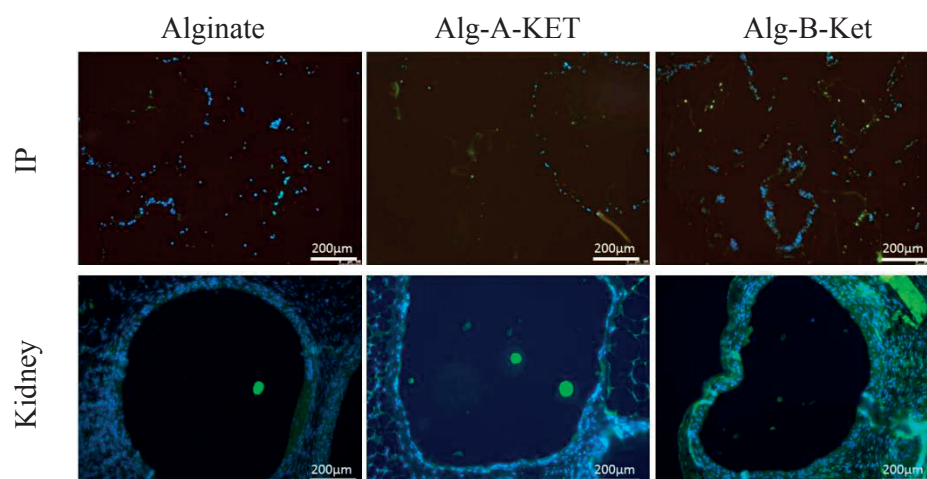


Figure 3.29: Insulin staining of encapsulated MIN6 cells 30 days after transplantation “Reprinted (adapted) with permission from *Antifibrotic Effect of Ketoprofen-Grafted Alginate Microcapsules in the Transplantation of Insulin Producing Cells*. *Bioconjug. Chem.* Copyright 2018.”

These results support that the long term functionality of transplanted encapsulated living cells (MIN6) could be enhanced with the use of ketoprofen containing hydrogels (alg-A-KET or alg-B-KET) by reduction of the fibrotic response when compared to pure alginate MS.

Within the context of cell therapy toward the treatment of T1D, the encapsulation of neo-natal pig islets having the ability to produce insulin was explored, as this source of cells has the potential to overcome the limitations associated with human cells. For this purpose, neo-natal pig islets were encapsulated in Ca-alg and alg-A-KET (10000 IEQ / ml of polymer). The islets viability was monitored with FDI/PI at day 1 and day 7. As shown on Figure 3.30 the viability of islets was not affected by the encapsulation in Ca-alg and alg-A-KET MS.

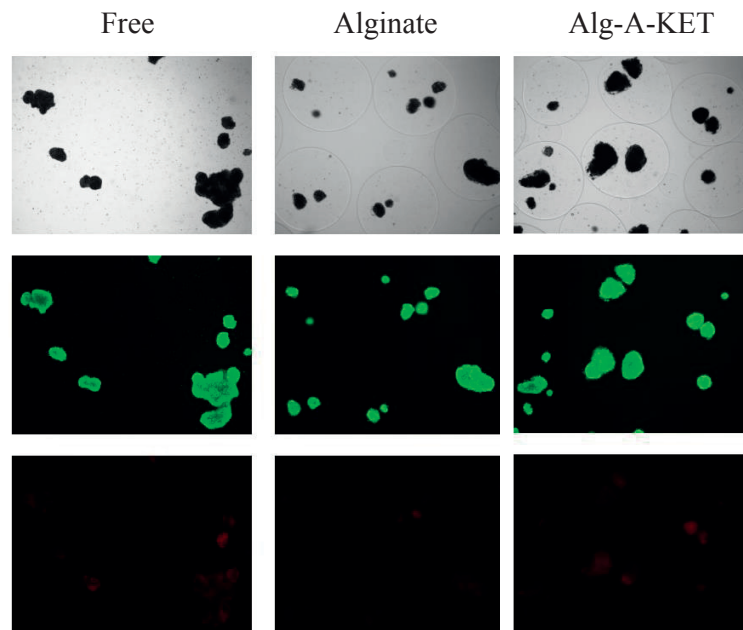


Figure 3.30: Microscopy image of neo natal pig islets, free, encapsulated in alginate and in alg-A-KET at day 7. Top panel: light microscopy, middle panel: staining of live cells with FDA (green), bottom panel: staining of dead cells with PI (red).

The functionality of encapsulated neo-natal pig islets was then assessed by monitoring the secretion of insulin in different conditions (basal, stimulated in 16.7 mM glucose and with theophylline), 3 and 7 days after encapsulation (Figure 3.31). Resulting data suggested that the secretion of insulin in response to stimulation remains regulated after encapsulation in Alg-A-KET, as compared with free islets but the quantity of insulin released is slightly reduced. This behavior should be overseen when considering transplantation of MS for glucose regulation in diabetic models.

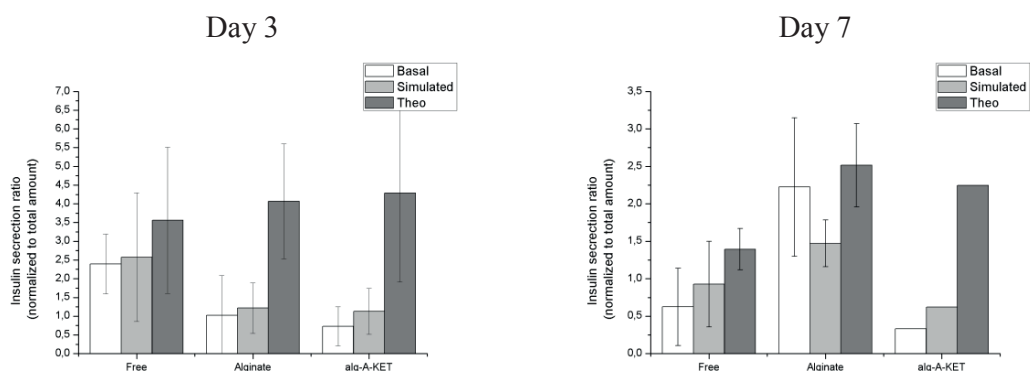


Figure 3.31: Glucose-stimulated insulin release for nonencapsulated neonatal pig islets (Free) and encapsulated in microspheres of alginate and alg-A-KET. Insulin release at basal glucose concentration (2.8 mM) upon stimulation at glucose concentration of 16.7 mM ($n=3$).

Overall, hydrogels formed from a mixture of Na-alg and ketoprofen functionalized alginate (alg-A-KET, alg-B-KET) appear as attractive materials for the encapsulation and transplantation of insulin producing cells. These new systems exhibited very promising

properties concerning the ability to reduce the formation of pericapsular overgrowth and to sustain the viability/functionality of encapsulated cells. The next objective of the study was to evaluate their mechanical properties, since this parameter impacts the long term durability of the transplanted systems.

3.5.3 Mechanical resistance

The resistance of alg-A-KET and alg-B-KET MS was evaluated by single and repeated compression to 90% of their initial diameter. In comparison with pure Ca-alg MS, the mechanical resistance of alg-(A/B)-KET was slightly lower exhibiting 1.48 and 1.79 [N/mm³] for alg-A-KET and alg-B-KET compared to 2.4 [N/mm³] for Ca-alg. The decrease of this mechanical properties may be attributed to the addition of extra polymer chain (PEG 2000) inducing steric hindrance within the hydrogel structure and not contributing to the hydrogel network.

The elasticity of these MS was also slightly reduced due to the presence of PEG within the hydrogel structure, exhibiting a decrease of shape recovery when compared to Ca-alg MS of the same size (Figure 3.32).

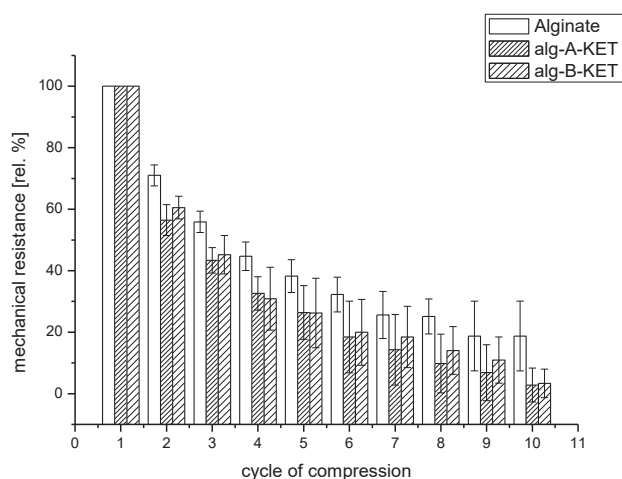


Figure 3.32: Shape recovery of alginate, alg-A-KET and alg-B-KET upon 10 successive compression to 90% of the initial diameter of the beads ($n=10$).

As these new polymers presented highly promising properties regarding their biocompatibility, the next investigations focused on the reinforcement of the hydrogel structure in order to increase both the mechanical resistance and the shape recovery performance.

3.6 THREE COMPONENTS SYSTEM

In order to combine the beneficial effect of ketoprofen containing alginate derivatives with reinforced hydrogel structures through covalent bonds, a recently developed hybrid hydrogel system was considered. This system, developed in the “Group for Functionalized Biomaterials” at EPFL (PhD thesis work of L.Szabó), involves the combination of two alginate derivatives functionalized with complementary heterobifunctional PEG polymers presenting reactive thiol or acrylate end moieties. When the hydrogel is produced in the presence of divalent cations, the

spontaneous 1,4-addition of thiol to acrylate functionality allows for the formation of a network of strong sulfur-carbon covalent linkages in addition to the electrostatic network, with the potential to reinforce the MS structure. Therefore, the combination of this system with alginate derivative **47** was assessed by mixing alg-PEG-SH, alg-PEG-acrylate and alg-PEG-ester-ketoprofen (**47**) in equivalent weight ratios (**3C-alg**) (Figure 3.33).

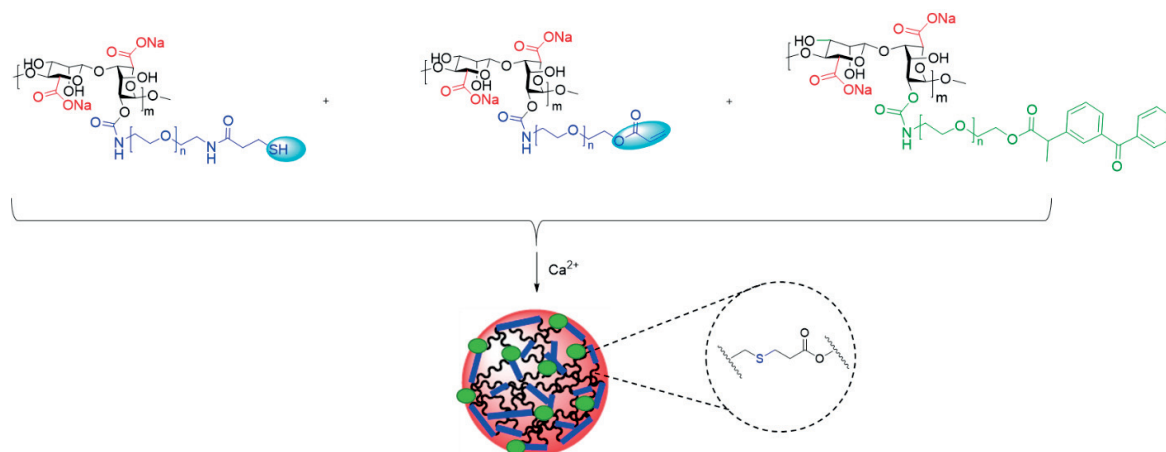


Figure 3.33: Representation of three components hybrid hydrogel formation with alg-PEG-SH, alg-PEG-acrylate and alg-PEG-ester-ketoprofen.

The three polymers were solubilized in MOPS buffer, alg-PEG-acrylate (3 wt. %), alg-PEG-thiol (3 wt. %), alg-PEG-ester-ket (**47**) (GD 20%, 2.5 wt. %) and mixed together (wt. ratio = 1:1:1) until homogenization of the resulting solution was achieved. The MS were then produced by extrusion of the solution into a gelation bath containing CaCl_2 yielding large MS (above 1 mm). Ca-alg MS of the same size were produced for comparison.

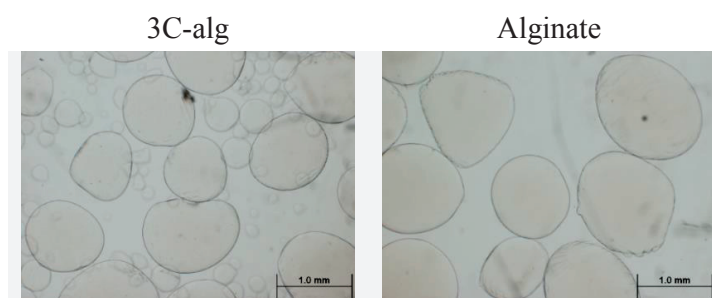
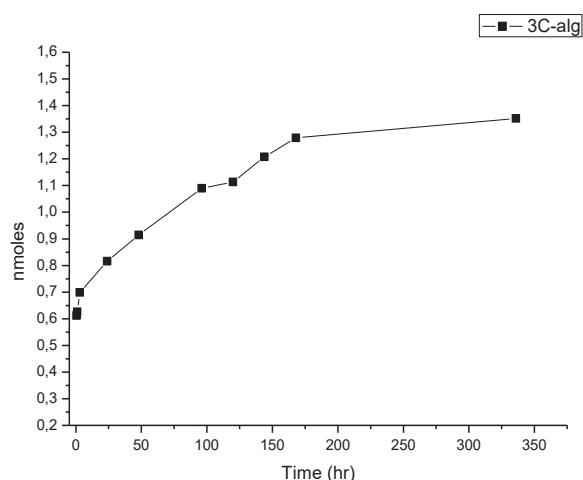


Figure 3.34: (left) images of microspheres prepared from a mixture of three polymers (**3C-alg**), (right) alginate MS.

Although, the shape and size distribution of the MS were not optimized, several parameters were assessed. Ketoprofen release from **3C-alg** MS was evaluated from a sample containing 1 mL of MS in 3 mL of gelation bath (MOPS, 100 mM CaCl_2). Aliquots of the supernatant were analyzed at regular time points over 2 weeks (0.5, 1, 3, 24, 48, 96, 120, 144, 168, 336 h). The quantification of ketoprofen released was performed by LC-MS analysis of the aliquots (Figure 3.35).



t (hr)	0.5	1	3	24	48	96	120	144	168	336
STD (3 comp.) [nmol]	0,09	0,036	0,048	0,036	0,009	0,024	0,027	0,006	0,027	0,018

Figure 3.35: In vitro cumulative ketoprofen release from 3C-alg in MOPS solution pH 7.4 ($n=3$).

3C-alg MS displayed regular release of ketoprofen during the time of the experiment with a profile similar than the one observed with alg-A-KET (Figure 3.24).

The mechanical resistance of 3C-alg MS was then evaluated at 1, 7 and 14 days after MS formation by single and repeated compression to 90% of their initial diameter. During this period, no significant size evolution was observed (Table 7).

Table 7: Sizes of microspheres 3C-alg at day 1, 7 and 14 ($n=10$)

	Alginate	3 components
Day 1	1030±123	1175±123
Day 7	986±118	1091±124
Day 14	1107±108	986±146

The resistance of 3C-alg MS to a single compression evolved from only 0.71 [N/mm³] at day 1 (against 1.60 [N/mm³] for Ca-alg MS of the same size) to 1.17 [N/mm³] after one week incubation in gelation bath. Interestingly pure Ca-alg MS resistance decreased after 7 days in the same conditions to 1.27 [N/mm³]. After two weeks both MS kept a stable resistance (1.10 [N/mm³] and 1.27 [N/mm³]). Similarly, the shape recovery of 3C-alg MS improved significantly during the first 7 days of incubation and stayed stable for the following week exhibiting 50 % recovery whereas Ca-alg MS displayed only 30% recovery at their best (Figure 3.36). The improvements of the mechanical properties of this system during the first week of incubation can be associated with the kinetics of the formation of the covalent network, which require several days to be completed.

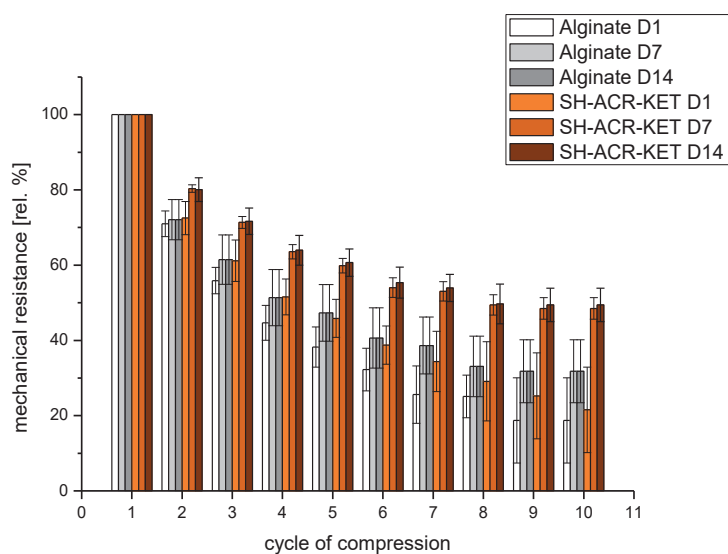


Figure 3.36: Shape recovery after 10 successive compressions to 90% of the initial diameter of 3C-alg and Ca-alginate microspheres ($n=10$).

These preliminary assays performed on 3C-alg MS showed that the shape recovery performance was significantly enhanced by the combination of a network of covalent bonds with the electrostatic network. In addition, sustained ketoprofen release was observed over two weeks as for the Na-alg/alg-A-KET hydrogel initially developed. In view of these promising results, the encapsulation of neo-natal pig islets in 3C-alg hydrogel systems and their transplantation into immune competent mice are currently investigated.

4 CONCLUSION

Cell-based therapies relying on the transplantation of xenogeneic cells into semi-permeable hydrogels have the potential to reduce or even avoid the use of chronic immunosuppression and to overcome the shortage human donor materials. The success of such an approach strongly relies on the properties of the material used for cell encapsulation. Since the pioneering developments of Bisceglie²⁷ and Chang,²⁸ significant progress was achieved to improve the performance of the material used for cell encapsulation, notably with the development of alginate-based hydrogels which provide spontaneous MS formation in the presence of divalent cations and high compatibility toward human and animal cells. Still, several limitations remain, especially when *in vivo* long term durability and functionality are required. Therefore, this thesis project was devoted to the development of alginate-based hydrogels able to overcome some of the current shortcomings, including the formation of pericapsular overgrowth and the lack of long term durability. For this purpose, several strategies were explored for the conjugation of anti-inflammatory compounds to alginate-based hydrogel networks and for the incorporation of covalent cross-linkings to reinforce the polymeric matrix.

First, new alginate-based hybrid hydrogels formed by functionalization on the hydroxyl group of Na-alg with heterobifunctional PEG derivatives containing end thiols or 1,2-dithiolane functionalities were characterized. The importance of the covalent link between the PEG linker and Na-alg was emphasized, leading to the development of a new synthetic route for the functionalization of the hydroxyl groups of Na-alg through carbamate bonds. The MS obtained from the derivatives of Na-alg containing either thiols or lipoyl moieties presented improved mechanical properties, in particular the shape recovery performance following multiple compressions, when compared with pure Ca-alg MS. It was then demonstrated that the length of the linear PEG linkers used for the introduction of the thiols or 1,2-dithiolanes had an influence on the mechanical properties of the resulting hydrogels. Shorter PEG (PEG 1000) linkers led to the formation of MS with higher resistance than PEG 2000. The potential of these hydrogels toward microencapsulation was demonstrated with the encapsulation of MIN6 cells which exhibited good viability in both MS types over two weeks. Good bioacceptance of the cell-free MS was also observed in preliminary *in vivo* studies. The so-developed hydrogels present several advantageous features for biomedical applications: i) the MS are obtained from a one-component polymer system containing the functionalities for both electrostatic and covalent cross-linking; ii) the conditions for MS production avoid the use of additional chemical cross-linkers, as the covalent bonds are spontaneously formed in aqueous medium, concomitantly to the formation of the electrostatic interactions. The functionalization strategy allows for the introduction of immune response modulators, which was explored in the second part of this project.

Three anti-fibrotic compounds were selected for their potential conjugation to the hydrogel network through covalent crosslinking (Curcumin, Ketoprofen and FAP- α inhibitor) to improve the biocompatibility of the MS by mitigation of the fibrotic response. In a first attempt, it was envisaged to take advantage of the chemical functionalities already present on functionalized alginate derivatives such as thiol and lipoyl moieties to bind the anti-inflammatory compounds

during MS production. Since the covalent conjugation and further release of anti-inflammatory compounds could not be evidenced through this approach, we turned to an alternative strategy relying on the direct conjugation of the anti-fibrotic compounds on the backbone of Na-alg prior to MS formation. For this approach, ketoprofen was PEGylated with either an ester or amide linkage. The resulting PEGylated drugs were grafted on the hydroxyl groups of Na-alg, resulting in alg-A-KET and alg-B-KET whose chemical structures were confirmed by DOSY-NMR. In combination with Na-alg, these polymers led to the formation of functionalized MS which were assessed for drug release, encapsulation of insulin producing cells and transplantation in immune competent mice. In particular, their ability to mitigate pericapsular fibrotic overgrowth was analyzed, in comparison with pure alginate-derived MS. Although only traces of ketoprofen were released from the hydrogel containing an amide linkage to ketoprofen, regular and sustained drug release was observed up to 14 days from the hydrogel containing an ester bond to ketoprofen. In presence of MIN6 cells, the release was accelerated during the first days following the encapsulation, which probably resulted from the action of cell esterase. The potential to inhibit the PFO was evaluated with the transplantation of both type of MS in immune-competent mice. For cell-free MS, a reduction of the pericapsular overgrowth was observed around the functionalized hydrogels when compared to pure alginate 30 days after transplantation. Moreover, the high increase of fibrotic tissue formation observed in the transplantation of encapsulated MIN6 cells in pure Ca-alg MS was significantly reduced around functionalized MS, in the same condition.

Hence, mitigation of PFO around cell-containing MS was achieved by controlled release of ketoprofen from the hydrogel matrix, resulting from the *in vivo* hydrolysis of the chemical bond used to conjugate the drug to PEG spacer. One of the main advantage of this approach is the long-term release providing the active compound over several days at the transplantation site which is highly advantageous for the mitigation PFO whereas simple co-encapsulation of anti-inflammatory compounds results in burst release of the drugs within the first hours limiting critically the duration of the anti-fibrotic action of the drugs. Furthermore, a variety of small molecular immune response modulators could be used with this strategy, including the possibility to combine several drugs for synergistic effects.

Finally, in order to combine the anti-fibrotic effect of alg-PEG-KET derivatives with a reinforced hydrogel matrix, the combination of alg-PEG-SH and alg-PEG-acrylate with alg-A-KET (3C-alg) was explored. Preliminary results showed that the release of ketoprofen was still sustained from this hydrogel including new functionalities in its structure. In addition, the mechanical properties of the MS were strengthened after an incubation time confirming the late formation of covalent bonds between acrylate and thiols.

These promising results will be the basis for further investigations, including:

- The development of other complementary alg-PEG derivatives for the production of hydrogel microspheres simultaneously stabilized by both ionotropic gelation and covalent cross-linking (thiol-maleimide and azide-alkyne combinations)
- The covalent conjugation of other immune response modulators on the hydrogel polymeric materials for sustained controlled delivery at the transplantation site

Conclusion

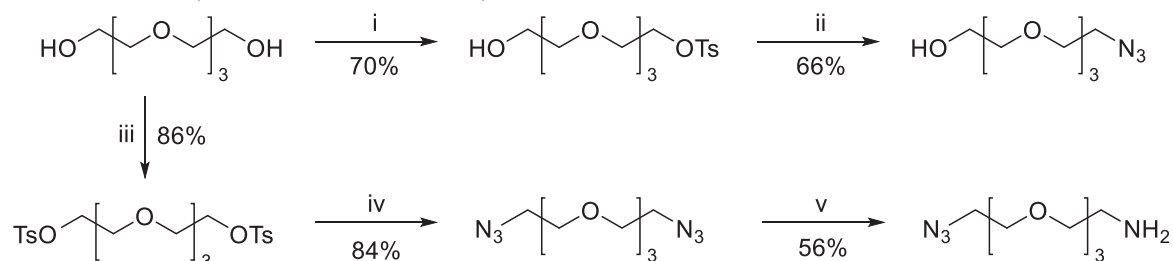
- The standardization of xenogeneic cells source for microencapsulation, including the stimulation of their secretion capacity by co-culture systems
- The validation of the capacity of the cell-transplant products in vivo with a longer follow-up period (6 months to one year)

5 EXPERIMENTAL SECTION

5.1 MATERIALS AND METHODS

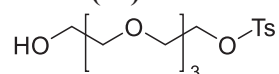
Na-alg Kelton HV (lot no. 61650A, $[\eta] = 813 \text{ mL g}^{-1}$ in 0.1 M NaCl, $T = 25 \text{ }^\circ\text{C}$, $G/M = 0.6$) was obtained from Kelco (San Diego, USA, CA). Linear PEG (TBOC-PEG2000-OH and TBOC-PEG2000-NH₂) were obtained from Jenkem Technology (Beijin, China). Other commercial reagents (Fluka, Sigma, Switzerland; TCI Europe, Zwijndrecht, Belgium) were used without further purification. Unless special mention, all reactions were performed under argon atmosphere (1 atm). Anhydrous solvents were obtained by filtration (Puresolv MD 5, Innovative Technology, Oldham, UK). Glassware was dried for 12 h in an oven ($T > 100 \text{ }^\circ\text{C}$) or under vacuum with a heat gun ($T > 200 \text{ }^\circ\text{C}$). Reactions were monitored by TLC (Merck silica gel 60F254 plates, Merck, Darmstadt, Germany). Detection was performed by UV light, KMnO₄, Ninhydrin or I₂. Purifications were performed by flash chromatography on silica gel (Merck N° 9385 silica gel 60, 240-400 mesh). NMR spectra were recorded on Bruker Avance III-400, Bruker Avance-400 or Bruker DRX-400 spectrometers at room temperature (rt) (400 MHz) (Bruker, Billerica, MA, USA). ¹H frequency is at 400.13 MHz, ¹³C frequency is at 100.62 MHz. Chemical shifts are expressed in parts per million (ppm) and coupling constants (J) in hertz (Hz). Solvents used for NMR spectroscopy were deuterated chloroform (CDCl₃, Acros), deuterated methanol (CD₃OD, Acros) and deuterated water (D₂O). Mass spectra were obtained on a Nermag R-10-10C spectrometer with chemical ionization (NH₃) and mode m/z (amu) [% relative base peak (100%)] (Nermag, Santa Clara, CA, USA). IR spectra were recorded on a Jasco FT/IR-4100 spectrometer outfitted with a PIKE technology MIRacle™ ATR accessory as neat films compressed onto a Zinc Selenide window. The spectra are reported in cm⁻¹. Mass spectra were obtained by using a Waters ACQUITY H-class UPLC/MS ACQ-SQD by electron ionization (EI positive and negative) or a Finnigan TSQ7000 by electrospray ionization (ESI+). The accurate masses were measured by ESI-TOF using a QTOF Ultima from Waters. Quantitative MS analyses were performed on and Agilent Accurate Mass Q-TOF LCMS mass spectrometer coupled to an Agilent 1290 series UHPLC system (Agilent Technologies, USA). The separation was achieved using an ACQUITY UPLC® BEH C18 1.7µm column, 2.1 mm x 50 mm (Waters) heated at 30°C.

5.2 TETRA(ETHYLENE GLYCOL) DERIVATIVES



Scheme 16: Synthesis of linkers derived from tetra(ethylene glycol). Reagents and conditions: i- NaOH, TsCl, 0°C to 23°C, 1 hr; ii- NaN₃, 90°C, 7 hr; iii- TsCl, Et₃N, DMAP, 0°C to 23°C, 16 hr; iv- NaN₃, 90°C, 16 hr; v- HCl 5%, PPh₃, 0°C to 23°C 6 hr.

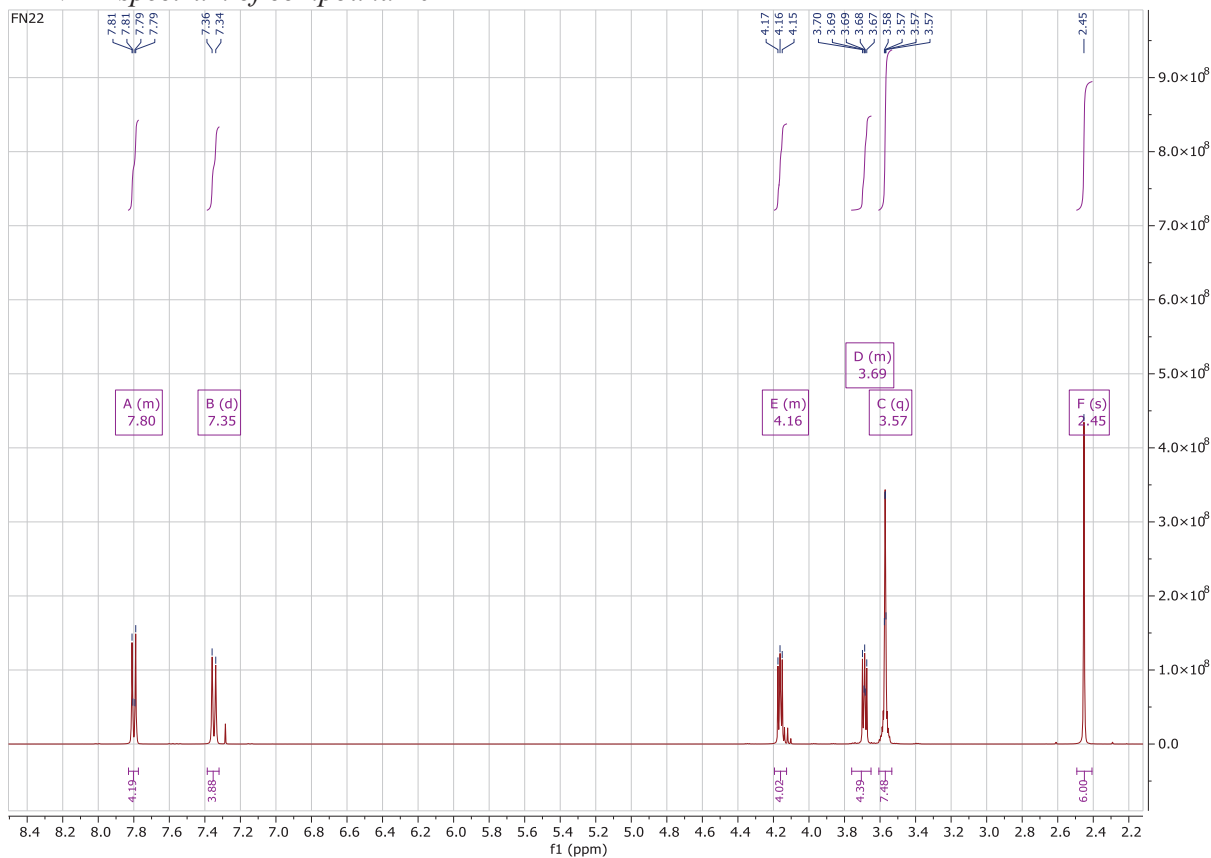
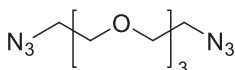
Tetraethylene glycol p-toluenesulfonate (18)



The following protocol was adapted from the procedure reported by Ligeour et al.²²⁶ Tetra(ethylene glycol) (43.3 mL, 250 mmol, 10 equiv) was dissolved in THF (10 mL) and the solution was cooled to 0°C. Aq. NaOH 50% (4.8 mL, 60 mmol, 2.4 equiv) was added and a solution of TsCl (4.77 g, 25 mmol, 1 equiv) in THF (15 mL) was introduced dropwise. The reaction mixture was stirred for 1 hr at 23°C. The solvent was then removed in vacuo and the residue was dissolved in chloroform. The solution was washed with water (3 x 30 mL), brine (30 mL), dried over MgSO₄ and concentrated in vacuo. The product was purified by FCC (EtOAc) to afford compound **1** as a colorless oil (6.100 g, 17.51 mmol, 70%). The analytical data were in agreement with literature report.

¹H NMR (400 MHz, CDCl₃) δ 7.76 (dt, J = 8.5, 1.1 Hz, 2H, CHar), 7.31 (d, J = 8.1 Hz, 2H, CHar), 4.13 (tt, J = 4.8, 3.9, 1.1 Hz, 2H, CH₂-OTs), 3.74 – 3.51 (m, 14H, CH₂-O), 2.41 (s, 3H, CH₃).

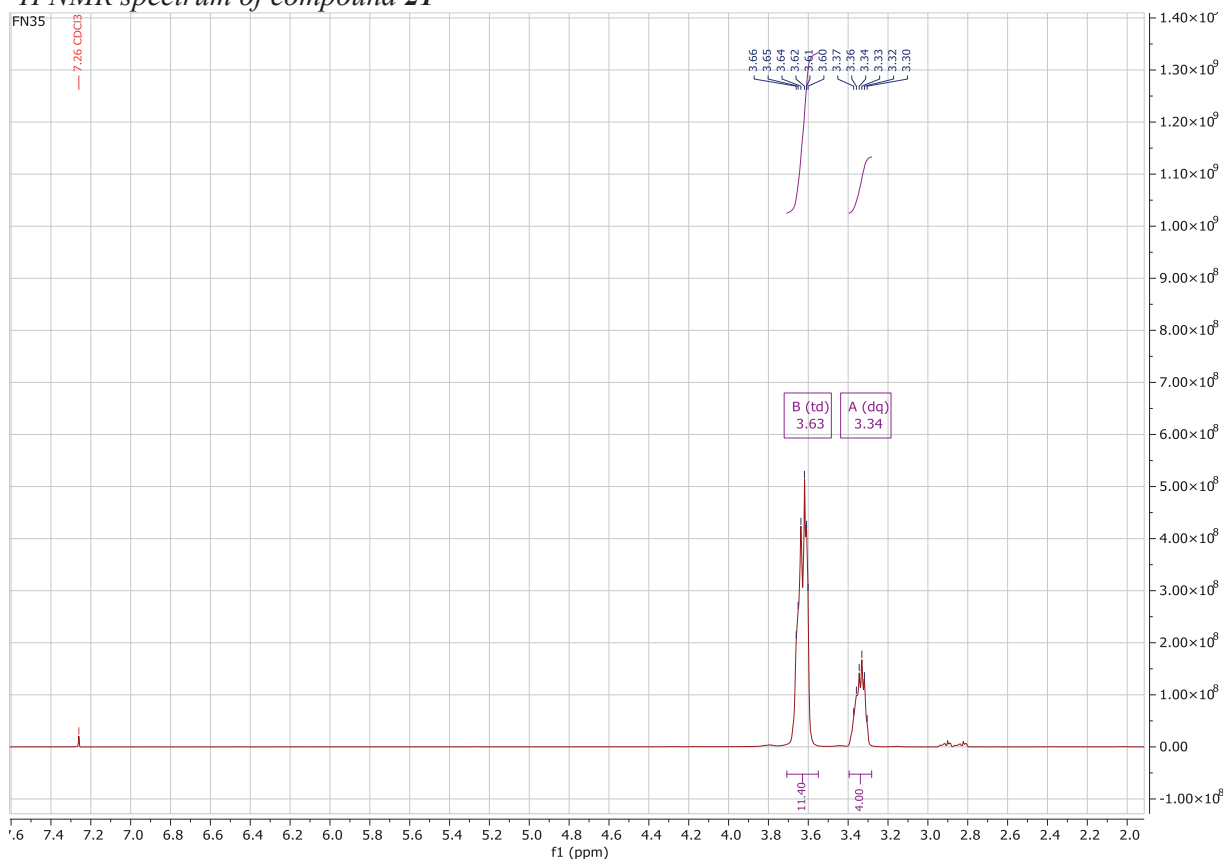
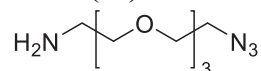
MS (ESI/QTOF) m/z: [M+Na]⁺ Calcd for C₁₅H₂₄NaO₇S⁺ 371.11; Found 371.33

¹H NMR spectrum of compound **20**Tetraethylene glycol di(azide) (**21**)

The following protocol was adapted from the procedure reported by Goswami et al.²²⁸ TEG ditosyl (**20**) (22.4 g, 44.5 mmol, 1 equiv) was dissolved in DMF (50 mL) and NaN₃ (6.95 g, 107 mmol, 2.4 equiv) was added. The reaction mixture was stirred for 16 hr at 90°C. The solvent was removed in vacuo and the residue was dissolved in water (30 mL). The solution was extracted with DCM (3 x 30 mL). The combined organic layers were washed with brine (2 x 20 mL), dried over MgSO₄ and concentrated in vacuo to afford TEG diazide (**21**) as a yellowish oil (37.34 mmol, 9.12 g, 84%). The analytical data were in agreement with literature report.

¹H NMR (400 MHz, CDCl₃) δ 3.63 (td, J = 8.3, 7.2, 3.4 Hz, 12H, CH₂-O), 3.34 (dq, J = 10.7, 5.5 Hz, 4H, 2 x CH₂-N₃).

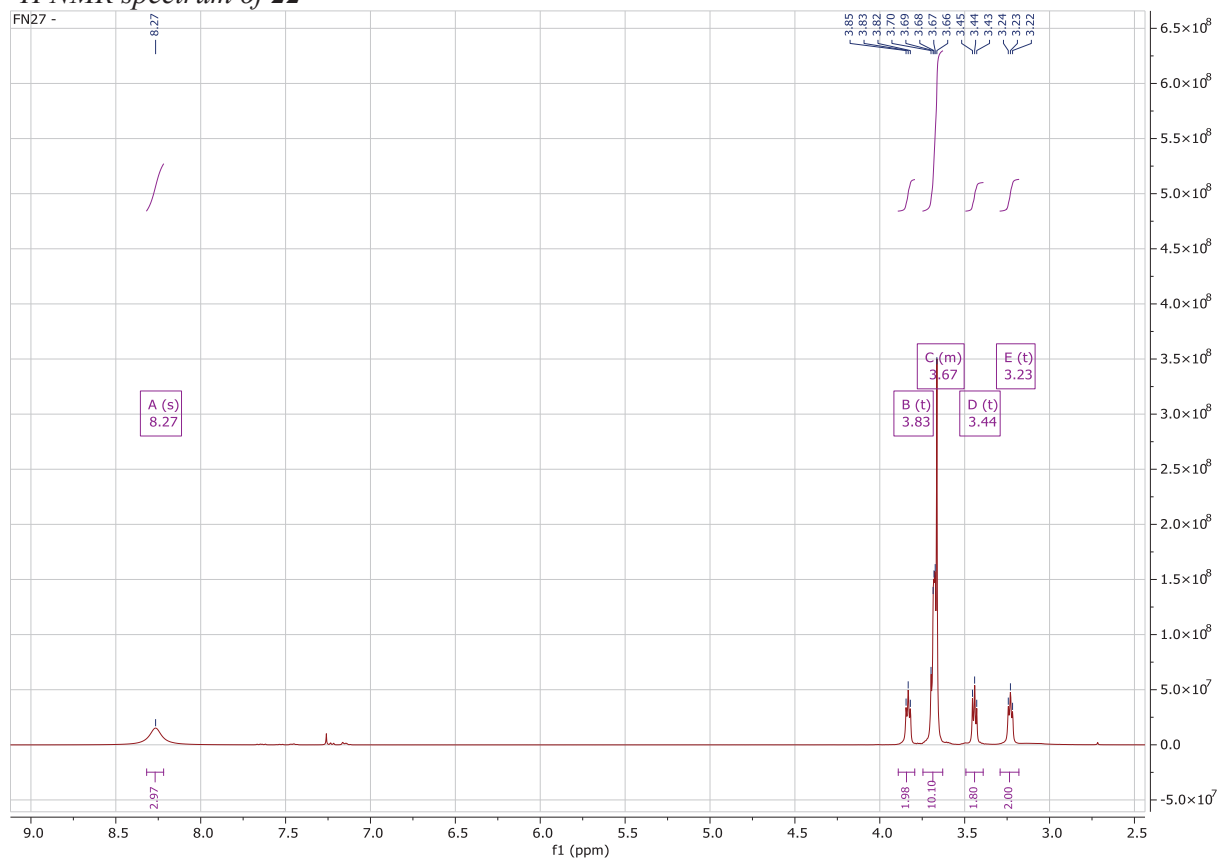
IR (cm⁻¹): 2871, 2104, 1294, 1125.

¹H NMR spectrum of compound **21****1-Amino, 11-azido-3,6,9-trioxaundecane (22)**

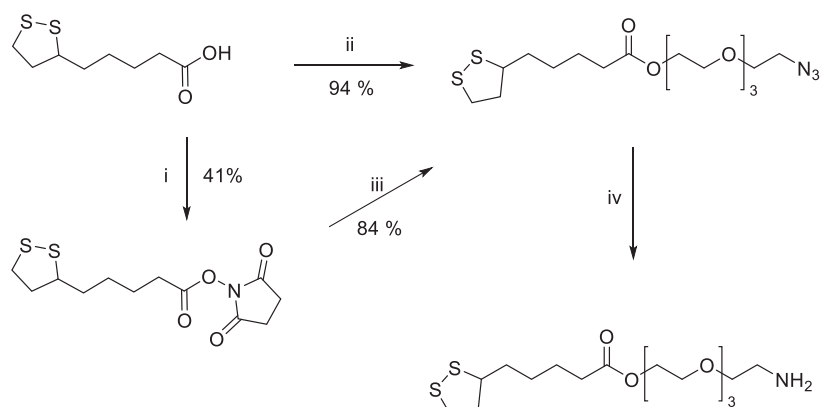
The following protocol was adapted from the procedure reported by Goswami et al.²²⁸ TEG diazide (**21**) (9.12 g, 37.3 mmol, 1 equiv) was dissolved in toluene (45 mL) and aq. HCl 5% (45 mL) was added. The solution was cooled to 0°C and PPh₃ (9.79 g, 37.3 mmol, 1 equiv) was added portion wise. The reaction mixture was then allowed to warm up to 23°C and stirred for 6 hr. The aqueous phase was recovered and co-evaporated with toluene under vacuo to afford amine-TEG-azide (**22**) as an opaque oil (4.55 g, 20.85 mmol, 56%). The analytical data were in agreement with literature report.

¹H NMR (400 MHz, CDCl₃) δ 8.27 (s, 2H, NH₂), 3.83 (t, J = 5.1 Hz, 2H, CH₂-NH₂), 3.75 – 3.63 (m, 10H, CH₂-O), 3.44 (t, J = 5.0 Hz, 2H, CH₂-CH₂-N₃), 3.23 (t, J = 5.0 Hz, 2H, CH₂-N₃).

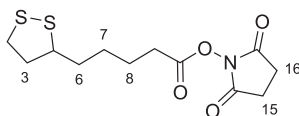
MS (ESI/QTOF) m/z: [M+H]⁺ Calcd for C₈H₁₉N₄O₃⁺ 219.14; Found 219.24

¹H NMR spectrum of 22

5.3 DERIVATIZATION OF LIPOIC ACID WITH TETRA(ETHYLENE GLYCOL) DERIVATIVES



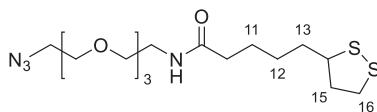
Scheme 17: Derivatization of lipoic acid with tetra(ethylene glycol) derivatives. Reagents and conditions: *i*- NHS, DCC, 0°C to 23°C, 12 hr; *ii*- HOBT, EDCI, DIPEA, 23°C, 12 hr, *iii*- NEt₃, 23°C, 12 hr, *iv*- PPh₃, THF, aq. HCl 5%, 23°C, 17 hr.

Lipoic Acid NHS-ester (23)

The following protocol was adapted from the procedure reported by Benito-Alifonso David et al.²²⁹ To a stirred solution of lipoic acid (15 g, 72.7 mmol, 1 equiv) in THF (60 mL) was added *N*-hydroxysuccinimide (10 g, 87.2 mmol, 1.2 equiv) portion wise. The solution was cooled to 4°C and a solution of DCC (18 g, 87.2 mmol, 1.2 equiv) in THF (25 mL) was added dropwise. The reaction mixture was allowed to warm up to 23°C and stirred for 12 hr. The solution was filtered through a pad of celite and solvent was removed in vacuo. The product was purified by FCC (EtOAc:PE = 1:2) to afford **23** as a yellow solid (9.14 g, 30.12 mmol, 41%). The analytical data were in agreement with literature report.

¹H NMR (400 MHz, CDCl₃) δ 3.58 (dq, *J* = 8.2, 6.4 Hz, 1H, CH-S), 3.24 – 3.07 (m, 2H, CH₂-S), 2.91 – 2.78 (m, 4H, 2 x CH₂ (15, 16)), 2.63 (t, *J* = 7.4 Hz, 2H, CH₂COO), 2.47 (dtd, *J* = 13.1, 6.6, 5.4 Hz, 1H, CH₂ (3')), 1.92 (dq, *J* = 12.6, 6.9 Hz, 1H, CH₂ (3'')), 1.84 – 1.65 (m, 4H, 2 x CH₂ (6, 8)), 1.64 – 1.51 (m, 2H, CH₂, (7)).

¹H NMR spectrum of 23

Lipoic acid-TEG-azide (24)

The following molecule was obtained through two different protocols. The former is adapted from the procedure reported by Benito-Alifonso David et al.²²⁹ Amine-TEG-azide (**22**) (200 mg, 785 μmol , 1 equiv) was dissolved in DMF (5 mL). Lipoic acid NHS-ester (**23**) (476 mg, 1.57 mmol, 2 equiv) and NEt_3 (120 μL , 864 μmol , 1.1 equiv) were added and the solution was stirred at 23°C for 12 hr. The solvent was removed in vacuo and the residue was dissolved in DCM (10 mL) and washed with aq. sat. NH_4Cl (3 x 10 mL) brine (10 mL). The organic phase was reduced in vacuo and the product was purified by FCC (DCM:MeOH = 1:0 \rightarrow 8:1) to afford **24** as a yellow oil (268 mg, 0.66, mmol, 84%). The analytical data were in agreement with literature report.

Lipoic acid (227 mg, 1.1 mmol, 1.2 equiv) was dissolved in DMF (3 mL) and EDCI (202 mg, 1.05 mmol, 1.15 equiv), HOBt (281 mg, 1.83 mmol, 2 equiv) and DIPEA (454 μL , 2.75 mmol, 3 equiv) were added to the solution. The reaction mixture was stirred for 10 min before the addition of a solution of amine-TEG-azide (**5**) (233 mg, 916 μmol , 1 equiv) in DMF (3 mL). The solution was stirred for 12 hr at 23°C. DMF was removed in vacuo. The residue was dissolved in water (7 mL) and extracted with DCM (3 x 5 mL). The combined organic phases were washed with sat. aq. NaHCO_3 (3 x 5 mL) and brine (5 mL). The solvent was removed in vacuo to afford **7** as a yellow oil (349 mg, 0.86 mmol, 94%).

^1H NMR (400 MHz, CDCl_3) δ 6.06 (d, $J = 6.5$ Hz, 1H, NH), 3.87 – 3.37 (m, 17H, $\text{CH}_2\text{-O} + \text{CH-S}$), 3.28 – 3.09 (m, 2H, CH_2 16), 2.48 (dq, $J = 12.4, 6.3$ Hz, 1H, 15'), 2.21 (t, $J = 7.5$ Hz, 2H, $\text{CH}_2\text{-CO}$), 1.93 (dd, $J = 13.0, 6.7$ Hz, 1H, 15''), 1.70 (tdd, $J = 15.3, 9.2, 5.2$ Hz, 4H, 2 x CH_2 11, 13), 1.50 (ddd, $J = 14.3, 8.2, 5.6$ Hz, 2H, CH_2 12).

^{13}C NMR (101 MHz, CDCl_3) δ 172.83 (CO), 70.86 (CH_2 TEG), 70.77 (CH_2 TEG), 70.71 (CH_2 TEG), 70.40 (CH_2 TEG), 70.21 (CH_2 TEG), 70.04 (CH_2 TEG), 56.56 (CH-S), 50.82 (CH_2 TEG), 40.36 (15), 39.29 (CH_2 TEG), 38.60 (16), 36.53 ($\text{CH}_2\text{-CO}$), 34.79 (13), 29.05 (12), 25.50 (11).

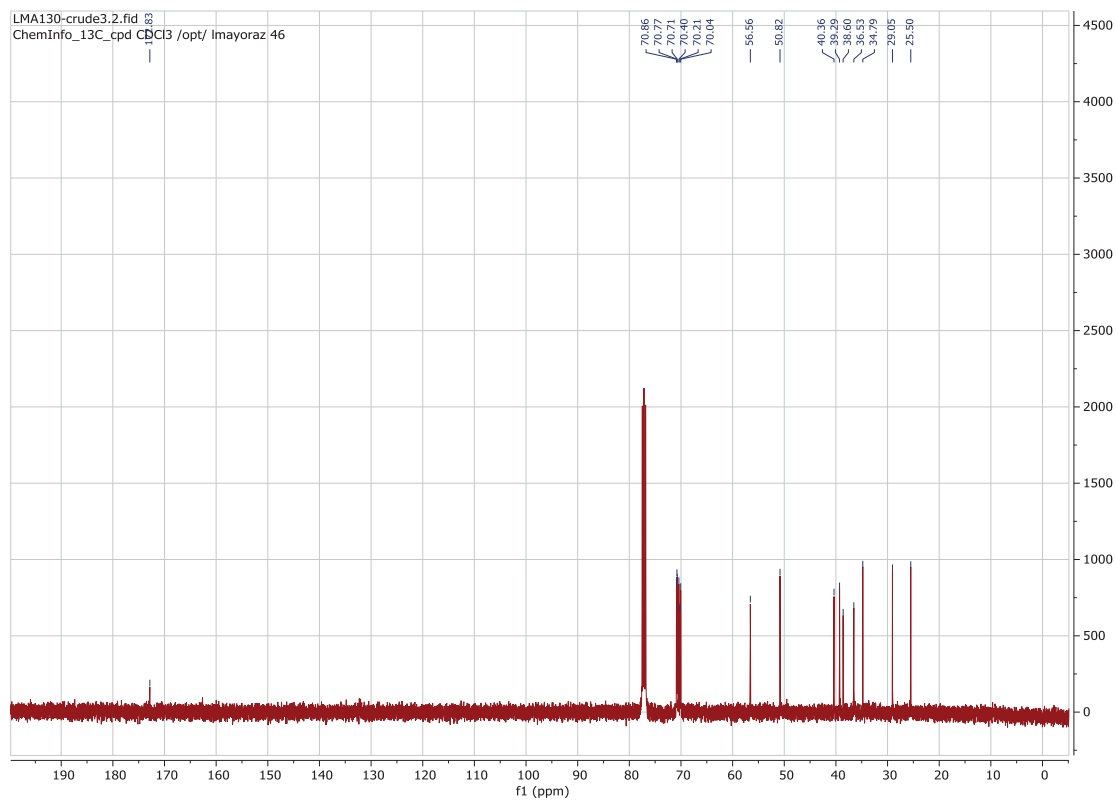
HRMS (ESI/QTOF) m/z : $[\text{M} + \text{Na}]^+$ Calcd for $\text{C}_{16}\text{H}_{30}\text{N}_4\text{NaO}_4\text{S}_2^+$ 429.1601; Found 429.1606

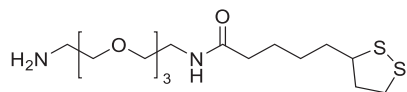
IR (cm^{-1}): 3283, 2921, 2872, 2098, 1649, 1537, 1288, 1100

¹H NMR spectrum of 24



¹³C NMR spectrum of 24

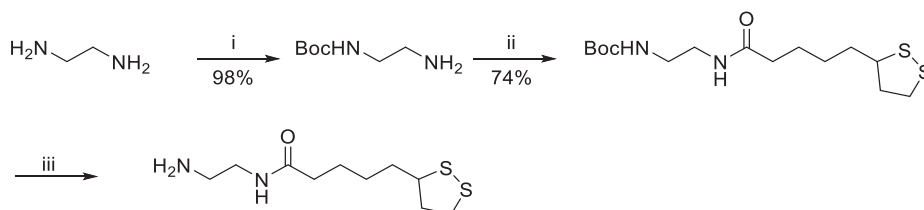


Lipoic acid-TEG-amine (25)

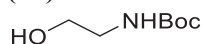
The following protocol was adapted from the procedure reported by Yuan Guo et al²³⁰. To a solution of azide-TEG-LA (**24**) (210 mg, 517 μmol , 1 equiv) in THF (15 mL) was added PPh_3 (190 mg, 724 μmol , 1.4 equiv). The reaction mixture was stirred for 1 hr at 23°C before the addition of aq. HCl 5% (1 mL). The reaction mixture was stirred for 16 hr at 23°C. THF was then removed in vacuo and water (8 mL) was added to the aqueous phase. The aqueous phase was then washed with a mixture EtOAc:PE = 1:1 (3 x 5 mL) and co-evaporated with toluene in vacuo to afford **25** as a yellow oil which was used without further purification. The analytical data were in agreement with literature report.

HRMS (ESI/QTOF) m/z: $[\text{M} + \text{H}]^+$ Calcd for $\text{C}_{16}\text{H}_{33}\text{N}_2\text{O}_4\text{S}_2^+$ 381.1876; Found 381.1877.

Ethylenediamine derivatization



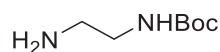
Scheme 18: Derivatization of lipoic acid with ethylene diamine. Reagents and conditions: i- Boc_2O , 23°C, 12 hr; ii- lipoic acid, EDCI, HOBt, DIPEA, 23°C, 12 hr; iii- TFA, 0°C to 23°C 1.5 hr.

tert-Butyl 2-hydroxyethylcarbamate (52)

The following protocol was adapted from the procedure reported by Becht et al.²³¹ To a solution of ethanolamine (2.98 g, 16.4 mmol, 1.2 equiv) in anhydrous DCM (16 mL) was added dropwise a solution of Boc_2O (2.92 mL, 13.6 mmol, 1 equiv) in anhydrous DCM (5 mL). The solution was stirred for 12 hr at 23°C. The reaction mixture was washed with sat. aq. NaHCO_3 (3 x 15 mL). The organic layer was dried over MgSO_4 and concentrated in vacuo. The product was purified by FCC (EtOAc:PE = 1:1) to afford **52** as a transparent oil (1.86 g, 11.54 mmol, 85%). The analytical data were in agreement with literature report.

^1H NMR (400 MHz, CDCl_3) δ 5.11 (s, 1H, NH), 3.66 (t, $J = 5.1$ Hz, 2H, $\text{CH}_2\text{-O}$), 3.25 (t, $J = 5.1$ Hz, 2H, $\text{CH}_2\text{-N}$), 2.97 (s, 1H, OH), 1.42 (s, 9H, 3 x CH_3).

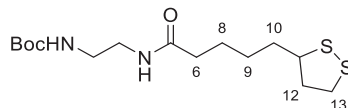
MS (ESI/QTOF) m/z: $[\text{M} + \text{Na}]^+$ Calcd for $\text{C}_8\text{H}_{19}\text{N}_4\text{O}_3^+$ 184.09; Found 184.12

¹H NMR spectrum of **52**N-Boc-ethylenediamine (**10**)

The following protocol was adapted from the procedure reported by Liu et al.⁵. A solution of Boc₂O (7.26 g, 33.28 mmol, 1 equiv) in DCM (300 mL) was added dropwise to a solution of ethylenediamine (12 g, 199.70 mmol, 6 equiv) in DCM (100 mL). The solution was stirred for 12h at 23°C. The volume of the solution was reduced to 20 mL. The mixture was then with sat. aq. Na₂CO₃ (2 x 100 mL). The organic layer was dried over MgSO₄ and concentrated in vacuo to afford N-Boc-Ethylenediamine (**10**) as a colorless oil (5.23 g, 32.64 mmol, 98%).

¹H NMR (400 MHz, CDCl₃) δ 5.05 (s, 1H, NH), 3.11 (q, J = 6.0 Hz, 2H, CH₂-NHBoc), 2.74 (t, J = 5.9 Hz, 2H, CH₂-NH₂), 1.39 (s, 9H, 3 x CH₃).

MS (ESI/QTOF) m/z: [M+H]⁺ Calcd for C₇H₁₇N₂O₂⁺ 161.13; Found 161.07

¹H NMR spectrum of **10**Lipoic acid-N-Boc-ethylenediamine (**15**)

EDCI (869 mg, 4.54 mmol, 1.15 equiv), HOBt (964 mg, 7.89 mmol, 2 equiv) and DIPEA (1.96 mL, 11.8 mmol, 3 equiv) were added to a solution of lipoic acid (814 mg, 3.94 mmol, 1 equiv) in DMF (10 mL). The reaction mixture was stirred for 15 min under argon atm and N-Boc-ethylenediamine (**10**) (758 mg, 4.73 mmol, 1.2 equiv) in DMF (4 mL) was added. The mixture was stirred for 12 hr at 23°C. DMF was then removed in vacuo and the residue was purified by FCC (EtOAc:PE = 8:2) to afford **15** as a yellow oil (1.02 g, 2.94 mmol, 74%).

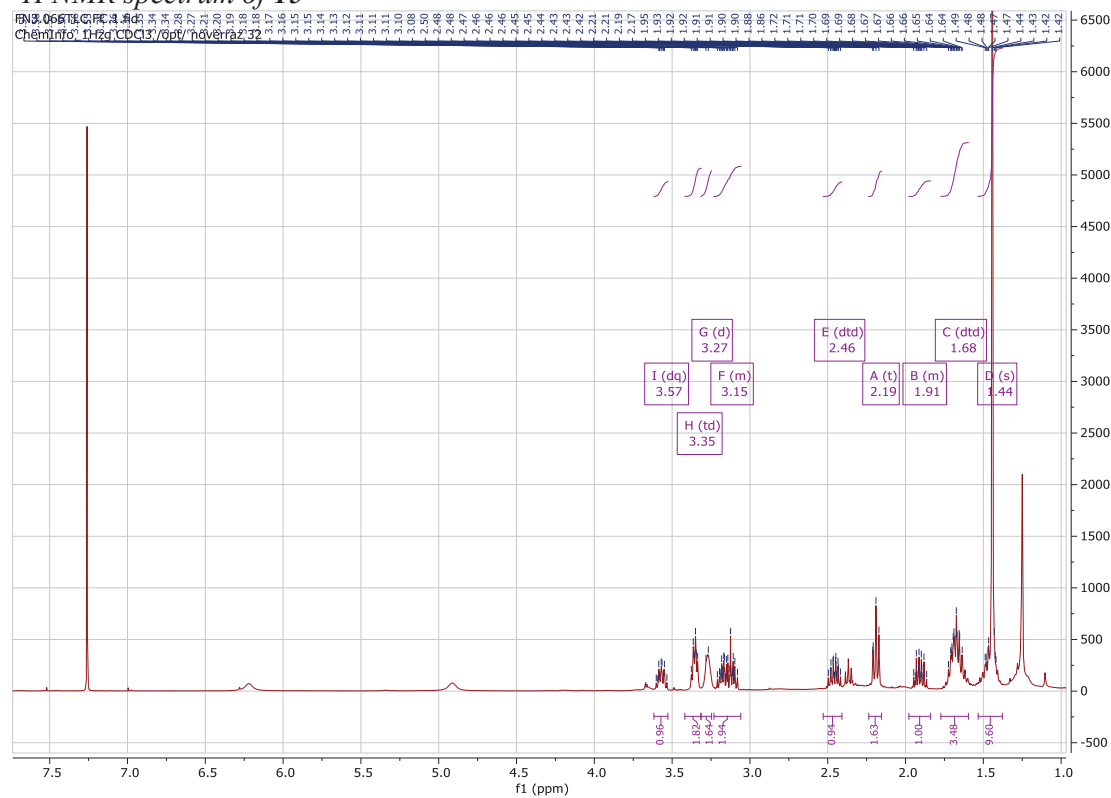
¹H NMR (400 MHz, CDCl₃) δ 3.57 (dq, J = 8.7, 6.4 Hz, 1H, CH-S), 3.35 (td, J = 6.4, 5.5, 4.3 Hz, 2H, CH₂-NHBoc), 3.27 (d, J = 6.1 Hz, 2H, CH₂-NH), 3.23 – 3.06 (m, 2H, CH₂-S), 2.46 (dtd, J = 10.2, 6.6, 5.4 Hz, 1H, (13')), 2.19 (t, J = 7.3 Hz, 2H, CH₂ (6)), 1.98 – 1.84 (m, 1H, (13'')), 1.68 (dtd, J = 15.1, 7.9, 7.2, 4.9 Hz, 4H, 2 x CH₂ (8, 10)), 1.44 (s, 11H, CH₂ (9) + 3 x CH₃).

¹³C NMR (101 MHz, CDCl₃) δ 173.53 (CO), 56.39 (CHS), 40.24 (CH₂ x 2 + CH₂ (12)), 38.48 (CH₂S), 36.40 (6), 34.62 (8), 28.37 (3 x CH₃ Boc), 25.34 (10).

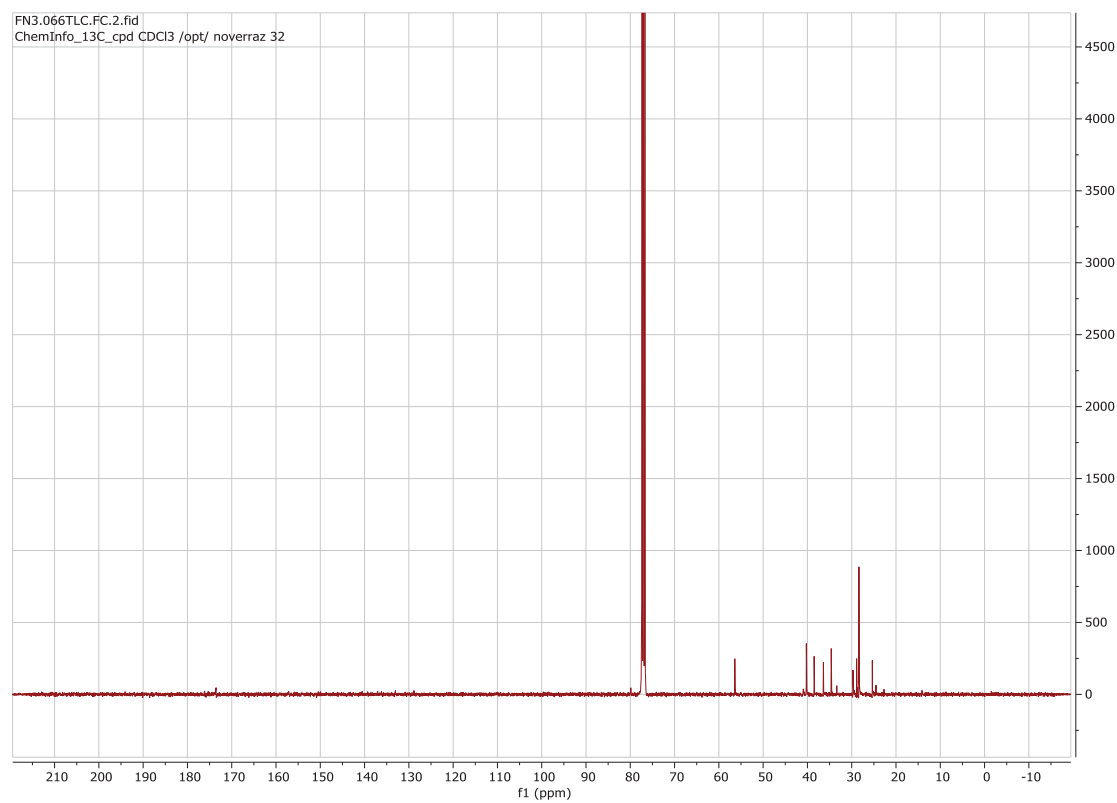
HRMS (ESI/QTOF) m/z: [M + Na]⁺ Calcd for C₁₅H₂₈N₂NaO₃S₂⁺ 371.1434; Found 371.1431

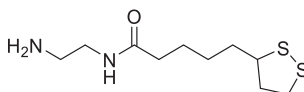
IR (cm⁻¹): 3333, 2930, 1701, 1644, 1518, 1254, 1165

¹H NMR spectrum of **15**

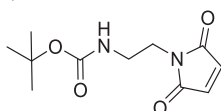


¹³C NMR spectrum of **15**



Lipoic acid-ethylenediamine (16)

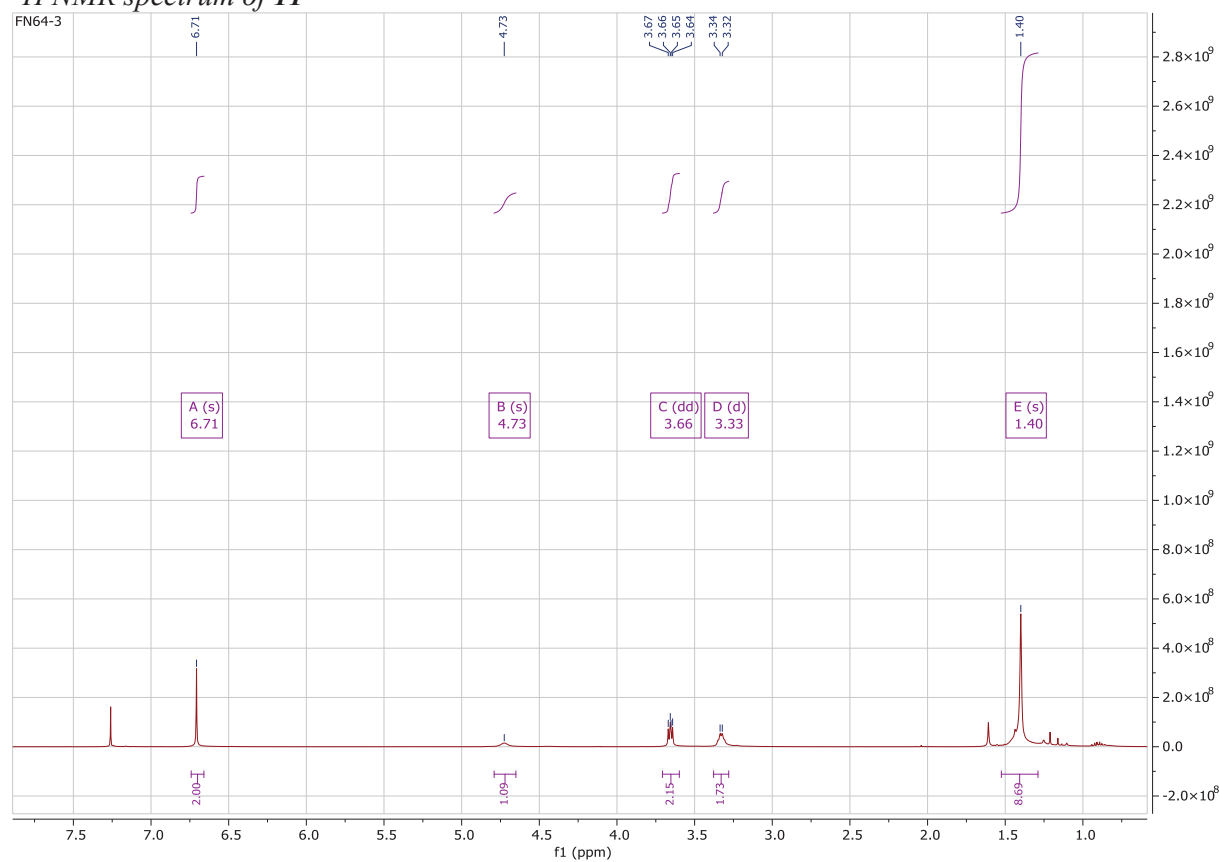
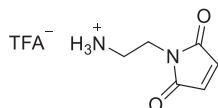
Product **15** (363 mg, 1.04 mmol, 1 equiv) was dissolved in DCM (5 mL) and the solution was cooled to 0°C. TFA (1.24 mL, 16.6 mmol, 16 equiv) was added dropwise and the reaction mixture was allowed to warm up to 23°C for 1.5 hr. The volatiles were removed in vacuo and product **16** was directly engaged in the next step.

N-Boc-(2-Aminoethyl)maleimide (11)

The following protocol was adapted from the procedure reported by Liu et al.⁵ A solution of maleic anhydride (2.67 g, 27.20 mmol, 1 equiv) in ethanol (200 mL) was added dropwise to a solution of *N*-Boc-ethylenediamine (**10**) (5.23 g, 32.64 mmol, 1.2 equiv) and triethylamine (4.55 mL, 32.64 mmol, 1.2 equiv) in ethanol (230 mL), cooled to 0°C. The reaction mixture was stirred for 4 hr. The solvent was removed in vacuo and the residue was dissolved in acetic anhydride (55 mL). Sodium acetate (2.23 g, 27.20 mmol, 1 equiv) was added and the solution was stirred at 60-70°C for 30 min. The reaction mixture was cooled to 23°C and water (50 mL) was added. The solution was extracted with EtOAc (3 x 60 mL). The combined organic layers were washed with sat. aq. NaHCO₃ (2 x 25 mL), dried over MgSO₄ and concentrated in vacuo. The product was purified by FCC (EtOAc:PE = 1:3) to afford **11** as a white solid (4.03 g, 16.79 mmol, 51%). The analytical data were in agreement with literature report.

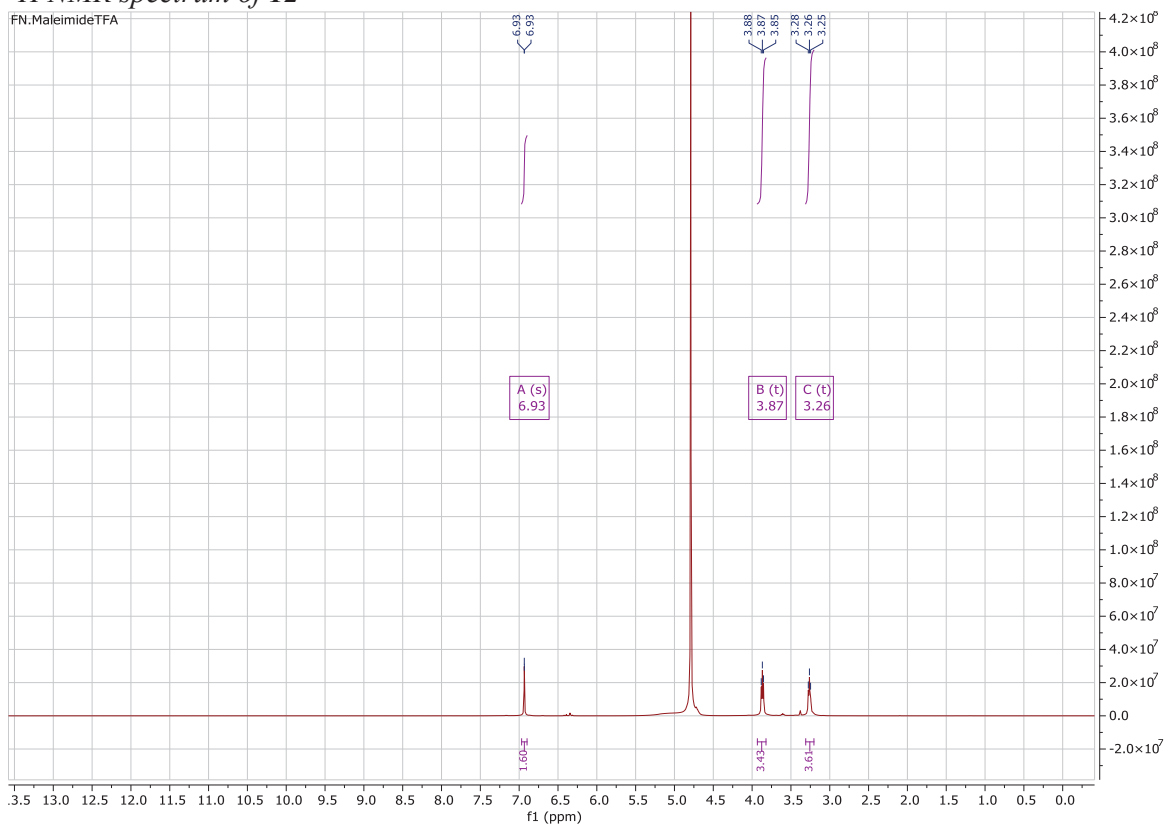
¹H NMR (400 MHz, CDCl₃) δ 6.71 (s, 2H, CH-CH), 4.71 (s, 1H, NH), 3.66 (m, 2H, CH₂-N), 3.33 (m, 2H, CH₂-NH), 1.40 (s, 9H, 3 x CH₃).

MS (ESI/QTOF) m/z: [M+K]⁺ Calcd for C₁₁H₁₆KN₂O₄⁺ 279.07; Found 279.26

¹H NMR spectrum of **11**N-(2-Aminoethyl) maleimide Trifluoroacetate Salt (**12**)

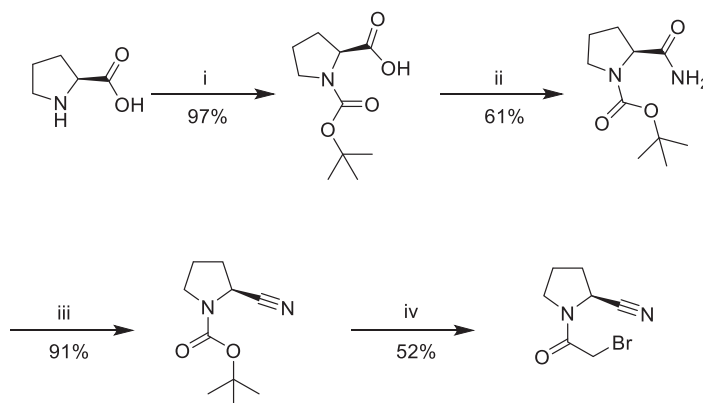
The following protocol was adapted from the procedure reported by Liu et al.⁵ To a solution of **11** (4.03 g, 16.79 mmol, 1 equiv) in DCM (40 mL), cooled to 0°C, was added trifluoroacetic acid (20.15 mL) and the reaction mixture was stirred for 1 hr. DCM was evaporated in vacuo and the residue was dissolved in methanol (12 mL). Precipitation with diethyl ether (200 mL), followed by filtration afforded **12** as a white solid (3.956 g, 16.54 mmol, quant.). The analytical data were in agreement with literature report.

¹H NMR (400 MHz, D₂O) δ 6.93 (s, 2H, CH=CH), 3.87 (t, *J* = 5.8 Hz, 2H, CH₂), 3.26 (t, *J* = 5.8 Hz, 2H, CH₂).

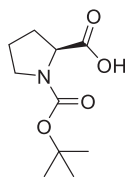
¹H NMR spectrum of 12

5.4 FAP-ALPHA INHIBITOR BLOCK 1

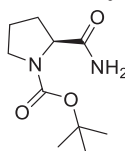
The synthesis of FAP- α inhibitor backbone was performed following the procedure described in Passemard. S doctoral thesis¹⁹⁹ with minor modifications.



Scheme 19: Synthesis of the cyano-pyrrolidine block. Reagents and conditions. i- Boc_2O , Et_3N , DCM , 23°C , 16 hr; ii- HOBt , EDCI , NH_3 , THF , 23°C , 16 hr; iii- TFAA , Et_3N , DCM , 0°C to 23°C , 16 hr; iv- 2-bromoacetyl bromide, MeCN , reduced pressure, 23°C , 1 hr

(S)-tert-Butyl 2-carbamoylpyrrolidine-1-carboxylate (1)

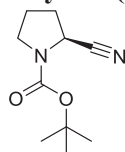
To a cooled suspension (0°C) of L-proline (10 g, 86.86 mmol, 1 equiv) in chloroform (330 mL), Boc₂O (19.90 mL, 91.20 mmol, 1.05 equiv) and NEt₃ (15.75 mL, 112.92 mmol, 1.3 equiv) were added dropwise. The reaction mixture was stirred for 16 hr at 23°C. The solution was washed with aq. HCl 1N (3 x 100 mL). The organic phase was dried over MgSO₄ and evaporated in vacuo to afford **1** as a white solid (18.2 g, 84.55 mmol, 97%). The product was used for the next step without purification.

(S)-tert-Butyl 2-carbamoylpyrrolidine-1-carboxylate (2)

To a solution of **1** (15 g, 69.69 mmol, 1 equiv) in THF (500 mL) were added HOBt (10.73 g, 69.69 mmol, 1 equiv) and EDCI (15.36 g, 80.14 mmol, 1.15 equiv). The solution was stirred at 23°C for 30 min and aq. ammonia 25 % (5.72 mL, 76.65 mmol, 1.1 equiv) was added dropwise. The mixture was stirred for an additional 16 hr at 23°C. The volatiles were evaporated in vacuo and the residue was dissolved in EtOAc (200 mL). The solution was washed with sat. aq. NaHCO₃ (200 mL), brine (200 mL), dried over MgSO₄ and evaporated in vacuo to afford **2** as a yellowish oil (9.2 g, 42.94 mmol, 61%).

¹H NMR (400 MHz, CDCl₃) δ 5- 4.62 (s, 1H, COOH), 4.40 - 4.17 (m, 1H, N-CH), 3.65 - 3.23 (m, 2H, N-CH₂), 2.14-1.80 (m, 4H, CH₂-CH₂), 1.56 – 1.33 (m, 9H, 3 x CH₃).

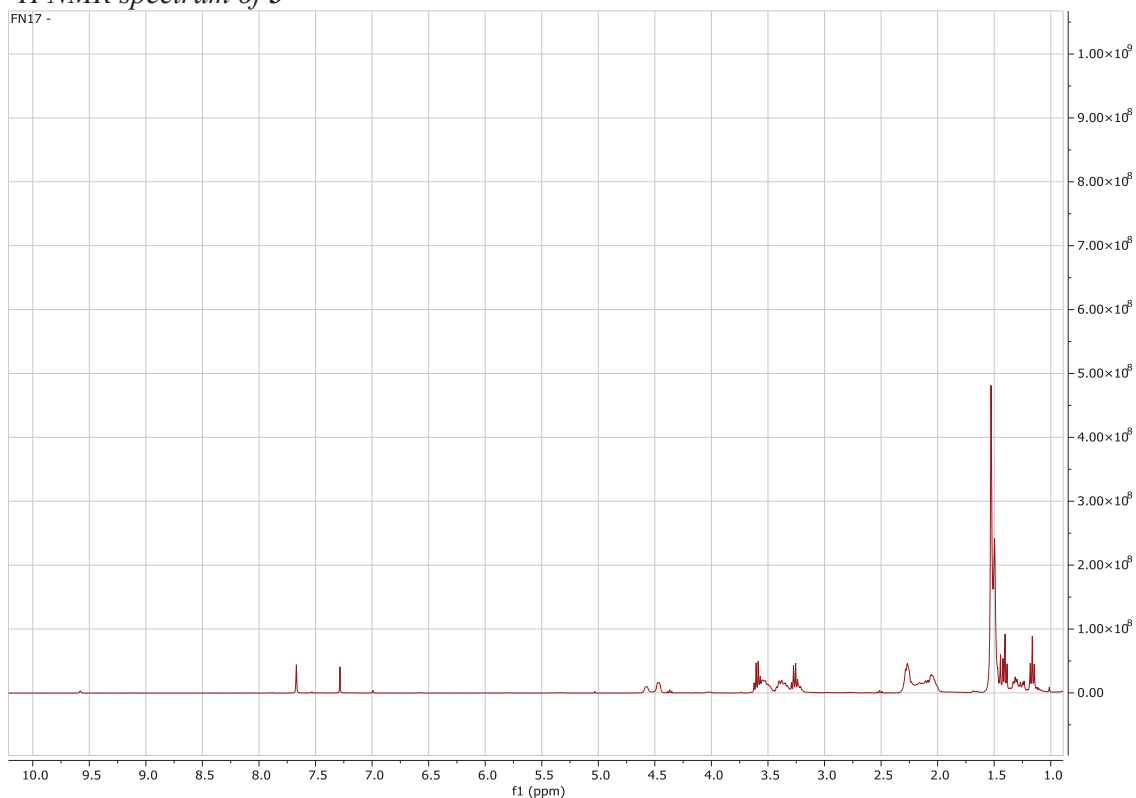
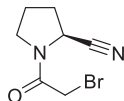
ESI-MS m/z: [M + Na]⁺ Calcd for C₁₀H₁₈N₂NaO₃⁺ 237.12; Found 237.08

(S)-tert-Butyl 2-cyanopyrrolidine-1-carboxylate (3)

To a cooled suspension (0°C) of **2** (9 g, 42.00 mmol, 1 equiv) and NEt₃ (25.52 mL, 189.02 mmol, 4.5 equiv) in DCM (200 mL), was added TFAA (11.68 mL, 84.01, 2 equiv) dropwise. The solution was allowed to warm up to 23°C and was stirred for 12 hr. The reaction mixture was washed with water (100 mL), aq. 0.5 M HCl (100 mL) and sat. aq. NaHCO₃ (100 mL). The organic phase was dried over MgSO₄ and evaporated in vacuo to afford **3** as a yellowish oil (38.22 mmol, 7.5 g, 91 %).

¹H NMR (400MHz, CDCl₃) δ 4.58 – 4.40 (m, 1H, N-CH), 3.61 – 3.14 (m, 2H, N-CH₂), 2.30–1.94 (m, 4H, CH₂-CH₂), 1.48 (m, 9H, 3 x CH₃).

ESI-MS m/z: [M + Na]⁺ Calcd for C₁₀H₁₆N₂NaO₂⁺ 219.11; Found 219.08

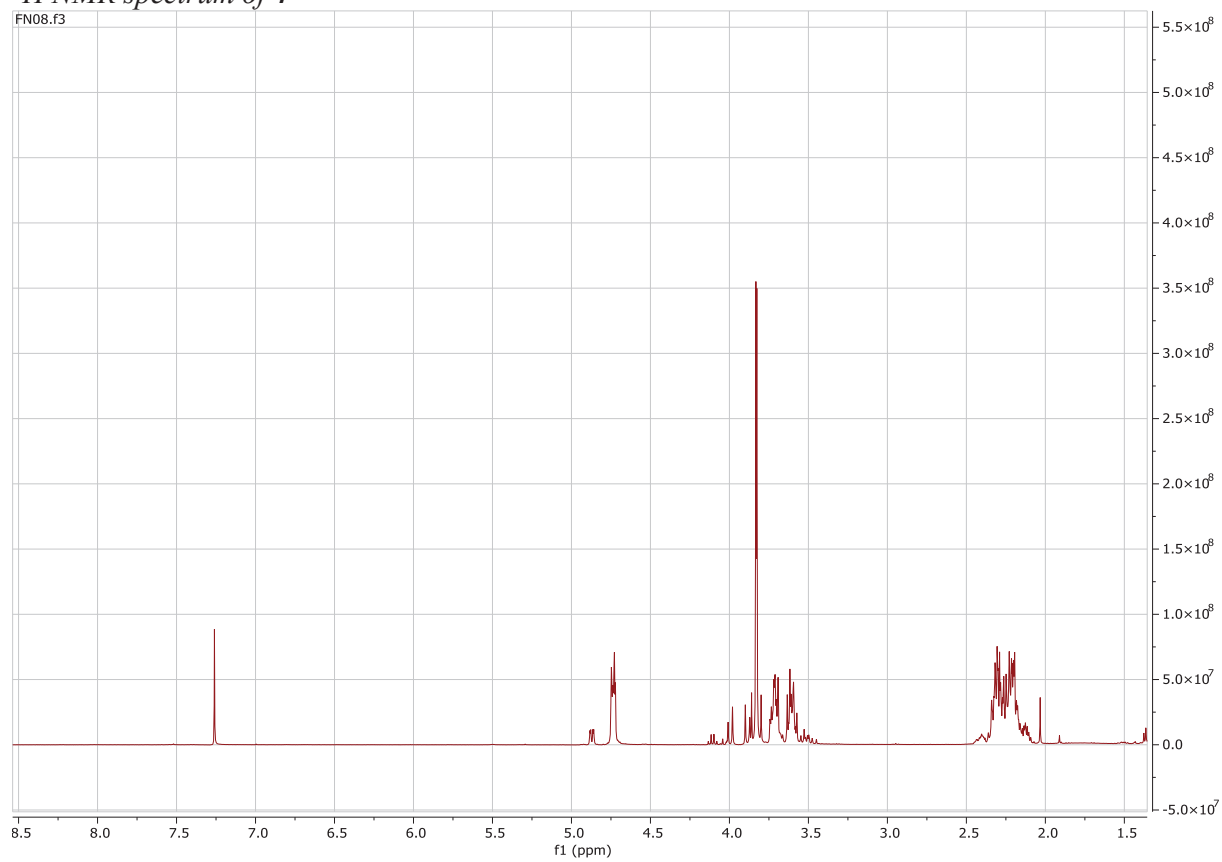
¹H NMR spectrum of **3****(S)**-1-(2-bromoacetyl) pyrrolidine-2-carbonitrile (**4**)

To a solution of **3** (7.5 g, 38.22 mmol, 1 equiv) in MeCN (75 mL) was added 2-bromoacetyl bromide (6.66 mL, 76.43 mmol, 2 equiv) and the pressure of the flask was reduced to 500 mbar. The mixture was stirred for 1 hr at 23°C and the volatiles were removed in vacuo. The product was purified by FCC (Pe:EtOAc = 6:4) to afford **4** as a yellowish oil (4.9 g, 19.99 mmol, 52%).

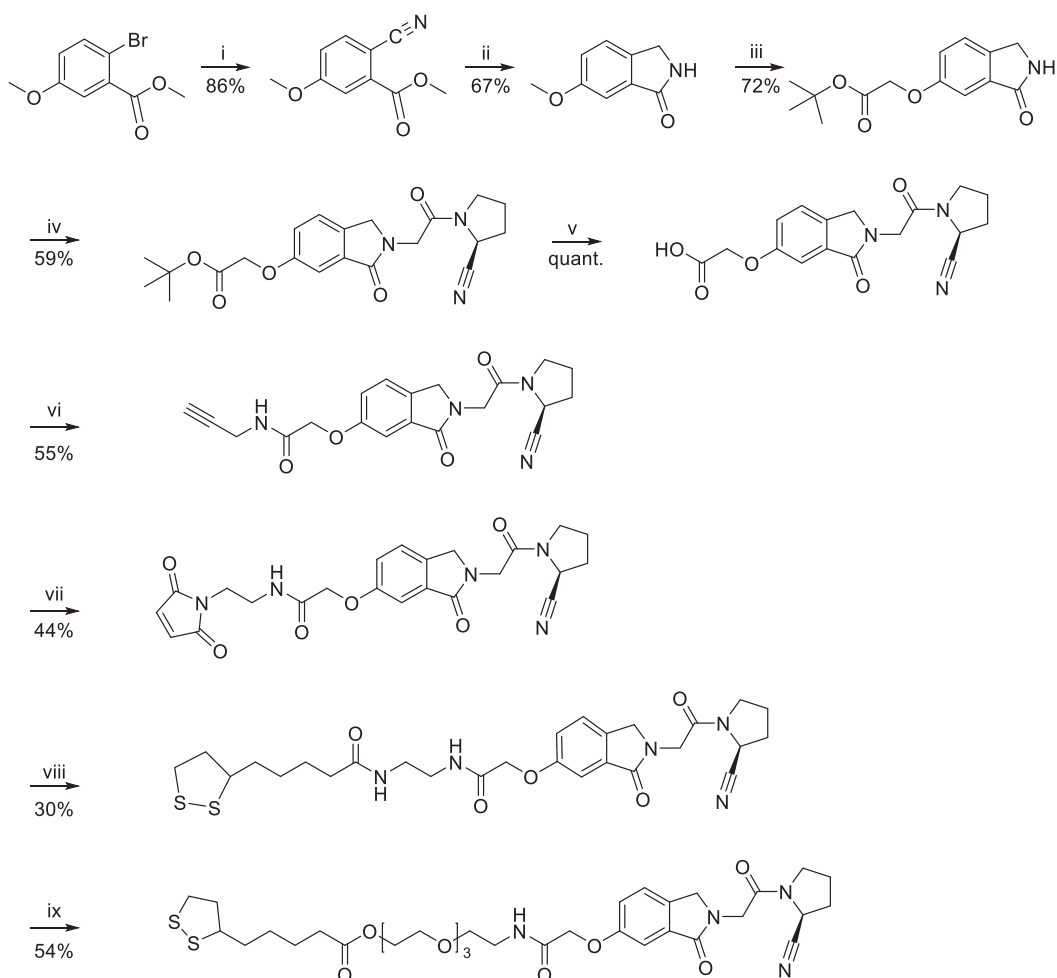
¹H NMR (400 MHz, CDCl₃) δ 4.91 – 4.69 (m, 1H, N-CH), 3.83 (s, 2H, Br-CH₂), 3.76 – 3.56 (m, 2H, N-CH₂), 2.35 – 2.15 (m, 4H, CH₂-CH₂).

ESI-MS m/z: [M + Na]⁺ Calcd for C₇H₉BrN₂NaO⁺ 238.99; Found 239.03

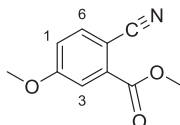
¹H NMR spectrum of **4**



5.5 FAP-ALPHA INHIBITOR BLOCK 2



Scheme 20 : Synthesis of FAP- α inhibitor derivative. Reagents and conditions: i- 1) CuCN, DMF, 140°C, 30 min, 2) KCN, H₂O, 50°C, 1 hr; ii- Ni raney, H₂, MeOH, 23°C, 16 hr; iii- 1) MsOH, methionine, 85°C, 16 hr, 2) tert-butyl bromoacetate, NaOH, TBAB, H₂O, DMF/DCM, 23°C, 16 hr; iv- LiHMDS, 0°C, **18**, THF, 23°C, 16 hr; v- SiO₂, toluene, reflux, 60 min; vi- HOBt, EDCl, DIPEA, propargylamine, 23°C, 12 hr; vii- TBTU, DIPEA, **14**, THF, 23°C, 16 hr; viii- EDCl, HOBt, DIPEA, **12**, 23°C, 16 hr; ix- TBTU, HOBt, DIPEA, **8**, 23°C, 16 hr

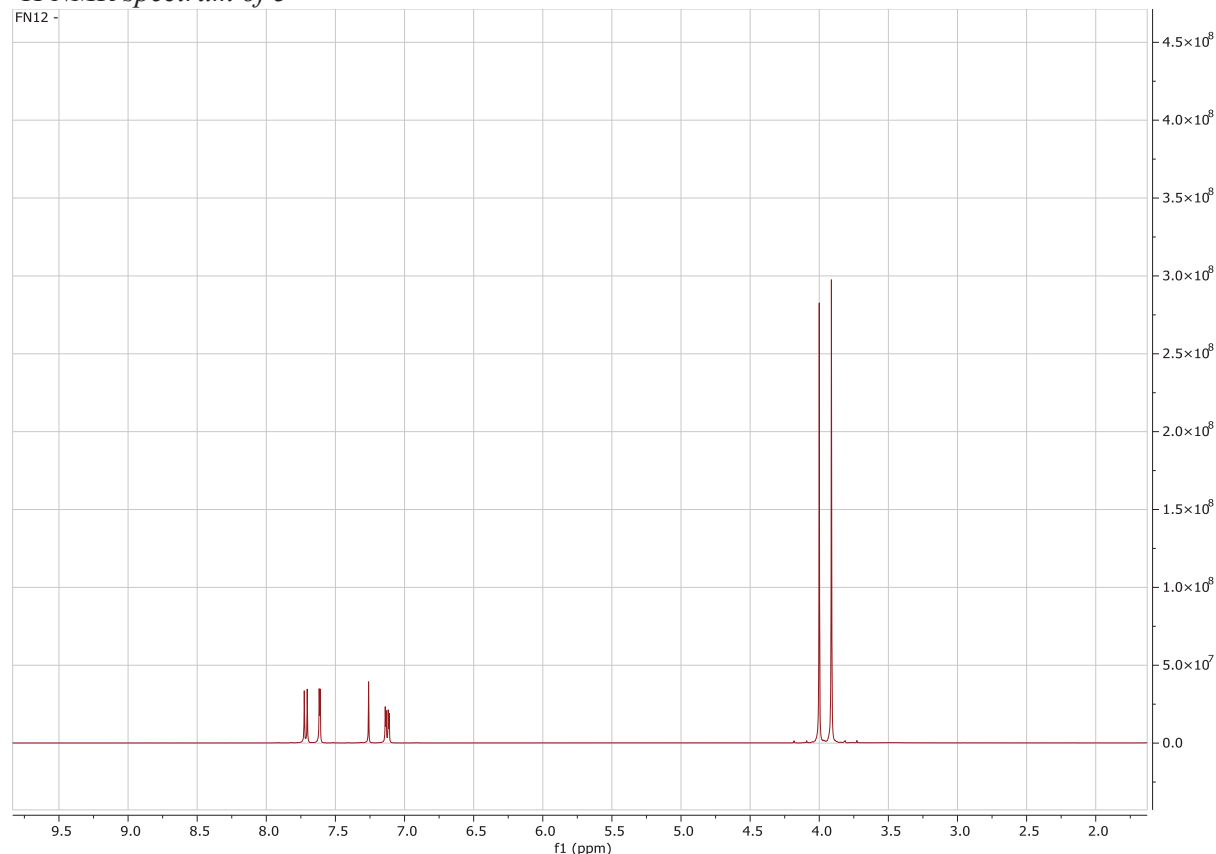
Methyl 2-cyano-5-methoxybenzoate (**5**)

CuCN (4.75 g, 53.05mmol, 1.3 equiv) was added to a solution of methyl 2-bromo-5-methoxybenzoate (10 g, 40.80 mmol, 1 equiv) in DMF (40 mL) and the reaction mixture was stirred for 30 min at 140°C. The mixture was cooled to 23°C and cold water (60 mL) was added. The resulting precipitate was filtered and dissolved in water (80 mL). KCN (7.97 g, 122.41 mmol, 3 equiv) was added and the mixture was stirred for 1 hr at 50°C. The resulting solid was filtered, washed with water and dissolved in CHCl₃ (100 mL). The solution was dried over MgSO₄ and concentrated in vacuo to afford **5** as a white solid (6.7 g, 35.04 mmol, 86%).

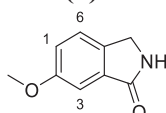
¹H NMR (400 MHz, CDCl₃) δ 7.71 (d, J = 8.6 Hz, 1H, CH_{ar}(6)), 7.62 (s, 1H, CH_{ar}(3)), 7.13 (d, J = 11.3 Hz, 1H, CH_{ar}(1)), 4.00 (s, 3H, CH₃-OCO), 3.91 (s, 4H, CH₃-O).

ESI-MS m/z: $[M + Na]^+$ Calcd for $C_{10}H_9NNaO_3^+$ 214.05; Found 214.04

¹H NMR spectrum of 5



6-Methoxy-2,3-dihydro-1H-isoindol-1-one (6)

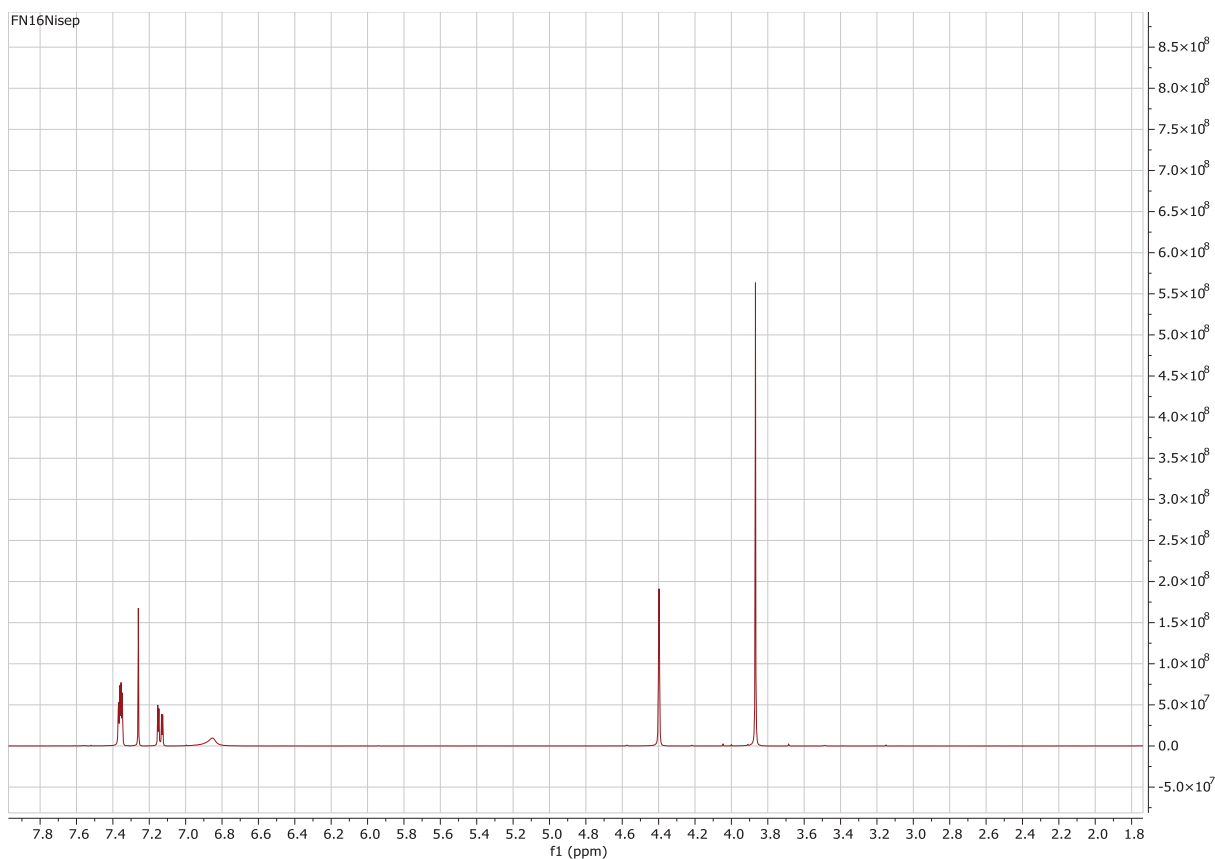


To a solution of **5** (6.7 g, 35.04 mmol, 1equiv) in MeOH (120 mL) under argon atm was added Raney Ni (5 mol %). The argon atm was then replaced by H₂ atm and the mixture was stirred for 16 hr at 23°C. The catalyst was removed by filtration on a pad of celite. Volatiles were removed in vacuo and the crude product was triturated in a minimal amount of EtOAc:isooctane = 1:1 at 60°C. The mixture was cooled to 23°C and the resulting precipitate was filtered and washed with cold EtOAc:isoOctane = 1:2 to afford **6** as a white solid (3.82 g, 23.41 mmol, 67 %).

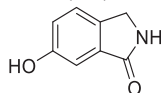
¹H NMR (400 MHz, CDCl₃) δ 7.41 – 7.36 (m, 2H, 3, 2 x CH_{ar}(6, 3)) 7.16 (dd, J = 8.4, 2.4 Hz, 1H, CH_{ar}(1)), 6.88 (s, 1H, NH), 4.42 (s, 2H, CH₂), 3.89 (s, 3H, CH₃).

ESI-MS m/z: $[M + H]^+$ Calcd for $C_9H_{10}NO_2^+$ 164.07; Found 164.08

¹H NMR spectrum of 6

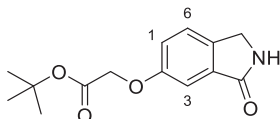


6-Hydroxy-2,3-dihydro-1H-isoindol-1-one (**6b**)



Methionine (42.13mmol, 6.29 g, 1.8 equiv) was added to a solution of **6** (23.41 mmol, 3.82 g, 1 equiv) in MsOH (468.21 mmol, 30.38 mL, 20 equiv) and the mixture was stirred at 85 °C for 16 hr. After cooling to 0 °C, cold water (5°C) was added and the mixture was stirred at 5°C for 1 hr. The resulting solid was recovered by filtration, washed with aq. 1% HCl, water and dried to afford **6b** as a white solid (16.76mmol, 2.5 g, 72%). This product was directly engaged in the next step.

tert-Butyl [(3-oxo-1,2-dihydro-1H-isoindol-5-yl)oxy] (**7**)

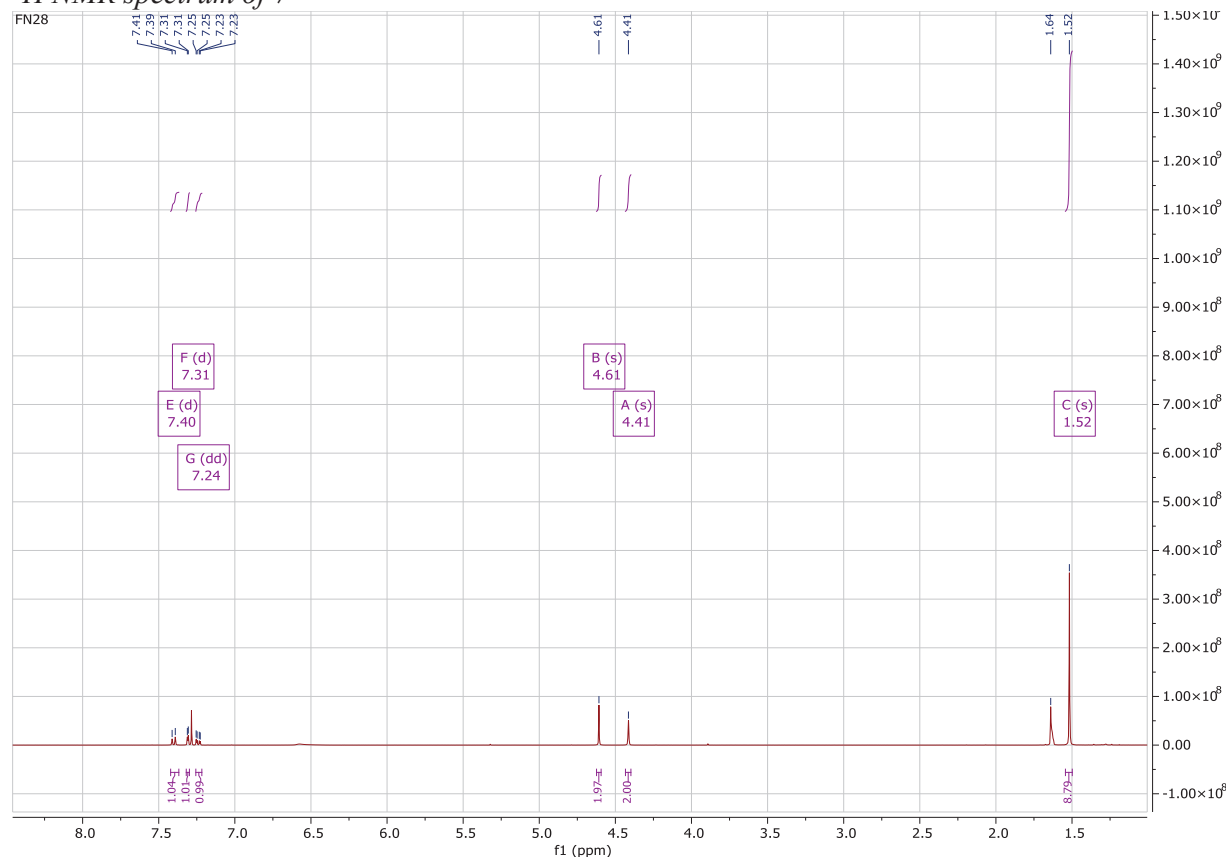


Compound **6b** (2.5 g, 16.76 mmol, 1equiv) was dissolved in DMF:DCM = 1:1 (30 mL). *Tert*-butyl bromoacetate (0.81 g, 18.43, 1.1 equiv), TBAB (0.27 g, 0.84 mmol, 0.05 equiv) and aq. 50% NaOH (1.88 g, 23.47 mmol, 1.4 equiv) were added successively. The mixture was stirred for 16 hr at 22 °C and the product was extracted with DCM (3 x 10 mL). The combined organic phases were dried over MgSO₄ and concentrated in vacuo. Purification by FCC (PE:EtOAc = 1:1) afforded **7** as a white solid (3.45 g, 13.12 mmol, 78%).

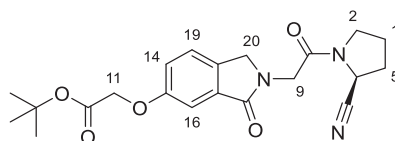
$^1\text{H NMR}$ (400 MHz, CDCl_3) δ 7.38 (d, $J = 8.3$ Hz, 1H, CH_{ar} (6)), 7.28 (d, $J = 2.5$ Hz, 1H, CH_{ar} (3)), 7.22 (dd, $J = 8.3, 2.5$ Hz, 1H, CH_{ar} (1)), 6.40 (s, 1H, NH), 4.58 (s, 2H, OCH_2), 4.39 (s, 3H, CH_2N), 1.49 (s, 9H, 3 x CH_3).

ESI-MS m/z : $[\text{M} + \text{Na}]^+$ Calcd for $\text{C}_{14}\text{H}_{17}\text{NNaO}_4^+$ 286.11; Found 286.17

$^1\text{H NMR}$ spectrum of 7



(*S*)-*tert*-Butyl 2-((2-(2-(2-cyanopyrrolidin-1-yl)-2-oxoethyl)-3-oxoisindolin-5-yl)oxy)acetate (**8**)



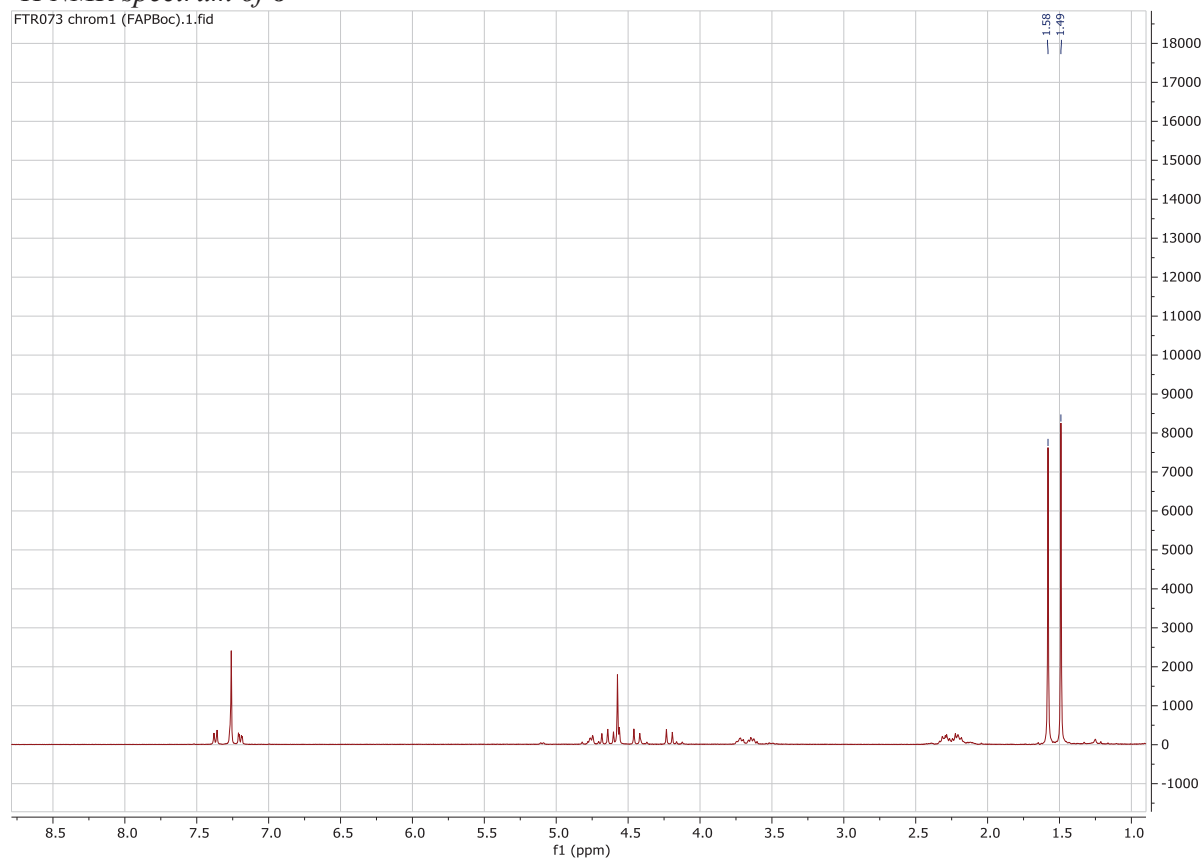
LiHMDS (1M) (4.32 mL, 4.32 mmol, 1.5 equiv) was added to a cooled (0°C) solution of **7** (756.8 mg, 25.88 mmol, 1 equiv) in THF (9 mL). After 30 min, a solution of **4** (811.8 mg, 3.74 mmol, 1.3 equiv) in THF (9 mL) was added dropwise. The mixture was allowed to warmup to 23°C and stirred for 10 hr. Volatiles were removed in vacuo and the residue was purified by FCC (EtOAc:PE = 4:1) to afford **8** as a white solid (683.5 mg, 1.71 mmol, 59%).

$^1\text{H NMR}$ (400 MHz, CDCl_3) δ 7.37 (d, $J = 8.3$ Hz, 1H, CH_{ar} (19)), 7.27 (d, $J = 8.3$ Hz, 1H, CH_{ar} (16)), 7.19 (dd, $J = 8.3, 2.5$ Hz, 1H, CH_{ar} (14)), 4.79 – 4.72 (m, 1H, $\text{CHC}\equiv\text{N}$), 4.57 (s, 2H, CH_2 (11)), 4.44 (d, $J = 16.4$ Hz, 1H, CH_2N (20)), 4.18 (dd, $J = 27.5, 16.1$ Hz, 1H, N- CH_2 (9)), 3.79 – 3.45 (m, 2H, CH_2 (2')), 2.43 – 2.03 (m, 4H, CH_2 (1'), CH_2 (5')), 1.49 (s, 9H, 3 x CH_3).

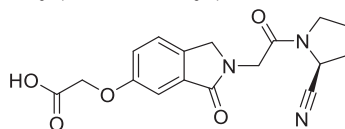
^{13}C NMR (100MHz, CDCl_3) δ 168.8 (8), 167.6 (21), 166.9 (12), 158.2 (15), 134.9 (18), 132.9 (17), 124.0 (19), 120.8 (14), 118.7 (6), 107.4 (16), 82.7 (26), 65.8 (11), 50.5 (20), 46.6 (4), 46.0 (2), 44.6 (9), 29.9 (5), 28.1 (27, 28, 29), 25.3 (1)

HRMS (ESI/QTOF) m/z : $[\text{M} + \text{H}]^+$ Calcd for $\text{C}_{21}\text{H}_{26}\text{N}_3\text{O}_5^+$ 400.1872; Found 400.2500

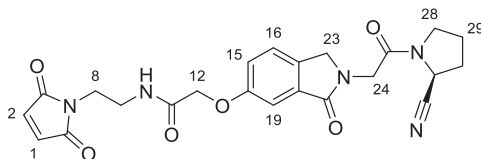
^1H NMR spectrum of **8**



(*S*)-2-((2-(2-(2-cyanopyrrolidin-1-yl)-2-oxoethyl)-3-oxoisindolin-5-yl)oxy)acetic acid (**9**)



Compound **8** (57 mg, 0.14 mmol, 1 equiv) was added to a suspension of silica (0.71 g) in toluene (3 mL). The mixture was stirred at reflux for 1 hr. Celite (150 mg) was added to the reaction mixture and a solution of DCM:MeOH = 4:1 (10 mL) was poured in the reaction mixture. The solids were filtered and rinsed with DCM:MeOH = 4:1 (20 mL). The filtrate was concentrated under reduced pressure to afford the free carboxylic acid (**9**) as a white solid in quantitative yield. This product was directly engaged in the next step.

(S)-2-((2-(2-(2-cyanopyrrolidin-1-yl)-2-oxoethyl)-3-oxoisindolin-5-yl)oxy)-N-(2-(2,5-dioxo-2,5-dihydro-1H-pyrrol-1-yl)ethyl)acetamide (13)

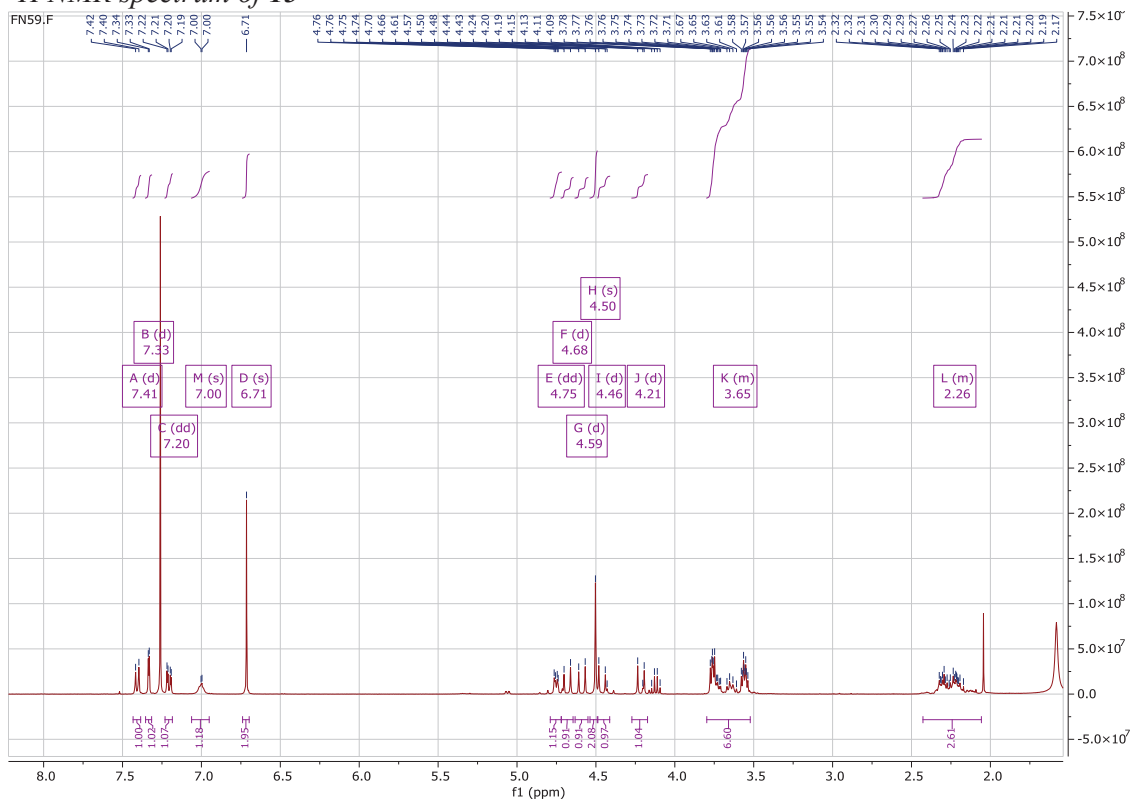
A solution of compound **9** (61 mg, 0.18 mmol, 1 equiv) in THF (5 mL) was cooled to 0°C. DIPEA (0.03 mL, 0.21 mmol, 1.2 equiv) and TBTU (69.35 mg, 0.216 mmol, 1.2 equiv) were added successively and the mixture was stirred for 30 min under Ar atm. A solution of **14** (54.2 mg, 0.21 mmol, 1.2 equiv) and DIPEA (0.03 mL, 0.21 mmol, 1.2 equiv) in THF (3 mL) was added. The mixture was allowed to warmup to 23°C and stirred for 12 hr. The solvent was removed in vacuo and the residue was dissolved in DCM (10 mL), washed with aq. HCl 1% (2 x 5 mL), NaHCO₃ (2 x 5 mL), brine (5 mL) and dried over MgSO₄. DCM was removed in vacuo and the product was purified by FCC (EtOAc:MeOH = 9:1). Further purification was obtained by precipitation in MeOH:DCM = 5:1 and n-pentane to afford (S)-2-((2-(2-(2-cyanopyrrolidin-1-yl)-2-oxoethyl)-3-oxoisindolin-5-yl)oxy)-N-(2-(2,5-dioxo-2,5-dihydro-1H-pyrrol-1-yl)ethyl)acetamide (**13**) (44 mg, 0.095 mmol, 44 %) as a white solid.

¹H NMR (400MHz, CDCl₃) δ 7.45 (d, J = 8.3 Hz, 1H, CH_{ar}(16)), 7.31 (d, J = 2.4 Hz, 1H, CH_{ar}(19)), 7.23 (dd, J = 8.3, 2.5 Hz, 1H, CH_{ar}(15)), 6.73 (s, 2H, CH-CH (1, 2)), 4.76 – 4.71 (m, 1H, CH-CN (31)), 4.56 - 4.52 (s, 2H, CH₂ (12)), 4.48 (m, 2H, CH₂-N (23)), 4.38 (d, J = 17.0 Hz, 1H, CH₂-N (24)), 3.75 (dt, J = 6.3, 3.7 Hz, 1H, CH₂-N (28')), 3.72 – 3.67 (m, 2H, CH₂-N (8)), 3.62 (td, J = 8.6, 8.0, 3.0 Hz, 1H, CH₂-N (28'')), 3.51 – 3.45 (m, 2H, CH₂-N (9)), 2.25 (m, 4H, CH₂-CH₂ (29, 30)).

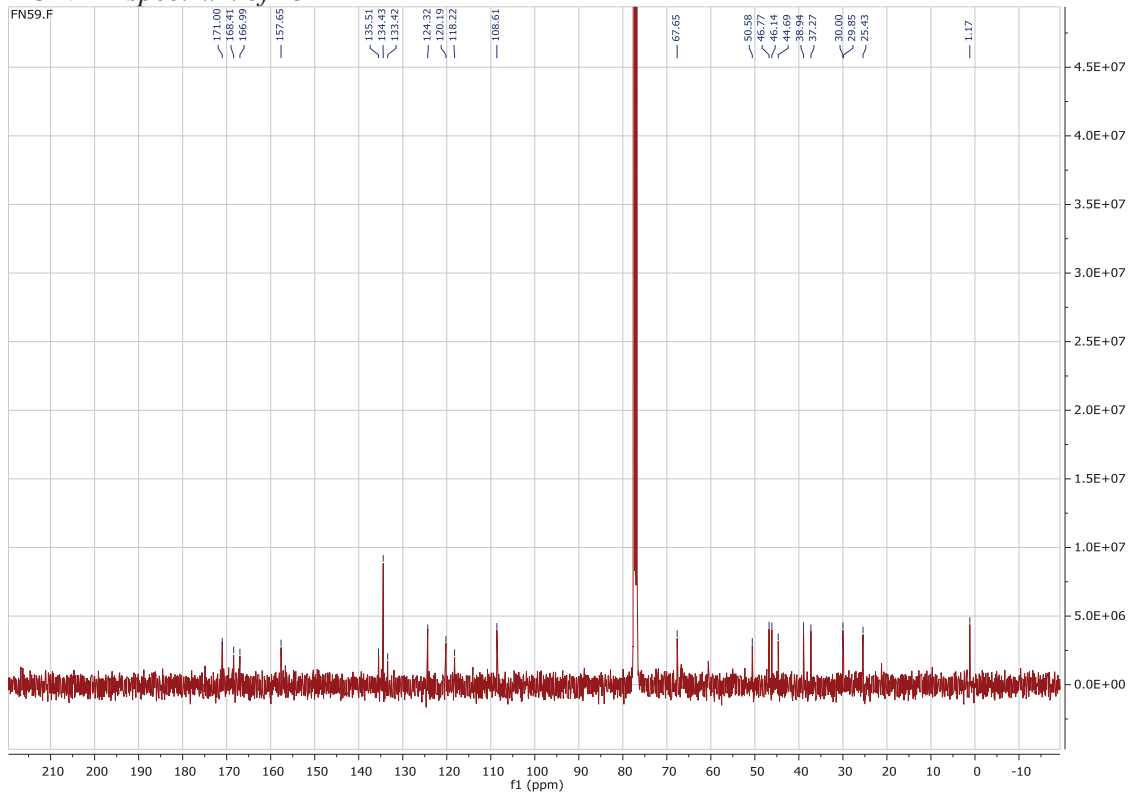
¹³C NMR (100 MHz, CDCl₃) δ 171.2 (3, 5), 169.5 (11), 167.3 (25), 157.8 (20), 135.4, (14), 134.2 (1, 2), 132.8 (17), 124.2 (16), 120.1 (15), 118.0 (18), 108.3 (19), 67.2 (12), 50.7 (23), 46.7 (31), 45.9 (28), 44.5 (24), 38.0 (9), 36.9 (8), 29.7 (30), 25.1 (29).

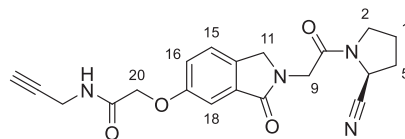
HRMS (ESI/QTOF) m/z: [M + Na]⁺ Calcd for C₂₃H₂₃N₅NaO₆⁺ 488.1546; Found 488.1546

¹H NMR spectrum of 13



¹³C NMR spectrum of 13

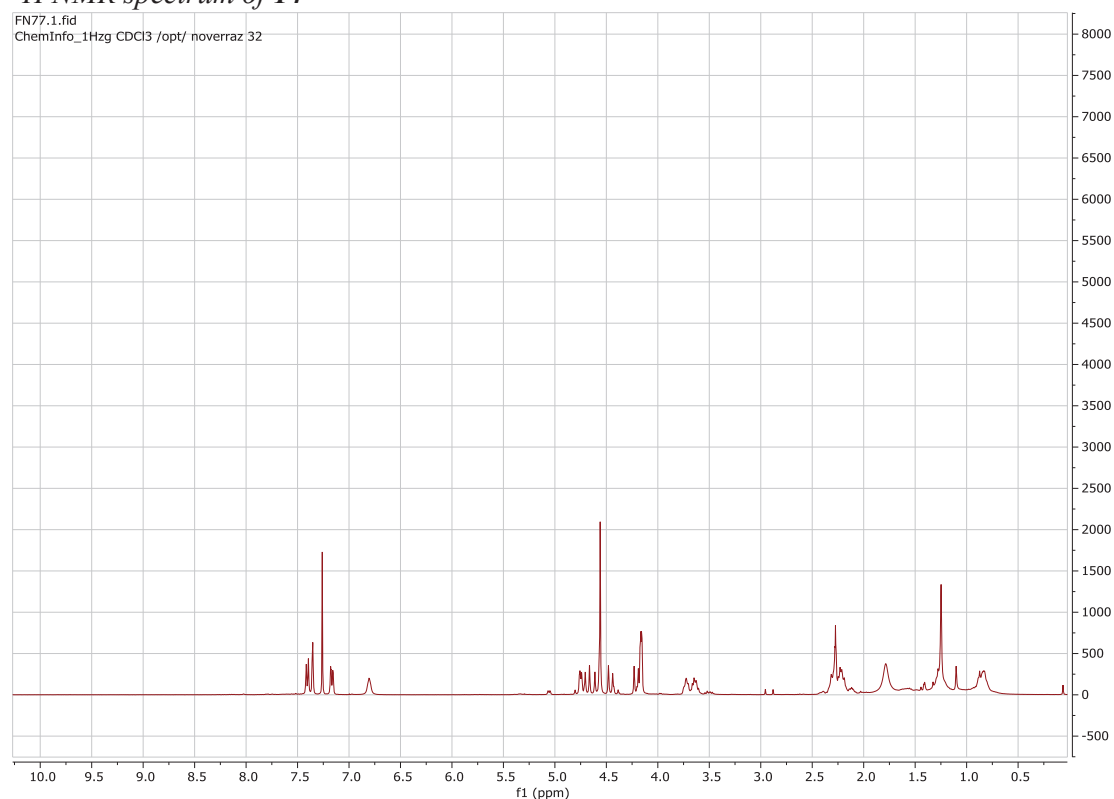


(S)-2-((2-(2-(2-cyanopyrrolidin-1-yl)-2-oxoethyl)-3-oxoisindolin-5-yl)oxy)-N-(prop-2-yn-1-yl)acetamide (14)

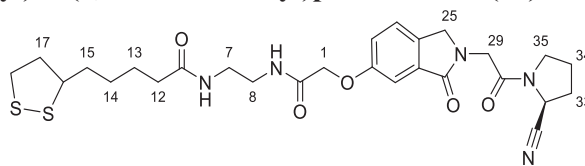
EDCI (31 mg, 0.31mmol, 2 equiv) HOBt (31.3 mg, 0.20 mmol, 1.3 equiv) and DIPEA (0.081 mL, 0.47mmol, 3 equiv) were added to a solution of **9** (54 mg, 0.16 mmol, 1 equiv) in DMF (5 mL). The reaction mixture was stirred for 15 min under Ar atm. Propargylamine (0.03mL, 0.47 mmol, 3 equiv) was added and the mixture was stirred for 12 hr at 23°C. DMF was removed in vacuo and the residue was purified by FCC (DCM:MeOH = 50:1 → 25:1) to afford (S)-2-((2-(2-(2-cyanopyrrolidin-1-yl)-2-oxoethyl)-3-oxoisindolin-5-yl)oxy)-N-(prop-2-yn-1-yl)acetamide (**14**) as a white solid (30 mg, 0.079mmol, 55 %).

¹H NMR (400 MHz, CDCl₃) δ 7.41 (d, J = 8.4 Hz, 1H, CH_{ar} (15)), 7.36 (d, J = 2.5 Hz, 1H, CH_{ar} (18)), 7.17 (dd, J = 8.2, 2.5 Hz, 1H, CH_{ar} (16)), 6.77 (s, 1H, 13), 4.76 (d, J = 7.2 Hz, 1H, CH-CN), 4.73 – 4.61 (m, 1H, 9', 20), 4.57 (s, 2H, CH₂-O (11)), 4.47 (d, J = 16.5 Hz, 1H, CH₂-CCH (24)), 4.22 – 4.13 (m, 1H, CCH), 3.79 – 3.54 (m, 2H, NCH₂ (2)), 2.47 – 2.03 (m, 3H, CH₂-CH₂ (1, 5)).

HRMS (ESI/QTOF) m/z: [M + Na]⁺ Calcd for C₂₀H₂₀N₄NaO₄⁺ 403.1377; Found 403, 1382

¹H NMR spectrum of 14

N-(2-(2-((2-(2-((S)-2-cyanopyrrolidin-1-yl)-2-oxoethyl)-3-oxoisindolin-5-yl)oxy)acetamido)ethyl)-5-(1,2-dithiolan-3-yl)pentanamide (17)



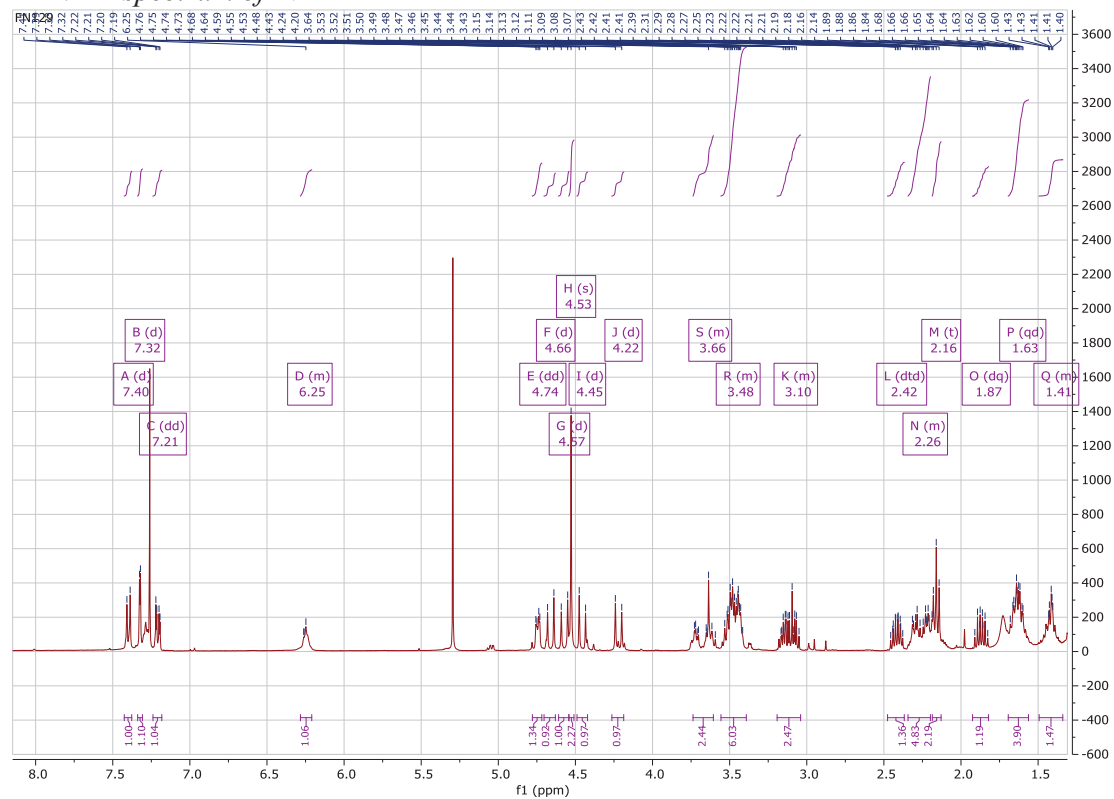
Compound **9** (0.200 g, 0.58 mmol, 1 equiv) was dissolved in DMF (10 mL) and DIPEA (0.29 mL, 1.75 mmol, 3 equiv), EDCI (128 mg, 0.670 mmol, 1.15 equiv) and HOBt (179 mg, 1.17 mmoles, 2 eq.) were added successively. The reaction mixture was stirred for 30 min under Ar atm. A solution of **16** (199 mg, 0.699 mmol, 1.2 equiv) in DMF (7 mL) was added and the reaction mixture was stirred for 12 hr. The solvent was then removed in vacuo and the residue was dissolved in DCM (10 mL) and washed with water (3 x 10 mL), brine (1 x 10 mL) and dried over MgSO₄. The DCM was then removed in vacuo and the product was purified by FCC (DCM:MeOH = 20:1) to afford **17** as a pale yellow solid (0.106 g, 0.18 mmol, 30%)

¹H NMR (400 MHz, CDCl₃) δ 7.40 (d, J = 8.4 Hz, 1H, CH_{ar}), 7.32 (d, J = 2.5 Hz, 1H, CH_{ar}), 7.21 (dd, J = 8.3, 2.5 Hz, 1H, CH_{ar}), 6.28 – 6.21 (m, 1H, NH), 4.74 (dd, J = 7.5, 2.8 Hz, 1H, CH-CN), 4.66 (d, J = 16.5 Hz, 1H, (25')), 4.57 (d, J = 16.6 Hz, 1H, (35')), 4.53 (s, 2H, (1)), 4.45 (d, J = 16.5 Hz, 1H, (25'')), 4.22 (d, J = 16.6 Hz, 1H, (35'')), 3.74 – 3.61 (m, 2H, (29)), 3.56 – 3.39 (m, 4H, (7+8)), 3.19 – 3.04 (m, 2H, CH₂-S), 2.42 (dtd, J = 12.9, 6.6, 5.3 Hz, 1H, (17')), 2.34 – 2.20 (m, 4H, (33 + 34)), 2.16 (t, J = 7.5 Hz, 2H, (12)), 1.87 (dq, J = 12.7, 6.9 Hz, 1H, (17'')), 1.63 (qd, J = 7.7, 7.2, 2.4 Hz, 4H, (15 + 13)), 1.49 – 1.34 (m, 2H, (14)).

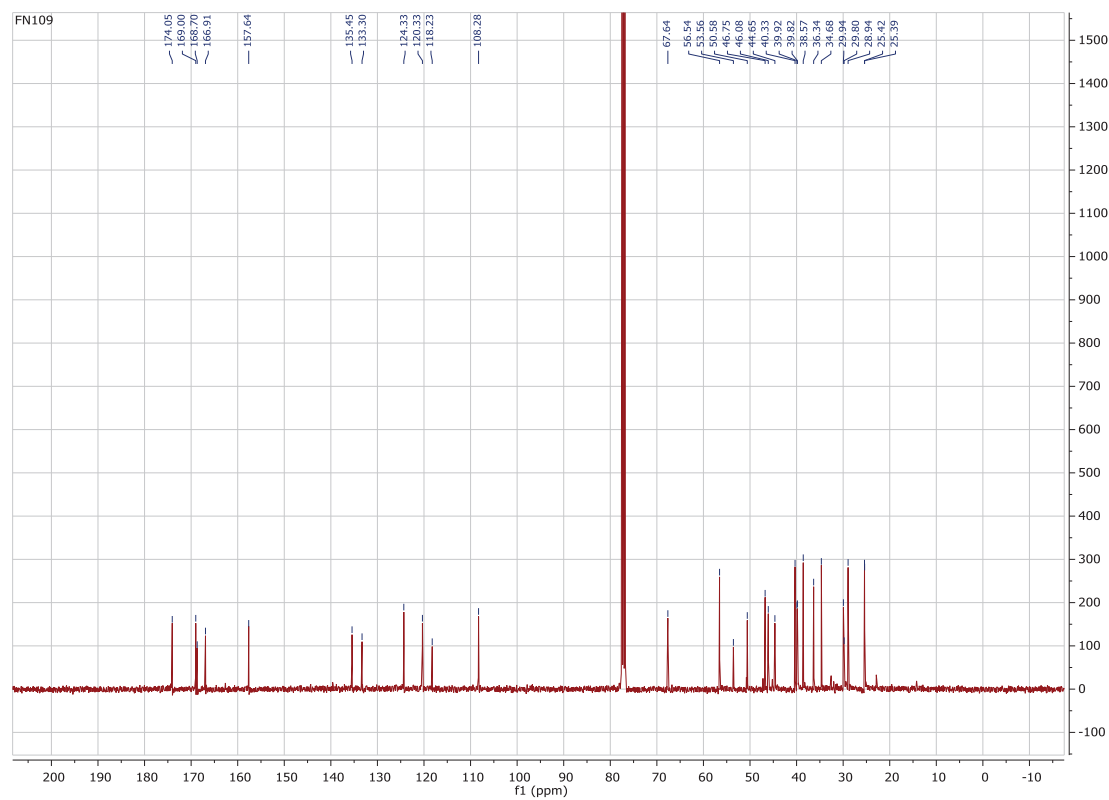
¹³C NMR (101 MHz, CDCl₃) δ 174.05(CO), 169.00 (CO), 168.70 (CO), 166.91 (CO), 157.64 (O-C_{ar}), 135.45 (C_{ar}), 133.30 (C_{ar}), 124.33 (C_{ar}), 120.33 (C_{ar}), 118.23 (CN), 108.28 (C_{ar}), 67.64 (1), 56.54 (CHS), 50.58 (25), 46.75 (CH-CN), 46.08 (29), 44.65 (35), 40.33 (17), 39.92 (7), 39.82 (8), 38.57 (CH₂S), 36.34 (12), 34.68 (15), 29.94 (33), 28.94 (14), 25.42 (13), 25.39 (34).

HRMS m/z: [M+H]⁺ Calcd for C₂₇H₃₆N₅O₅S₂⁺ 574.2152; Found 574.2151

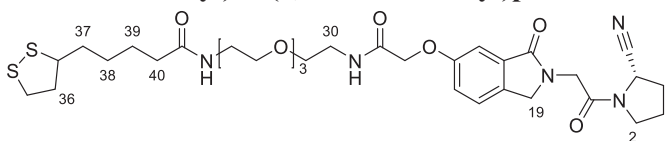
¹H NMR spectrum of 17



¹³C NMR spectrum of 17



N-(1-((2-(2-((S)-2-cyanopyrrolidin-1-yl)-2-oxoethyl)-3-oxoisindolin-5-yl)oxy)-2-oxo-6,9,12-trioxa-3-azatetradecan-14-yl)-5-(1,2-dithiolan-3-yl)pentanamide (26)



Compound **9** (0.200 g, 0.58 mmol, 1 equiv) was dissolved in DMF (5 mL) and DIPEA (0.29 mL, 1.75 mmol, 3 equiv), TBTU (0.374 g, 1.17 mmol, 2 equiv) and HOBt (0.107 g, 0.699 mmol, 1.2 equiv) were added successively. The reaction mixture was stirred for 30 min under Ar atm and a solution of **25** (0.266 g, 0.7 mmol, 1.2 equiv) in DMF (6 mL) was added. The reaction mixture was stirred for 12 hr and the solvent were removed in vacuo. The residue was purify by FCC (EtOAc → DCM:MeOH = 10:1). To afford the desired product (**26**) as a yellowish oil (0.220 g, 0.316 mmol, 54%)

¹H NMR (400 MHz, CDCl₃) δ 7.45 (d, J = 8.3 Hz, 1H, CH_{ar}), 7.41 (d, J = 2.5 Hz, 1H, CH_{ar}), 7.20 (dd, J = 8.3, 2.5 Hz, 1H, CH_{ar}), 7.05 (d, J = 8.9 Hz, 1H, NH (29)), 6.21 (s, 1H, NH (31)), 4.81 – 4.77 (m, 1H, CH-CN), 4.72 (d, J = 16.4 Hz, 1H, (19'')), 4.62 (d, J = 18.3 Hz, 3H, (2') + (NOC-CH₂-O)), 4.51 (d, J = 16.4 Hz, 1H, (19'')), 4.26 (d, J = 16.5 Hz, 1H, 2''), 3.84 – 3.55 (m, 17H, CH₂ TEG + CH-S + CH₂ (9)), 3.47 (q, J = 5.2 Hz, 2H, CH₂ (30)), 3.25 – 3.10 (m, 2H, CH₂-S), 2.54 – 2.44 (m, 1H, CH₂ (36')), 2.41 – 2.24 (m, 4H, (1 + 5)), 2.22 (t, J = 7.5 Hz, 2H, CH₂ (40)), 1.94 (dq, J = 12.7, 6.9 Hz, 1H, CH₂ (36'')), 1.79 – 1.63 (m, 4H, 2 x CH₂ (37, 39)), 1.56 – 1.43 (m, 2H, CH₂ (38)).

¹³C NMR (101 MHz, CDCl₃) δ 172.95 (CO), 167.86 (CO), 166.93 (CO), 157.72 (CO), 135.50 (C_{ar}), 133.50 (C_{ar}), 124.33 (C_{ar}), 119.79 (C_{ar}), 118.20 (C_{ar}), 109.07 (C_{ar}), 70.68 (CH₂ TEG), 70.66 (CH₂ TEG), 70.51 (CH₂ TEG), 70.36 (CH₂ TEG), 70.08 (CH₂ TEG), 69.85 (CH₂ TEG), 67.94 (OC-CH₂-O), 56.61 (CH-S), 50.60 (19), 46.78 (CH-C≡N), 46.13 (N-CH₂-CO), 44.68 (2), 40.39 (36), 39.30 (30), 39.00 (CH₂-NH), 38.62 (32), 36.50 (40), 34.80 (37), 30.01 (1), 29.08 (38), 25.53 (39), 25.43 (5).

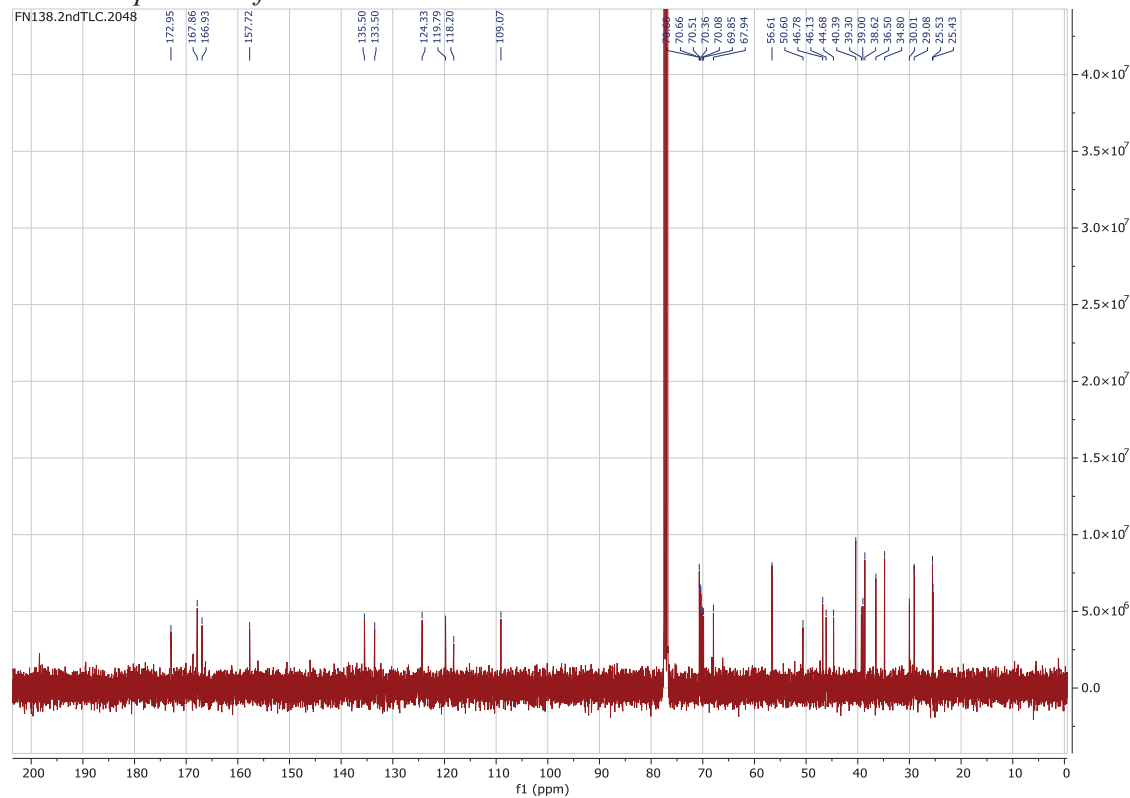
HRMS (ESI/QTOF) m/z: [M + Na]⁺ Calcd for C₃₃H₄₇N₅NaO₈S₂⁺ 728.2758; Found 728.2759.

IR (cm⁻¹): 2924, 2363, 1758, 1670, 1430, 1216, 1285

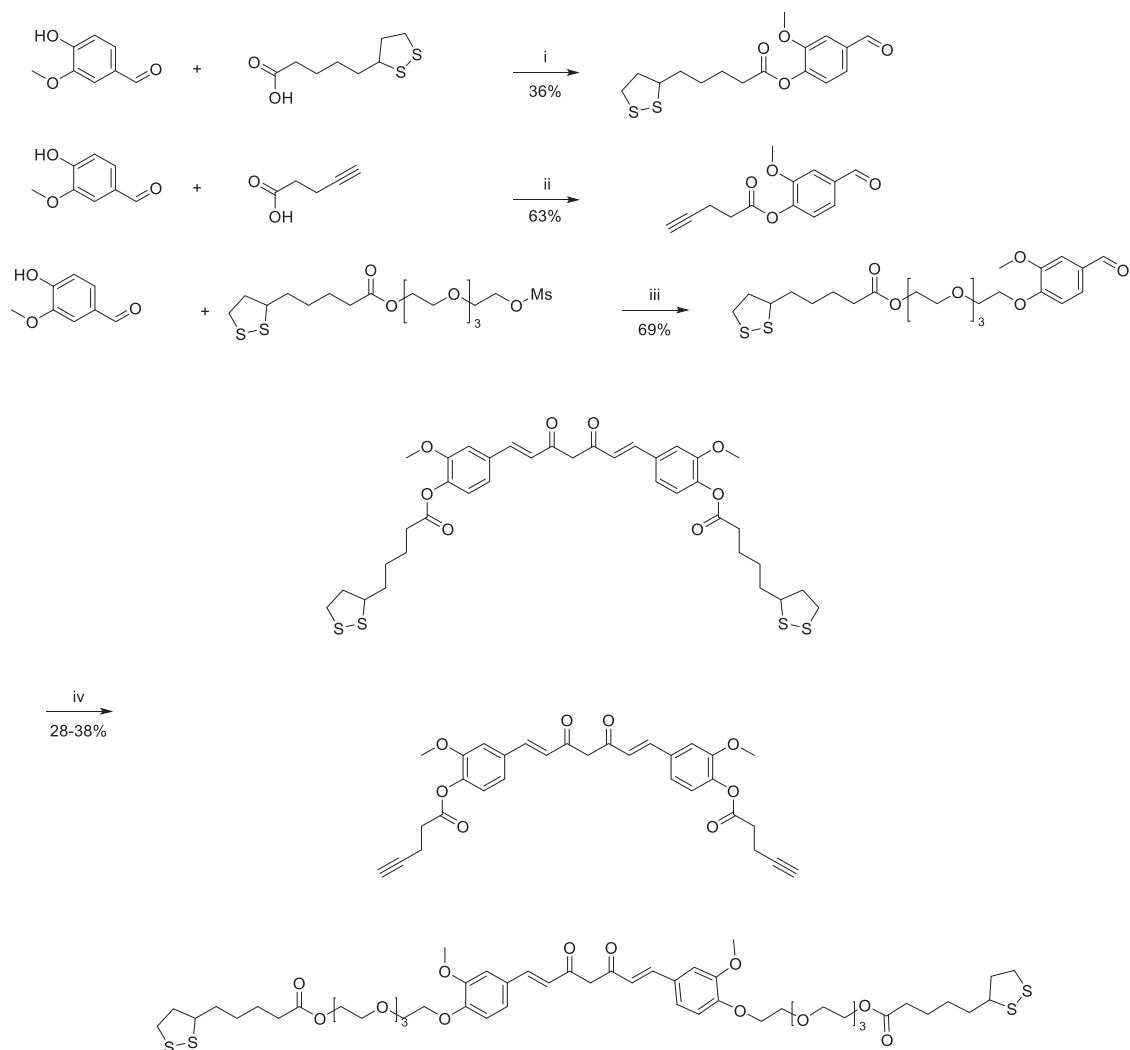
¹H NMR spectrum of 26



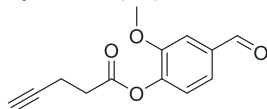
¹³C NMR spectrum of 26



5.6 CURCUMIN DERIVATIVES



Scheme 21: Synthesis of curcumin derivatives. Reagents and conditions: i- DMAP, DCC, 23°C, 12 hr; ii- DMAP, DCC, 0°C to 23°C, 12 hr; iii- K₂CO₃, KI, 90°C, 12 hr; iv- BO₃, 2,4-pentanedione, **29** or **30** or **33**, tributyl borate, *n*-butylamine, HCl (0.5 M) 80°C to 23°C, 3 hr.

4-Formyl-2-methoxyphenyl pent-4-ynoate (**28**)

To a solution of 4-pentynoic acid (387 mg, 3.94 mmol, 1.2 equiv) in DCM (5 mL) cooled to 0°C was added vanillin (500 mg, 3.29 mmol, 1 equiv), DMAP (80.3 mg, 657 μmol, 0.2 equiv) and DCC (1.08 g, 5.26 mmol, 1.6 equiv). The reaction was allowed to warmup to 23°C and stirred overnight. The reaction mixture was then filtered on Buchner. The filtrate was recovered and purified by FCC (EtOAc:PE = 17:5) to yield 4-formyl-2-methoxyphenyl pent-4-ynoate (**28**) as a white solid (0.483 g, 2.08 mmol, 63%).

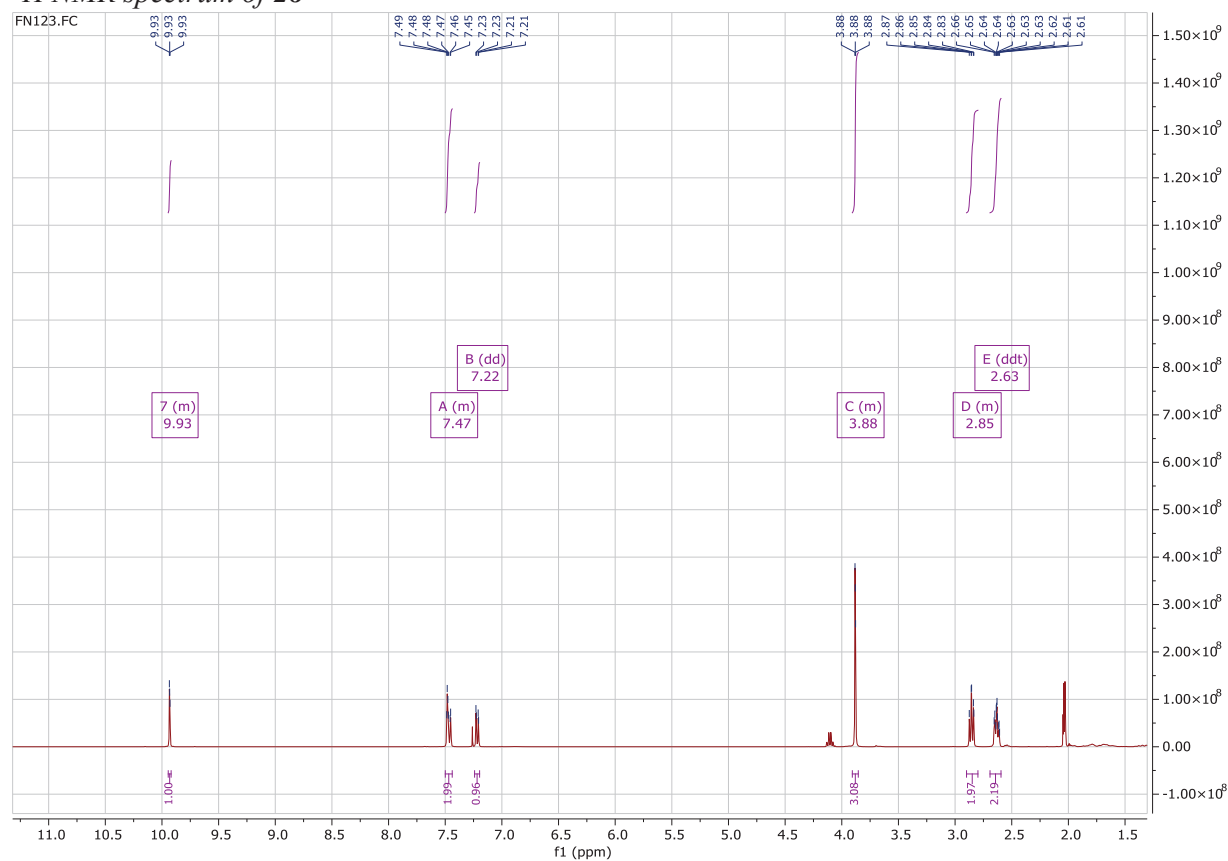
¹H NMR (400 MHz, CDCl₃) δ 9.94 – 9.92 (m, 1H, CHO), 7.50 – 7.44 (m, 2H, CH_{ar}), 7.22 (dd, J = 7.9, 1.4 Hz, 1H, CH_{ar}), 3.91 – 3.85 (m, 3H, CH₃), 2.90 – 2.80 (m, 2H, CH₂), 2.63 (ddt, J = 7.3, 5.8, 2.4 Hz, 2H, CH₂), 2.03 (s, 1H, ≡CH).

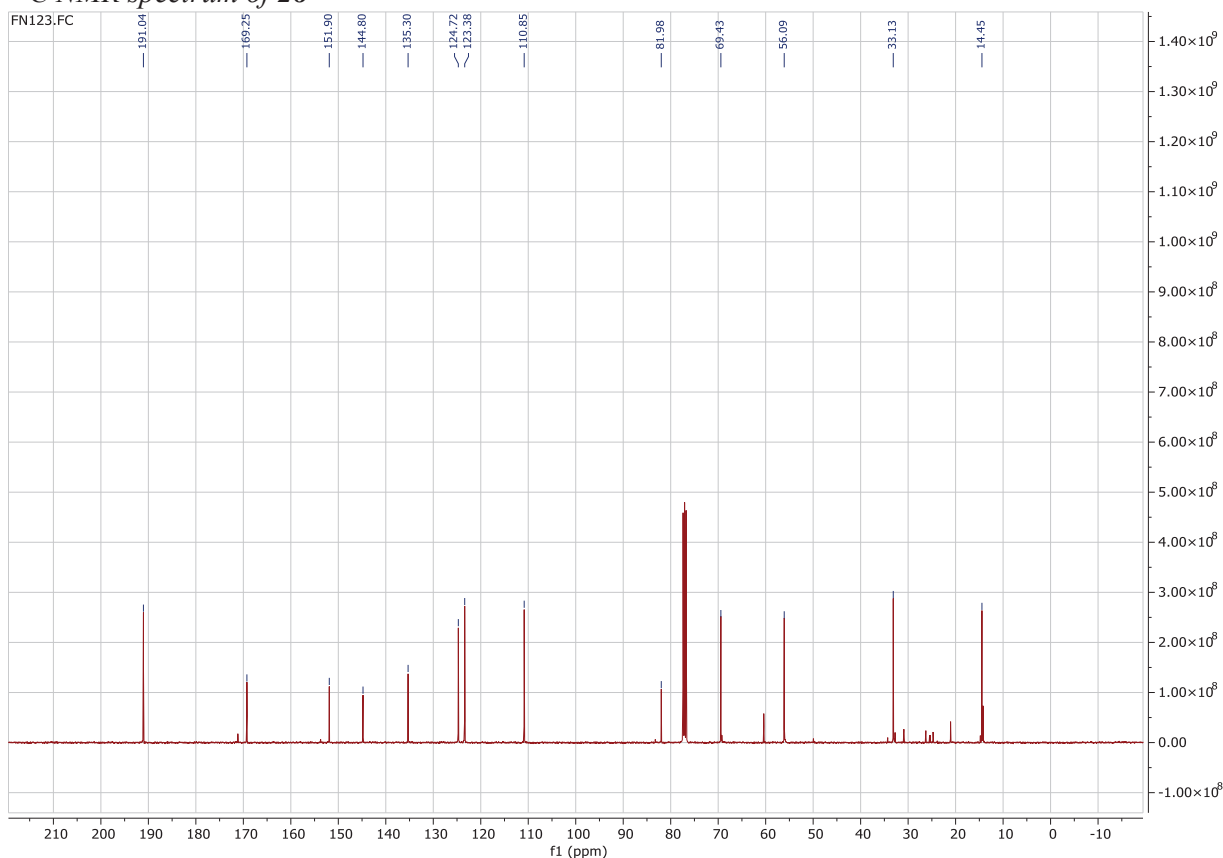
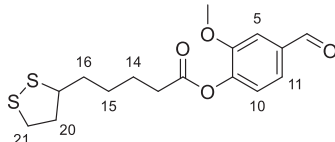
^{13}C NMR (101 MHz, CDCl_3) δ 191.04 (COH), 169.25 (CO), 151.90 (C_{ar}), 144.80 (C_{ar}), 135.30 (C_{ar}), 124.72 (CH_{ar}), 123.38 (CH_{ar}), 110.85 (CH_{ar}), 81.98 ($\text{C}\equiv\text{CH}$), 69.43 ($\text{C}\equiv\text{CH}$), 56.09 (CH_3), 33.13 (CH_2), 14.45 (CH_2).

HRMS (APPI/QTOF) m/z : $[\text{M} + \text{H}]^+$ Calcd for $\text{C}_{13}\text{H}_{13}\text{O}_4^+$ 233.0808; Found 233.0809

IR (cm^{-1}): 3275, 1762, 1692, 1273, 1127, 1608

^1H NMR spectrum of **28**

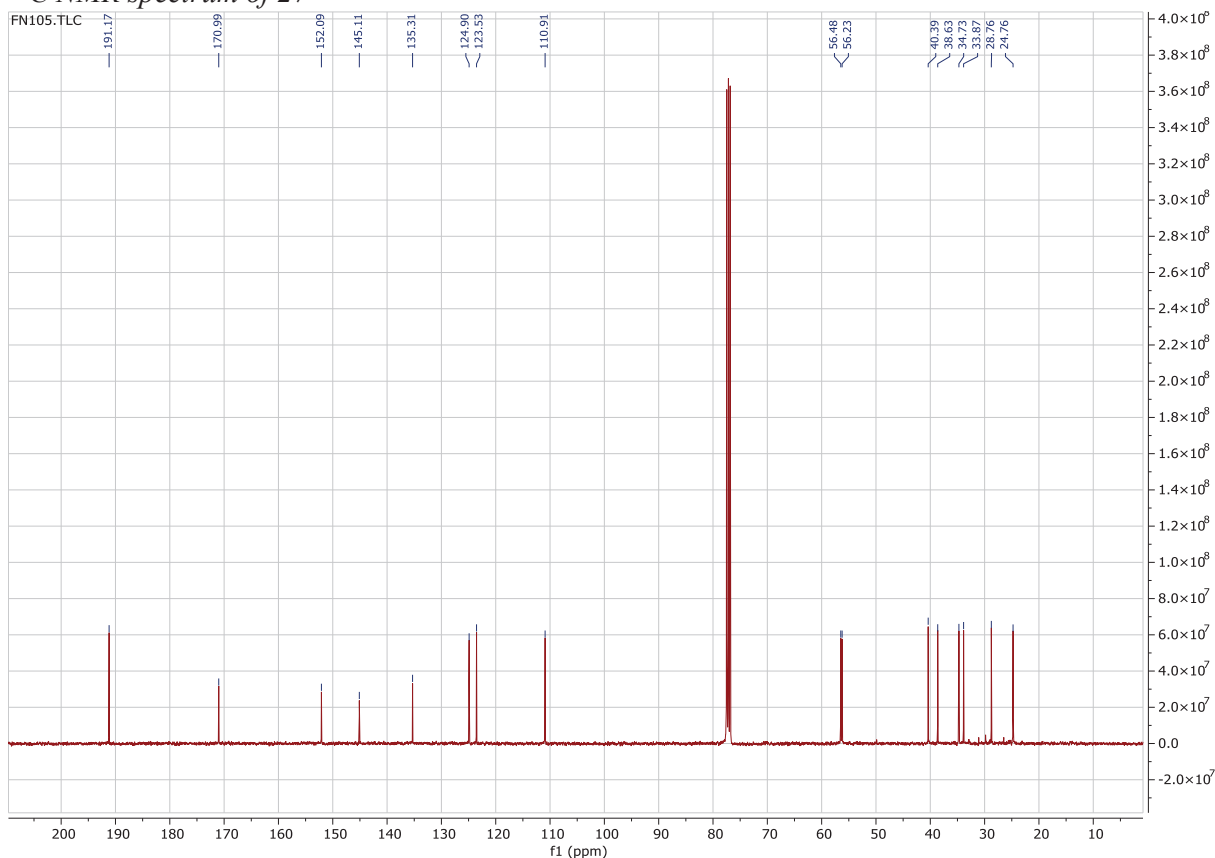
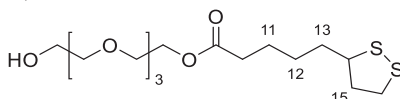


¹³C NMR spectrum of **28**4-Formyl-2-methoxyphenyl 5-(1,2-dithiolan-3-yl)pentanoate (**27**)

To a solution of vanillin (0.5 g, 3.29 mmol, 1 equiv) in DCM (5 mL) was added lipoic acid (814 mg, 3.94 mmol, 1.2 equiv), DMAP (20.1 mg, 164 μ mol, 0.05 equiv) and DCC (1.08 g, 5.26 mmol, 1.6 equiv). The reaction mixture was stirred overnight at 23°C and water (7 mL) was added to the reaction mixture. The aqueous phase was extracted with DCM (3 x 5 mL). The organic phases were combined, washed with brine (10 mL), dried over MgSO₄ and the solvent was removed in vacuo. The product was purified by FCC (EtOAc:PE = 1:1) to afford 4-formyl-2-methoxyphenyl 5-(1,2-dithiolan-3-yl)pentanoate (**27**) as a yellowish oil (0.406 g, 1.19 mmol, 36%).

¹H NMR (400 MHz, CDCl₃) δ 9.94 (s, 1H, CHO), 7.51 – 7.45 (m, 2H, CH_{ar}), 7.21 (d, J = 7.8 Hz, 1H, CH_{ar}), 3.90 (s, 3H, CH₃), 3.68 – 3.56 (m, 1H, CH 17), 3.25 – 3.06 (m, 2H, CH₂ 20), 2.63 (t, J = 7.4 Hz, 2H, CH₂-CO), 2.48 (dtd, J = 13.0, 6.6, 5.3 Hz, 1H, CH₂ 21'), 1.93 (dq, J = 12.7, 6.9 Hz, 1H, CH₂ 21''), 1.86 – 1.69 (m, 4H, 2 x CH₂ 14, 16), 1.59 (m, 2H, CH₂ 15).

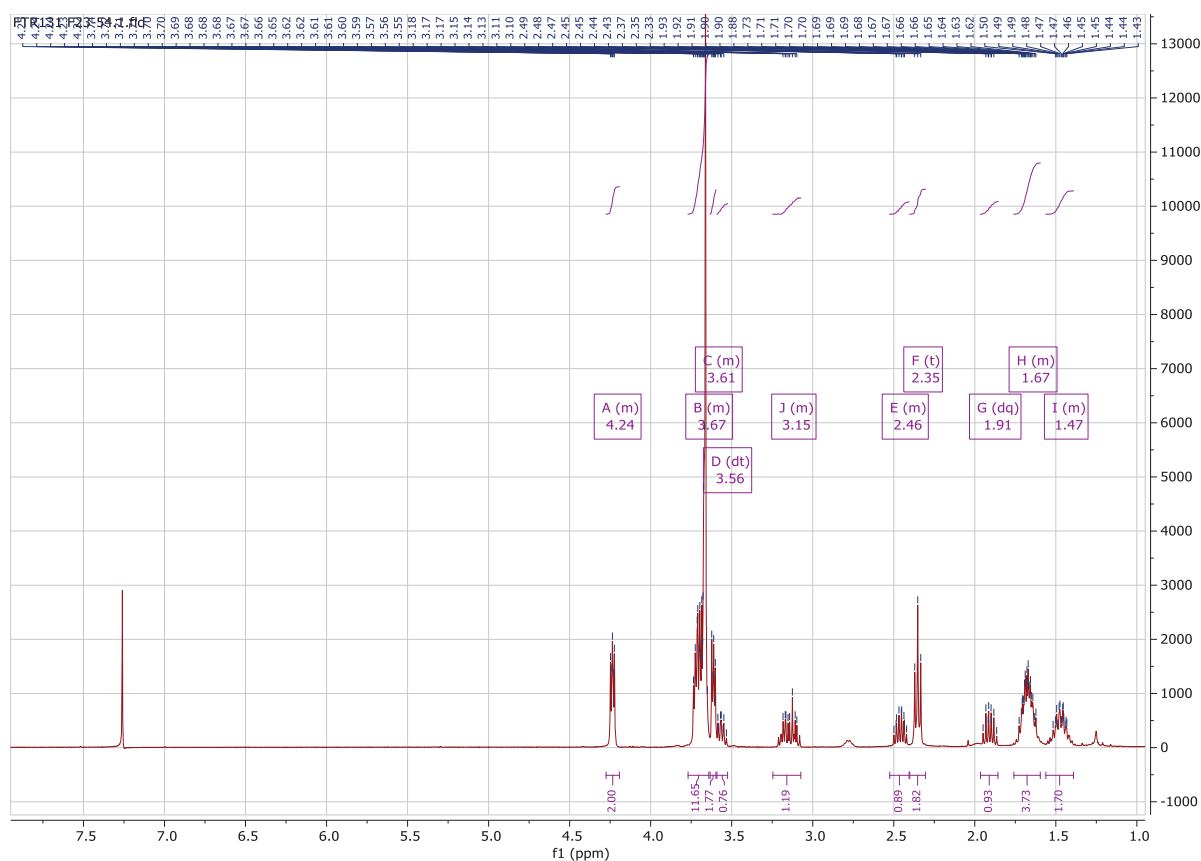
¹³C NMR (101 MHz, CDCl₃) δ 191.17 (CHO), 170.99 (CO), 152.09 (C_{ar}), 145.11 (C_{ar}), 135.31 (C_{ar}), 124.90 (C_{ar}), 123.53 (C_{ar}), 110.91 (C_{ar}), 56.48 (CHS), 56.23 (CH₃), 40.39 (20), 38.63 (21), 34.73 (16), 33.87 (CH₂-CO), 28.76(15), 24.76 (14).

¹³C NMR spectrum of 27**Lipoic acid-TEG-hydroxyl (29)**

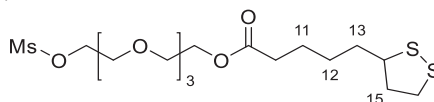
The following protocol was adapted from the procedure reported by Zhu et al.²³². Lipoic acid (1 g, 4.85 mmol, 1 equiv) and tetra(ethylene glycol) (3.36 mL, 19.4 mmol, 4 equiv) were dissolved in anhydrous DCM (75 mL). EDCI (2.79 g, 14.5 mmol, 3 equiv) and DMAP (88.8 mg, 727 μ mol, 0.15 equiv) were added and reaction mixture was stirred for 10 hr at 23°C. The reaction was quenched with the addition of aq. NH_4Cl (100 mL) and extracted with DCM (3 x 50 mL). The combined organic phase was washed with water (3 x 100 mL) and concentrated in vacuo. The product was then purified by FCC (PE:EtOAc = 1:1) to afford Lipoic acid-TEG-OH (**29**) as a yellow oil (1.161 g, 3.03 mmol, 63%). The analytical data were in agreement with literature report.

¹H NMR (400 MHz, CDCl_3) δ 4.28 – 4.19 (m, 2H, $\text{CH}_2\text{-OCO}$), 3.77 – 3.64 (m, 12H, $\text{CH}_2\text{-O}$), 3.63 – 3.60 (m, 2H, $\text{CH}_2\text{-OH}$), 3.56 (m, 1H, CH-S), 3.25 – 3.07 (m, 2H, $\text{CH}_2\text{-S}$), 2.52 – 2.41 (m, 1H, CH_2 (15')), 2.35 (t, $J = 7.4$ Hz, 2H, $\text{CH}_2\text{-COO}$), 1.91 (dq, $J = 12.7, 6.9$ Hz, 1H, CH_2 (15'')), 1.76 – 1.60 (m, 4H, 2 x CH_2 (11, 13)), 1.56 – 1.39 (m, 2H, CH_2 (12)).

¹H NMR spectrum of 29



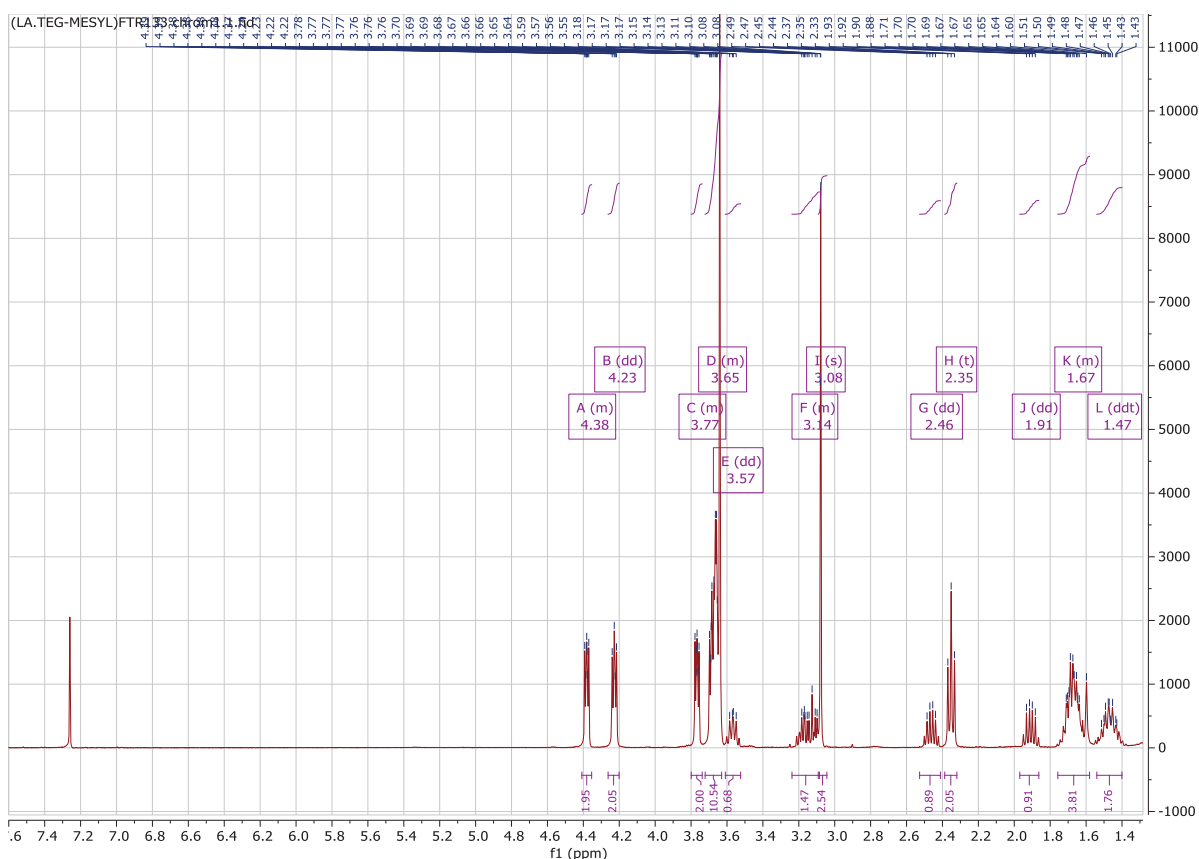
Lipoic acid-TEG-MesyI (**30**)



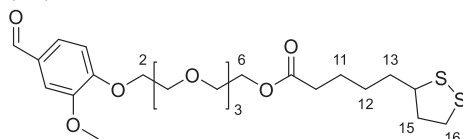
The following protocol was adapted from the procedure reported by Zhu et al.²³². Compound **29** (1 g, 2.61 mmol, 1 equiv) was dissolved in dry DCM (15 mL) and cooled to 0°C. NEt₃ (400 μL, 2.88 mmol, 1.1 eq.) and methanesulfonyl chloride (223 μL, 2.88 mmol, 1.1 eq.) were added to the solution under stirring. The reaction was allowed to warmup to 23°C and stirred overnight. The reaction mixture was diluted with the addition of DCM (50 mL) and washed with aq. HCl 5% (3 x 20 mL), aq. sat. NaHCO₃ (3 x 20 mL) and water (20 mL). The organic phase was then reduced in vacuo and the product was purified by FCC (EtOAc:PE = 1:1) to afford the desired product **30** as a yellow oil (0.325 g, 0.71 mmol, 27%).

¹H NMR (400 MHz, CDCl₃) δ 4.41 – 4.35 (m, 2H, CH₂-OCO), 4.23 (dd, J = 5.8, 3.8 Hz, 2H, CH₂-OMs), 3.80 – 3.74 (m, 2H, CH₂-CH₂OMs), 3.72 – 3.63 (m, 10H, CH₂-O), 3.57 (dd, J = 8.3, 6.3 Hz, 1H, CH-S), 3.24 – 3.09 (m, 2H, CH₂-S), 3.08 (s, 3H, CH₃), 2.46 (dd, J = 12.6, 6.3 Hz, 1H, CH₂ (15')), 2.35 (t, J = 7.4 Hz, 2H, CH₂-COO), 1.91 (dd, J = 13.0, 6.7 Hz, 1H, CH₂ (15')), 1.76 – 1.58 (m, 4H, 2 x CH₂ (11, 13)), 1.47 (m, 2H, CH₂ (12)).

¹H NMR spectrum of 30



Lipoic acid-TEG-Vanillin (**31**)



A solution of **30** (224 mg, 486 μ mol, 1 eq.) in DMF (0.97 mL) was added dropwise to a suspension of vanillin (76.8 μ L, 535 μ mol, 1.1 eq.) K_2CO_3 (101 mg, 729 μ mol, 1.5 eq.) and KI (8 mg, 48.6 μ mol, 0.1 eq.) in DMF (6 mL). The reaction mixture was heated to 90°C and stirred for 12 hr. After cooled to 23°C the solid residues were filtered and the filtrate was concentrated in vacuo. The product was purified by FCC (EtOAc:PE 7:3 \rightarrow 1:0) to yield **31** as a yellowish solid (174 mg, 0.337 mmol, 69%).

¹H NMR (400 MHz, CDCl₃) δ 9.85 (s, 1H, CHO), 7.47 – 7.37 (m, 2H, 2 x CH_{ar}), 7.01 (d, J = 8.1 Hz, 1H, CH_{ar}), 4.27 (t, J = 5.1 Hz, 2H, CH₂ (2)), 4.24 – 4.20 (m, 2H, CH₂ (6)), 3.92 (d, J = 5.7 Hz, 6H, CH₃ + CH₂(-2)), 3.76 – 3.62 (m, 10H, CH₂-O), 3.56 (dd, J = 8.2, 6.2 Hz, 1H, CH-S), 3.23 – 3.06 (m, 2H, CH₂ (16)), 2.46 (dq, J = 12.5, 6.3 Hz, 1H, CH₂ (15')), 2.34 (t, J = 7.4 Hz, 2H, CH₂-COO), 1.90 (dq, J = 13.6, 6.9 Hz, 1H, CH₂ (15'')), 1.67 (m, 4H, 2 x CH₂ (11, 13)), 1.54 – 1.40 (m, 2H, CH₂ (12)).

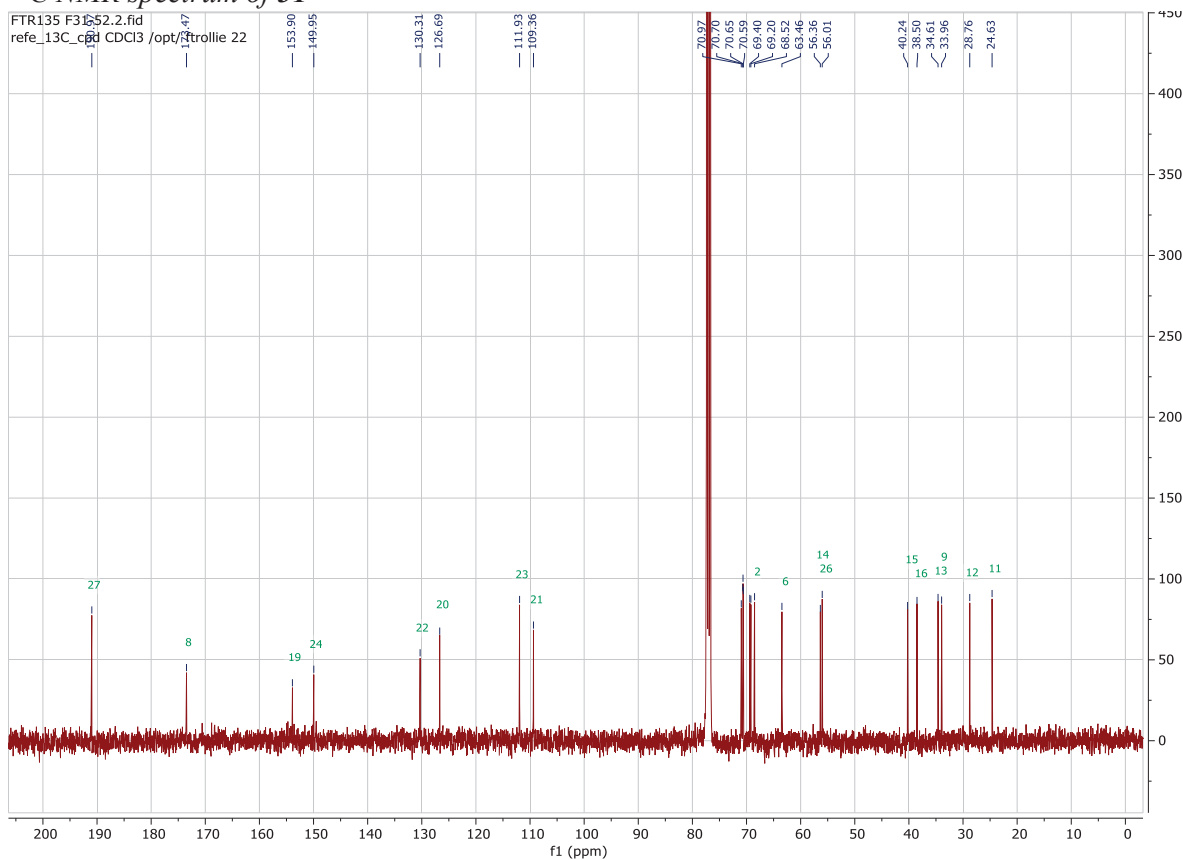
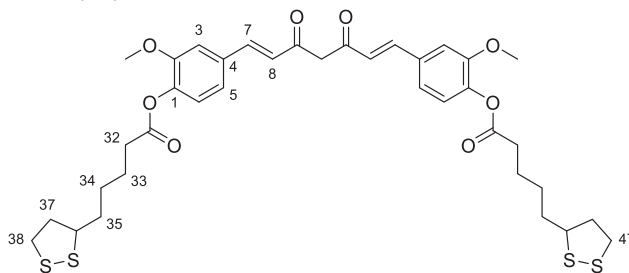
¹³C NMR (101 MHz, CDCl₃) δ 190.97 (CHO), 173.47 (CO), 153.90 (C_{ar}), 149.95 (C_{ar}), 130.31 (C_{ar}), 126.69 (CH_{ar}), 111.93 (CH_{ar}), 109.36 (CH_{ar}), 70.97 (CH₂), 70.70 (CH₂), 70.65 (CH₂), 70.59 (CH₂), 69.40 (CH₂), 69.20 (CH₂), 68.52 (CH₂), 63.46 (CH₂), 56.36 (CH), 56.01 (CH₃), 40.24 (CH₂), 38.50 (CH₂-S), 34.61 (13), 33.96 (CH₂COO), 28.76 (12), 24.63 (11).

HRMS (ESI/QTOF) m/z : $[M + H]^+$ Calcd for $C_{24}H_{37}O_8S_2^+$ 517.1924; Found 517.1940.

IR (cm^{-1}): 2942, 2356, 1260

1H NMR spectrum of **31**



¹³C NMR spectrum of 31**Di(lipoic acid)-curcumin (32)**

Boron oxide (12.5 μL , 441 μmol , 1 equiv) was added to a solution of 2,4-pentanedione (45.2 μL , 441 μmol , 1 equiv) in DMF (5 mL) and the solution was heated to 80°C under stirring. After 30 min a solution of compound **27** (300 mg, 881 μmol , 2 equiv) and tributyl borate (476 μL , 1.76 mmol, 4 equiv) in DMF (6 mL) and a solution of N-butylamine (17.4 μL , 176 μmol , 0.4 equiv) in DMF (0.5 mL) were added dropwise successively. After 2 hr during which the reaction became red-orange, aq. HCl 0.5 M (5 mL) was added and the reaction mixture was allowed to cool to 23°C for 1 hr under stirring. The solvent was then removed in vacuo and the residue was dissolved in water (10 mL) and extracted with EtOAc (3 x 10 mL). The organic phases were combined and washed with aq. LiCl 5% (2 x 10 mL). EtOAc was removed in vacuo and the product was purified by FCC (PE:EtOAc = 8:2) to afford di(lipoic acid)-curcumin (**32**) as a dark yellow solid gel. (102 mg, 0.14 mmol, 31%).

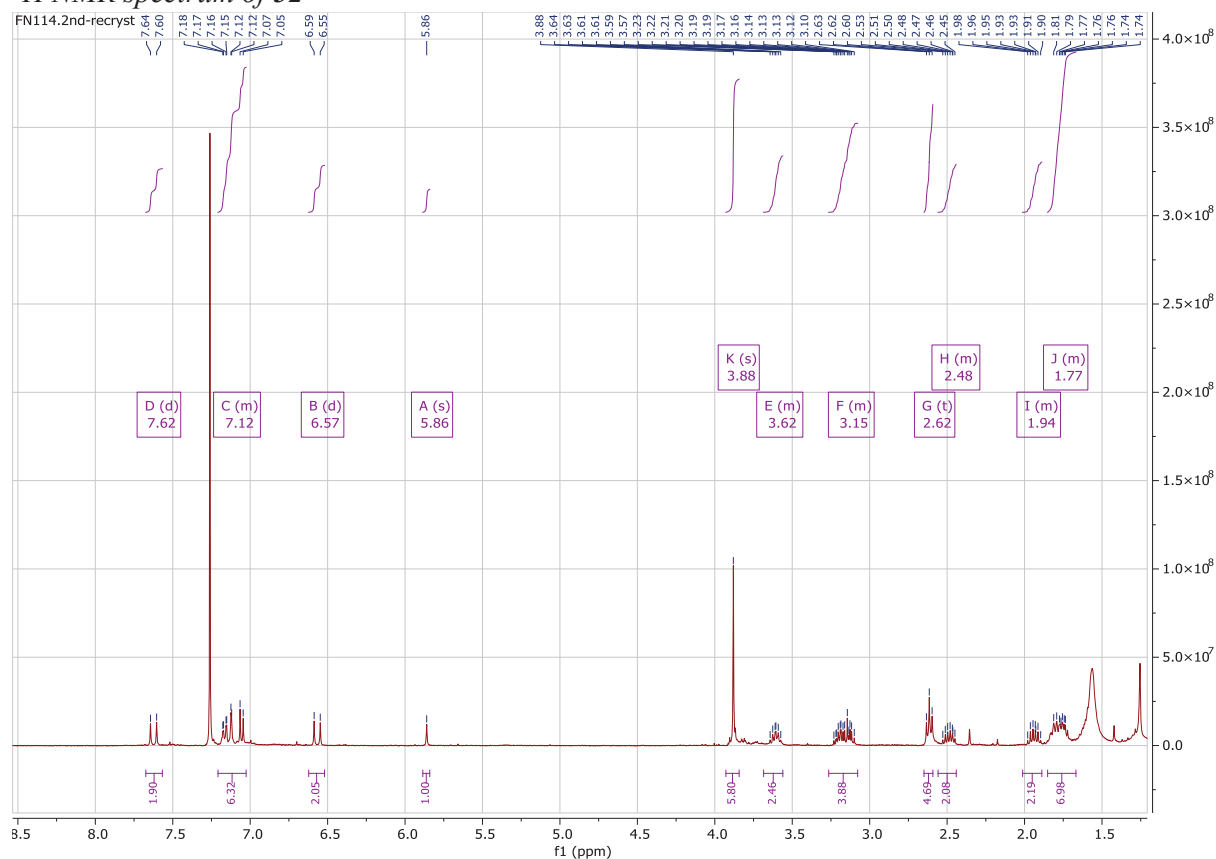
^1H NMR (400 MHz, CDCl_3) δ 7.62 (d, $J = 15.8$ Hz, 2H, CH- C_{ar}), 7.21 – 7.03 (m, 6H, CH_{ar}), 6.57 (d, $J = 15.8$ Hz, 2H, 2 x CH-C=O), 5.86 (s, 1H, O=C-CH-C=O), 3.88 (s, 6H, 2 x CH_3), 3.68 – 3.56 (m, 2H, 2 x CH-S), 3.26 – 3.08 (m, 4H, 2 x CH_2 -S), 2.62 (t, $J = 7.3$ Hz, 4H, 2 x CH_2 -CO), 2.56 – 2.44 (m, 2H, 2 x (37')), 2.01 – 1.89 (m, 2H, 2 x (37'')), 1.85 – 1.67 (m, 8H, 2 x (35) + 2 x (33)).

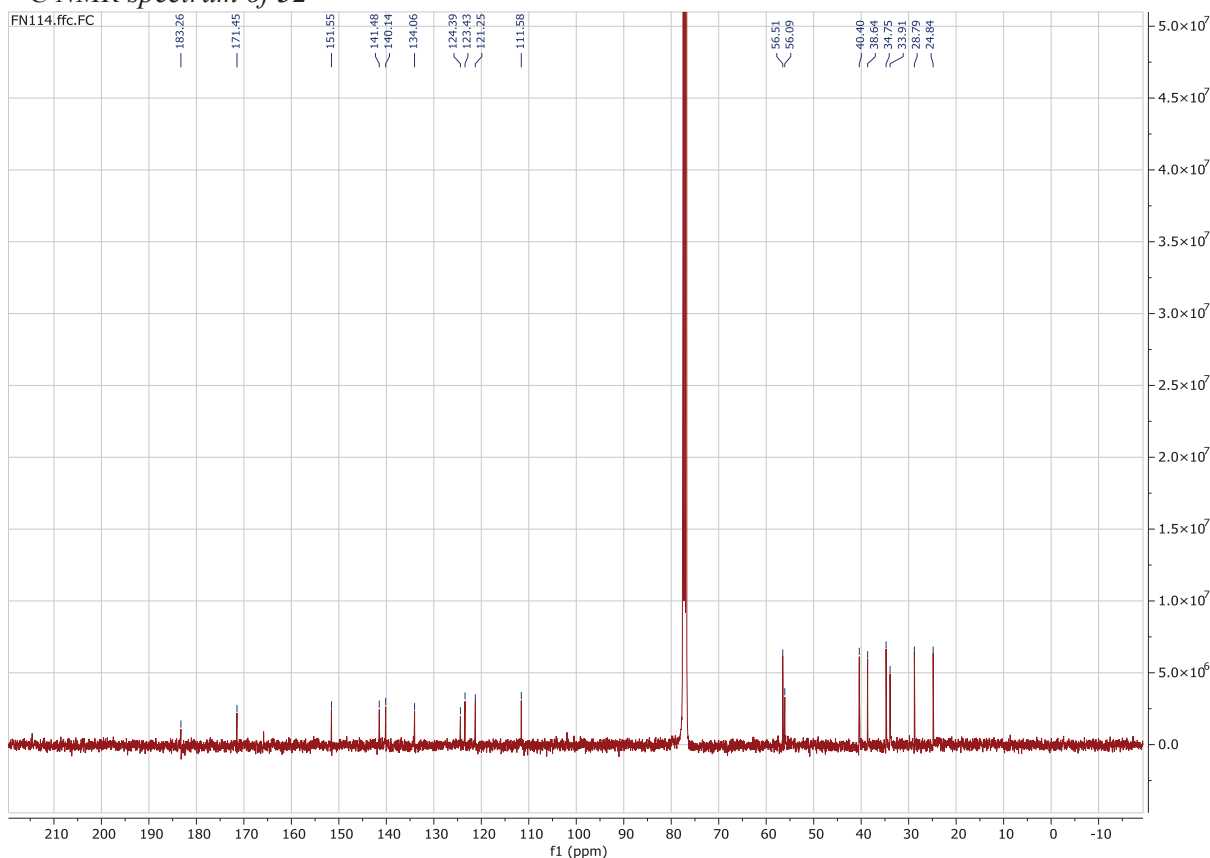
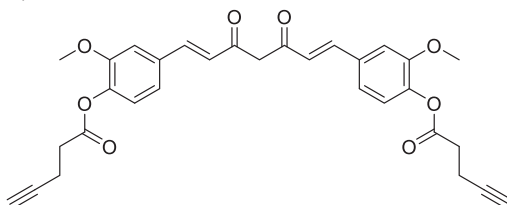
^{13}C NMR (101 MHz, CDCl_3) δ 183.26 (CO), 171.45 (CO), 151.55 (C_{ar}), 141.48 (C_{ar}), 140.14 (CH), 134.06 (C_{ar}), 124.39 (CH), 123.43 (CH_{ar}), 121.25 (CH_{ar}), 111.58 (CH_{ar}), 56.51 (CH-S), 56.09 (CH_3), 40.40 (37), 38.64 (CH_2 -S), 34.75 (35), 33.91 (CH_2 -COO), 28.79 (34), 24.84 (33).

HRMS m/z : $[\text{M} + \text{H}]^+$ Calcd for $\text{C}_{37}\text{H}_{45}\text{O}_8\text{S}_4^+$ 745.1992; Found 745.1974.

IR (cm^{-1}): 3326, 2923, 1625, 1575

^1H NMR spectrum of 32



¹³C NMR spectrum of **32**Di(pentyne)-curcumin (**33**)

Boron oxide (29.4 μL , 1.04 mmol, 1 equiv) was added to a solution of 2,4-pentanedione (107 μL , 1.04 mmol, 1 equiv) in DMF (6 mL) and the solution was heated to 80°C under stirring. After 30 min a solution of compound **28** (483 mg, 2.08 mmol, 2 equiv) and tributyl borate (1.12 mL, 4.16 mmol, 4 equiv) in DMF (6 mL) and a solution of N-butylamine (41.1 μL , 416 μmol , 0.4 equiv) in DMF (0.5 mL) were added dropwise successively. After 2 hr during which the reaction became red-orange, aq. HCl 0.5 M (5 mL) was added and the reaction mixture was allowed to cool to 23°C for 1 hr under stirring. The solvent was then removed in vacuo and the residue was dissolved in water (10 mL) and extracted with EtOAc (3 x 10 mL). The organic phases were combined and washed with aq. LiCl 5% (2 x 10 mL). EtOAc was removed in vacuo and the product was purified by FCC (PE:EtOAc 1:0 \rightarrow 13:7) and further purified with a second FCC (PE:DCM:MeOH = 10:10:1) to afford di(pentyne)-curcumin (**33**) as a yellow solid (0.153 g, 0.29 mmol, 28%).

¹H NMR (400 MHz, CDCl₃) δ 7.62 (d, J = 15.8 Hz, 2H, CH-C_{ar}), 7.20 – 7.04 (m, 6H, CH_{ar}), 6.57 (d, J = 15.8 Hz, 2H, 2 x CH-C=O), 5.86 (s, 1H, O=C-CH-C=O), 3.88 (s, 6H, 2 x CH₃), 2.86

Experimental section

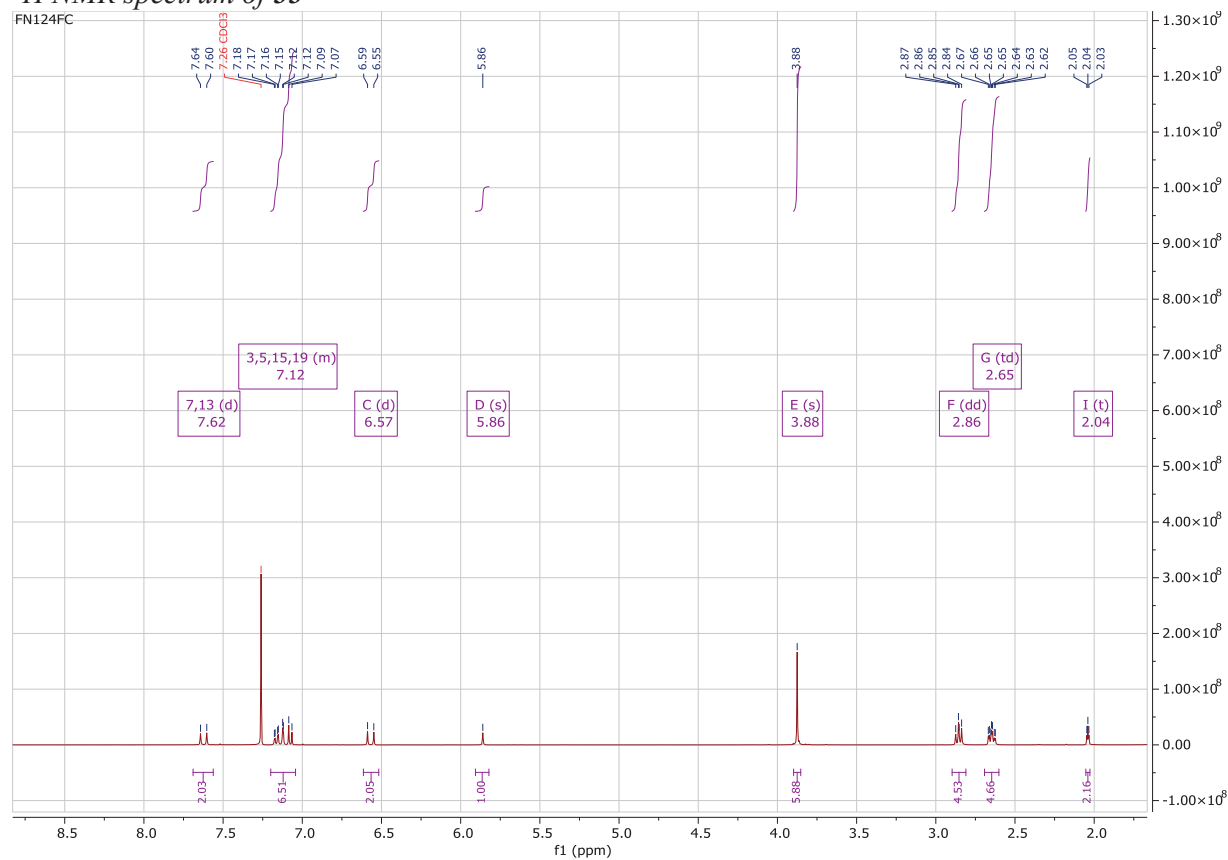
(dd, $J = 8.3, 6.6$ Hz, 4H, 2 x CH₂-C=O), 2.65 (td, $J = 7.6, 7.1, 2.7$ Hz, 4H, 2 x CH₂-C), 2.04 (t, $J = 2.6$ Hz, 2H, 2 x C≡CH).

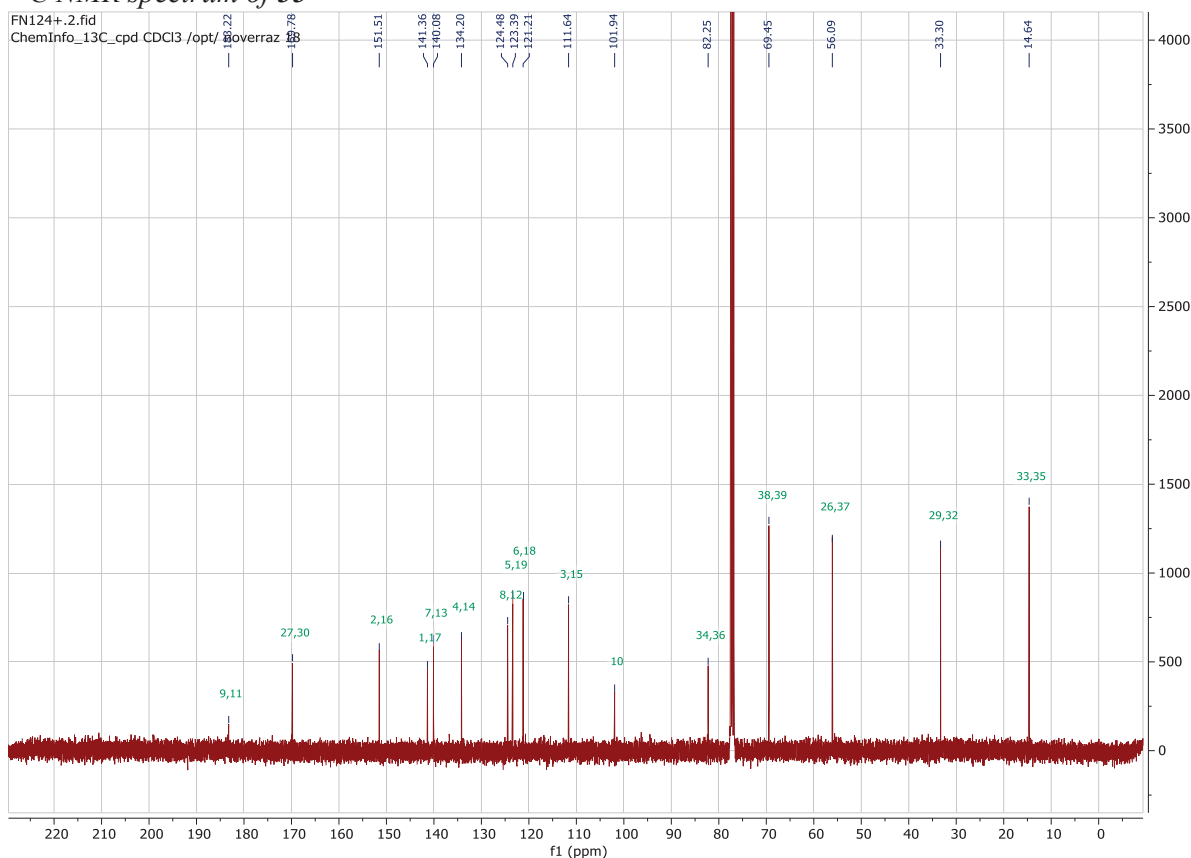
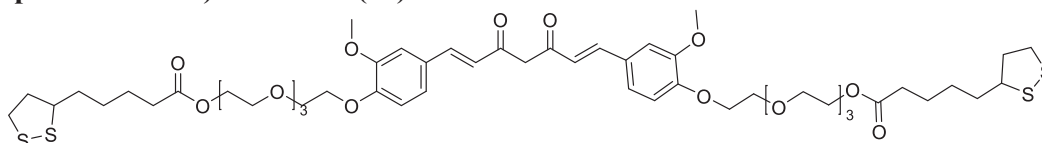
¹³C NMR (101 MHz, CDCl₃) δ 183.22 (CO), 169.78 (CO), 151.51 (C_{ar}O), 141.36 (C_{ar}O), 140.08 (CH), 134.20 (C_{ar}), 124.48 (C_{ar}), 123.39 (CH), 121.21 (C_{ar}), 111.64 (C_{ar}), 101.94 (O=C-CH-C=O), 82.25 (C≡CH), 69.45 (C≡CH), 56.09 (CH₃), 33.30 (CH₂), 14.64 (CH₂).

HRMS (ESI/QTOF) m/z : [M + Na]⁺ Calcd for C₃₁H₂₈NaO₈⁺ 551.1676; Found 551.1677

IR (cm⁻¹): 3289, 1755, 1587, 1512, 1631, 1125, 1250, 1300, 1026, 963, 913, 845, 1419

¹H NMR spectrum of 33



¹³C NMR spectrum of **33**Di(lipoic acid-TEG)-curcumin (**34**)

Boron oxide (33.7 μ L, 1.19 mmol, 1 equiv) was added to a solution of 2,4-pentanedione (122 μ L, 1.19 mmol, 1 equiv) in DMF (6 mL) and the solution was heated to 80°C under stirring. After 30 min a solution of compound **31** (1.23 g, 2.38 mmol, 2 equiv) and tributyl borate (1.28 mL, 4.76 mmol, 4 equiv) in DMF (6 mL) and a solution of N-butylamine (47.1 μ L, 476 μ mol, 0.4 equiv) in DMF (0.5 mL) were added dropwise successively. After 2 hr during which the reaction became red-orange, aq. HCl 0.5 M (5 mL) was added and the reaction mixture was allowed to cool to 23°C for 1 hr under stirring. The solvent was then removed in vacuo and the residue was dissolved in water (10 mL) and extracted with EtOAc (3 x 10 mL). The organic phases were combined and washed with aq. LiCl 5% (2 x 10 mL). EtOAc was removed in vacuo and the product was purified by FCC (PE:EtOAc 1:0 \rightarrow 13:7). Further purification was obtained with a second FCC (PE:EtOAc = 1:0 \rightarrow 1:1) to yield di(lipoic acid-TEG)-Curcumin (**34**) as a yellow-orange solid (0.501 g, 0.456 mmol, 38%).

¹H NMR (400 MHz, CDCl₃) δ 7.59 (d, J = 15.8 Hz, 2H, 2 x CH=CH), 7.16 – 7.04 (m, 4H, CH_{ar}), 6.91 (d, J = 8.3 Hz, 2H, CH_{ar}), 6.49 (d, J = 15.8 Hz, 2H, 2 x CH=CH), 5.82 (s, 1H, O=C-CH-C=O), 4.22 (dd, J = 5.4, 3.5 Hz, 8H, 4 x CH₂-O), 3.91 (m, 12H, 2 x CH₃ + 2 x CH₂-CH₂-O), 3.77 – 3.62 (m, 20H, CH₂ TEG), 3.61 – 3.51 (m, 2H, 2 x CH-S), 3.23 – 3.05 (m, 4H,

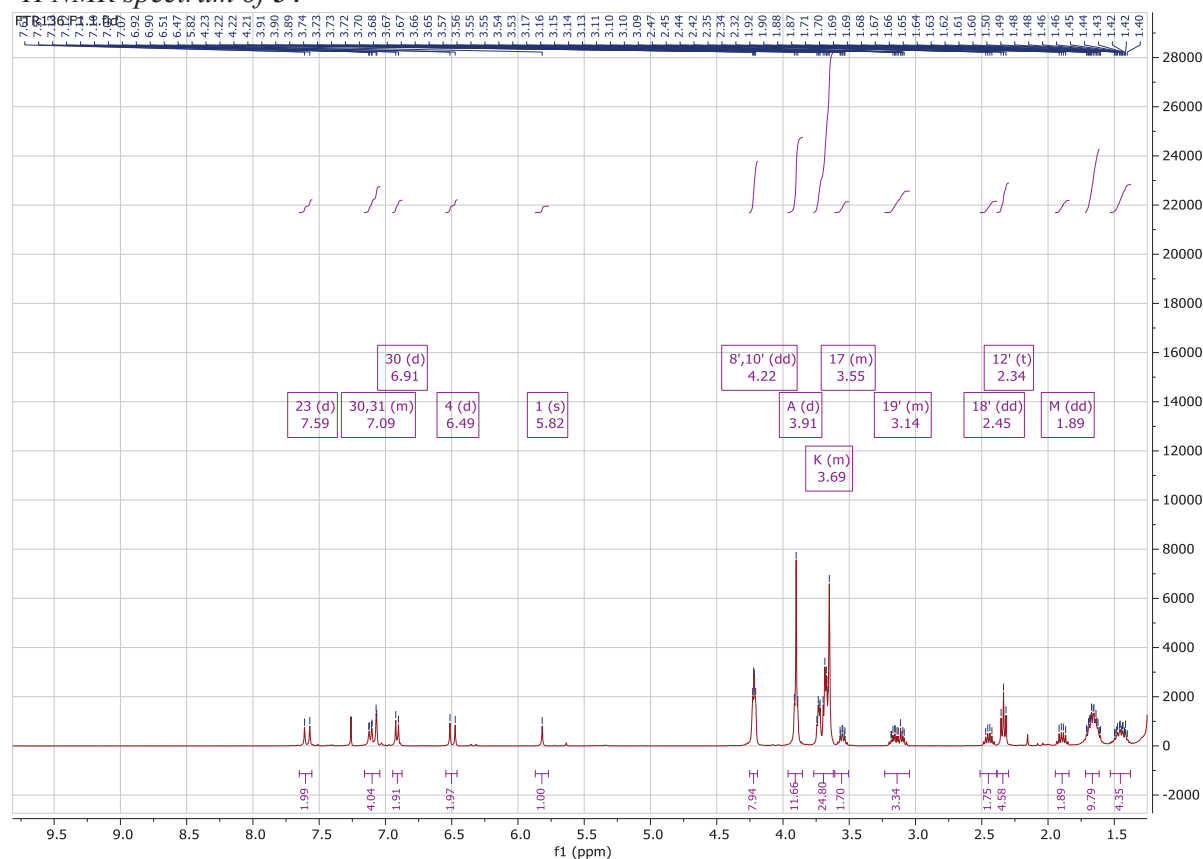
2 x CH₂-S), 2.45 (dd, J = 12.6, 6.2 Hz, 2H, 2 x CH₂'-CH-S), 2.34 (t, J = 7.4 Hz, 4H, 2 x CH₂-CO), 1.89 (dd, J = 13.0, 6.7 Hz, 2H, CH₂''-CH-S), 1.72 – 1.61 (m, 8H, 2 x CO-CH₂-CH₂ + 2x CH₂-CH-S), 1.46 (ddd, J = 18.3, 9.2, 6.6 Hz, 4H, 2 x CH₂-CH₂-C=O).

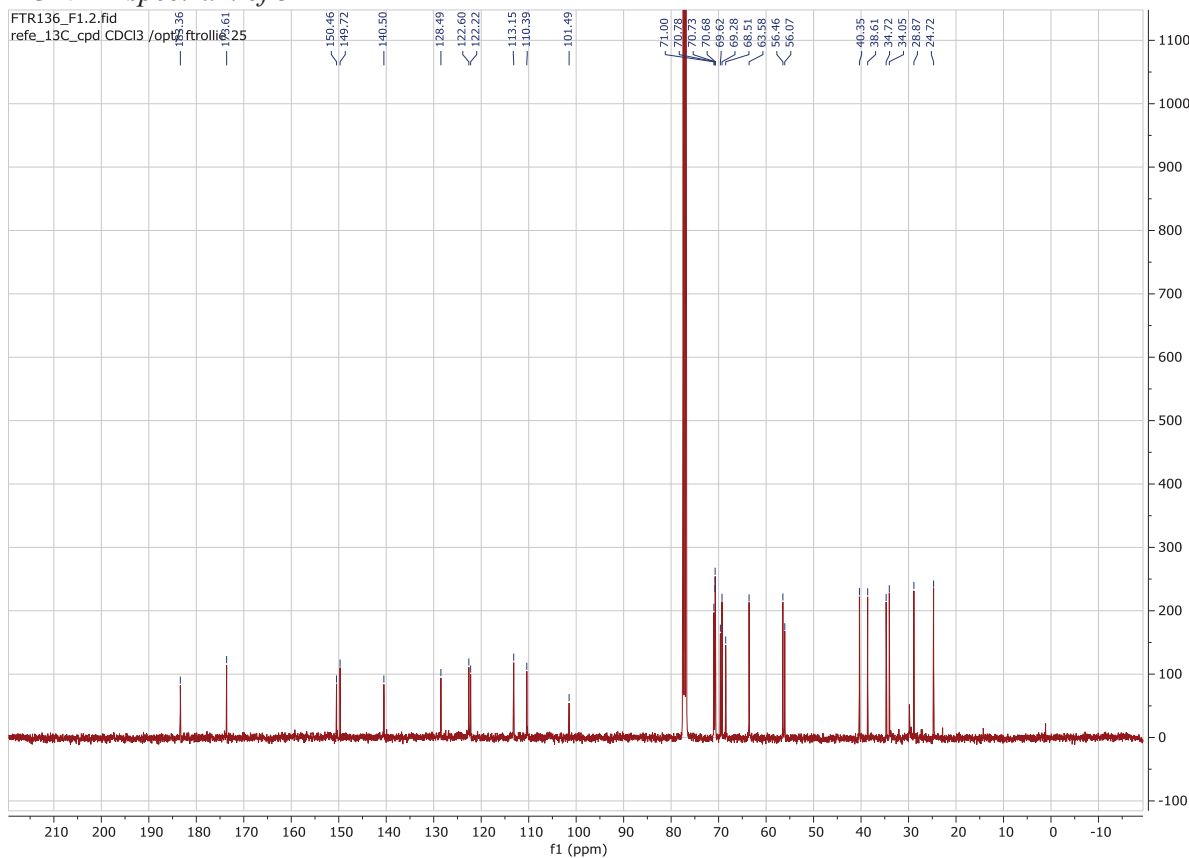
¹³C NMR (101 MHz, CDCl₃) δ 183.36 (CO), 173.61 (CO), 150.46 (C_{ar}), 149.72 (C_{ar}), 140.50 (CH), 128.49 (C_{ar}), 122.60 (CH_{ar}), 122.22 (CH), 113.15 (CH_{ar}), 110.39 (CH_{ar}), 101.49 (OC-CH-CO), 71.00 (CH₂), 70.78 (CH₂), 70.73 (CH₂), 70.68 (CH₂), 69.62 (CH₂), 69.28 (CH₂), 68.51 (CH₂), 63.58 (CH₂), 56.46 (CH-S), 56.07 (CH₃), 40.35 (CH₂), 38.61 (CH₂), 34.72 (CH₂), 34.05 (CH₂), 28.87 (CH₂), 24.72 (CH₂).

HRMS (ESI/QTOF) m/z: [M + Na]⁺ Calcd for C₅₃H₇₆NaO₁₆S₄⁺ 1119.3908; Found 1119.3920

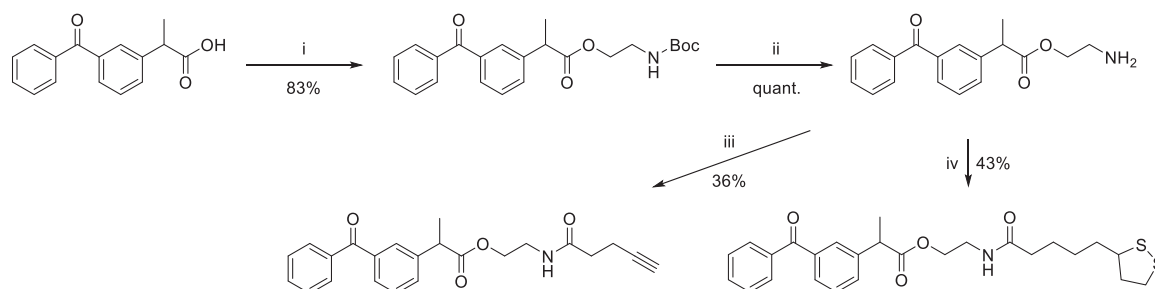
IR (cm⁻¹): 2924, 2366, 2346, 1732, 1617, 1582, 1511, 1456, 1265, 1139, 954

¹H NMR spectrum of **34**

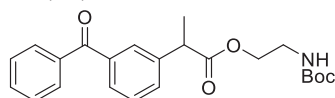


¹³C NMR spectrum of **34**

5.7 KETOPROFEN DERIVATIVES



Scheme 22 : Synthesis ketoprofen derivatives with short (ethyl) linkers. Reagents and conditions: i- *N*-Boc-ethanolamine, DMAP, DCC, 0°C to 23°C, 12 hr; ii- TFA, 23°C, 2 hr; iii- 4-pentynoic acid, HOBt, EDCl, DIPEA, 23°C, 12 hr; iv- lipoic acid, HOBt, EDCl, DIPEA, 23°C, 12 hr

Ketoprofen-*N*-boc-ethanolamine (**35**)

A stirred solution of *N*-Boc-ethanolamine (**52**) (0.288 g, 1.79 mmol, 1 equiv) and ketoprofen (0.5 g, 1.97 mmol, 1.1 equiv) in DCM (10 mL) was cooled to 0°C. DMAP (21.8 mg, 0.18 mmol, 0.1 equiv) and DCC (0.406 g, 1.97 mmol, 1.1 equiv) were added successively. The

reaction mixture was stirred at 0°C for 20 min, warmup to 23°C and stirred for 12 hr. EtOAc (20mL) was added and the solution was filtered on through a pad of celite. The solvent was removed in vacuo and the product was purified by FCC (EtOAc:PE = 1:3 → 1:0) to yield ketoprofen-N-Boc-ethanolamine (**35**) as a transparent oil (0.649 g, 1.633 mmol, 83%).

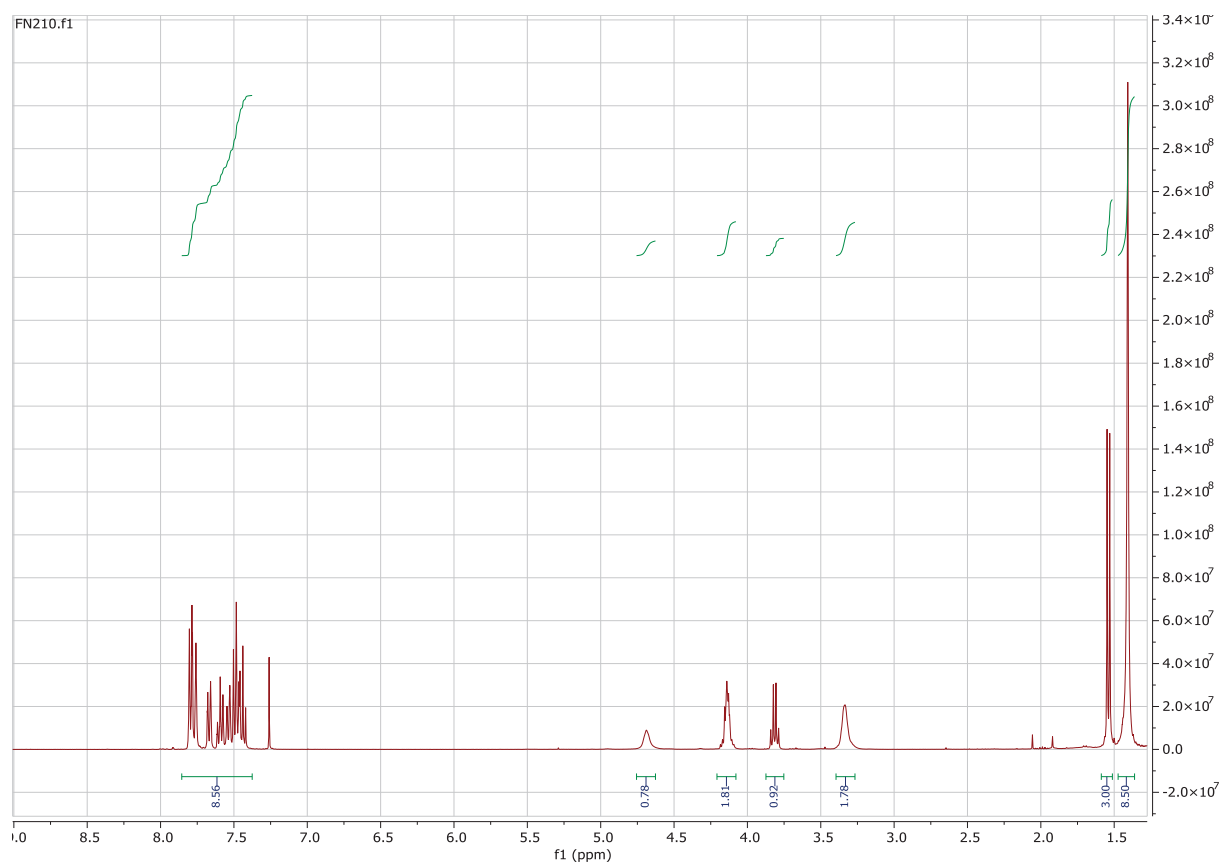
¹H NMR (400 MHz, CDCl₃) δ 7.77 – 7.34 (m, 10H, CH_{ar}), 4.07 (ddd, J = 7.5, 5.2, 2.8 Hz, 2H, O-CH₂), 3.75 (q, J = 7.2 Hz, 1H, CH), 3.34 – 3.19 (m, 2H, N-CH₂), 1.48 (d, J = 7.2 Hz, 3H, CH-CH₃), 1.34 (s, 9H, 3 x CH₃(Boc)).

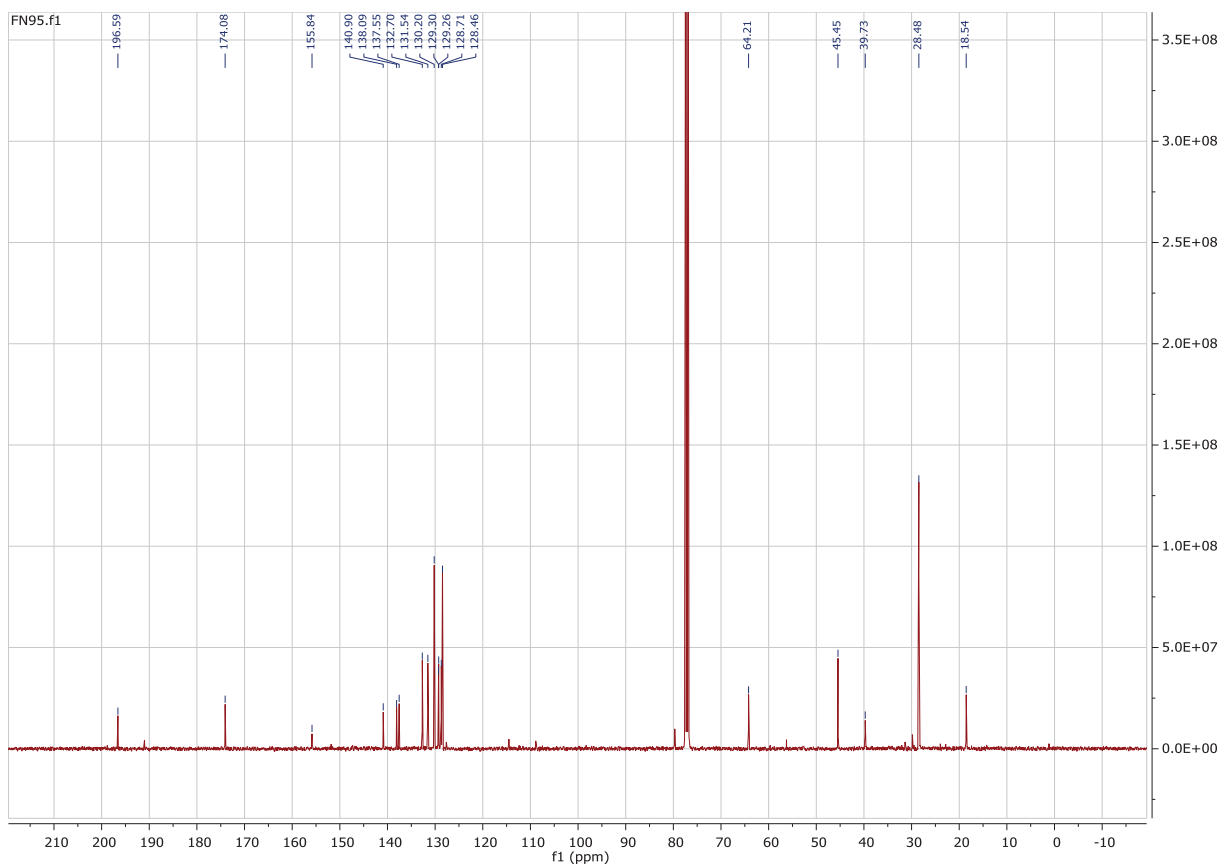
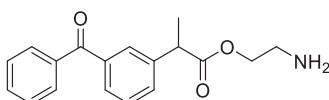
¹³C NMR (101 MHz, CDCl₃) δ 196.59 (CO), 174.08 (CO), 155.84 (CO), 140.90 (C_{ar}), 138.09 (C_{ar}), 137.55 (C_{ar}), 132.70 (C_{ar}), 131.54 (C_{ar}), 130.20 (2 x C_{ar}), 129.30 (C_{ar}), 129.26 (C_{ar}), 128.71 (C_{ar}), 128.46 (2 x C_{ar}), 64.21 (O-CH₂), 45.45 (CH), 39.73 (N-CH₂), 28.48 (3 x CH₃ (Boc)), 18.54 (CH₃).

HRMS (ESI/QTOF) m/z: [M + Na]⁺ Calcd for C₂₃H₂₇NNaO₅⁺ 420.1781; Found 420.1783.

IR (cm⁻¹): 711, 1156, 1272, 1282, 1509, 1691, 2984, 3383

¹H NMR spectrum of 35



¹³C NMR spectrum of **35**Ketoprofen-ethanolamine (**36**)

To a solution of Ketoprofen-N-Boc-ethanolamine (**35**) (500 mg, 1.26 mmol, 1 equiv) in DCM (8 mL), TFA (0.93 mL, 12.6 mmol, 10 equiv) was added dropwise. The reaction mixture was stirred for 2 hr until completion of the reaction. The volatiles were removed in vacuo and the residue dissolved in EtOAc (10 mL) and washed with aq. sat. K₂CO₃ (3 x 10 mL). The organic layer was then evaporated in vacuo to afford the desired product (**36**) (0.36 g, 1.20 mmol, quant.).

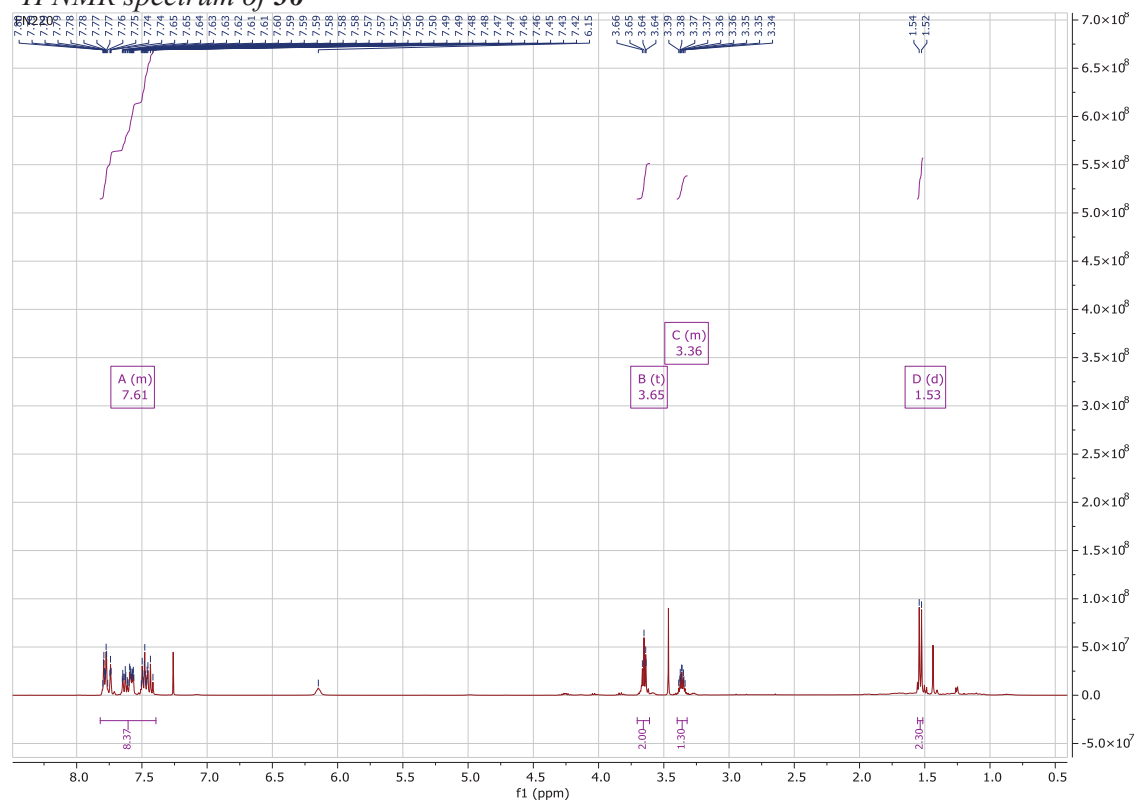
¹H NMR (400 MHz, CDCl₃) δ 7.82 – 7.39 (m, 9H), 3.65 (t, J = 5.1 Hz, 2H, O-CH₂), 3.40 – 3.32 (m, 1H, CH), 1.53 (d, J = 7.2 Hz, 2H, HN-CH₂).

¹³C NMR (101 MHz, CDCl₃) δ 195.90 (CO), 173.93 (CO), 140.97 (C_{ar}), 137.16 (C_{ar}), 136.42 (C_{ar}), 131.83 (C_{ar}), 130.70 (C_{ar}), 129.24 (2 x C_{ar}), 128.30 (C_{ar}), 128.17 (C_{ar}), 127.89 (C_{ar}), 127.51 (2 x C_{ar}), 61.27 (O-CH₂), 45.96 (CH), 41.67 (HN-CH₂), 17.79 (CH₃).

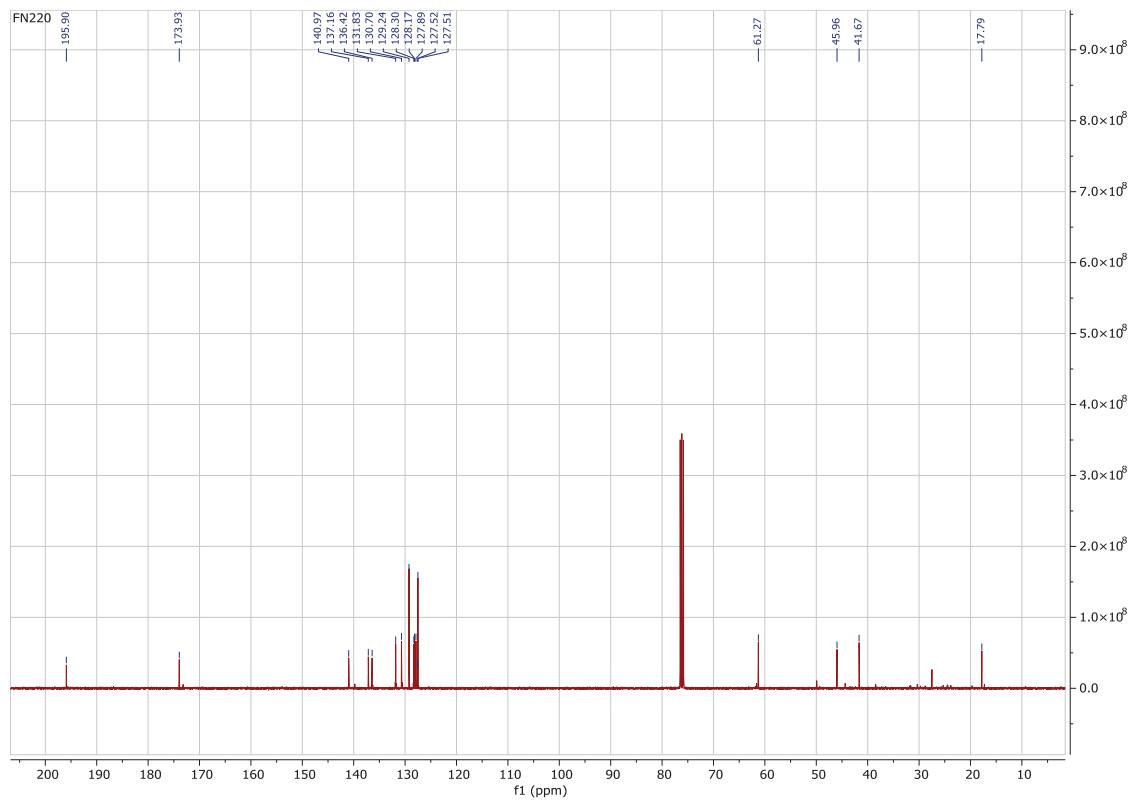
HRMS (ESI/QTOF) m/z: [M + Na]⁺ Calcd for C₁₈H₁₉NNaO₃⁺ 320.1257; Found 320.1265.

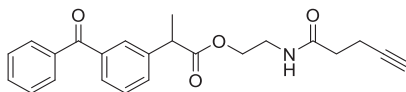
IR (cm⁻¹): 800, 1013, 1108, 1257

¹H NMR spectrum of 36



¹³C NMR spectrum of 36



Ketoprofen-ethanolamine-pentyne (37)

4-Pentynoic acid (191 mg, 1.95 mmol, 1.2 equiv) was dissolved in DMF (4 mL). Ketoprofen-ethanolamine (**36**) (483 mg, 1.62 mmol, 1 equiv), HOBt (498 mg, 3.25 mmol, 2 equiv), EDCI (374 mg, 1.95 mmol, 1.2 equiv) and DIPEA (805 μ L, 4.87 mmol, 3 equiv) were added. The reaction mixture was stirred at 23°C for 12 hr. The solvent was removed in vacuo and the residue was dissolved in EtOAc (10 mL), washed with water (2 x 10 mL) and brine (1 x 10 mL). The organic phase was dried over MgSO₄ and concentrated in vacuo. The product was purified by FCC on silica gel (EtOAc:PE = 1:1) to afford ketoprofen-ethanolamine-pentyne (**37**) as a white solid (220 mg, 0.58 mmol, 36%).

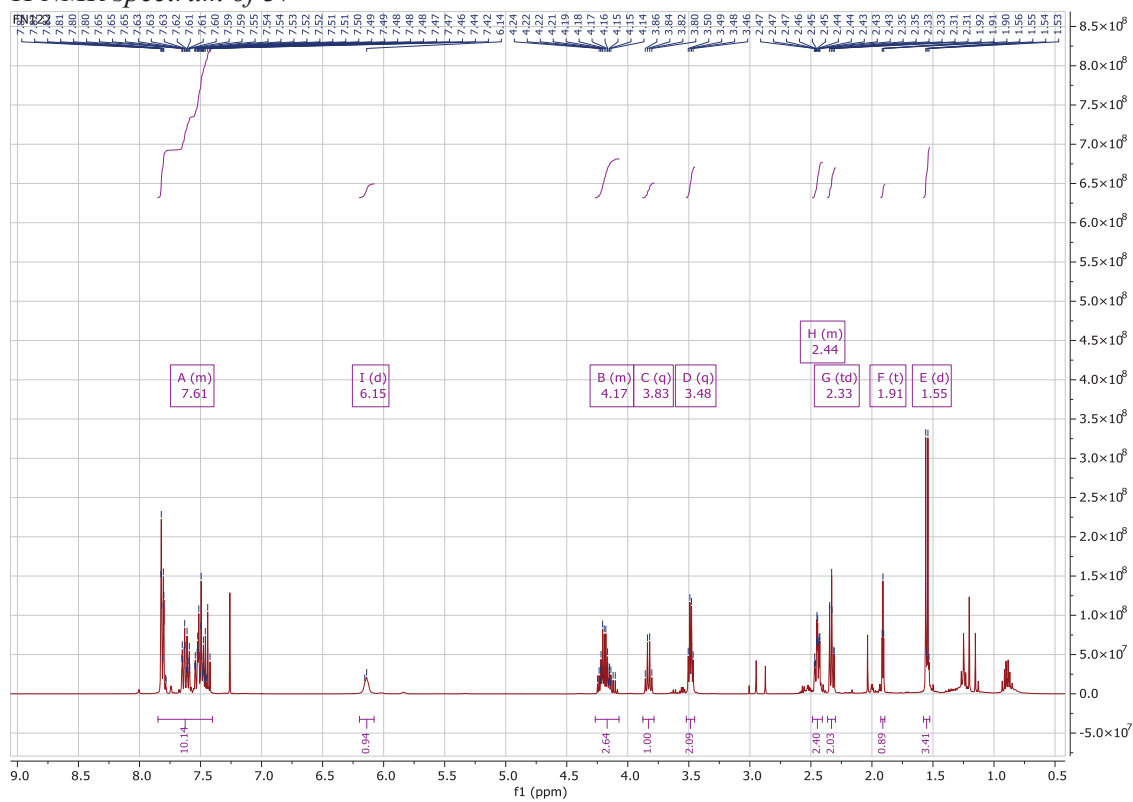
¹H NMR (400 MHz, CDCl₃) δ 7.85 – 7.40 (m, 9H, CH_{ar}), 6.15 (d, J = 6.4 Hz, 1H, NH), 4.27 – 4.07 (m, 2H, O-CH₂), 3.83 (q, J = 7.2 Hz, 1H, CH), 3.48 (q, J = 5.4 Hz, 2H, HN-CH₂), 2.49 – 2.41 (m, 2H, ONHC-CH₂), 2.33 (td, J = 7.2, 1.0 Hz, 2H, \equiv C-CH₂), 1.91 (t, J = 2.6 Hz, 1H, \equiv CH), 1.55 (d, J = 7.2 Hz, 3H, CH₃).

¹³C NMR (101 MHz, CDCl₃) δ 196.85 (CO), 173.98 (CO), 171.38 (CO), 141.08 (C_{ar}), 138.14 (C_{ar}), 137.28 (C_{ar}), 132.91 (C_{ar}), 131.57 (C_{ar}), 130.28 (2 x C_{ar}), 129.31 (C_{ar}), 129.18 (C_{ar}), 128.64 (C_{ar}), 128.52 (2 x C_{ar}), 83.01 (C \equiv CH), 69.33 (C \equiv CH), 63.90 (CH), 45.46 (CH₂), 38.85 (CH₂), 35.18 (CH₂), 18.30 (CH₂), 14.92 (CH₃).

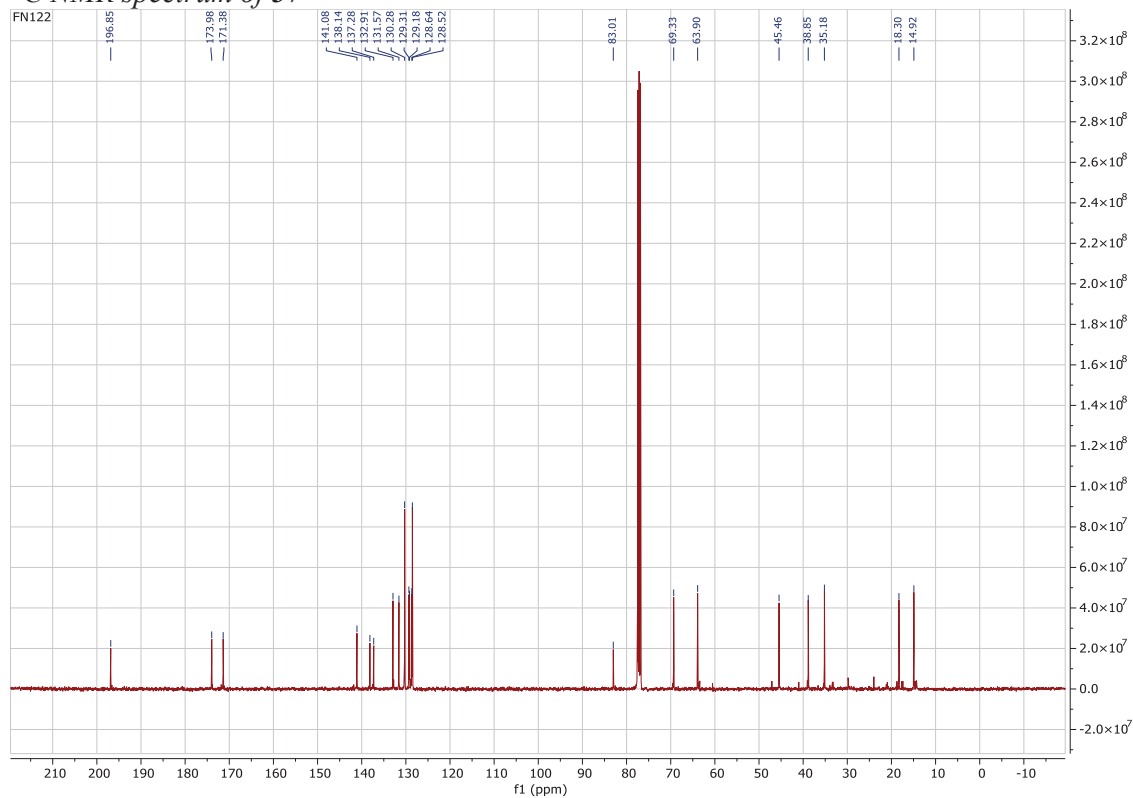
HRMS (ESI/QTOF) m/z: [M + Na]⁺ Calcd for C₂₃H₂₃NNaO₄⁺ 400.1519; Found 400.1523.

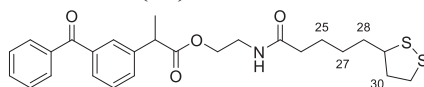
IR (cm⁻¹): 701, 920, 1175, 1281, 1537, 1656, 1730, 3296

¹H NMR spectrum of 37



¹³C NMR spectrum of 37



Lipoic acid Ketoprofen-ethanolamine (38)

Lipoic acid (213 mg, 1.03 mmol, 1 eq.) was dissolved in DMF (5 mL). Ketoprofen-ethanolamine (**36**) (413 mg, 1.24 mmol, 1.2 eq.), HOBt (316 mg, 2.06 mmol, 2 eq.), EDCI (237 mg, 1.24 mmol, 1.2 eq.) and DIPEA (511 μ L, 3.09 mmol, 3 eq.) were added. The reaction mixture was stirred at 23°C for 12 hr. The solvent was removed in vacuo and the residue was dissolved in EtOAc (10 mL). The solution was washed with water (2 x 10 mL) and brine (1 x 10 mL). The organic phase was dried over $MgSO_4$ and concentrated in vacuo. The product was purified by FCC on silica gel (EtOAc:PE = 0:1 \rightarrow 1:1) to afford the desired product (**38**) as a yellowish solid (0.213 g, 0.44 mmol, 43%).

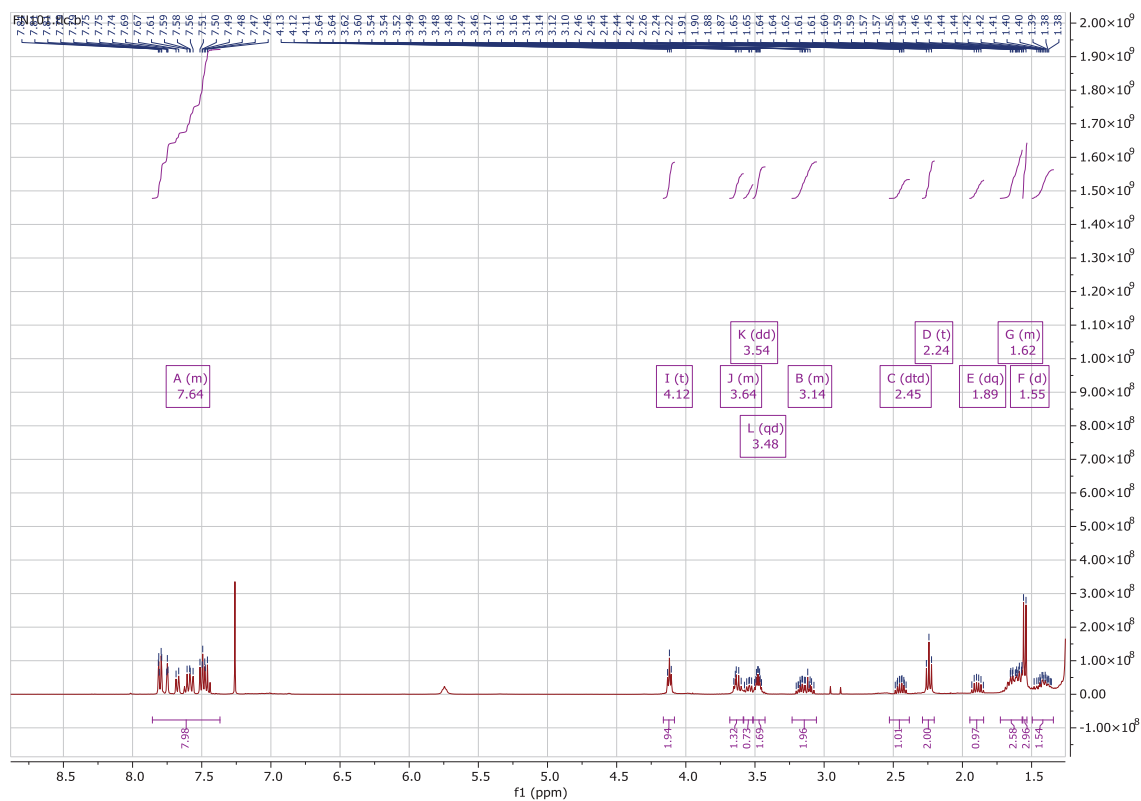
1H NMR (400 MHz, $CDCl_3$) δ 7.86 – 7.37 (m, 9H, CH_{ar}), 4.12 (t, J = 5.4 Hz, 2H, (CH_2-NHC)), 3.68 – 3.58 (m, 1H ($CH-CH_3$)), 3.54 (dd, J = 8.1, 6.1 Hz, 1H, ($CH-S$)), 3.48 (qd, J = 5.5, 3.7 Hz, 2H, (CH_2-OCO)), 3.23 – 3.06 (m, 2H, CH_2-S), 2.45 (dtd, J = 13.0, 6.6, 5.4 Hz, 1H, CH_2 (30')), 2.24 (t, J = 7.4 Hz, 2H, CH_2-CON), 1.89 (dq, J = 13.6, 6.9 Hz, 1H, CH_2 (30'')), 1.73 – 1.57 (m, 4H, 2 x CH_2 (25, 26)), 1.55 (d, J = 7.2 Hz, 3H, (CH_3)), 1.49 – 1.34 (m, 2H, CH_2 (27)).

^{13}C NMR (101 MHz, $CDCl_3$) δ 196.58 (CO), 173.80 (CO), 173.62 (CO), 141.84 (C_{ar}), 138.24 (C_{ar}), 137.50 (C_{ar}), 132.78 (C_{ar}), 131.64 (C_{ar}), 130.22 (2 x C_{ar}), 129.33 (C_{ar}), 129.24 (C_{ar}), 128.93 (C_{ar}), 128.52 (2 x C_{ar}), 63.07 (CH_2-O), 56.49 ($CH-C_{ar}$), 47.13 ($CH-S$), 40.40 (30), 39.21 (CH_2-NH), 38.63 (CH_2-S), 34.67 (25), 33.94 (CH_2-CON), 28.84 (27), 24.67 (28), 18.79 (CH_3)

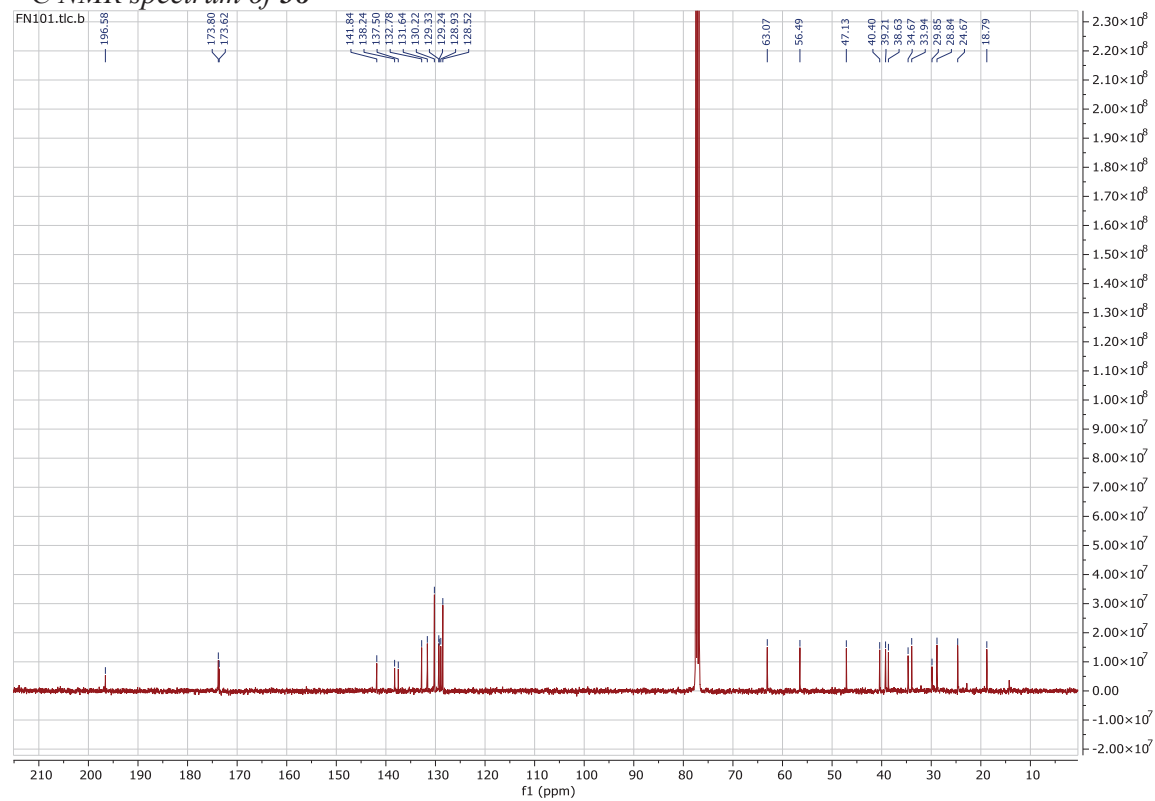
HRMS (ESI/QTOF) m/z : $[M + Na]^+$ Calcd for $C_{26}H_{31}NNaO_4S_2^+$ 508.1587; Found 508.1589

IR (cm^{-1}): 718, 1172, 1291, 1657, 1739, 1531, 1449, 2929, 3307

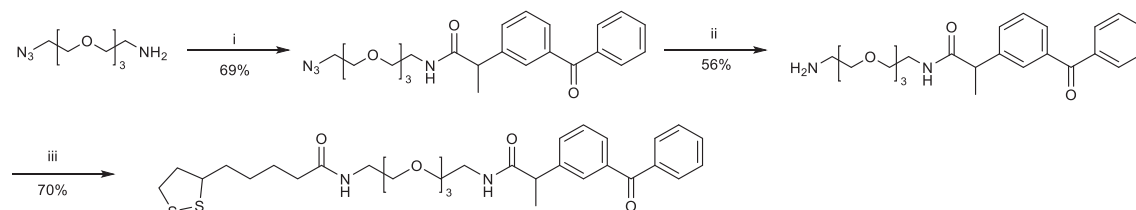
^1H NMR spectrum of **38**



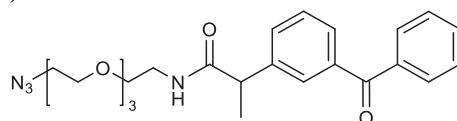
^{13}C NMR spectrum of **38**



KET-TEG-LA



Scheme 23 : Synthesis ketoprofen derivatives with TEG linkers. Reagents and conditions: *i*- ketoprofen, EDCI, HOBT, DIPEA, 23°C, 12 hr; *ii*- PPh₃, H₂O, 23°C, 12 hr; *iii*- lipoic acid, HOBT, EDCI, DIPEA, 23°C, 12 hr

Ketoprofen-TEG-azide (**39**)

Tetra(ethylene glycol) derivative, amine-TEG-azide (**22**) (0.182 g, 0.71 mmol, 1 equiv) was dissolved in DMF (4 mL). Ketoprofen (0.184 g, 0.72 mmol, 1.01 equiv), HOBT (0.164 g, 1.07 mmol, 1.5 equiv), EDCI (0.274 g, 1.42 mmol, 2.0 equiv) and DIPEA (0.354 mL, 2.14 mmol, 3.0 equiv) were added to the solution. The reaction mixture was stirred at 23°C for 12 hr. The solvent was removed in vacuo and the residue was dissolved in DCM (10 mL). The solution was washed with sat. aq. NH₄Cl solution (2 x 10 mL) and brine (1 x 10 mL). The organic phase was dried over MgSO₄ and concentrated in vacuo. The product was purified by FCC (DCM:MeOH = 20:1 → 9:1) to afford ketoprofen-TEG-azid (**39**) as a yellow oil (0.223 g, 0.49 mmol, 69%).

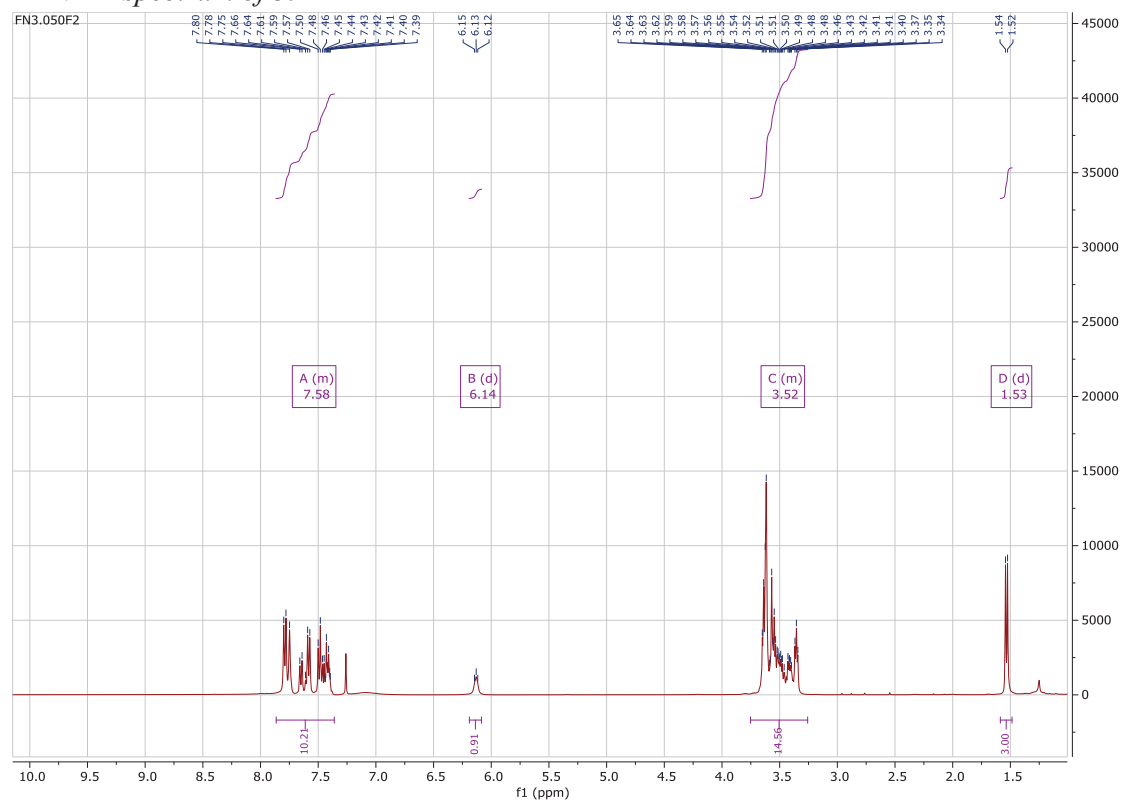
¹H NMR (400 MHz, CDCl₃) δ 7.83 – 7.40 (m, 9H, CH_{ar}), 6.07 (d, J = 5.3 Hz, 1H, NH), 3.70 – 3.30 (m, 17H, CH₂-CH₂-O + CH), 1.54 (d, J = 7.1 Hz, 2H, CH₃).

¹³C NMR (101 MHz, CDCl₃) δ 196.65 (CO), 173.79 (CO), 142.35 (C ar), 137.91 (C ar), 137.60 (C ar), 132.58 (C ar), 131.62 (C ar), 130.14 (2 X C ar), 129.23 (C ar), 128.97 (C ar), 128.64 (C ar), 128.63 (C ar), 128.40 (2 x C ar), 70.55 (CH₂), 70.52 (CH₂), 70.29 (CH₂), 70.18 (CH₂), 70.01 (CH₂), 46.77 (CH-CH₃), 39.51 (CH₂), 18.85 (CH₃).

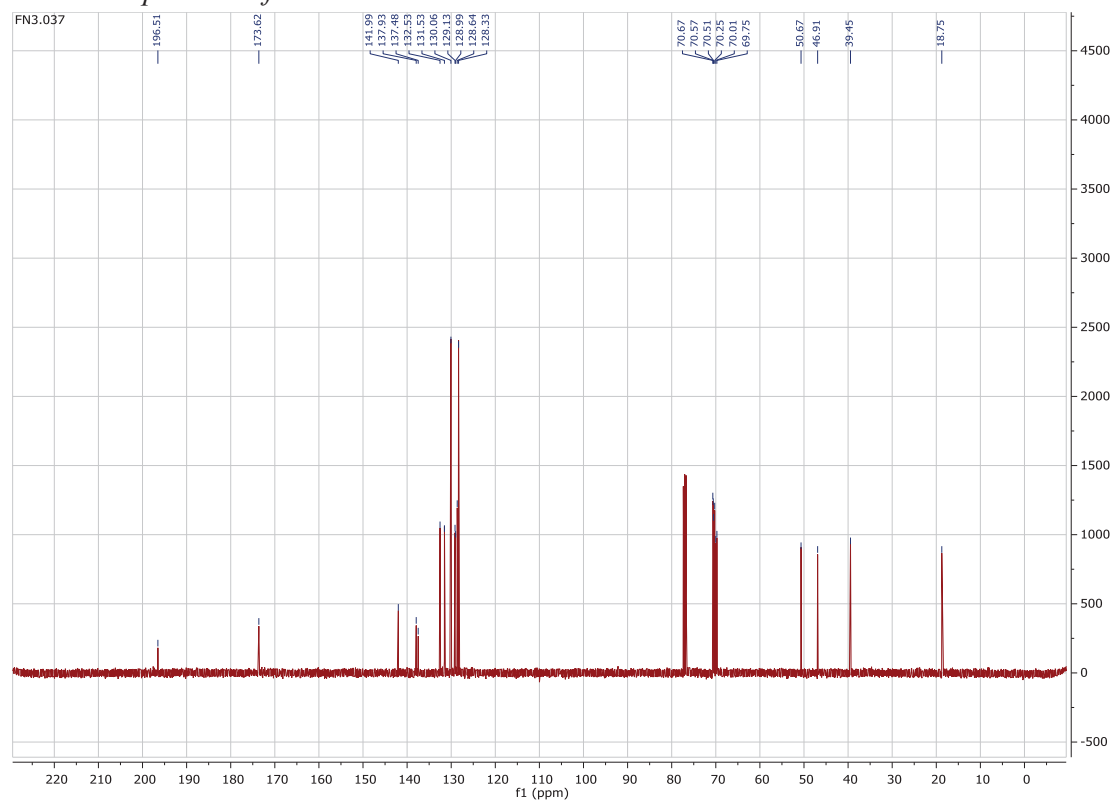
HRMS (ESI/QTOF) m/z: [M + Na]⁺ Calcd for C₂₄H₃₀N₄NaO₅⁺ 477.2114; Found 477.2127

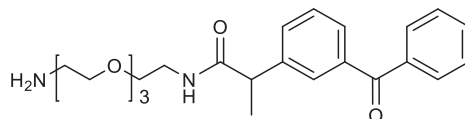
IR (cm⁻¹): 2880, 2095, 1655, 1285, 1115

¹H NMR spectrum of 39



¹³C NMR spectrum of 39



Ketoprofen-TEG-amine (40)

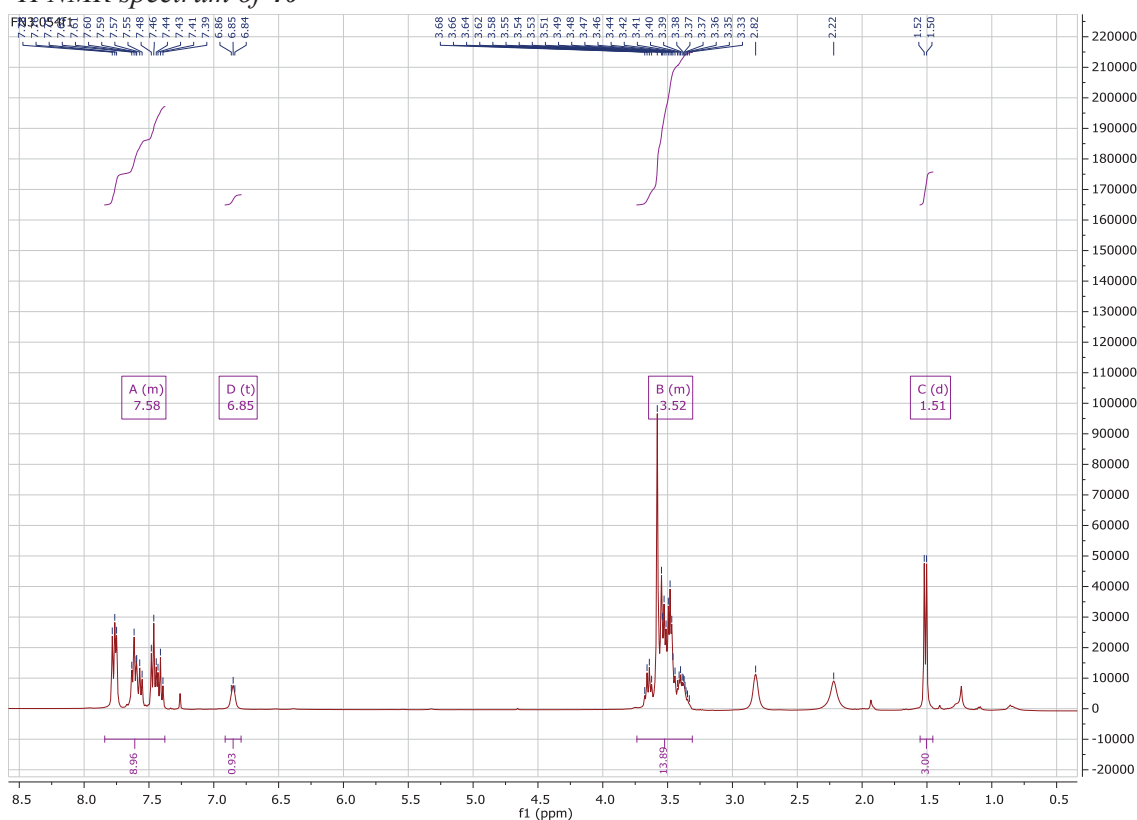
Ketoprofen-TEG-azide (**39**) (0.368 g, 0.81 mmol, 1.0 equiv,) was dissolved in THF (6 mL). Triphenylphosphine (0.297 g, 1.1 mmol, 1.4 equiv) was added and the solution was stirred at 23°C for 1 hr. Water (1 mL) was added and the reaction mixture was stirred at 23°C for 12 hr. The solvent was removed in vacuo. The residue was purified by FCC (DCM:MeOH:NEt₃ = 10:1:0.1) to afford ketoprofen-TEG-amine (**40**) as a yellow oil (0.195 g, 0.45 mmol, 56%).

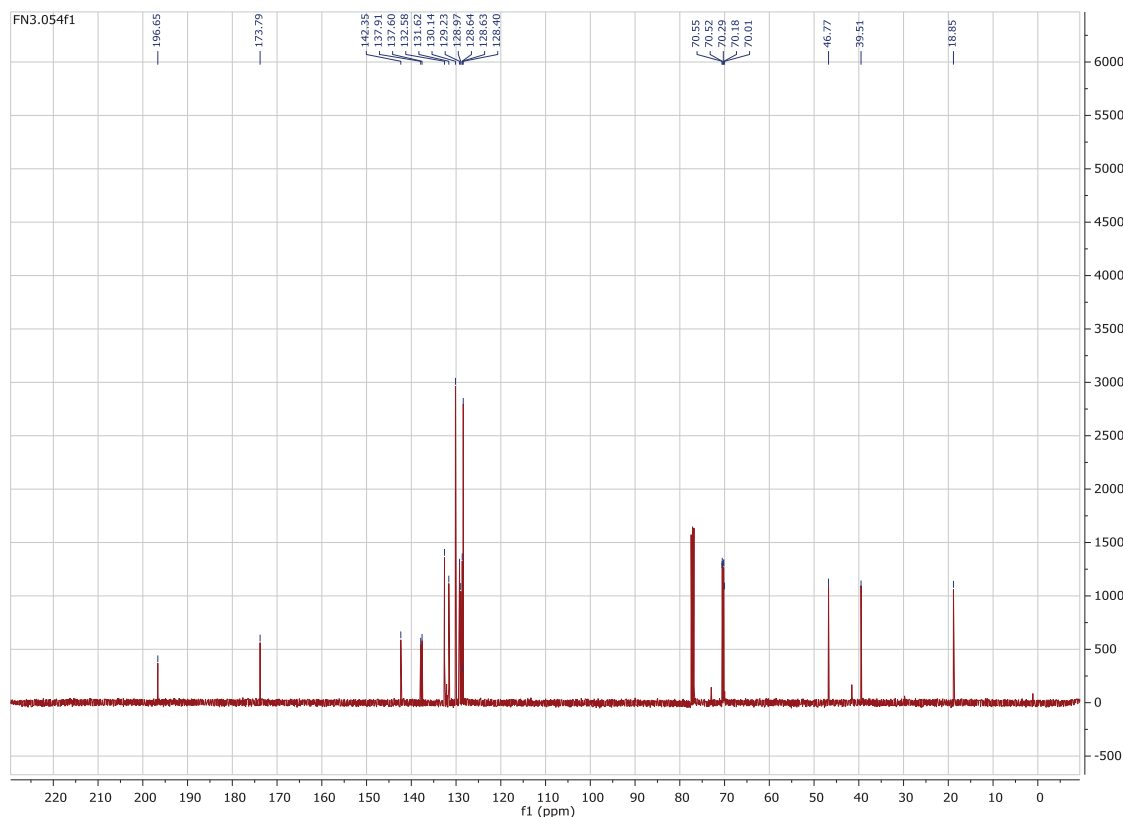
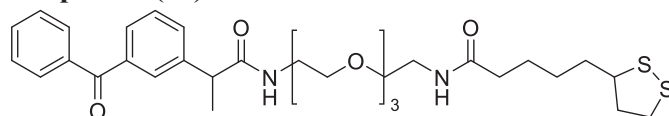
¹H NMR (400 MHz, CDCl₃) δ 7.84 – 7.38 (m, 9H, ar.), 6.85 (t, J = 5.4 Hz, 1H, NH), 3.74 – 3.31 (m, 17H, CH₂-CH₂-O + CH), 1.51 (d, J = 7.1 Hz, 3H, CH₃).

¹³C NMR (101 MHz, CDCl₃) δ 196.65 (CO), 173.79 (CO), 142.35 (C ar.), 137.91 (C ar), 137.60 (C ar), 132.58 (C ar), 131.62 (C ar), 130.14 (2 X C ar), 129.23 (C ar), 128.97 (C ar), 128.64 (C ar), 128.63 (C ar), 128.40 (2 x C ar), 70.55 (CH₂), 70.52 (CH₂), 70.29 (CH₂), 70.18 (CH₂), 70.01 (CH₂), 46.77 (CH-CH₃), 39.51 (CH₂), 18.85 (CH₃).

HRMS (ESI/QTOF) m/z: [M + H]⁺ Calcd for C₂₄H₃₃N₂O₅⁺ 429.2384; Found 429.2379.

IR (cm⁻¹): 2925, 1660, 1080.

¹H NMR spectrum of 40

¹³C NMR spectrum of **40**Lipoic acid-TEG-Ketoprofen (**41**)

To a solution of **40** (0.519 g, 1.21 mmol, 1 equiv) in DMF (4 mL), were added lipoic acid (0.3 g, 1.45 mmol, 1.2 equiv), HOBt (0.371 g, 2.42 mmol, 2 equiv), EDCI (0.28 g, 1.45 mmol, 1.2 equiv) and DIPEA (0.51 ml, 3.64 mmol, 3 equiv). The reaction mixture was stirred at 23°C for 12 hr. The solvent was removed in vacuo and the residue was dissolved in DCM (5 mL). The solution was washed with water (3 x 5 mL) and the organic phase was dried over MgSO₄ and concentrated in vacuo. The product was purified by FCC (DCM:MeOH = 20:1) to afford **41** as a yellowish solid (0.52 g, 0.85 mmol, 70%).

¹H NMR (400 MHz, CDCl₃) δ 7.84 – 7.40 (m, 9H, ar.), 6.17 (2 bs, 2H, 2 x NH), 3.68 – 3.36 (m, 18H, CH₂-CH₂-O, CH-Me, CH-S), 3.22 – 3.05 (m, 2H, CH₂-S), 2.44 (dq, J = 12.5, 6.3 Hz, 1H, CH₂-CH₂S), 2.16 (t, J = 7.5 Hz, 2H, CH₂-C(O)NH), 1.89 (dq, J = 13.7, 7.0 Hz, 1H, CH₂-CH₂S), 1.75 – 1.58 (m, 4H, 2 x CH₂), 1.54 (d, J = 7.1 Hz, 3H, CH₃), 1.44 (ddd, J = 14.8, 8.3, 5.8 Hz, 2H, CH₂).

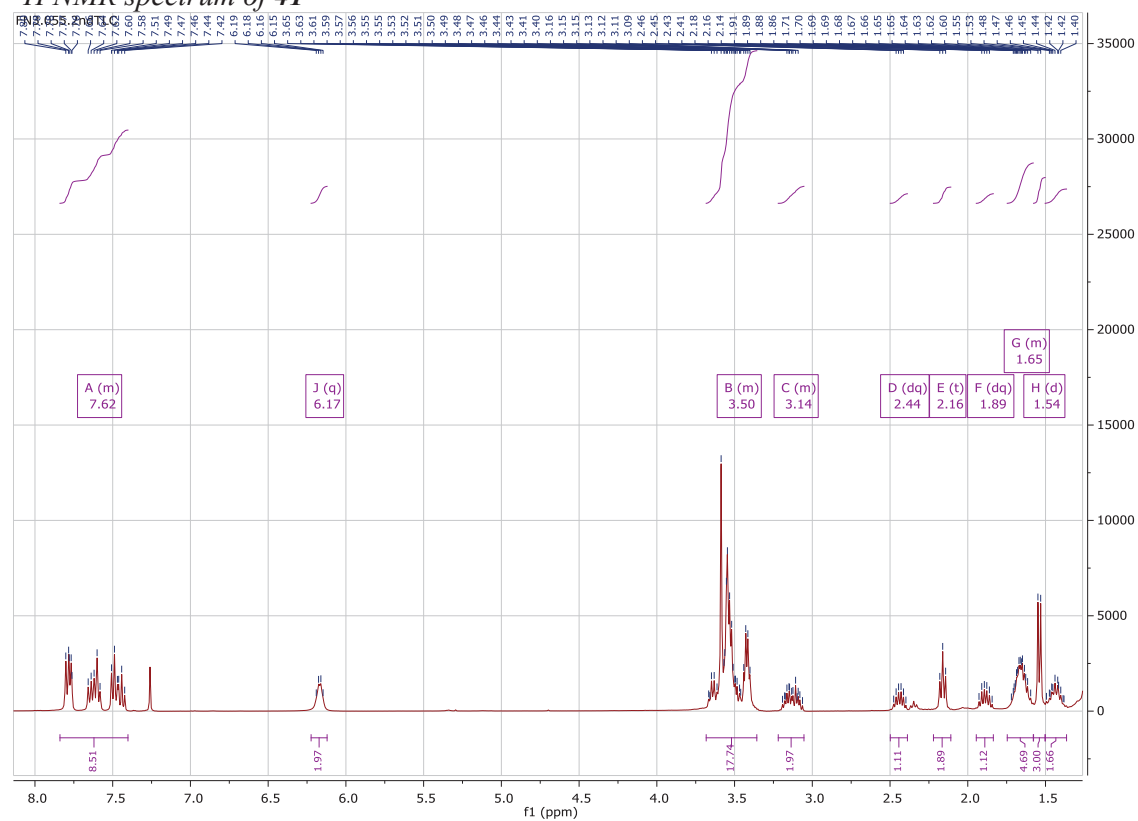
¹³C NMR (101 MHz, CDCl₃) δ 196.70 (CO), 173.75 (CO), 173.00 (CO), 142.19 (C ar.), 138.05 (C ar.), 137.57 (C ar.), 132.73 (C ar.), 131.68 (C ar.), 130.20 (2 x C ar.), 129.26 (C ar.), 129.20 (C ar.), 128.78 (C ar.), 128.50 (2 x C ar.), 70.58 (CH₂), 70.55 (CH₂), 70.36 (CH₂), 70.30 (CH₂),

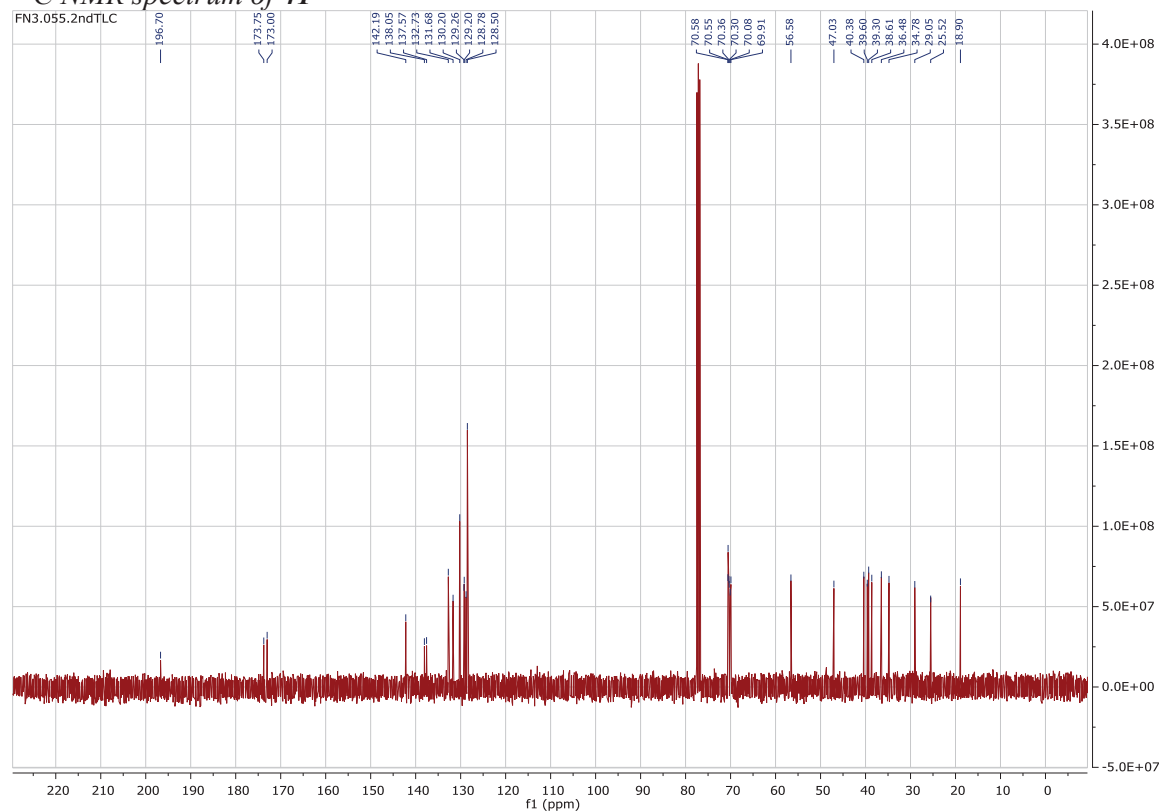
70.08 (CH₂), 69.91 (CH₂), 56.58 (CH), 47.03 (CH), 40.38 (CH₂), 39.60 (CH₂), 39.30 (CH₂), 38.61 (CH₂), 36.48 (CH₂), 34.78 (CH₂), 29.05 (CH₂), 25.52 (CH₂), 18.90 (CH₃).

HRMS (ESI/QTOF) m/z: [M + H]⁺ Calcd for C₃₂H₄₅N₂O₆S₂⁺ 617.2719; Found 617.2718

IR (cm⁻¹): 3314, 2938, 1657, 1560, 1452, 1370, 1267, 1097

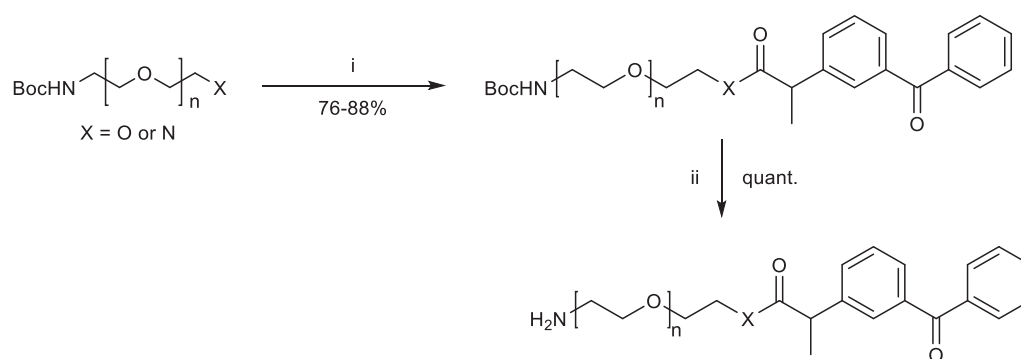
¹H NMR spectrum of 41



¹³C NMR spectrum of 41

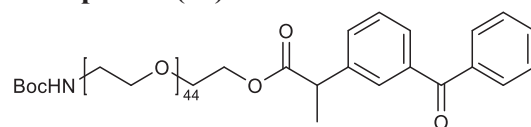
5.8 PREPARATION OF PEG-KET AND GRAFTING ON ALGINATE

The following synthesis has been published in Antifibrotic Effect of Ketoprofen-Grafted Alginate Microcapsules in the Transplantation of Insulin Producing Cells. *Bioconjug. Chem.* Copyright 2018.²²⁵



Scheme 24: Synthesis ketoprofen derivatives with PEG linkers. Reagents and conditions: i- ketoprofen, [DCC, DMAP] or [HOBt, EDCI, DIPEA] 23°C, 12 hr; ii-HCl 4N, 23°C, 2 hr.

N-Boc-amine-PEG-ester-ketoprofen (42)



(0.234 g, 0.111 mmol, 1.0 equiv) of TBOC-PEG2000-OH was dissolved in DCM (2 mL). Ketoprofen (29 mg, 0.112 mmol, 1.01 equiv), DCC (0.025 mg, 0.1224 mmol, 1.1 equiv) and DMAP (1 mg, 0.011 mmol, 0.1 equiv) were added to the reaction mixture. The reaction was stirred at 23°C for 12 hr. After concentration under reduced pressure, the crude residue was purified by FCC (DCM:MeOH = 30:1→10:1) to afford a white solid (0.234 g, 0.098 mmol, 88%).

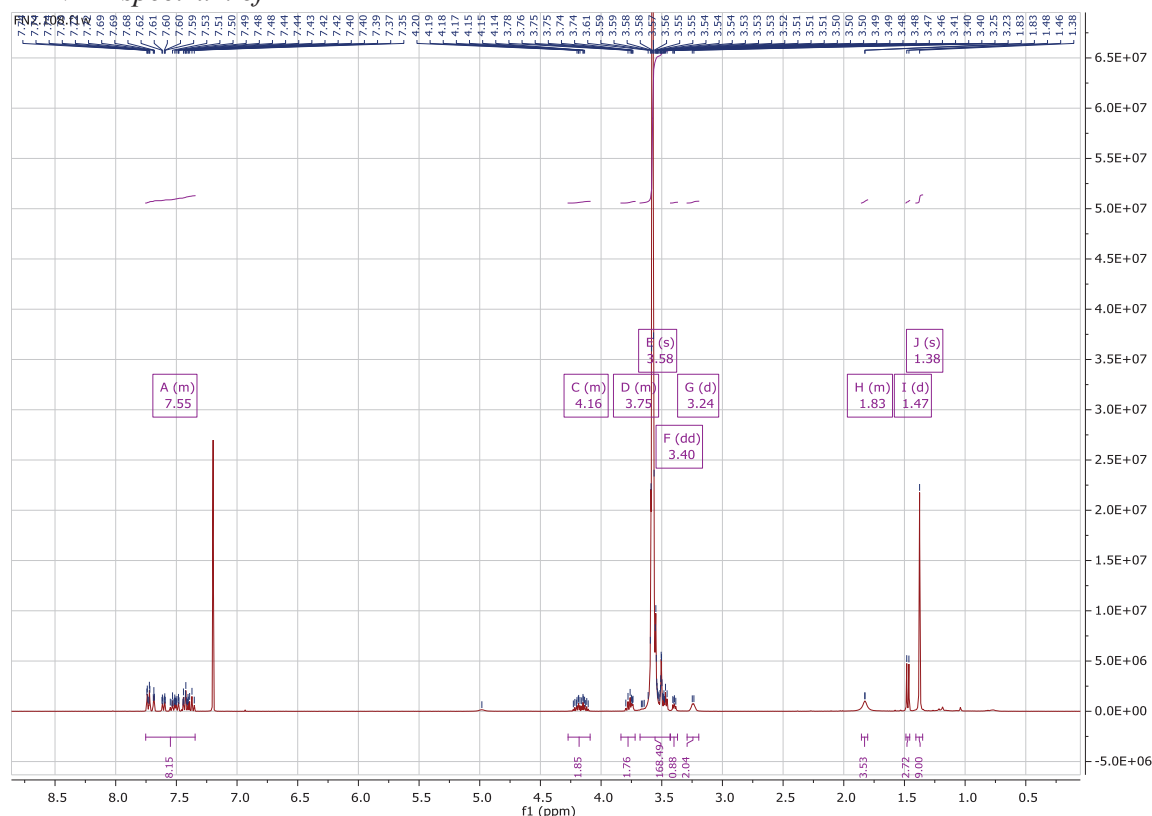
¹H-NMR spectrum (400 MHz, CDCl₃) δ 7.75 – 7.35 (m, 9H, CH_{ar}), 4.27 – 4.09 (m, 2H, CH₂-NHBoc), 3.84 – 3.72 (m, 2H, CH₂-OC(O)), 3.58 (s, 174H, CH₂, PEG), 3.40 (dd, J = 5.8, 4.1 Hz, 1H, CH-Me), 3.24 (d, J = 5.4 Hz, 2H, CH₂-CH₂O), 1.89 – 1.78 (bs, 1H, NH), 1.47 (d, J = 7.2 Hz, 3H, CH₃), 1.38 (s, 9H, CH₃(Boc)).

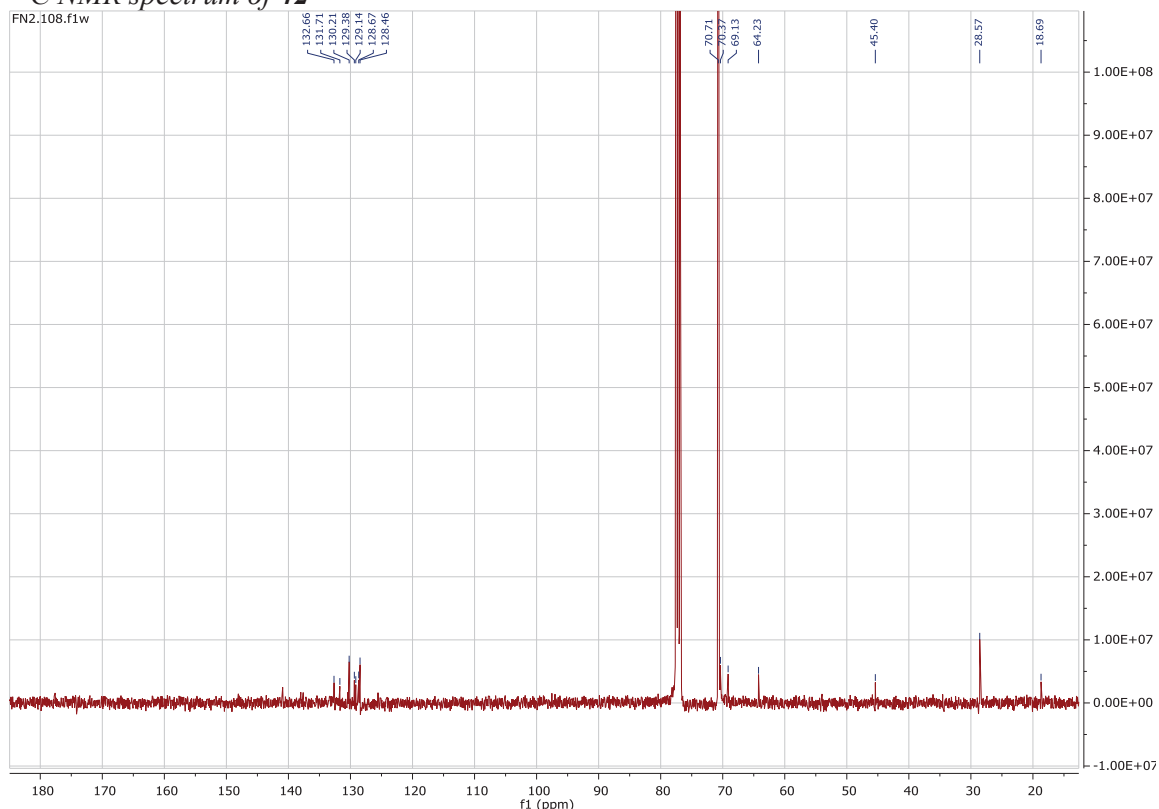
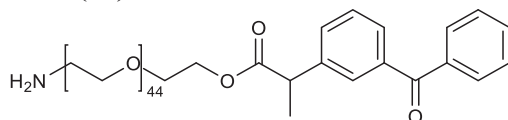
¹³C-NMR spectrum (101 MHz, CDCl₃) δ 132.66 (C_{ar}), 131.71 (C_{ar}), 130.21 (2 x C_{ar}), 129.38 (C_{ar}), 129.14 (C_{ar}), 128.67 (C_{ar}), 128.46 (2 x C_{ar}), 70.71 (CH₂), 70.37 (CH₂), 69.13 (CH₂), 64.23 (CH₂), 45.40 (CH), 28.57 (CH₂), 18.69 (3 x CH₃), 18.69 (CH₃).

Mass MALDI m/z: [M + Na]⁺ Calcd for C₁₁₁H₂₀₃NNaO₄₉⁺ 2357.3321; Found 2356.599

IR (cm⁻¹): 2870, 1350, 1250, 1105

¹H NMR spectrum of 42



¹³C NMR spectrum of **42**Amine-PEG-ester-ketoprofen (**44**)

N-Boc-amine-PEG-ester-ketoprofen (**42**) (0.234 g, 0.100 mmol, 1.0 equiv) was dissolved in a solution of HCl 4N in dioxane (3 mL) and the mixture was stirred at 23°C until completion of the reaction (2 hr, monitored by TLC). The volatiles were removed under air flow and the product was dried in vacuo to afford amine-PEG-ester-ketoprofen (**44**) as a beige solid (0.225 g, quant.) which was used without further purification.

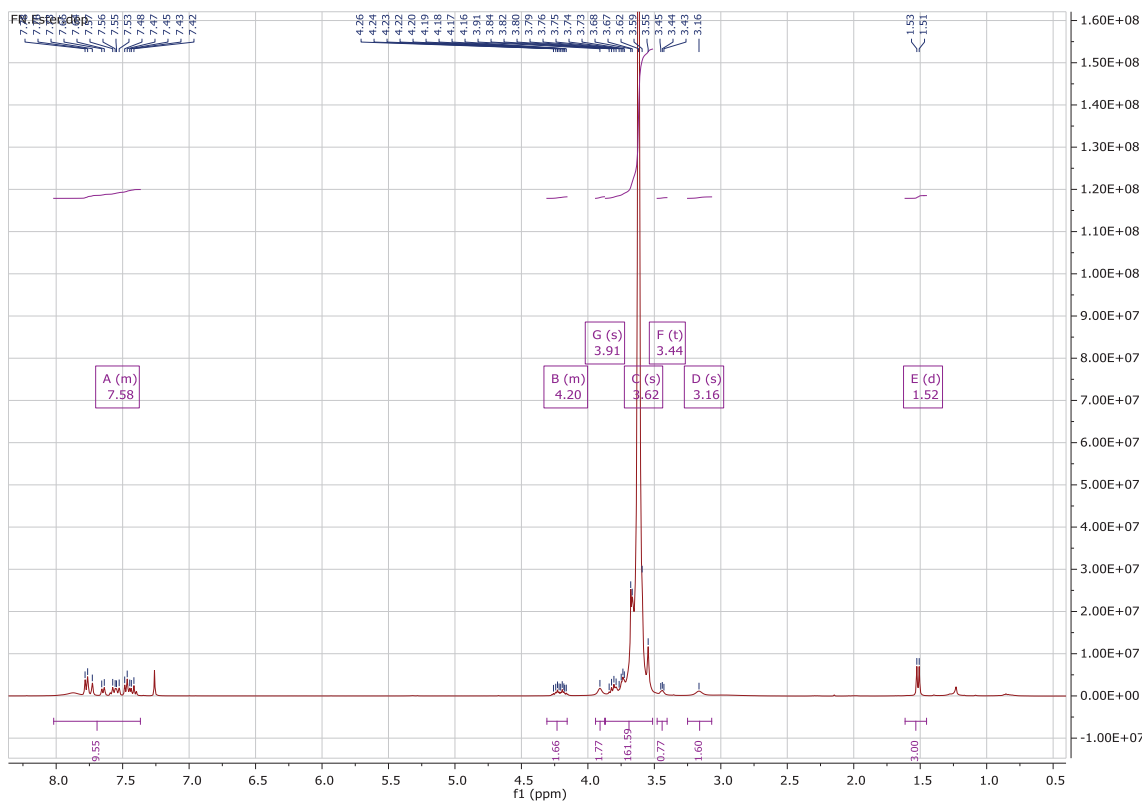
¹H-NMR spectrum (400 MHz, CDCl₃) δ 7.8.02 – 7.37 (m, 9H, CH_{ar}), 4.31 – 4.16 (m, 2H, CH₂-NH₂), 3.91 (s, 2H, CH₂-OC(O)), 3.62 (s, 174H, PEG), 3.44 (t, J = 4.8 Hz, 1H, CH-Me), 3.16 (s, 2H, CH₂-CH₂O), 1.52 (d, J = 7.2 Hz, 3H, CH₃).

¹³C NMR (101 MHz, CDCl₃) δ 196.49 (CO), 174.08 (CO), 140.88 (C_{ar}), 137.96 (C_{ar}), 137.58 (C_{ar}), 132.58(C_{ar}), 131.65 (C_{ar}), 130.14 (2 x C_{ar}), 129.31 (C_{ar}), 129.06 (C_{ar}), 128.60 (C_{ar}), 128.40 (2 x C_{ar}), 70.67 (n x CH₂), 69.08 (CH₂), 67.18 (CH₂), 64.18 (CH₂), 45.37 (CH), 18.64 (CH₃).

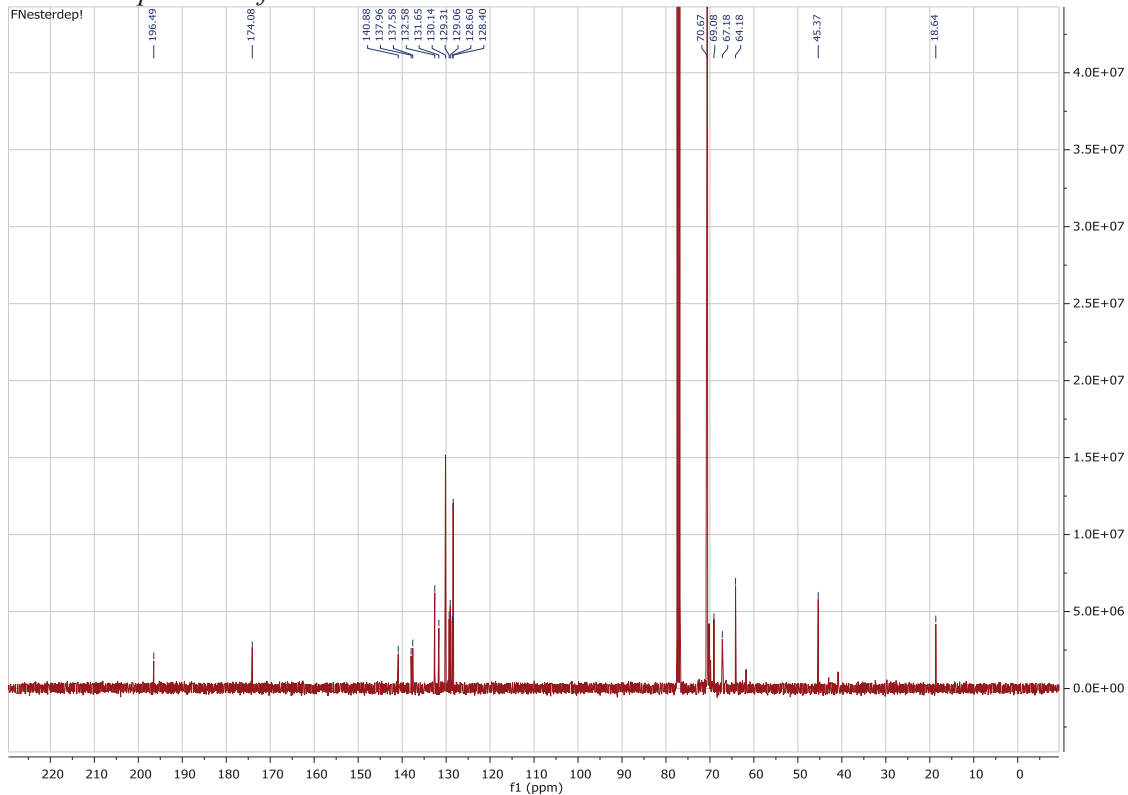
HRMS (ESI/QTOF) m/z: [M + H]⁺ Calcd for C₁₀₆H₁₉₆NO₄₇⁺ 2235.2979; Found 2235.2905

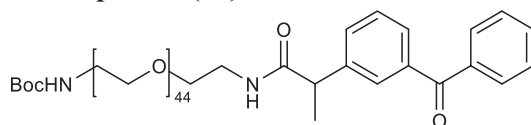
IR (cm⁻¹): 2880, 1465, 1345, 1280, 1240, 1105, 960, 840

¹H NMR spectrum of 44



¹³C NMR spectrum of 44



N-Boc-amine-PEG-amide-ketoprofen (43)

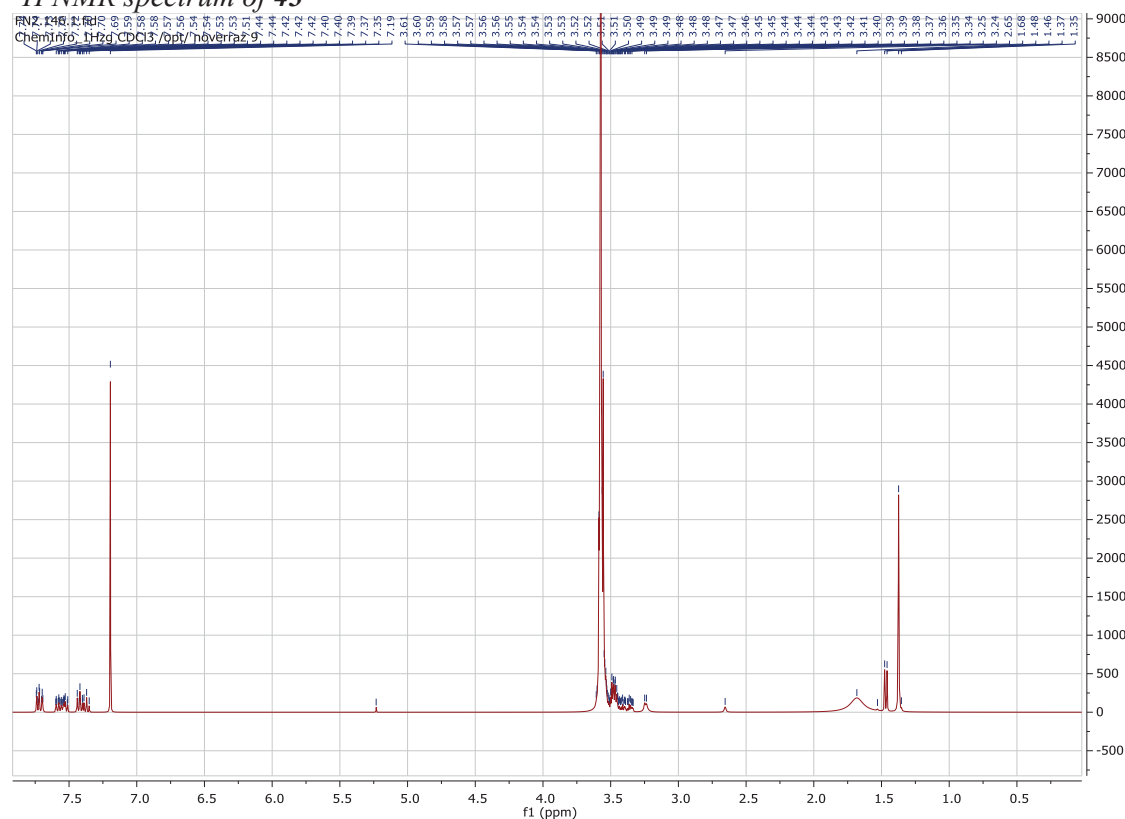
(0.100 g, 0.047 mmol, 1.0 equiv) of TBOC-PEG2000-NH₂ was dissolved in DMF (5 mL). Ketoprofen (0.012 g, 0.047 mmol, 1.01 equiv), HOBt (0.011 g, 0.070 mmol, 1.5 equiv), EDCI (0.018 g, 0.094 mmol, 2.0 equiv) and DIPEA (0.023 mL, 0.140 mmol, 3.0 equiv) were added. The reaction mixture was stirred at 23°C for 12 hr. The solvent was removed under vacuum. The residue was dissolved in DCM (10 mL) and washed with sat. NH₄Cl solution (2 x 10 mL) and brine (1 x 10 mL). The organic layer was dried with MgSO₄ and concentrated under vacuum. Purification by FCC on silica gel (DCM:MeOH = 20:1 → 9:1) afforded **43** as a white solid (0.084 g, 0.036 mmol, 76%).

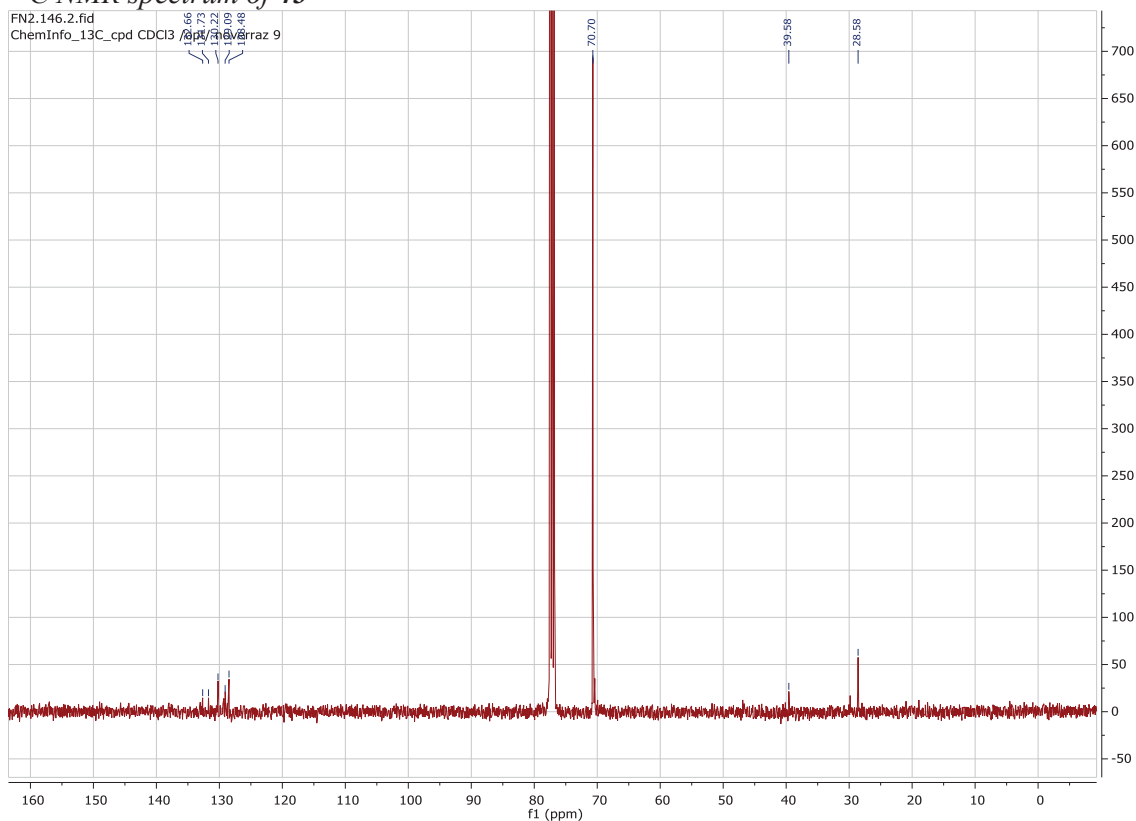
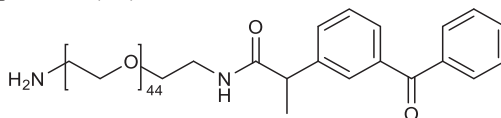
¹H NMR spectrum (400 MHz, CDCl₃) δ 7.84 – 7.35 (m, 9H, CH_{ar}), 3.70 – 3.29 (m, 176H, CH₂, PEG), 1.53 (d, *J* = 7.1 Hz, 3H, CH₃), 1.44 (s, 9H, CH₃(Boc)).

¹³C NMR (101 MHz, CDCl₃) δ 132.66 (C_{ar}), 131.73 (C_{ar}), 130.22 (2 x C_{ar}), 129.09 (C_{ar}), 128.48 (2 x C_{ar}), 70.70 (n x CH₂), 39.58 (CH₂), 28.58(CH₂).

HRMS (ESI/QTOF) *m/z*: [M + Na]⁺ Calcd for C₁₁₁H₂₀₄N₂NaO₄₈⁺ 2356.3481; Found 2356.3481

IR (cm⁻¹): 2866, 1106

¹H NMR spectrum of 43

¹³C NMR spectrum of 43**Amine-PEG-amide-ketoprofen (45)**

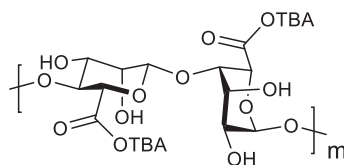
N-Boc-amine-PEG-amide-ketoprofen (**43**) (0.084 g, 1 equiv, 0.036 mmol) was dissolved in a solution of HCl 4N in dioxane (3 mL) and the mixture was stirred at 23°C until completion of the reaction (monitored by TLC). The volatiles were removed under air flow and the product was dried in vacuo to afford amine-PEG-amide-ketoprofen (**45**) as a beige solid (0.083 g, quant.) which was used without further purification.

¹H NMR (400 MHz, CDCl₃) δ 7.84 – 7.38 (m, 9H, ar.), 6.85 (t, J = 5.4 Hz, 1H, NH), 3.74 – 3.31 (m, 14H, CH₂-CH₂-O), 1.51 (d, J = 7.1 Hz, 3H, CH₃).

¹³C NMR (101 MHz, CDCl₃) δ 196.58(CO), 173.66(CO), 142.14 (C ar.), 137.99 (C ar.), 137.58 (C ar.), 132.62 (C ar.), 131.67 (C ar.), 130.16 (2 x C ar.), 129.25 (C ar.), 129.06 (C ar.), 128.72 (C ar.), 128.43 (2 x C ar.), 70.67 (n x CH₂), 66.89 (CH₂), 46.92 (CH), 40.63 (CH₂), 39.55 (CH₂), 29.80 (CH₂), 18.91 (CH₃).

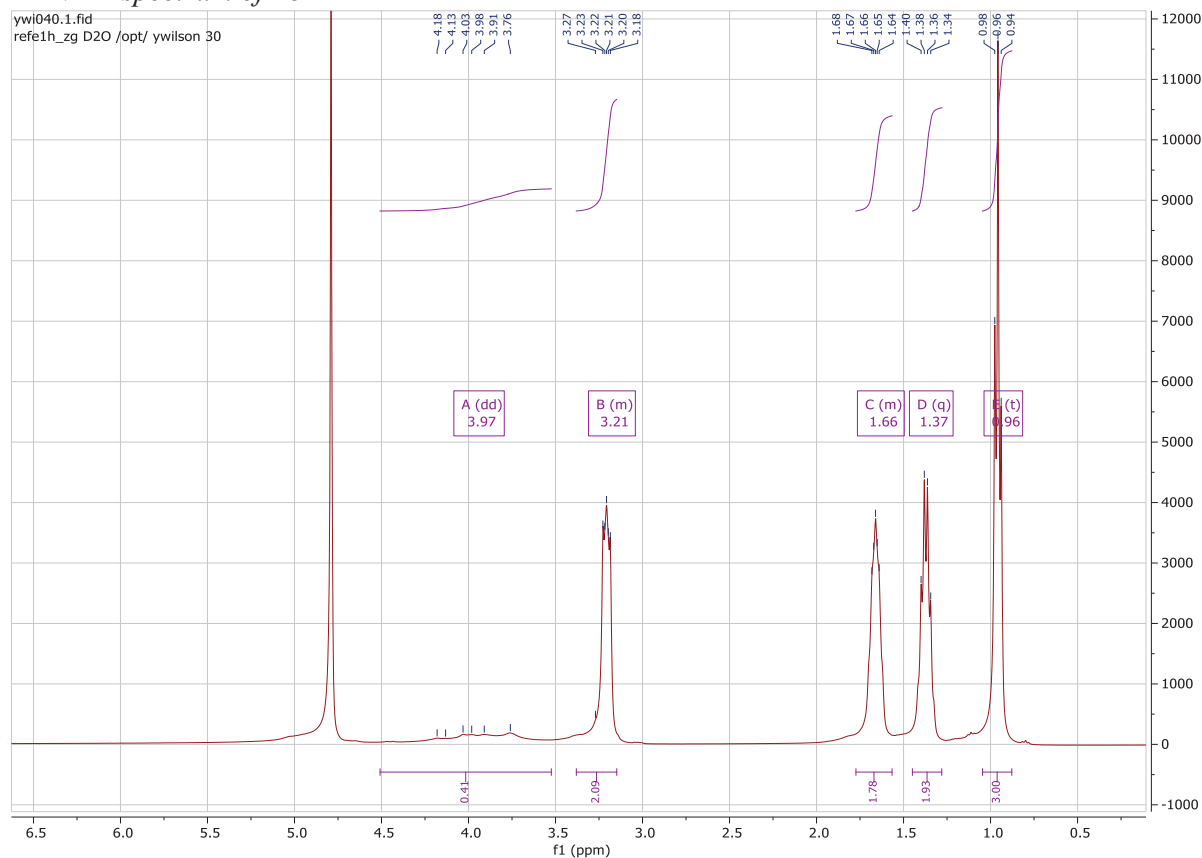
HRMS (ESI/QTOF) m/z: [M + H]⁺ Calcd for C₁₀₆H₁₉₇N₂O₄₆⁺ 2234.3137; Found 2234.3108

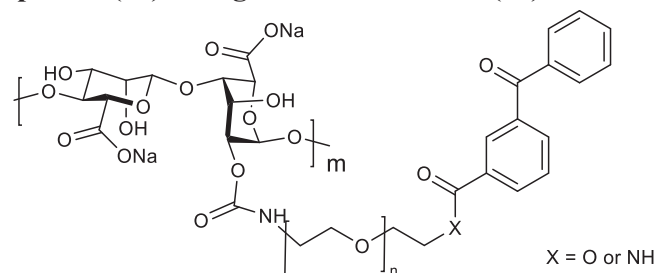
IR (cm⁻¹): 2890, 1103

TBA-Alginate (46)

The following protocol was reported by Passemard et al.¹⁹⁷ Na-alg (Kelton HV) (2 g) was suspended in ethanol (100 mL) and cooled to 0°C under stirring. To the suspension a solution of EtOH:HCOOH = 4:1 (100 mL) was added and the suspension was kept under stirring overnight at 0°C. The suspension was then recover on a vacuum filter, washed with EtOH:H₂O = 1:1 (3 x 50 mL) and acetone (3 x 50 mL). The solid was then re-suspended in water (200 mL) and the solution was basified with the addition of aq. TBAOH (1.5 M) until the pH reached 7-8 which lead to the dissolution of alginate. The mixture was directly freeze in liquid nitrogen and placed in a freeze drier to yield TBA-alg (**46**) (2.3 g, quant.) as a white solid foam.

¹H NMR (400 MHz, Deuterium Oxide) δ 3.97 (dd, $J = 108.6, 59.7$ Hz, alg), 3.38 – 3.15 (m, 2H, CH₂ (TBA)), 1.77 – 1.57 (m, 2H, CH₂ (TBA)), 1.37 (q, $J = 7.4$ Hz, 2H, CH₂ (TBA)), 0.96 (t, $J = 7.4$ Hz, 3H, CH₃ (TBA)).

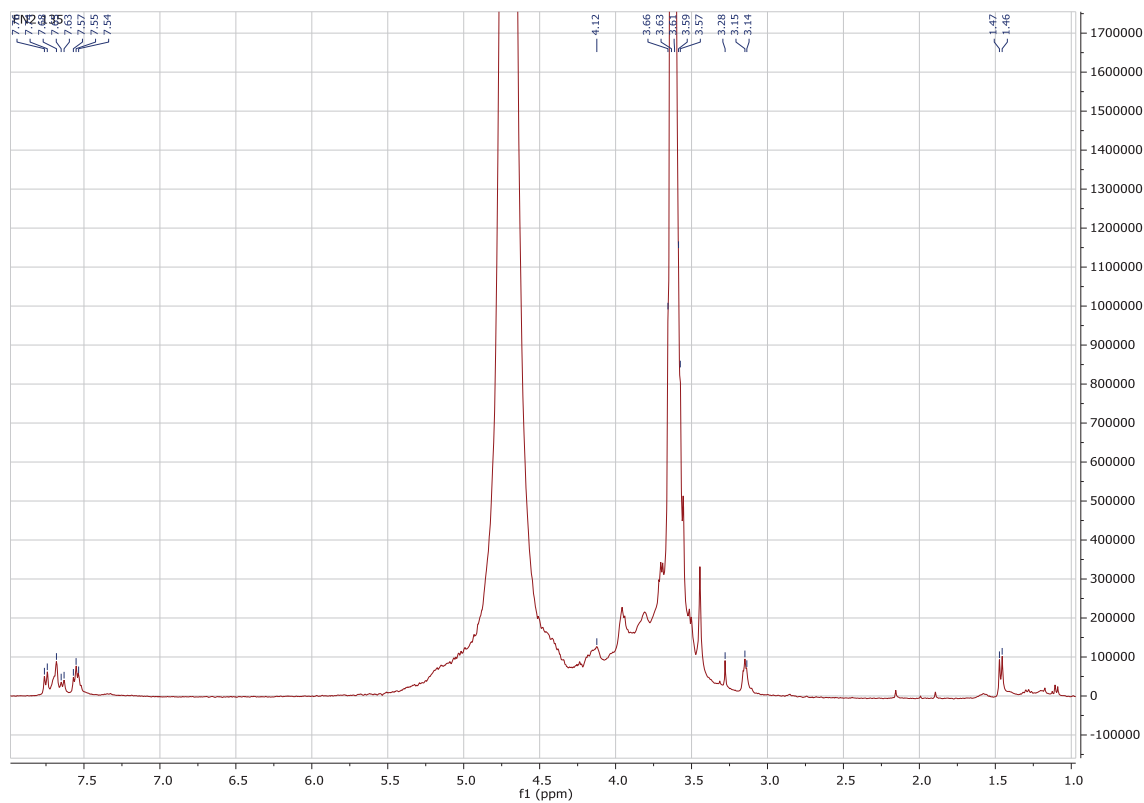
¹H NMR spectrum of 46

Alg-PEG-ester-ketoprofen (47) & Alg-PEG-amide-KET (48)

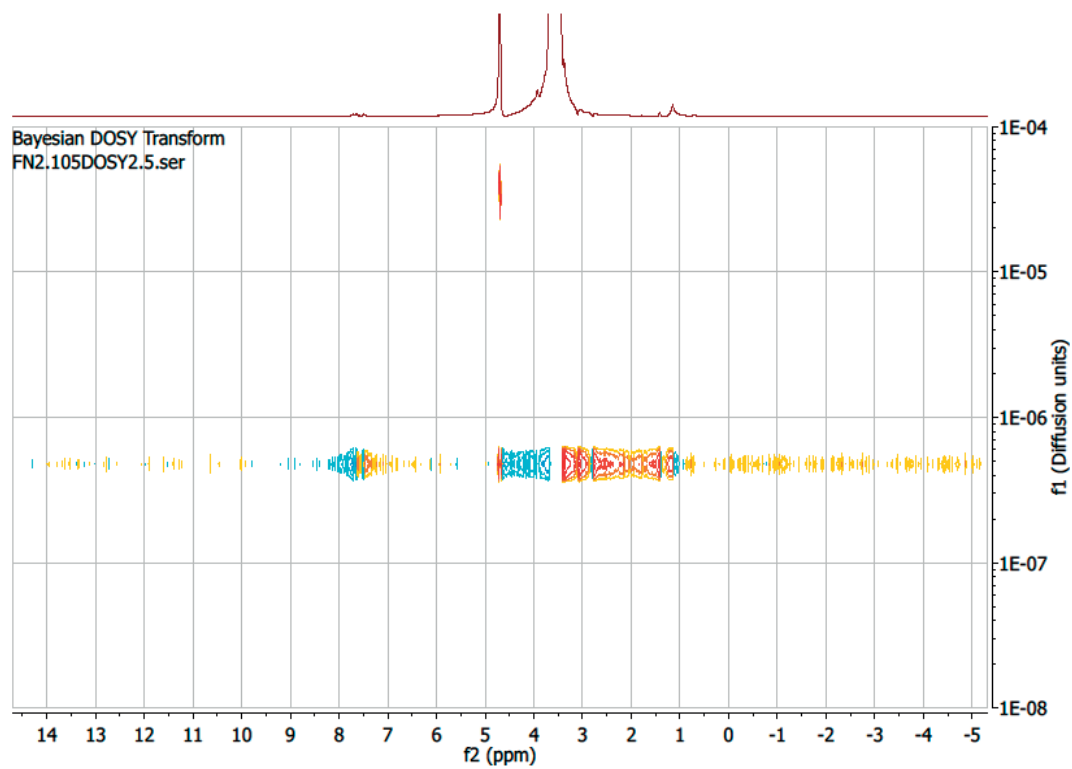
TBA-Alg (**46**) (0.100 g, 0.239 mmol, 1.0 equiv) was dissolved in DMSO (20 mL) and the solution was stirred at 23°C for 12 hr to ensure homogeneity. 1,1'-Carbonyldiimidazole (0.039 g, 0.239 mmol, 1.0 equiv) previously dissolved in a minimum volume of DMSO was added and the reaction mixture was stirred at 23°C for 30 min. To enhance precipitation of the imidazolidine-alginate intermediate, acetone (40 mL) was added. The resulting precipitate was filtered (70 μm) and washed with acetone (3×10 mL). The solid was further dried for 15 min under vacuum at 40 °C and transferred to a round-bottom flask. Distilled water was added (10 mL), and the mixture was stirred until complete dissolution. **44** or **45** (0.0239 mmol, 0.10 equiv.) previously dissolved in a minimum volume of water was added. The solution was stirred at 23°C for 2 hr. The reaction was quenched by addition of 0.05 M NaOH solution until reaching pH 11. The solution was directly transferred into a dialysis membrane (14 kDa) and dialyzed against distilled water. The first day, water was changed once. The dialysis was continued the next day (changing water 3 times that day). The last day, the dialysis was continued against water, with the addition of NaHCO_3 (180 mg in 9 L distilled water) in the dialysis bucket, to reach pH 7. The solution was filtered (70 and 0.22 μm) and freeze-dried to obtain Alg-PEG-ester-KET (**47**) or Alg-PEG-amide-KET (**48**) as white solids.

^1H NMR (400 MHz, D_2O) δ 7.76 – 7.51 (m, CH_{ar}), 4.10 – 3.40 (m, $\text{CH-Alg} + \text{CH}_2\text{-CH}_2\text{-O}$), 3.14 (m, $\text{CH}_2\text{-NHC(O)}$), 1.46 (d, $J = 7.1$ Hz, CH_3).

^1H NMR spectrum of 47

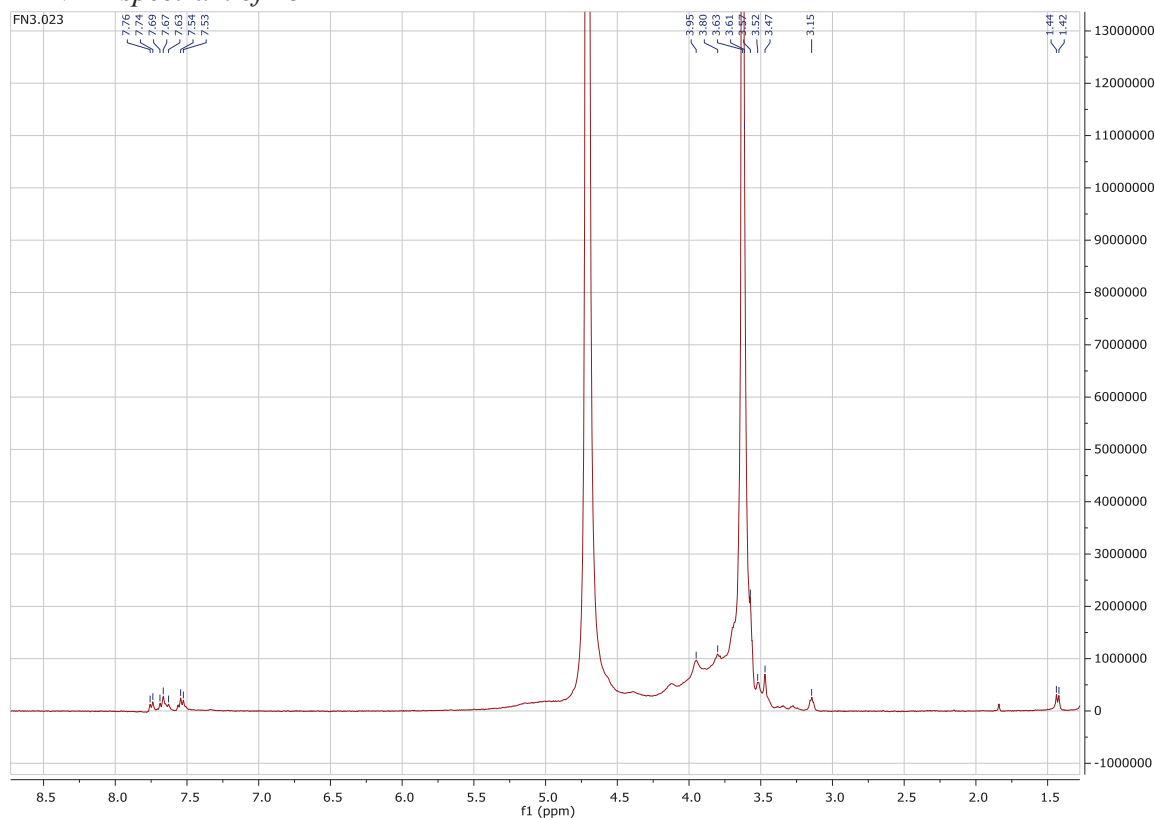


¹H DOSY spectrum of 47



Alg-PEG-amide-KET (48)

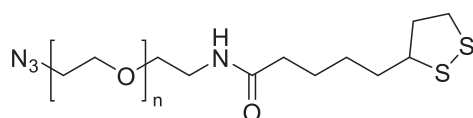
$^1\text{H NMR}$ (400 MHz, D_2O) δ 7.76 – 7.53 (m, CH_{ar}), 4.10 – 3.47 (m, $\text{CH-Alg} + \text{CH}_2\text{-CH}_2\text{-O}$), 3.15 (m, $\text{CH}_2\text{-NHC(O)}$), 1.43 (d, $J = 7.1$ Hz, CH_3).

 $^1\text{H NMR}$ spectrum of 48

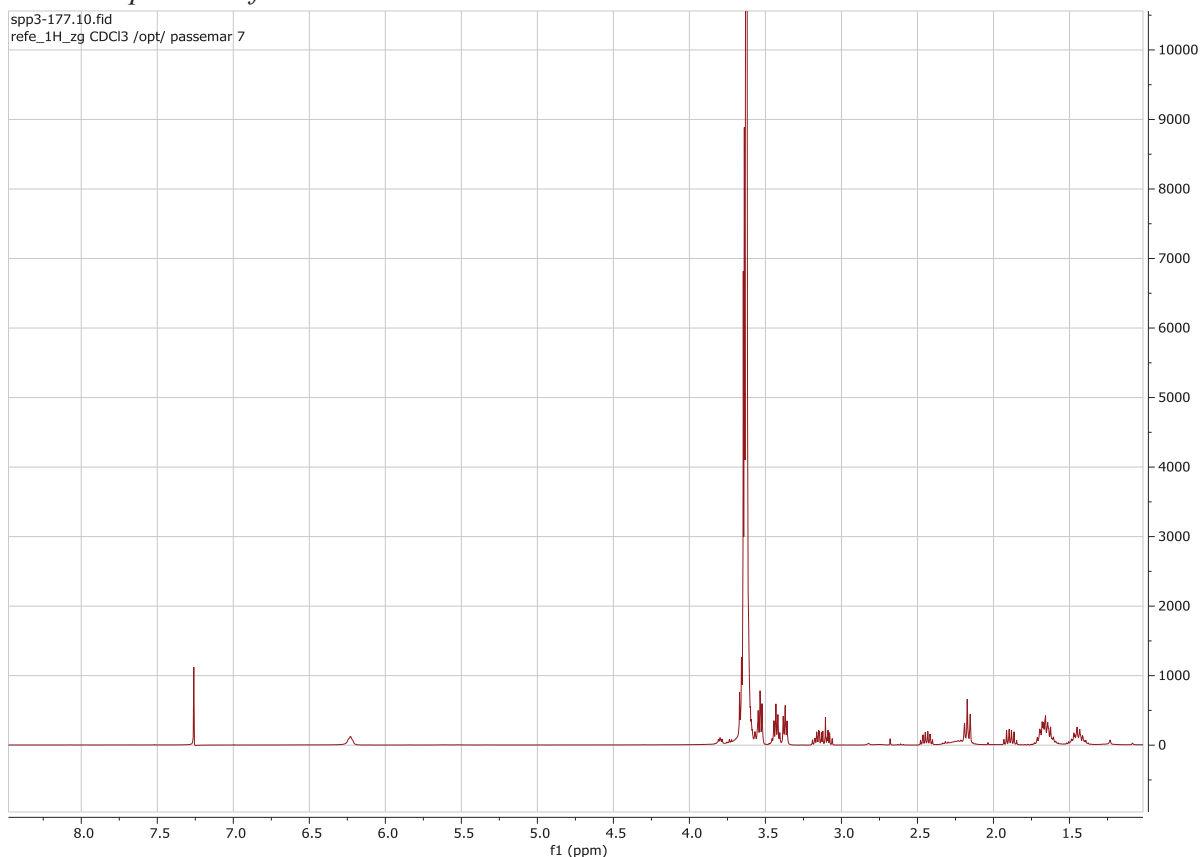
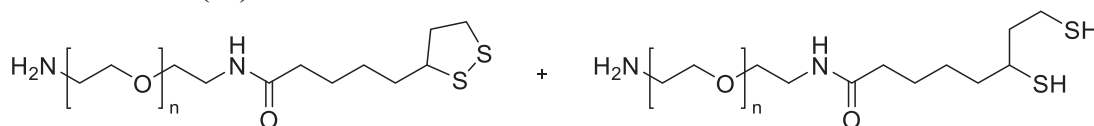
5.9 SYNTHESIS OF ALGINATE-LIPOIC ACID

The following synthesis was reported in “Synthesis Strategies to Extend the Variety of Alginate-Based Hybrid Hydrogels for Cell Microencapsulation” by Passemard et al.¹⁹⁷

Azide-PEG-LA (49)

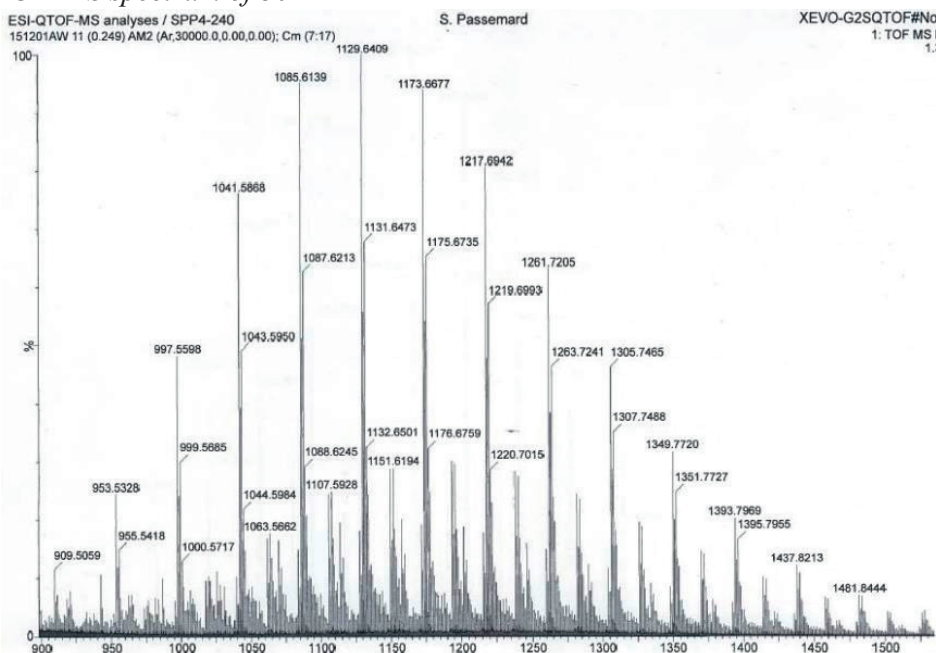
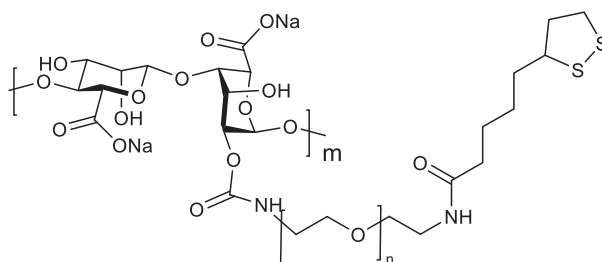


To a solution of compounds azide-PEG-amine (5 g, 4.72 mmol, 1 equiv) and **6** (2.86 g, 9.44 mmol, 2 equiv) in DMF (35 mL), Et_3N (477 mg, 4.72 mmol, 1 equiv) was added. The reaction mixture was stirred for 48 h at 23°C . The solvent was removed under reduced pressure. The crude product was dissolved in DCM (100 mL) and washed with sat. NH_4Cl (2×40 mL). The organic phase was dried (MgSO_4) and concentrated in vacuo. The product was purified by FCC (DCM:MeOH = 17:1) to afford **49** as a yellowish amorphous solid (4.63 g, 3.71 mmol, 78%).

¹H NMR spectrum of 49**Amine-PEG-LA (50)**

Compound **49** (1 g, 866 μmol , 1 equiv) was dissolved in THF (5 mL). LiAlH_4 (66 mg, 1.73 mmol, 2 equiv) was added portion wise, and the reaction was stirred for 40 min at 23°C. The reaction was quenched by slow addition of EtOAc (2 mL), then water (20 mL), and the product was extracted with DCM (3 \times 30 mL). The combined organic layers were dried (MgSO_4) and concentrated in vacuo to afford amine-PEG-LA (**50**) as a white amorphous solid (895 mg, 791 μmol , 91%).

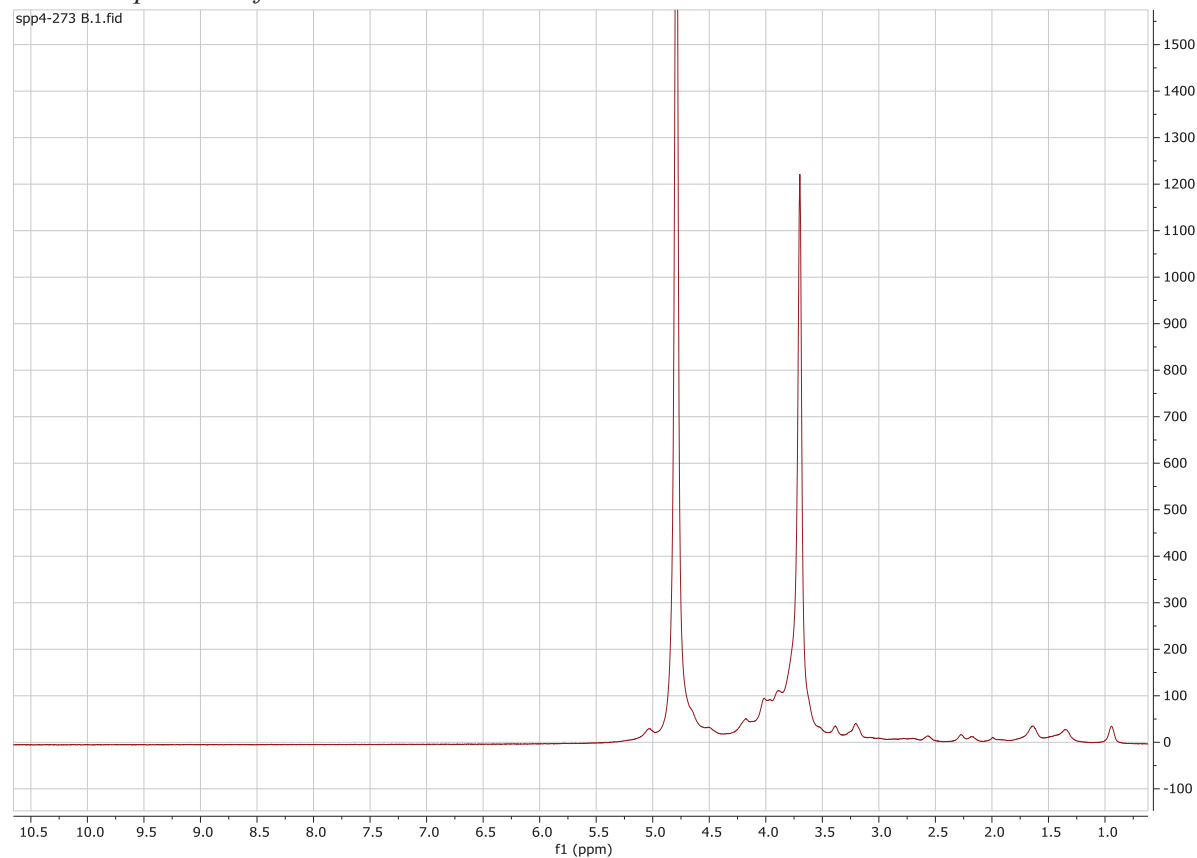
HRMS (ESI/QTOF) m/z: Calcd. for $\text{C}_{52}\text{H}_{106}\text{N}_2\text{O}_{22}\text{S}_2$: 1175.6757; Found: 1175.6735

ESI-QTOF-MS spectrum of 50**Alg-PEG-LA (51)**

TBA-**alg (46)** (100 mg, 0.239 mmol, 1 equiv) was dissolved in DMSO (20 mL), and the solution was stirred for 12 h to ensure homogeneity. CDI (38.7 mg, 0.239 mmol, 1 equiv) previously dissolved in a minimum volume of DMSO was added, and the reaction mixture was stirred at 23°C for 30 min. To enhance precipitation of the imidazolide-alginate intermediate, acetone (40 mL) was added. The resulting precipitate was filtered and washed with acetone (3 × 10 mL). The solid was further dried for 15 min under vacuum at 40 °C and transferred to a round-bottom flask. Distilled water was added (10 mL), and the mixture was stirred until complete dissolution. Heterobifunctional PEG derivative (47.9 μmol, 0.2 equiv,) previously dissolved in a minimum volume of water was added. The solution was stirred at 23°C for 2 h. The reaction was quenched by addition of 0.05 M NaOH solution until reaching pH 11. The solution was directly transferred into a dialysis membrane and dialyzed against distilled water. The first day, water was changed once. A second water change was performed with prior addition of TCEP (0.1 M, 1 mL) in the dialysis tube. The dialysis was continued for 2 more days, adding TCEP (0.1 M, 1 mL) one more time to the dialysis tube, and followed by dialysis against distilled water the second day (changing water 3 times that day). The last day the dialysis was continued against water, with the addition of NaHCO₃ (180 mg in 9 L distilled water) in the dialysis

bucket, to reach pH 7. The solution was filtered (70 and 0.22 μm) and freeze-dried to obtain the PEG-grafted alginates (**51**) as white solid.

¹H NMR spectrum of 51



5.10 MICROSPHERES FORMATION

Formation of empty microspheres from pure polymer

Alg-PEG-KET (**47** or **48**) polymer was dissolved in MOPS buffer (100 mM, pH = 7.4) to obtain 1 mL of a 3 wt % solution. The mixture was extruded into a gelation bath (100 mM CaCl₂ in 100 mM MOPS buffer, pH 7.4) containing tween 80 (diluted 1/10 000) using a coaxial air-flow droplet generator. MS were rinsed with MOPS buffer and kept in MOPS solution (3 mL) containing CaCl₂ (100 mM). Quantification of ketoprofen release was performed over different time period by LC-MS analysis of aliquots from the supernatant at regular time points (0.5, 1, 3, 6, 24, 48, 72, 96, 168 h).

Formation of empty microspheres from a mixture of polymer (alg-A-KET, alg-B-KET)

Na-alg and Alg-PEG-KET (**47** or **48**) polymers were dissolved in in MOPS buffer (100 mM) adjusted to pH 7.4 to obtain respectively 2 mL of a 1.5 wt. % solution and 0.86 mL of a 3.5 wt. % solution. The two solutions of polymer were mixed until homogenization. The resulting mixture was extruded into a gelation bath (100 mM CaCl₂ in 100 mM MOPS buffer, pH 7.4) containing tween 80 (diluted 1/10 000). MS were produced employing a coaxial air-flow droplet generator (Encapsulator B-395 Pro, Büchi Labortechnik AG, Flawil, Switzerland). The MS were collected by filtration, washed twice for 10 minutes with NaCl 0.9%, and finally stored in this solution at 4 °C. The release of ketoprofen was quantified by LC-MS from the supernatant at regular time points (0.5, 1, 3, 6, 24, 48, 72, 96, 168 and 336 h).

Formation of empty microspheres from a mixture of polymer (3C-alg)

Alg-PEG-acrylate 3 wt. % alg-PEG-thiol 3wt. % and alg-PEG-ester-KET 2.5wt. % were dissolved in MOPS buffer adjusted to pH 7.4 to obtain respectively 1 mL 3 wt. %, 1 mL 3 wt. % and 1.2 mL 2.5 wt. %. The three solutions of polymer were mixed until homogenization. The mixture was extruded into a gelation bath (100 mM CaCl₂ in 100 mM MOPS buffer, pH 7.4) containing tween 80 (diluted 1/10 000) using a coaxial air-flow droplet generator. MS were rinsed with MOPS buffer and kept in MOPS solution (3 mL) containing CaCl₂ (100 mM). Quantification of ketoprofen release was performed over different time period by LC-MS analysis of aliquots from the supernatant at regular time points (0.5, 1, 3, 24, 48, 96, 120, 144, 168, 336 h).

Formation of microspheres with MIN6 cells and porcine Islets

MIN6 cells were cultured in Dulbecco Modified Eagle's Medium (DMEM) supplemented with 1 mM Na-Pyruvate, 71 µM β-mercaptoethanol, 15% decomplexed fetal calf serum (FCS), 25 mM glucose, penicillin and streptomycin (DMEM complete medium). MIN6 cells (3 x 10⁶) were centrifuged at 250 g for 5 minutes and the supernatant was completely removed. The remaining cell pellet was dispersed in 1 mL of Na-alg-PEG solution using a 10 mL syringe. MS were produced using the same procedure as described above for the formation of empty MS. Encapsulated MIN6 cells were then cultured in DMEM complete medium at 37°C with 5% CO₂. The release of ketoprofen was quantified by LC-MS from the supernatant at regular time points (0.5, 1, 3, 6, 24, 48, 72, 96, 168 and 336 h).

Porcine Islets were cultured in neonatal porcine islet culture medium from Corning. The islets were placed in a falcon tubes for 5 min and after sedimentation the supernatant was removed. The remaining cell pellet was dispersed in 1 mL of the polymers solution using a 10 mL syringe to obtain 10000 or 20000 IEQ / ml of polymer. MS were produced using the same procedure

described above. Encapsulated Islet were then cultured in Neonatal porcine islet culture medium from Corning at 37°C with 5% CO₂ and the medium was changed two times per week.

5.11 DETERMINATION OF THE DEGREE OF GRAFTING

The procedure is described for alg-PEG-ester-KET (**47**). The same methodology was performed on alg-PEG-amide-KET (**48**).

1D ¹H-NMR of alg-PEG-ester-KET (**47**) was run at 800 MHz with a repetition delay of 5s as ¹H longitudinal relaxation time constants (T₁) of **47** and alginate were measured to be T₁ < 1s. Line broadening was set to 0.3 Hz. The baseline was automatically corrected with Bruker Topspin routine, using degree 5 polynomial. The percentage of grafting was estimated by comparison of integration of ¹H resonances of PEG fragment (176 protons) and alginate unit (5 protons). Due to overlap, separation between PEG and alginate resonances was performed by deconvolution with Lorentzian functions, using Bruker Topspin curve fitting and line shape analysis tool. The grafting degrees of **47** are of 7% and 20% when using 0.1 and 0.2 equiv. of PEG-ester-KET (**44**), respectively, in the coupling procedure.

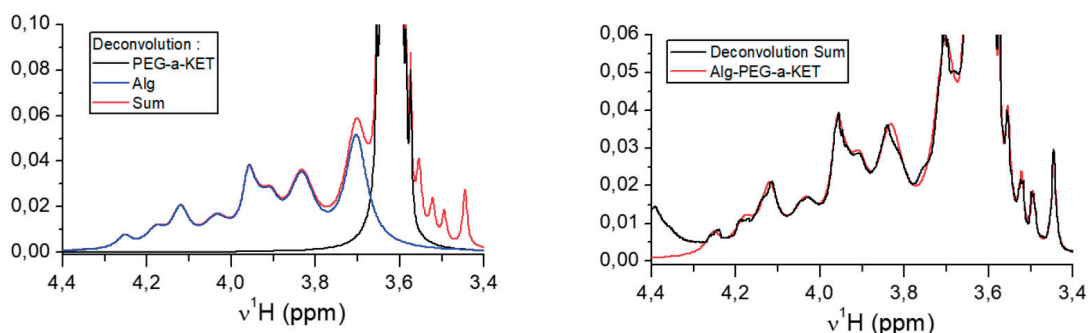


Figure 5.1: (left): Simulated spectra of PEG-a-KET, Alg, D₂O and their sum calculated from lorentzian functions. (right): The method was validated by superimposition of the recorded spectrum of Alg-PEG-a-KET with the simulated spectrum obtained from the sum of the lorentzian functions

5.12 QUANTITATIVE ANALYSIS BY UHPLC-ESI-HRMS

MS quantitative analysis were performed on a Agilent 6530 Accurate Mass Q-TOF LCMS mass spectrometer coupled to an Agilent 1290 series UHPLC system (Agilent Technologies, USA). The separation was achieved using an ACQUITY UPLC[®] BEH C18 1.7 μ m column, 2.1 mm x 50 mm (Waters) heated at 30°C. Mobile phase consisted of 0.1% formic acid in water as eluent A and 0.1% formic acid in acetonitrile as eluent B. The separation was carried out at 0.4 mL/min over a 6 min total run time using the following program: 0-0.5 min, 1-5% B; 0.5-3 min, 5-95% B; 3-3.5 min, 95-1% B; 3.5-6 min, 1% B to reequilibrated the system in initial conditions. The sample manager was system temperature was fixed at 10°C and the injection volume was 5 μ L. Mass spectrometer detection was operated in positive ionization using the Dual AJS Jet stream ESI Assembly. The QTOF instrument was operated in the 4 GHz High Resolution mode in profile mode. The Instrument was calibrated in positive full scan mode using ESI-L+ solution (Agilent Technologies, USA). The TOF mass spectra were acquired over the range of m/z 100-1000 at an acquisition rate of 3 spectra/s. ESI AJS settings were as follows RF drying gas flow, 8 L/min; drying gas temperature, 300°C; nebulizer pressure, 35psi; capillary voltage, 3500V; nozzle voltage, 1000V; fragmentor voltage, 175V; skimmer voltage, 65V; octopole 1 RF voltage, 750V; Sheath gas temperature, 350°C; Sheath gas low; 11L/min. Data was processed using the MassHunter Workstation (Agilent Technologies, USA). Extracted ions chromatograms (XIC) were based on a retention time (RT) window of ± 0.2 min with a mass-extraction-window (MEW) of ± 50 ppm centered on m/z_{theor} . Calibration curves were fitted with a polynomial order 2 equation, with $R^2 > 0.995$.

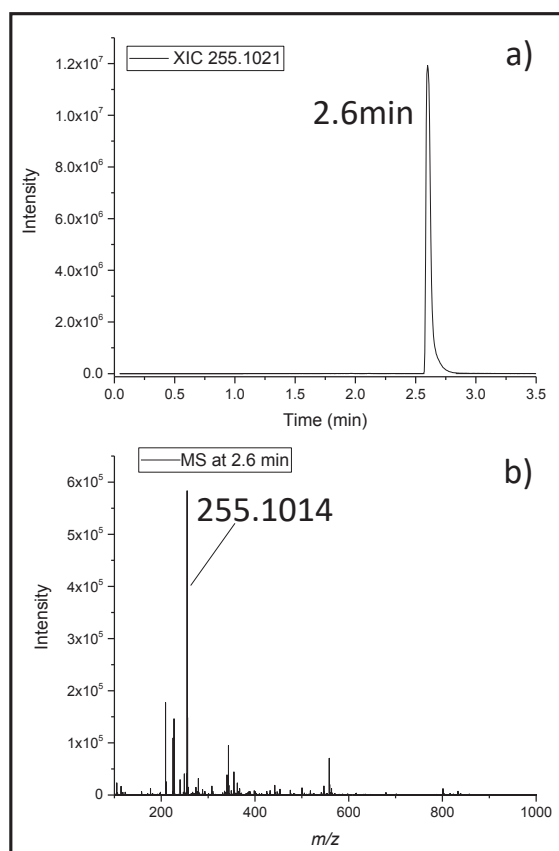


Figure 5.2: Typical XIC (255.1021 MEW of ± 50 ppm) of ketoprofen standard (b) Typical MS of ketoprofen standard at 2.6 min

5.13 TRANSPLANTATION OF MICROSPHERES IN MICE

All animal experiments were approved by the Geneva veterinary authorities (license GE/ 34/13 and license GE/151/16). After production, MS were kept for 1 day in culture. Prior to transplantation, MS were rinsed three times for 15 min in Hank's Balanced Salt Solution (HBSS), containing Ca^{2+} . Once MS have settled on the bottom of the tube, the supernatant was removed and remaining MS were dispersed in minimal amount of HBSS for transplantation. 1.5 mL of MS, corresponding to $\sim 12\,700$ MS (We considered the average diameter of MS as 0.55 mm and used the formula $\frac{4}{3} \pi r^3$ to calculate the sphere volume. Hence, the sphere volume of one MS was determined as 0.087 mm³. Total volume of transplanted MS is, 1500 mm³ (1.5 mL), adjusted by the Kepler conjecture $1500 \cdot 0.74$ resulting in 1110 mm³. Therefore the total number of MS contained in 1.5 mL of solution is $1110 \text{ mm}^3 / 0.087 \text{ mm}^3 = 12\,758$), were introduced through a small incision into the peritoneum of C57BL/6 mice anesthetized by isoflurane. For kidney transplantation, kidneys were exposed through a small dorsal incision and $\sim 100 \mu\text{L}$ of MS were injected under the kidney capsule using a 18G catheter. Thirty days after transplantation mice were sacrificed and kidneys and MS from peritoneum were retrieved for histological analysis.

5.14 HISTOLOGICAL ANALYSIS.

MS were collected from the peritoneum using a spatulas microspoon and added without washing to a small volume of NaCl 0.9% for immediate image acquisition using inverted bright-field microscopy (Leica DM IL) and LAS v 4.5 software (Leica Microsystem, Heerbrugg, Switzerland). Kidneys were harvested, fixed in formalin for 24 h, and embedded in paraffin. Histological sections of 4 μm of tissue were stained for collagen using Goldner's trichrome, images were acquired by Zeiss Axioscan.Z1 and processed with ZEN 2.3 lite (Carl Zeiss).

5.15 QUANTIFICATION OF PERICAPSULAR FIBROTIC OVERGROWTH.

Fibrotic overgrowth around MS retrieved from peritoneum was quantified using ImageJ. Briefly, each selected MS was processed with the same parameters for color threshold and brightness during analysis. Total area of each MS was determined after manual selection of MS shape, which was set as 100%. The pericapsular fibrotic overgrowth (gray levels) was then evaluated in the selected area and normalized to the value of the area of each MS and therefore expressed as percentage of fibrotic overgrowth/MS. At least, 5 MS per type of polymer were analyzed to determine the percentage of fibrotic overgrowth. All values are means \pm standard deviation (SD). Collagen quantification around MS transplanted under the kidney capsule was performed using Definiens Software. Five kidney sections per polymer were quantified. Collagen depositions (in green) were quantified and normalized to the number of MS present in each section. Since MS size differed in each section, values were additionally normalized to the mean of the total area of MS present in a given section; therefore values are expressed as fibrosis area/MS count/mean of area. All values are means \pm standard deviation (SD).

5.16 REAL-TIME RT-PCR.

mRNA expression of α -SMA, COL1A1, and MMP was analyzed by real-time reverse transcription PCR (RT-PCR), as previously described.³⁸ Briefly, 1.5×10^5 human fibroblasts were plated in DMEM supplemented with 100 IU/mL penicillin, 100 mg/ml streptomycin (P-S, Gibco-Invitrogen), and 10% FCS (Gibco- Invitrogen) at 37 °C in humidified air containing 5% CO₂. After 8 h, medium was removed and replaced by DMEM without FCS for 1 day. Then, 10 ng/mL of TGF β 1 diluted in DMEM with 1% FCS was added to all conditions (except negative control) and supplemented with increasing concentrations of KET-TEG-LA (0.125, 0.25, 0.5, 1 mg/mL). After 24 h of incubation, total RNA was extracted using the Qiagen RNeasy Mini kit (Qiagen, San Diego, CA, USA) according to the manufacturer's instructions. Primers listed in Figure 5.3 were designed using Primer3 online software (<http://primer3.ut.ee>), tested with Primer Biosoft (<http://www.premierbiosoft.com>), and blasted on BLAST (<http://blast.ncbi.nlm.nih.gov/Blast.cgi>). Expression of housekeeping ribosomal protein large P0 was used to normalize expression values obtained for α -SMA, COL1A1, and MMP.

H-RPLP0	Fwd 5'-TGC ATC AGT ACC CCA TTC TAT CAT-3' Rev 5'-AAG GTG TAA TCC GTC TCC ACA GA-3'
H-αSMA	Fwd 5'-ACT GGG ACG ACA TGG AAA AG-3' Rev 5'-TAC ATG GCT GGG ACA TTG AA-3'
H-COL1A1	Fwd 5'-CCA GGC AGA GAT GGT GAA GA-3' Rev 5'-GCA GGT CCT TGG AAA CCT TG-3'
H-MMP-1	Fwd 5'-GGA GGA AAA GCA GCT CAA GAA-3' Rev 5'-TCC AGG GTG ACA CCA GTG ACT-3'

Figure 5.3: *H-RPLP0*, human ribosomal protein large P0; *H- α SMA*, human α smooth muscle actine; *H-COL1A1*, human type 1 collagen; *H-MMP-1*, human metalloproteinase-1.

5.17 INSULIN SECRETION TEST

Insulin release in response to acute glucose stimulation was determined by incubating the islets or MIN6 cells for 1 hour in RPMI 10% FCS medium containing low glucose (2.8 mM) for basal secretion, followed by an additional hour of incubation in high glucose (16.8 mM) medium or 16.8 mM glucose medium supplemented with 5 mM of theophylline. Supernatants were collected, frozen and insulin concentrations were determined using insulin ELISA Kit according to the manufacturer's instructions (Merckodia, Uppsala, Sweden). Results were normalized to the total insulin content of the islets as measured by the same ELISA kit and following ice-cold acid-ethanol extraction. Due to interexperimental variability, and depending upon the time of culture and the encapsulation, insulin secretion was expressed relative to the basal levels (stimulation index).

6 ANNEXES

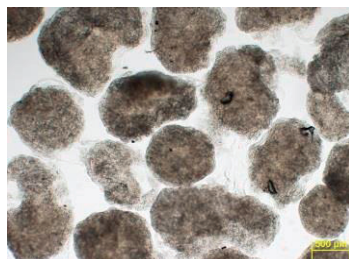


Figure 6.1: Alg-[carbamate]-PEG-(triazole)-SH

Table 8: Size of Alg-[carbamate]-PEG-(triazole)-SH MS at day 1 and 7

Alg-PEG-SH 7.7% 2 w. %	
Size (μm) Day 1	983 ± 168
Size (μm) Day 7	935 ± 142

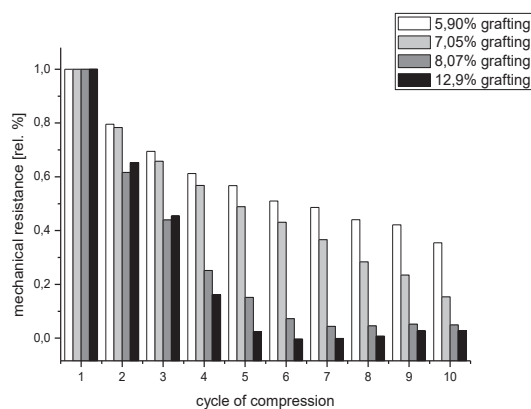


Figure 6.2: Shape recovery of alg-PEG1000-SH with different degree of grafting

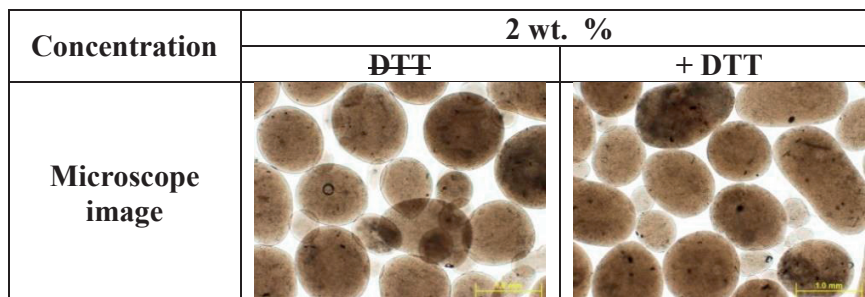


Figure 6.3: Alg-PEG-triazole-L.A

Table 9: Alg-PEG-triazole-LA

	No DTT	DTT
Day 1	1040 ± 214	1103 ± 121
Day 7	1079 ± 117	1134 ± 108

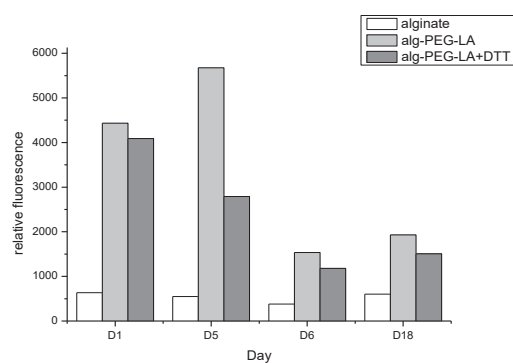


Figure 6.4: fluorescence of un-modified curcumin in supernatant

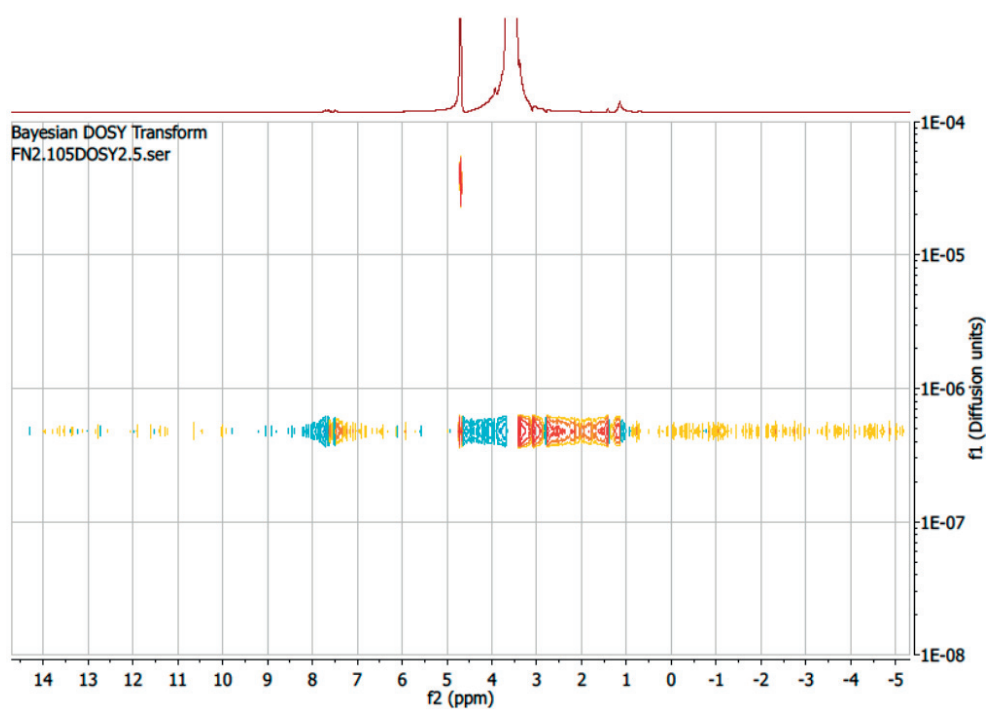


Figure 6.5: Dosey spectrum of alg-PEG-KET

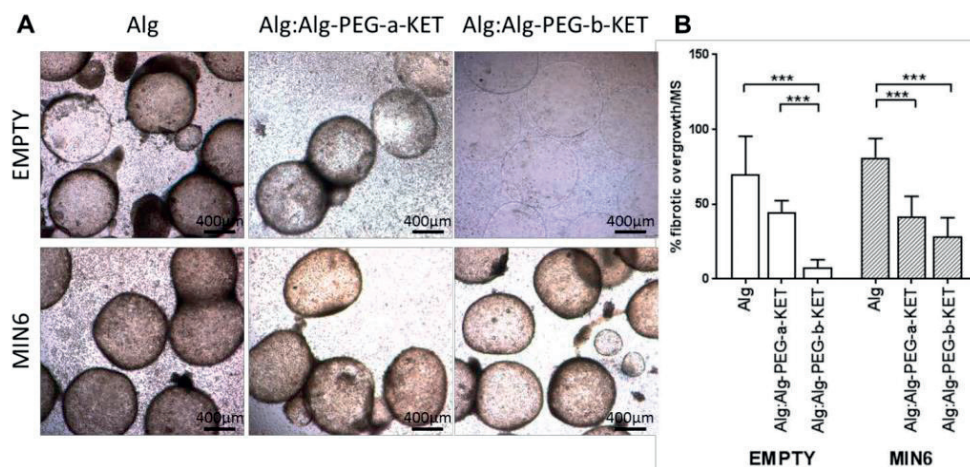


Figure 6.6: (A) Bright-field microscopy images of MS retrieved from the peritoneum following 15 days of transplantation. Na-alg (left rows), Alg:Alg-PEG-a-KET (middle rows) and Alg:Alg-PEG-b-KET (right rows); cell-free MS (upper panels) and MS with MIN6 cells (lower panels). (B) Pericapsular fibrotic overgrowth was quantified using ImageJ and expressed as a percentage of fibrotic overgrowth. For each MS, fibrotic overgrowth (grey levels) were normalized to the total area of MS measured. Fibrotic overgrowth for empty MS (white bars) and for MS with MIN6 cells (striped bars) are represented. All values are means \pm standard deviation (SD) of at least 5 MS. *** $p < 0.001$.

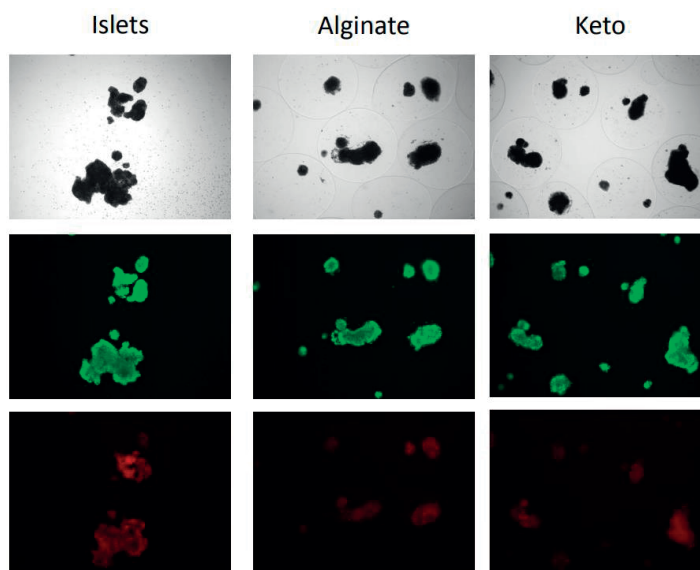


Figure 6.7: Microscopy image of neo natal pig islets, free, encapsulated in alginate and in alg-A-KET at day 1. Top panel: light microscopy, middle panel: staining of live cells with FDA (green), bottom panel: staining of dead cells with PI (red).

7 REFERENCES

- (1) Saini, V. Molecular Mechanisms of Insulin Resistance in Type 2 Diabetes Mellitus. *World J. Diabetes* **2010**, *1* (3), 68–75.
- (2) Whaley, B.; Stone, A.; Brady, S.; Whaley, R. Explaining Diabetes: Studying the Effects of Using Analogies to Talk about Illness - Journal of Diabetes Nursing. *J. Diabetes Nurs.* **2014**, *18* (2), 72–75.
- (3) Bae, J. P.; Lage, M. J.; Mo, D.; Nelson, D. R.; Hoogwerf, B. J. Obesity and Glycemic Control in Patients with Diabetes Mellitus: Analysis of Physician Electronic Health Records in the US from 2009–2011. *J. Diabetes Complications* **2016**, *30* (2), 212–220.
- (4) *Global Report on Diabetes*; Roglic, G., World Health Organization, Eds.; World Health Organization: Geneva, Switzerland, 2016.
- (5) Drive, A. D. A. 2451 C.; Arlington, S. 900; Va 22202 1-800-Diabetes. History of Diabetes <http://www.diabetes.org/research-and-practice/student-resources/history-of-diabetes.html> (accessed May 28, 2018).
- (6) Rosenfeld, L. Insulin: Discovery and Controversy. *Clin. Chem.* **2002**, *48* (12), 2270–2288.
- (7) What Is Insulin Therapy? <http://insulinnation.com/treatment/what-is-insulin-therapy/> (accessed May 17, 2018).
- (8) Federal Register. Application of current statutory authorities to human somatic cell therapy products and gene therapy products <https://www.fda.gov/downloads/BiologicsBloodVaccines/SafetyAvailability/UCM148113.pdf> (accessed May 26, 2018).
- (9) Niehans, P. *Introduction to Cellular Therapy*; Pageant Books, 1960.
- (10) Q Fever Outbreak Among Travelers to Germany Who Received Live Cell Therapy — United States and Canada, 2014 <https://www.cdc.gov/mmwr/preview/mmwrhtml/mm6438a3.htm> (accessed May 30, 2018).
- (11) Starzl, T. E. History of Clinical Transplantation. *World J. Surg.* **2000**, *24* (7), 759–782.
- (12) History of Cell Therapy <https://okyanos.com/history-of-cell-therapy/> (accessed May 30, 2018).
- (13) Gatti, R.; Meuwissen, H.; Allen, H.; Hong, R.; Good, R. IMMUNOLOGICAL RECONSTITUTION OF SEX-LINKED LYMPHOPENIC IMMUNOLOGICAL DEFICIENCY. *The Lancet* **1968**, *292* (7583), 1366–1369.
- (14) Heathman, T. R. J.; Nienow, A. W.; McCall, M. J.; Coopman, K.; Kara, B.; Hewitt, C. J. The Translation of Cell-Based Therapies: Clinical Landscape and Manufacturing Challenges. *Regen. Med.* **2015**, *10* (1), 49–64.
- (15) Fischbach, M. A.; Bluestone, J. A.; Lim, W. A. Cell-Based Therapeutics: The next Pillar of Medicine. *Sci. Transl. Med.* **2013**, *5* (179), 179ps7.

- (16) Gschweng, E.; De Oliveira, S.; Kohn, D. B. Hematopoietic Stem Cells for Cancer Immunotherapy. *Immunol. Rev.* **2014**, *257* (1), 237–249.
- (17) Jackson, C. J.; Tønseth, K. A.; Utheim, T. P. Cultured Epidermal Stem Cells in Regenerative Medicine. *Stem Cell Res. Ther.* **2017**, *8*.
- (18) Pellegrini, G.; Lambiase, A.; Macaluso, C.; Pocobelli, A.; Deng, S.; Cavallini, G. M.; Esteki, R.; Rama, P. From Discovery to Approval of an Advanced Therapy Medicinal Product-Containing Stem Cells, in the EU. *Regen. Med.* **2016**, *11* (4), 407–420.
- (19) Volarevic, V.; Markovic, B. S.; Gazdic, M.; Volarevic, A.; Jovicic, N.; Arsenijevic, N.; Armstrong, L.; Djonov, V.; Lako, M.; Stojkovic, M. Ethical and Safety Issues of Stem Cell-Based Therapy. *Int. J. Med. Sci.* **2018**, *15* (1), 36–45.
- (20) Martin, U. Therapeutic Application of Pluripotent Stem Cells: Challenges and Risks. *Front. Med.* **2017**, *4*.
- (21) Poulos, J. The Limited Application of Stem Cells in Medicine: A Review. *Stem Cell Res. Ther.* **2018**, *9*, 1.
- (22) Tolosa, L.; Pareja, E.; Gómez-Lechón, M. J. Clinical Application of Pluripotent Stem Cells: An Alternative Cell-Based Therapy for Treating Liver Diseases? *Transplantation* **2016**, *100* (12), 2548–2557.
- (23) Kimbrel, E. A.; Lanza, R. Current Status of Pluripotent Stem Cells: Moving the First Therapies to the Clinic. *Nat. Rev. Drug Discov.* **2015**, *14* (10), 681–692.
- (24) Barton, F. B.; Rickels, M. R.; Alejandro, R.; Hering, B. J.; Wease, S.; Naziruddin, B.; Oberholzer, J.; Odorico, J. S.; Garfinkel, M. R.; Levy, M.; et al. Improvement in Outcomes of Clinical Islet Transplantation: 1999–2010. *Diabetes Care* **2012**, *35* (7), 1436–1445.
- (25) Gabardi, S. Understanding Risk Evaluation and Mitigation Strategies in Organ Transplantation. *Pharmacother. J. Hum. Pharmacol. Drug Ther.* **2012**, *31* (7), 714–722.
- (26) Wang, J.-Z.; Ding, Z.-Q.; Zhang, F.; Ye, W.-B. Recent Development in Cell Encapsulations and Their Therapeutic Applications. *Mater. Sci. Eng. C* **2017**, *77*, 1247–1260.
- (27) Bisceglie, V. Über die antineoplastische Immunität. *Z. Für Krebsforsch.* **1934**, *40* (1), 122–140.
- (28) Chang, T. M. S. Semipermeable Microcapsules. *Science* **1964**, *146* (3643), 524–525.
- (29) Mahou, R.; Passemard, S.; Carvello, M.; Petrelli, A.; Noverraz, F.; Gerber-Lemaire, S.; Wandrey, C. Contribution of Polymeric Materials to Progress in Xenotransplantation of Microencapsulated Cells: A Review. *Xenotransplantation* **2016**, *23* (3), 179–201.
- (30) Ellis, C.; Ramzy, A.; Kieffer, T. J. Regenerative Medicine and Cell-Based Approaches to Restore Pancreatic Function. *Nat. Rev. Gastroenterol. Hepatol.* **2017**, *14* (10), 612–628.
- (31) Aebischer P; Buchser, E; Joseph, J M. TRANSPLANTATION IN HUMANS OF ENCAPSULATED XENOGENEIC CELLS WITHOUT IMMUNOSUPPRESSION. *Transplantation* **1994**, *58* (11), 1275–1277.

- (32) Bonavita, A. G.; Quaresma, K.; Cotta-de-Almeida, V.; Pinto, M. A.; Saraiva, R. M.; Alves, L. A. Hepatocyte Xenotransplantation for Treating Liver Disease. *Xenotransplantation* **2010**, *17* (3), 181–187.
- (33) Teng, Y.; Wang, Y.; Li, S.; Wang, W.; Gu, R.; Guo, X.; Nan, X.; Ma, X.; Pei, X. Treatment of Acute Hepatic Failure in Mice by Transplantation of Mixed Microencapsulation of Rat Hepatocytes and Transgenic Human Fetal Liver Stromal Cells. *Tissue Eng. Part C Methods* **2010**, *16* (5), 1125–1134.
- (34) Qiu, L.; Wang, J.; Wen, X.; Wang, H.; Wang, Y.; Lin, Q.; Du, Z.; Duan, C.; Wang, C.; Wang, C. Transplantation of Co-Microencapsulated Hepatocytes and HUVECs for Treatment of Fulminant Hepatic Failure. *Int. J. Artif. Organs* **2012**, *35* (6), 458–465.
- (35) Coussa, R.; Martoni, C.; Bhathena, J.; Urbanska, A. M.; Prakash, S. Oral Microencapsulated Live *Saccharomyces Cerevisiae* Cells for Use in Renal Failure Uremia: Preparation and In Vivo Analysis. *J. Biomed. Biotechnol.* **2010**, *2010*, 1–7.
- (36) Jain, P.; Shah, S.; Coussa, R.; Prakash, S. Potentials and Limitations of Microorganisms as Renal Failure Biotherapeutics. *Biol. Targets Ther.* **2009**, *3*, 233–243.
- (37) Brodie, J. C.; Humes, H. D. Stem Cell Approaches for the Treatment of Renal Failure. *Pharmacol. Rev.* **2005**, *57* (3), 299–313.
- (38) Salmons, B.; Gunzburg, W. H. Therapeutic Application of Cell Microencapsulation in Cancer. In *Therapeutic Applications of Cell Microencapsulation*; PHD, J. L. P., Orive, G., Eds.; Advances in Experimental Medicine and Biology; Springer New York, 2010; pp 92–103.
- (39) Basta, G.; Calafiore, R. Immunoisolation of Pancreatic Islet Grafts with No Recipient's Immunosuppression: Actual and Future Perspectives. *Curr. Diab. Rep.* **2011**, *11* (5), 384–391.
- (40) Montanucci, P.; Pennoni, I.; Pescara, T.; Basta, G.; Calafiore, R. Treatment of Diabetes Mellitus with Microencapsulated Fetal Human Liver (FH-B-TPN) Engineered Cells. *Biomaterials* **2013**, *34* (16), 4002–4012.
- (41) Dufrane, D.; Gianello, P. Macro- or Microencapsulation of Pig Islets to Cure Type 1 Diabetes. *World J. Gastroenterol. WJG* **2012**, *18* (47), 6885–6893.
- (42) Dolgin, E. Encapsulate This. *Nat. Med.* **2014**, *20* (1), 9–11.
- (43) Wichterle, O.; Lim, D. Hydrophilic Gels for Biological Use. *Nature* **1960**, *185* (4706), 117–118.
- (44) Gupta, P.; Vermani, K.; Garg, S. Hydrogels: From Controlled Release to PH-Responsive Drug Delivery. *Drug Discov. Today* **2002**, *7* (10), 569–579.
- (45) Hoffman, A. S. Hydrogels for Biomedical Applications. *Adv. Drug Deliv. Rev.* **2012**, *64*, Supplement, 18–23.
- (46) Censi, R.; Di Martino, P.; Vermonden, T.; Hennink, W. E. Hydrogels for Protein Delivery in Tissue Engineering. *J. Controlled Release* **2012**, *161* (2), 680–692.
- (47) Liu, L. S.; Kost, J.; Yan, F.; Spiro, R. C. Hydrogels from Biopolymer Hybrid for Biomedical, Food, and Functional Food Applications. *Polymers* **2012**, *4* (2), 997–1011.

- (48) Mawad, D.; Anne Boughton, E.; Boughton, P.; Lauto, A. Advances in Hydrogels Applied to Degenerative Diseases. *Curr. Pharm. Des.* **2012**, *18* (18), 2558–2575.
- (49) Seliktar, D. Designing Cell-Compatible Hydrogels for Biomedical Applications. *Science* **2012**, *336* (6085), 1124–1128.
- (50) Selimović, Š.; Oh, J.; Bae, H.; Dokmeci, M.; Khademhosseini, A. Microscale Strategies for Generating Cell-Encapsulating Hydrogels. *Polymers* **2012**, *4* (3), 1554–1579.
- (51) Billiet, T.; Vandenhoute, M.; Schelfhout, J.; Van Vlierberghe, S.; Dubruel, P. A Review of Trends and Limitations in Hydrogel-Rapid Prototyping for Tissue Engineering. *Biomaterials* **2012**, *33* (26), 6020–6041.
- (52) Gauvin, R.; Parenteau-Bareil, R.; Dokmeci, M. R.; Merryman, W. D.; Khademhosseini, A. Hydrogels and Microtechnologies for Engineering the Cellular Microenvironment. *Wiley Interdiscip. Rev. Nanomed. Nanobiotechnol.* **2012**, *4* (3), 235–246.
- (53) Borg, D. J.; Bonifacio, E. The Use of Biomaterials in Islet Transplantation. *Curr. Diab. Rep.* **2011**, *11* (5), 434–444.
- (54) Habibi, Y.; Lucia, L. A.; Rojas, O. J. Cellulose Nanocrystals: Chemistry, Self-Assembly, and Applications. *Chem. Rev.* **2010**, *110* (6), 3479–3500.
- (55) Keerl, M.; Smirnovas, V.; Winter, R.; Richtering, W. Copolymer Microgels from Mono- and Disubstituted Acrylamides: Phase Behavior and Hydrogen Bonds. *Macromolecules* **2008**, *41* (18), 6830–6836.
- (56) Wang, H.-J.; Hong, X.-Z.; Ba, X.-W. Sol–Gel Transition in Nonlinear Hydrogen Bonding Solutions. *Macromolecules* **2007**, *40* (15), 5593–5598.
- (57) Du, X.-W.; Wu, H.-L.; Zhu, Y.-F.; Hu, J.-B.; Jin, F.; Lv, R.-P.; Sun, S.; Wang, H.-Y.; Xu, J.-W. Experimental Study of Therapy of Bone Marrow Mesenchymal Stem Cells or Muscle-like Cells/Calcium Alginate Composite Gel for the Treatment of Stress Urinary Incontinence. *Neurourol. Urodyn.* **2013**, *32* (3), 281–286.
- (58) Lee, J.-H.; Lee, D.-H.; Park, J.-K.; Kim, S.-K.; Kwon, C. H. D.; Lee, S.-K. Potentiality of Immobilized Pig Hepatocyte Spheroids in Bioartificial Liver System. *Transplant. Proc.* **2012**, *44* (4), 1012–1014.
- (59) Dufrane, D.; Steenberghe, M. van; Goebbels, R.-M.; Saliez, A.; Guiot, Y.; Gianello, P. The Influence of Implantation Site on the Biocompatibility and Survival of Alginate Encapsulated Pig Islets in Rats. *Biomaterials* **2006**, *27* (17), 3201–3208.
- (60) Moyer, H. R.; Kinney, R. C.; Singh, K. A.; Williams, J. K.; Schwartz, Z.; Boyan, B. D. Alginate Microencapsulation Technology for the Percutaneous Delivery of Adipose-Derived Stem Cells: *Ann. Plast. Surg.* **2010**, *65* (5), 497–503.
- (61) Man, Y.; Wang, P.; Guo, Y.; Xiang, L.; Yang, Y.; Qu, Y.; Gong, P.; Deng, L. Angiogenic and Osteogenic Potential of Platelet-Rich Plasma and Adipose-Derived Stem Cell Laden Alginate Microspheres. *Biomaterials* **2012**, *33* (34), 8802–8811.
- (62) Endres, M.; Wenda, N.; Woehlecke, H.; Neumann, K.; Ringe, J.; Erggelet, C.; Lerche, D.; Kaps, C. Microencapsulation and Chondrogenic Differentiation of Human Mesenchymal

- Progenitor Cells from Subchondral Bone Marrow in Ca-Alginate for Cell Injection. *Acta Biomater.* **2010**, *6* (2), 436–444.
- (63) Schneider, S.; Feilen, P. J.; Brunnenmeier, F.; Minnemann, T.; Zimmermann, H.; Zimmermann, U.; Weber, M. M. Long-Term Graft Function of Adult Rat and Human Islets Encapsulated in Novel Alginate-Based Microcapsules After Transplantation in Immunocompetent Diabetic Mice. *Diabetes* **2005**, *54* (3), 687–693.
- (64) Malpique, R.; Osório, L. M.; Ferreira, D. S.; Ehrhart, F.; Brito, C.; Zimmermann, H.; Alves, P. M. Alginate Encapsulation as a Novel Strategy for the Cryopreservation of Neurospheres. *Tissue Eng. Part C Methods* **2009**, *16* (5), 965–977.
- (65) Penolazzi, L.; Tavanti, E.; Vecchiatini, R.; Lambertini, E.; Vesce, F.; Gambari, R.; Mazzitelli, S.; Mancuso, F.; Luca, G.; Nastruzzi, C.; et al. Encapsulation of Mesenchymal Stem Cells from Wharton's Jelly in Alginate Microbeads. *Tissue Eng. Part C Methods* **2009**, *16* (1), 141–155.
- (66) Qi, M.; Mørch, Y.; Lacík, I.; Formo, K.; Marchese, E.; Wang, Y.; Danielson, K. K.; Kinzer, K.; Wang, S.; Barbaro, B.; et al. Survival of Human Islets in Microbeads Containing High Galuronic Acid Alginate Crosslinked with Ca²⁺ and Ba²⁺. *Xenotransplantation* **2012**, *19* (6), 355–364.
- (67) Wikström, J.; Elomaa, M.; Syväjärvi, H.; Kuokkanen, J.; Yliperttula, M.; Honkakoski, P.; Urtti, A. Alginate-Based Microencapsulation of Retinal Pigment Epithelial Cell Line for Cell Therapy. *Biomaterials* **2008**, *29* (7), 869–876.
- (68) Draget, K. I.; Skjåk-Braek, G.; Smidsrød, O. Alginate Based New Materials. *Int. J. Biol. Macromol.* **1997**, *21* (1), 47–55.
- (69) Smidsrød, O.; Skjåk-Braek, G. Alginate as Immobilization Matrix for Cells. *Trends Biotechnol.* **1990**, *8*, 71–78.
- (70) Rokstad, A. M.; Brekke, O.-L.; Steinkjer, B.; Ryan, L.; Kolláriková, G.; Strand, B. L.; Skjåk-Braek, G.; Lambris, J. D.; Lacík, I.; Mollnes, T. E.; et al. The Induction of Cytokines by Polycation Containing Microspheres by a Complement Dependent Mechanism. *Biomaterials* **2013**, *34* (3), 621–630.
- (71) Nicodemus, G. D.; Bryant, S. J. Cell Encapsulation in Biodegradable Hydrogels for Tissue Engineering Applications. *Tissue Eng. Part B Rev.* **2008**, *14* (2), 149–165.
- (72) Xu, K.; Fu, Y.; Chung, W.; Zheng, X.; Cui, Y.; Hsu, I. C.; Kao, W. J. Thiol–Ene-Based Biological/Synthetic Hybrid Biomatrix for 3-D Living Cell Culture. *Acta Biomater.* **2012**, *8* (7), 2504–2516.
- (73) Fu, Y.; Xu, K.; Zheng, X.; Giacomini, A. J.; Mix, A. W.; Kao, W. J. 3D Cell Entrapment in Crosslinked Thiolated Gelatin-Poly(Ethylene Glycol) Diacrylate Hydrogels. *Biomaterials* **2012**, *33* (1), 48–58.
- (74) Phelps, E. A.; Enemchukwu, N. O.; Fiore, V. F.; Sy, J. C.; Murthy, N.; Sulchek, T. A.; Barker, T. H.; García, A. J. Maleimide Cross-Linked Bioactive PEG Hydrogel Exhibits Improved Reaction Kinetics and Cross-Linking for Cell Encapsulation and In Situ Delivery. *Adv. Mater.* **2012**, *24* (1), 64–70.

- (75) Nimmo, C. M.; Owen, S. C.; Shoichet, M. S. Diels–Alder Click Cross-Linked Hyaluronic Acid Hydrogels for Tissue Engineering. *Biomacromolecules* **2011**, *12* (3), 824–830.
- (76) Almany, L.; Seliktar, D. Biosynthetic Hydrogel Scaffolds Made from Fibrinogen and Polyethylene Glycol for 3D Cell Cultures. *Biomaterials* **2005**, *26* (15), 2467–2477.
- (77) Ossipov, D. A.; Hilborn, J. Poly(Vinyl Alcohol)-Based Hydrogels Formed by “Click Chemistry.” *Macromolecules* **2006**, *39* (5), 1709–1718.
- (78) Cho, N.-J.; Elazar, M.; Xiong, A.; Lee, W.; Chiao, E.; Baker, J.; Frank, C. W.; Glenn, J. S. Viral Infection of Human Progenitor and Liver-Derived Cells Encapsulated in Three-Dimensional PEG-Based Hydrogel. *Biomed. Mater.* **2009**, *4* (1), 011001.
- (79) Hong, Y.; Gong, Y.; Gao, C.; Shen, J. Collagen-Coated Polylactide Microcarriers/Chitosan Hydrogel Composite: Injectable Scaffold for Cartilage Regeneration. *J. Biomed. Mater. Res. A* **2008**, *85A* (3), 628–637.
- (80) Liu, Y.; Chan-Park, M. B. A Biomimetic Hydrogel Based on Methacrylated Dextran-Graft-Lysine and Gelatin for 3D Smooth Muscle Cell Culture. *Biomaterials* **2010**, *31* (6), 1158–1170.
- (81) Choh, S.-Y.; Cross, D.; Wang, C. Facile Synthesis and Characterization of Disulfide-Cross-Linked Hyaluronic Acid Hydrogels for Protein Delivery and Cell Encapsulation. *Biomacromolecules* **2011**, *12* (4), 1126–1136.
- (82) Young, C. J.; Poole-Warren, L. A.; Martens, P. J. Combining Submerged Electrospray and UV Photopolymerization for Production of Synthetic Hydrogel Microspheres for Cell Encapsulation. *Biotechnol. Bioeng.* **2012**, *109* (6), 1561–1570.
- (83) Schmidt, J. J.; Rowley, J.; Kong, H. J. Hydrogels Used for Cell-Based Drug Delivery. *J. Biomed. Mater. Res. A* **2008**, *87A* (4), 1113–1122.
- (84) Dusseault, J.; Leblond, F. A.; Robitaille, R.; Jourdan, G.; Tessier, J.; Ménard, M.; Henley, N.; Hallé, J.-P. Microencapsulation of Living Cells in Semi-Permeable Membranes with Covalently Cross-Linked Layers. *Biomaterials* **2005**, *26* (13), 1515–1522.
- (85) Mazumder, M. A. J.; Burke, N. A. D.; Shen, F.; Potter, M. A.; Stöver, H. D. H. Core-Cross-Linked Alginate Microcapsules for Cell Encapsulation. *Biomacromolecules* **2009**, *10* (6), 1365–1373.
- (86) Gardner, C. M.; Stöver, H. D. H. Reactive Polyanions Based on Poly(4,4-Dimethyl-2-Vinyl-2-Oxazoline-5-One-Co-Methacrylic Acid). *Macromolecules* **2011**, *44* (18), 7115–7123.
- (87) Mahou, R.; Tran, N. M.; Dufresne, M.; Legallais, C.; Wandrey, C. Encapsulation of Huh-7 Cells within Alginate-Poly(Ethylene Glycol) Hybrid Microspheres. *J. Mater. Sci. Mater. Med.* **2012**, *23* (1), 171–179.
- (88) Meier, R. P. H.; Mahou, R.; Morel, P.; Meyer, J.; Montanari, E.; Muller, Y. D.; Christofilopoulos, P.; Wandrey, C.; Gonelle-Gispert, C.; Bühler, L. H. Microencapsulated Human Mesenchymal Stem Cells Decrease Liver Fibrosis in Mice. *J. Hepatol.* **2015**, *62* (3), 634–641.

- (89) Mahou, R.; Meier, R.; Bühler, L.; Wandrey, C. Alginate-Poly(Ethylene Glycol) Hybrid Microspheres for Primary Cell Microencapsulation. *Materials* **2014**, *7* (1), 275–286.
- (90) Mahou, R.; Wandrey, C. Alginate–Poly(Ethylene Glycol) Hybrid Microspheres with Adjustable Physical Properties. *Macromolecules* **2010**, *43* (3), 1371–1378.
- (91) Mahou, R.; Borcard, F.; Crivelli, V.; Montanari, E.; Passemard, S.; Noverraz, F.; Gerber-Lemaire, S.; Bühler, L.; Wandrey, C. Tuning the Properties of Hydrogel Microspheres by Adding Chemical Cross-Linking Functionality to Sodium Alginate. *Chem. Mater.* **2015**, *27* (12), 4380–4389.
- (92) Gattás-Asfura, K. M.; Stabler, C. L. Chemoselective Cross-Linking and Functionalization of Alginate via Staudinger Ligation. *Biomacromolecules* **2009**, *10* (11), 3122–3129.
- (93) Hall, K. K.; Gattás-Asfura, K. M.; Stabler, C. L. Microencapsulation of Islets within Alginate/Poly(Ethylene Glycol) Gels Cross-Linked via Staudinger Ligation. *Acta Biomater.* **2011**, *7* (2), 614–624.
- (94) Poncelet, D.; Lencki, R.; Beaulieu, C.; Halle, J. P.; Neufeld, R. J.; Fournier, A. Production of Alginate Beads by Emulsification/Internal Gelation. I. Methodology. *Appl. Microbiol. Biotechnol.* **1992**, *38* (1), 39–45.
- (95) Poncelet, D.; Babak, V.; Dulieu, C.; Picot, A. A Physico-Chemical Approach to Production of Alginate Beads by Emulsification-Internal Ionotropic Gelation. *Colloids Surf. Physicochem. Eng. Asp.* **1999**, *155* (2), 171–176.
- (96) Bilancetti, L.; Poncelet, D.; Loisel, C.; Mazzitelli, S.; Nastruzzi, C. A Statistical Approach to Optimize the Spray Drying of Starch Particles: Application to Dry Powder Coating. *AAPS PharmSciTech* **2010**, *11* (3), 1257–1267.
- (97) De Vos, P.; De Haan, B.; Pater, J.; Van Schilfgaarde, R. ASSOCIATION BETWEEN CAPSULE DIAMETER, ADEQUACY OF ENCAPSULATION, AND SURVIVAL OF MICROENCAPSULATED RAT ISLET ALLOGRAFTS1: *Transplantation* **1996**, *62* (7), 893–899.
- (98) Ceausoglu, I.; Hunkeler, D. A New Microencapsulation Device for Controlled Membrane and Capsule Size Distributions. *J. Microencapsul.* **2002**, *19* (6), 725–735.
- (99) Serp, D.; Cantana, E.; Heinzen, C.; Stockar, U. V.; Marison, I. W. Characterization of an Encapsulation Device for the Production of Monodisperse Alginate Beads for Cell Immobilization. *Biotechnol. Bioeng.* **2000**, *70* (1), 41–53.
- (100) Hallé, J.-P.; Leblond, F. A.; Pariseau, J.-F.; Jutras, P.; Brabant, M.-J.; Lepage, Y. STUDIES ON SMALL (<300 Mm) MICROCAPSULES: II - PARAMETERS GOVERNING THE PRODUCTION OF ALGINATE BEADS BY HIGH VOLTAGE ELECTROSTATIC PULSES. *Cell Transplant.* **1994**, *3* (5), 365–372.
- (101) Brandenberger, H.; Widmer, F. A New Multinozzle Encapsulation/Immobilisation System to Produce Uniform Beads of Alginate. *J. Biotechnol.* **1998**, *63* (1), 73–80.

- (102) Poncelet, D.; Neufeld, R.; Bugarski, B.; Amsden, B. G.; Zhu, J.; Goosen, M. F. A. A Parallel Plate Electrostatic Droplet Generator: Parameters Affecting Microbead Size. *Appl. Microbiol. Biotechnol.* **1994**, *42* (2–3), 251–255.
- (103) Prüße, U.; Fox, B.; Kirchhoff, M.; Bruske, F.; Breford, J.; Vorlop, K.-D. New Process (Jet Cutting Method) for the Production of Spherical Beads from Highly Viscous Polymer Solutions. *Chem. Eng. Technol.* **1999**, *21* (1), 29–33.
- (104) Mazzitelli, S.; Capretto, L.; Quinci, F.; Piva, R.; Nastruzzi, C. Preparation of Cell-Encapsulation Devices in Confined Microenvironment. *Adv. Drug Deliv. Rev.* **2013**, *65* (11–12), 1533–1555.
- (105) Kang, A.; Park, J.; Ju, J.; Jeong, G. S.; Lee, S.-H. Cell Encapsulation via Microtechnologies. *Biomaterials* **2014**, *35* (9), 2651–2663.
- (106) Kim, C.; Park, J.; Kang, J. Y. A Microfluidic Manifold with a Single Pump System to Generate Highly Mono-Disperse Alginate Beads for Cell Encapsulation. *Biomicrofluidics* **2014**, *8* (6), 066504.
- (107) Chau, M.; Abolhasani, M.; Thérien-Aubin, H.; Li, Y.; Wang, Y.; Velasco, D.; Tumarkin, E.; Ramachandran, A.; Kumacheva, E. Microfluidic Generation of Composite Biopolymer Microgels with Tunable Compositions and Mechanical Properties. *Biomacromolecules* **2014**, *15* (7), 2419–2425.
- (108) Luo, R.-C.; Chen, C.-H. Structured Microgels through Microfluidic Assembly and Their Biomedical Applications. *Soft* **2012**, *01* (01), 1–23.
- (109) Shim, T. S.; Kim, S.-H.; Yang, S.-M. Elaborate Design Strategies Toward Novel Microcarriers for Controlled Encapsulation and Release. *Part. Part. Syst. Charact.* **2013**, *30* (1), 9–45.
- (110) Mendes, A. C.; Baran, E. T.; Lisboa, P.; Reis, R. L.; Azevedo, H. S. Microfluidic Fabrication of Self-Assembled Peptide-Polysaccharide Microcapsules as 3D Environments for Cell Culture. *Biomacromolecules* **2012**, *13* (12), 4039–4048.
- (111) Liu, K.; Deng, Y.; Zhang, N.; Li, S.; Ding, H.; Guo, F.; Liu, W.; Guo, S.; Zhao, X.-Z. Generation of Disk-like Hydrogel Beads for Cell Encapsulation and Manipulation Using a Droplet-Based Microfluidic Device. *Microfluid. Nanofluidics* **2012**, *13* (5), 761–767.
- (112) *Nanotechnology 2012: Electronics, Devices, Fabrication, MEMS, Fluidics and Computational*; Laudon, M., Nano-Science and Technology Institute, Nanotech Conference and Expo, Eds.; CRC Press: Boca Raton, Fla., 2012.
- (113) Martinez, C. J.; Kim, J. W.; Ye, C.; Ortiz, I.; Rowat, A. C.; Marquez, M.; Weitz, D. A Microfluidic Approach to Encapsulate Living Cells in Uniform Alginate Hydrogel Microparticles. *Macromol. Biosci.* **2012**, *12* (7), 946–951.
- (114) Velasco, D.; Tumarkin, E.; Kumacheva, E. Microfluidic Encapsulation of Cells in Polymer Microgels. *Small* **2012**, *8* (11), 1633–1642.
- (115) Rossow, T.; Heyman, J. A.; Ehrlicher, A. J.; Langhoff, A.; Weitz, D. A.; Haag, R.; Seiffert, S. Controlled Synthesis of Cell-Laden Microgels by Radical-Free Gelation in Droplet Microfluidics. *J. Am. Chem. Soc.* **2012**, *134* (10), 4983–4989.

- (116) Headen, D. M.; Aubry, G.; Lu, H.; García, A. J. Microfluidic-Based Generation of Size-Controlled, Biofunctionalized Synthetic Polymer Microgels for Cell Encapsulation. *Adv. Mater.* **2014**, *26* (19), 3003–3008.
- (117) Akbari, S.; Pirbodaghi, T. Microfluidic Encapsulation of Cells in Alginate Particles via an Improved Internal Gelation Approach. *Microfluid. Nanofluidics* **2013**, *16* (4), 773–777.
- (118) Wu, L.; Chen, P.; Dong, Y.; Feng, X.; Liu, B.-F. Encapsulation of Single Cells on a Microfluidic Device Integrating Droplet Generation with Fluorescence-Activated Droplet Sorting. *Biomed. Microdevices* **2013**, *15* (3), 553–560.
- (119) Tendulkar, S.; Mirmalek-Sani, S.-H.; Childers, C.; Saul, J.; Opara, E. C.; Ramasubramanian, M. K. A Three-Dimensional Microfluidic Approach to Scaling up Microencapsulation of Cells. *Biomed. Microdevices* **2012**, *14* (3), 461–469.
- (120) de Vos, P.; Bučko, M.; Gemeiner, P.; Navrátil, M.; Švitel, J.; Faas, M.; Strand, B. L.; Skjak-Braek, G.; Morch, Y. A.; Vikartovská, A.; et al. Multiscale Requirements for Bioencapsulation in Medicine and Biotechnology. *Biomaterials* **2009**, *30* (13), 2559–2570.
- (121) Lacík, I. Polymer Chemistry in Diabetes Treatment by Encapsulated Islets of Langerhans: Review to 2006. *Aust. J. Chem.* **2006**, *59* (8), 508–524.
- (122) Robitaille, R.; Halle, J. P. Characterization and Evaluation of the Properties and Functions of the Microcapsules. *BIOARTIFICIAL PANCREAS Biohybrid Ther.* **2009**, 67–85.
- (123) Rokstad, A. M. A.; Lacík, I.; de Vos, P.; Strand, B. L. Advances in Biocompatibility and Physico-Chemical Characterization of Microspheres for Cell Encapsulation. *Adv. Drug Deliv. Rev.* **2014**, *67–68*, 111–130.
- (124) Drury, J. L.; Dennis, R. G.; Mooney, D. J. The Tensile Properties of Alginate Hydrogels. *Biomaterials* **2004**, *25* (16), 3187–3199.
- (125) Hinkley, J. A.; Morgret, L. D.; Gehrke, S. H. Tensile Properties of Two Responsive Hydrogels. *Polymer* **2004**, *45* (26), 8837–8843.
- (126) Rosiński, S.; Grigorescu, G.; Lewińska, D.; Ritzén, L. G.; Viernstein, H.; Teunou, E.; Poncelet, D.; Zhang, Z.; Fan, X.; Serp, D.; et al. Characterization of Microcapsules: Recommended Methods Based on Round-Robin Testing. *J. Microencapsul.* **2002**, *19* (5), 641–659.
- (127) Thu, B.; Bruheim, P.; Espevik, T.; Smidsrød, O.; Soon-Shiong, P.; Skjåk-Bræk, G. Alginate Polycation Microcapsules: I. Interaction between Alginate and Polycation. *Biomaterials* **1996**, *17* (10), 1031–1040.
- (128) Kobayashi, T.; Aomatsu, Y.; Iwata, H.; Kin, T.; Kanehiro, H.; Hisanaga, M.; Ko, S.; Nagao, M.; Nakajima, Y. Indefinite Islet Protection from Autoimmune Destruction in Nonobese Diabetic Mice by Agarose Microencapsulation without Immunosuppression. *Transplantation* **2003**, *75* (5), 619–625.
- (129) Desai, T. A.; West, T.; Cohen, M.; Boiarski, T.; Rampersaud, A. Nanoporous Microsystems for Islet Cell Replacement. *Adv. Drug Deliv. Rev.* **2004**, *56* (11), 1661–1673.

- (130) Trivedi, N.; Steil, G. M.; Colton, C. K.; Bonner-Weir, S.; Weir, G. C. Improved Vascularization of Planar Membrane Diffusion Devices Following Continuous Infusion of Vascular Endothelial Growth Factor. *Cell Transplant.* **2000**, *9* (1), 115–124.
- (131) O’Sullivan, E. S.; Vegas, A.; Anderson, D. G.; Weir, G. C. Islets Transplanted in Immunoisolation Devices: A Review of the Progress and the Challenges That Remain. *Endocr. Rev.* **2011**, *32* (6), 827–844.
- (132) Park, S. J.; Shin, S.; Koo, O. J.; Moon, J. H.; Jang, G.; Ahn, C.; Lee, B. C.; Yoo, Y. J. Functional Improvement of Porcine Neonatal Pancreatic Cell Clusters *via* Conformal Encapsulation Using an Air-Driven Encapsulator. *Exp. Mol. Med.* **2012**, *44* (1), 20–25.
- (133) Mørch, Ý. A.; Donati, I.; Strand, B. L.; Skjåk-Bræk, G. Molecular Engineering as an Approach to Design New Functional Properties of Alginate. *Biomacromolecules* **2007**, *8* (9), 2809–2814.
- (134) Mørch, Ý. A.; Donati, I.; Strand, B. L. Effect of Ca²⁺, Ba²⁺, and Sr²⁺ on Alginate Microbeads. *Biomacromolecules* **2006**, *7* (5), 1471–1480.
- (135) Uludag, H.; De Vos, P.; Tresco, P. A. Technology of Mammalian Cell Encapsulation. *Adv. Drug Deliv. Rev.* **2000**, *42* (1), 29–64.
- (136) Briššová, M.; Petro, M.; Lacík, I.; Powers, A. C.; Wang, T. Evaluation of Microcapsule Permeability via Inverse Size Exclusion Chromatography. *Anal. Biochem.* **1996**, *242* (1), 104–111.
- (137) Bertz, A.; Wöhl-Bruhn, S.; Miethe, S.; Tiersch, B.; Koetz, J.; Hust, M.; Bunjes, H.; Menzel, H. Encapsulation of Proteins in Hydrogel Carrier Systems for Controlled Drug Delivery: Influence of Network Structure and Drug Size on Release Rate. *J. Biotechnol.* **2013**, *163* (2), 243–249.
- (138) Cooper, D. K. C.; Bottino, R.; Satyananda, V.; Wijkstrom, M.; Trucco, M. Toward Clinical Islet Xenotransplantation – Are Revisions to the IXA Guidelines Warranted? *Xenotransplantation* **2013**, *20* (2), 68–74.
- (139) Reichart, B.; Niemann, H.; Chavakis, T.; Denner, J.; Jaeckel, E.; Ludwig, B.; Marckmann, G.; Schnieke, A.; Schwinzer, R.; Seissler, J.; et al. Xenotransplantation of Porcine Islet Cells as a Potential Option for the Treatment of Type 1 Diabetes in the Future. *Horm. Metab. Res.* **2015**, *47* (01), 31–35.
- (140) Zhu, H.; Yu, L.; He, Y.; Lyu, Y.; Wang, B. Microencapsulated Pig Islet Xenotransplantation as an Alternative Treatment of Diabetes. *Tissue Eng. Part B Rev.* **2015**, *21* (5), 474–489.
- (141) Nagaraju, S.; Bottino, R.; Wijkstrom, M.; Trucco, M.; Cooper, D. K. C. Islet Xenotransplantation: What Is the Optimal Age of the Islet-Source Pig? *Xenotransplantation* **2014**, *22* (1), 7–19.
- (142) Bürck, L. van; Seissler, J. The Potential of Local Immunomodulation and Tolerance Induction in Porcine Islet Xenotransplantation. *Xenotransplantation* **2013**, *20* (1), 51–51.

- (143) Jimenez-Vera, E.; Davies, S.; Phillips, P.; O'Connell, P. J.; Hawthorne, W. J. Long-Term Cultured Neonatal Islet Cell Clusters Demonstrate Better Outcomes for Reversal of Diabetes: In Vivo and Molecular Profiles. *Xenotransplantation* **2015**, *22* (2), 114–123.
- (144) Meier, R. P. H.; Muller, Y. D.; Balaphas, A.; Morel, P.; Pascual, M.; Seebach, J. D.; Buhler, L. H. Xenotransplantation: Back to the Future? *Transpl. Int.* **2018**, *31* (5), 465–477.
- (145) Niu, D.; Wei, H.-J.; Lin, L.; George, H.; Wang, T.; Lee, I.-H.; Zhao, H.-Y.; Wang, Y.; Kan, Y.; Shrock, E.; et al. Inactivation of Porcine Endogenous Retrovirus in Pigs Using CRISPR-Cas9. *Science* **2017**, *357* (6357), 1303–1307.
- (146) Wright, J. R.; Yang, H.; Hyrtsenko, O.; Xu, B.-Y.; Yu, W.; Pohajdak, B. A Review of Piscine Islet Xenotransplantation Using Wild-Type Tilapia Donors and the Production of Transgenic Tilapia Expressing a “Humanized” Tilapia Insulin. *Xenotransplantation* **2014**, *21* (6), 485–495.
- (147) White, D. J. Fish Islet Xenografts. *Xenotransplantation* **2014**, *21* (2), 124–126.
- (148) Safley, S. A.; Cui, H.; Cauffiel, S. M. D.; Xu, B.-Y.; Wright, J. R.; Weber, C. J. Encapsulated Piscine (Tilapia) Islets for Diabetes Therapy: Studies in Diabetic NOD and NOD-SCID Mice. *Xenotransplantation* **2014**, *21* (2), 127–139.
- (149) Shin, J. S.; Kim, J. M.; Kim, J. S.; Min, B. H.; Kim, Y. H.; Kim, H. J.; Jang, J. Y.; Yoon, I. H.; Kang, H. J.; Kim, J.; et al. Long-Term Control of Diabetes in Immunosuppressed Nonhuman Primates (NHP) by the Transplantation of Adult Porcine Islets. *Am. J. Transplant.* **2015**, *15* (11), 2837–2850.
- (150) Nöth, U.; Gröhn, P.; Jork, A.; Zimmermann, U.; Haase, A.; Lutz, J. 19F-MRI in Vivo Determination of the Partial Oxygen Pressure in Perfluorocarbon-Loaded Alginate Capsules Implanted into the Peritoneal Cavity and Different Tissues. *Magn. Reson. Med.* **1999**, *42* (6), 1039–1047.
- (151) Toso, C.; Mathe, Z.; Morel, P.; Oberholzer, J.; Bosco, D.; Sainz-Vidal, D.; Hunkeler, D.; Buhler, L. H.; Wandrey, C.; Berney, T. Effect of Microcapsule Composition and Short-Term Immunosuppression on Intraportal Biocompatibility. *Cell Transplant.* **2005**, *14* (2–3), 159–167.
- (152) Mai, G.; Huy, N. T.; Morel, P.; Mei, J.; Andres, A.; Bosco, D.; Baertschiger, R.; Toso, C.; Berney, T.; Majno, P.; et al. Treatment of Fulminant Liver Failure by Transplantation of Microencapsulated Primary or Immortalized Xenogeneic Hepatocytes. *Xenotransplantation* **2005**, *12* (6), 457–464.
- (153) Kobayashi, T.; Arefanian, H.; Harb, G.; Tredget, E. B.; Rajotte, R. V.; Korbitt, G. S.; Rayat, G. R. Prolonged Survival of Microencapsulated Neonatal Porcine Islet Xenografts in Immune-Competent Mice without Antirejection Therapy. *Cell Transplant.* **2008**, *17* (10–11), 1243–1256.
- (154) Cantarelli, E.; Piemonti, L. Alternative Transplantation Sites for Pancreatic Islet Grafts. *Curr. Diab. Rep.* **2011**, *11* (5), 364.

- (155) Ao, Z.; Matayoshi, K.; Lakey, J. R.; Rajotte, R. V.; Warnock, G. L. Survival and Function of Purified Islets in the Omental Pouch Site of Outbred Dogs. *Transplantation* **1993**, *56* (3), 524–529.
- (156) Banerjee, A.; Patra, S.; Ganguly, S. Alginate-Gelatin Blend with Embedded Voids for Controlled Release Applications. *J. Appl. Polym. Sci.* **2017**, *134* (18), n/a-n/a.
- (157) Kobayashi, T.; Aomatsu, Y.; Iwata, H.; Kin, T.; Kanehiro, H.; Hisanga, M.; Ko, S.; Nagao, M.; Harb, G.; Nakajima, Y. Survival of Microencapsulated Islets at 400 Days Posttransplantation in the Omental Pouch of NOD Mice. *Cell Transplant.* **2006**, *15* (4), 359–365.
- (158) Petrelli, A.; Carvello, M.; Vergani, A.; Lee, K. M.; Tezza, S.; Du, M.; Kleffel, S.; Chengwen, L.; Mfarrej, B. G.; Hwu, P.; et al. IL-21 Is an Antitolerogenic Cytokine of the Late-Phase Alloimmune Response. *Diabetes* **2011**, *60* (12), 3223–3234.
- (159) Juang, J.-H.; Shen, C.-R.; Wang, J.-J.; Kuo, C.-H.; Lin, M.-Y.; Wu, S.-T.; Tsai, Z.-T.; Yen, T.-C. Magnetic Resonance Imaging Study of Mouse Islet Allotransplantation. *Transplant. Proc.* **2010**, *42* (10), 4217–4220.
- (160) Vèriter, S.; Mergen, J.; Goebbels, R.-M.; Aouassar, N.; Grégoire, C.; Jordan, B.; Levêque, P.; Gallez, B.; Gianello, P.; Dufrane, D. In Vivo Selection of Biocompatible Alginates for Islet Encapsulation and Subcutaneous Transplantation. *Tissue Eng. Part A* **2009**, *16* (5), 1503–1513.
- (161) Wang, W.; Gu, Y.; Tabata, Y.; Miyamoto, M.; Hori, H.; Nagata, N.; Touma, M.; Balamurugan, A. N.; Kawakami, Y.; Nozawa, M.; et al. Reversal of Diabetes in Mice by Xenotransplantation of a Bioartificial Pancreas in a Prevascularized Subcutaneous Site. *Transplantation* **2002**, *73* (1), 122–129.
- (162) Christoffersson, G.; Henriksnäs, J.; Johansson, L.; Rolny, C.; Ahlström, H.; Caballero-Corbalan, J.; Segersvärd, R.; Permert, J.; Korsgren, O.; Carlsson, P.-O.; et al. Clinical and Experimental Pancreatic Islet Transplantation to Striated Muscle: Establishment of a Vascular System Similar to That in Native Islets. *Diabetes* **2010**.
- (163) Lund, T.; Korsgren, O.; Aursnes, I. A.; Scholz, H.; Foss, A. Sustained Reversal of Diabetes Following Islet Transplantation to Striated Musculature in the Rat. *J. Surg. Res.* **2010**, *160* (1), 145–154.
- (164) Fort, A.; Fort, N.; Ricordi, C.; Stabler, C. L. Biohybrid Devices and Encapsulation Technologies for Engineering a Bioartificial Pancreas. *Cell Transplant.* **2008**, *17* (9), 997–1003.
- (165) Calafiore, R.; Basta, G.; Luca, G.; Boselli, C.; Bufalari, A.; Bufalari, A.; Cassarani, M. P.; Giustozzi, G. M.; Brunetti, P. Transplantation of Pancreatic Islets Contained in Minimal Volume Microcapsules in Diabetic High Mammals. *Ann. N. Y. Acad. Sci.* **2006**, *875* (1), 219–232.
- (166) Giovagnoli, S.; Luca, G.; Blasi, P.; Mancuso, F.; Schoubben, A.; Arato, I.; Calvitti, M.; Falabella, G.; Basta, G.; Bodo, M.; et al. Alginates in Pharmaceuticals and Biomedicine: Is the Future so Bright? *Curr. Pharm. Des.* **2015**, *21* (33), 4917–4935.

- (167) Moya, M. L.; Morley, M.; Khanna, O.; Opara, E. C.; Brey, E. M. Stability of Alginate Microbead Properties in Vitro. *J. Mater. Sci. Mater. Med.* **2012**, *23* (4), 903–912.
- (168) Fritschy, W. M.; Vos, P. de; Groen, H.; Klatter, F. A.; Pasma, A.; Wolters, G. H. J.; Schilfgaarde, R. van. The Capsular Overgrowth on Microencapsulated Pancreatic Islet Grafts in Streptozotocin and Autoimmune Diabetic Rats. *Transpl. Int.* **1994**, *7* (4), 264–271.
- (169) Tuch, B. E.; Keogh, G. W.; Williams, L. J.; Wu, W.; Foster, J. L.; Vaithilingam, V.; Philips, R. Safety and Viability of Microencapsulated Human Islets Transplanted into Diabetic Humans. *Diabetes Care* **2009**, *32* (10), 1887–1889.
- (170) Williams, D. F. On the Mechanisms of Biocompatibility. *Biomaterials* **2008**, *29* (20), 2941–2953.
- (171) Anderson, J. M.; Rodriguez, A.; Chang, D. T. Foreign Body Reaction to Biomaterials. *Semin. Immunol.* **2008**, *20* (2), 86–100.
- (172) Nilsson, B.; Korsgren, O.; Lambris, J. D.; Ekdahl, K. N. Can Cells and Biomaterials in Therapeutic Medicine Be Shielded from Innate Immune Recognition? *Trends Immunol.* **2010**, *31* (1), 32–38.
- (173) Franz, S.; Rammelt, S.; Scharnweber, D.; Simon, J. C. Immune Responses to Implants – A Review of the Implications for the Design of Immunomodulatory Biomaterials. *Biomaterials* **2011**, *32* (28), 6692–6709.
- (174) Říhová, B. Immunocompatibility and Biocompatibility of Cell Delivery Systems. *Adv. Drug Deliv. Rev.* **2000**, *42* (1–2), 65–80.
- (175) Ward, P. A.; Lentsch, A. B. The Acute Inflammatory Response and Its Regulation. *Arch. Surg.* **1999**, *134* (6), 666–669.
- (176) Tam, S. K.; Haan, B. J. de; Faas, M. M.; Hallé, J.-P.; Yahia, L.; Vos, P. de. Adsorption of Human Immunoglobulin to Implantable Alginate-Poly-L-Lysine Microcapsules: Effect of Microcapsule Composition. *J. Biomed. Mater. Res. A* **2008**, *89A* (3), 609–615.
- (177) Roach, P.; Farrar, D.; Perry, C. C. Interpretation of Protein Adsorption: Surface-Induced Conformational Changes. *J. Am. Chem. Soc.* **2005**, *127* (22), 8168–8173.
- (178) Sethuraman, A.; Han, M.; Kane, R. S.; Belfort, G. Effect of Surface Wettability on the Adhesion of Proteins. *Langmuir* **2004**, *20* (18), 7779–7788.
- (179) Bexborn, F.; Andersson, P. O.; Chen, H.; Nilsson, B.; Ekdahl, K. N. The Tick-over Theory Revisited: Formation and Regulation of the Soluble Alternative Complement C3 Convertase (C3(H₂O)Bb). *Mol. Immunol.* **2008**, *45* (8), 2370–2379.
- (180) Guo, R.-F.; Ward, P. A. Role of C5a in Inflammatory Responses. *Annu. Rev. Immunol.* **2004**, *23* (1), 821–852.
- (181) Ricklin, D.; Hajishengallis, G.; Yang, K.; Lambris, J. D. Complement: A Key System for Immune Surveillance and Homeostasis. *Nat. Immunol.* **2010**, *11* (9), 785–797.
- (182) Paredes-Juarez, G. A.; de Haan, B. J.; Faas, M. M.; de Vos, P. The Role of Pathogen-Associated Molecular Patterns in Inflammatory Responses against Alginate Based Microcapsules. *J. Controlled Release* **2013**, *172* (3), 983–992.

- (183) Paredes-Juarez, G. A.; Sahasrabudhe, N. M.; Tjoelker, R. S.; Haan, B. J. de; Engelse, M. A.; Koning, E. J. P. de; Faas, M. M.; Vos, P. de. DAMP Production by Human Islets under Low Oxygen and Nutrients in the Presence or Absence of an Immunoisolating-Capsule and Necrostatin-1. *Sci. Rep.* **2015**, *5*, 14623.
- (184) Jacobs-Tulleneers-Thevissen, D.; Chintinne, M.; Ling, Z.; Gillard, P.; Schoonjans, L.; Delvaux, G.; Strand, B. L.; Gorus, F.; Keymeulen, B.; Pipeleers, D.; et al. Sustained Function of Alginate-Encapsulated Human Islet Cell Implants in the Peritoneal Cavity of Mice Leading to a Pilot Study in a Type 1 Diabetic Patient. *Diabetologia* **2013**, *56* (7), 1605–1614.
- (185) Rokstad, A.; Strand, B.; Espevik, T.; Mollnes, T. Biocompatibility and Biotolerability Assessment of Microspheres Using a Whole Blood Model. *Micro Nanosyst.* **2013**, *5* (3), 177–185.
- (186) Rokstad, A. M.; Brekke, O.-L.; Steinkjer, B.; Ryan, L.; Kolláriková, G.; Strand, B. L.; Skjåk-Bræk, G.; Lacík, I.; Espevik, T.; Mollnes, T. E. Alginate Microbeads Are Complement Compatible, in Contrast to Polycation Containing Microcapsules, as Revealed in a Human Whole Blood Model. *Acta Biomater.* **2011**, *7* (6), 2566–2578.
- (187) Vaithilingam, V.; Evans, M. D. M.; Rowe, A.; Bean, P. A.; Tuch, B. E. Coencapsulation of Target Effector Cells with Mesenchymal Stem Cells Reduces Pericapsular Fibrosis and Improves Graft Survival in a Xenotransplanted Animal Model. *Cell Transplant.* **2016**, *25* (7), 1299–1317.
- (188) Vaithilingam, V.; Evans, M. D. M.; Lewy, D. M.; Bean, P. A.; Bal, S.; Tuch, B. E. Co-Encapsulation and Co-Transplantation of Mesenchymal Stem Cells Reduces Pericapsular Fibrosis and Improves Encapsulated Islet Survival and Function When Allografted. *Sci. Rep.* **2017**, *7* (1), 10059.
- (189) Zheng, J. N.; Xie, H. G.; Yu, W. T.; Liu, X. D.; Xie, W. Y.; Zhu, J.; Ma, X. J. Chitosan-g-MPEG-Modified Alginate/Chitosan Hydrogel Microcapsules: A Quantitative Study of the Effect of Polymer Architecture on the Resistance to Protein Adsorption. *Langmuir* **2010**, *26* (22), 17156–17164.
- (190) Yang, H. K.; Ham, D.-S.; Park, H.-S.; Rhee, M.; You, Y. H.; Kim, M. J.; Shin, J.; Kim, O.-Y.; Khang, G.; Hong, T. H.; et al. Long-Term Efficacy and Biocompatibility of Encapsulated Islet Transplantation With Chitosan-Coated Alginate Capsules in Mice and Canine Models of Diabetes. *Transplantation* **2016**, *100* (2), 334–343.
- (191) Dang, T. T.; Thai, A. V.; Cohen, J.; Slosberg, J. E.; Siniakowicz, K.; Doloff, J. C.; Ma, M.; Hollister-Lock, J.; Tang, K. M.; Gu, Z.; et al. Enhanced Function of Immuno-Isolated Islets in Diabetes Therapy by Co-Encapsulation with an Anti-Inflammatory Drug. *Biomaterials* **2013**, *34* (23), 5792–5801.
- (192) Azadi, S. A.; Vasheghani-Farahani, E.; Hashemi-Najafbabadi, S.; Godini, A. Co-Encapsulation of Pancreatic Islets and Pentoxifylline in Alginate-Based Microcapsules with Enhanced Immunosuppressive Effects. *Prog. Biomater.* **2016**, *5* (2), 101–109.
- (193) Park, H.-S.; Kim, J.-W.; Lee, S.-H.; Yang, H. K.; Ham, D.-S.; Sun, C.-L.; Hong, T. H.; Khang, G.; Park, C.-G.; Yoon, K.-H. Antifibrotic Effect of Rapamycin Containing Polyethylene

- Glycol-Coated Alginate Microcapsule in Islet Xenotransplantation. *J. Tissue Eng. Regen. Med.* **2017**, *11* (4), 1274–1284.
- (194) Ricci, M.; Blasi, P.; Giovagnoli, S.; Rossi, C.; Macchiarulo, G.; Luca, G.; Basta, G.; Calafiore, R. Ketoprofen Controlled Release from Composite Microcapsules for Cell Encapsulation: Effect on Post-Transplant Acute Inflammation. *J. Controlled Release* **2005**, *107* (3), 395–407.
- (195) Bhujbal, S. V.; Paredes-Juarez, G. A.; Niclou, S. P.; de Vos, P. Factors Influencing the Mechanical Stability of Alginate Beads Applicable for Immunoisolation of Mammalian Cells. *J. Mech. Behav. Biomed. Mater.* **2014**, *37*, 196–208.
- (196) Veiseh, O.; Doloff, J. C.; Ma, M.; Vegas, A. J.; Tam, H. H.; Bader, A. R.; Li, J.; Langan, E.; Wyckoff, J.; Loo, W. S.; et al. Size- and Shape-Dependent Foreign Body Immune Response to Materials Implanted in Rodents and Non-Human Primates. *Nat. Mater.* **2015**, *14* (6), 643–651.
- (197) Passemard, S.; Szabó, L.; Noverraz, F.; Montanari, E.; Gonelle-Gispert, C.; Bühler, L. H.; Wandrey, C.; Gerber-Lemaire, S. Synthesis Strategies to Extend the Variety of Alginate-Based Hybrid Hydrogels for Cell Microencapsulation. *Biomacromolecules* **2017**.
- (198) Lawandi, J.; Gerber-Lemaire, S.; Juillerat-Jeanneret, L.; Moitessier, N. Inhibitors of Prolyl Oligopeptidases for the Therapy of Human Diseases: Defining Diseases and Inhibitors. *J. Med. Chem.* **2010**, *53* (9), 3423–3438.
- (199) Passemard, S. Functionalization of Nanoparticles for Targeted Cancer Imaging and Diagnosis, Ecole Polytechnique Fédérale De Lausanne: Lausanne, 2014.
- (200) Poplawski, S. E.; Lai, J. H.; Li, Y.; Jin, Z.; Liu, Y.; Wu, W.; Wu, Y.; Zhou, Y.; Sudmeier, J. L.; Sanford, D. G.; et al. Identification of Selective and Potent Inhibitors of Fibroblast Activation Protein and Prolyl Oligopeptidase. *J. Med. Chem.* **2013**, *56* (9), 3467–3477.
- (201) Meek, I. L.; van de Laar, M. A. F. J.; Vonkeman, H. E. Non-Steroidal Anti-Inflammatory Drugs: An Overview of Cardiovascular Risks. *Pharmaceuticals* **2010**, *3* (7), 2146–2162.
- (202) Jones, R. Nonsteroidal Anti-Inflammatory Drug Prescribing: Past, Present, and Future. *Am. J. Med.* **2001**, *110* (1A), 4S-7S.
- (203) Selvam, C.; Jachak, S. M.; Thilagavathi, R.; Chakraborti, A. K. Design, Synthesis, Biological Evaluation and Molecular Docking of Curcumin Analogues as Antioxidant, Cyclooxygenase Inhibitory and Anti-Inflammatory Agents. *Bioorg. Med. Chem. Lett.* **2005**, *15* (7), 1793–1797.
- (204) Cryer, B.; Feldman, M. Cyclooxygenase-1 and Cyclooxygenase-2 Selectivity of Widely Used Nonsteroidal Anti-Inflammatory Drugs. *Am. J. Med.* **1998**, *104* (5), 413–421.
- (205) T, K.; H, K.; H, K.; T, Y. Studies on the Effects of Anti-Inflammatory Action of Benzoyl-Hydrotropic Acid (Ketoprofen) and Other Drugs, with Special Reference to Prostaglandin Synthesis. *Arch. Int. Pharmacodyn. Ther.* **1979**, *237* (1), 169–176.
- (206) Anand, P.; Thomas, S. G.; Kunnumakkara, A. B.; Sundaram, C.; Harikumar, K. B.; Sung, B.; Tharakan, S. T.; Misra, K.; Priyadarsini, I. K.; Rajasekharan, K. N.; et al. Biological

- Activities of Curcumin and Its Analogues (Congeners) Made by Man and Mother Nature. *Biochem. Pharmacol.* **2008**, *76* (11), 1590–1611.
- (207) Aggarwal, B. B.; Harikumar, K. B. Potential Therapeutic Effects of Curcumin, the Anti-Inflammatory Agent, against Neurodegenerative, Cardiovascular, Pulmonary, Metabolic, Autoimmune and Neoplastic Diseases. *Int. J. Biochem. Cell Biol.* **2009**, *41* (1), 40–59.
- (208) Murphy, C. J.; Tang, H.; Van Kirk, E. A.; Shen, Y.; Murdoch, W. J. Reproductive Effects of a Pegylated Curcumin. *Reprod. Toxicol.* **2012**, *34* (1), 120–124.
- (209) Tang, H.; Murphy, C. J.; Zhang, B.; Shen, Y.; Sui, M.; Van Kirk, E. A.; Feng, X.; Murdoch, W. J. Amphiphilic Curcumin Conjugate-Forming Nanoparticles as Anticancer Prodrug and Drug Carriers: In Vitro and in Vivo Effects. *Nanomed.* **2010**, *5* (6), 855–865.
- (210) Babazadeh, M. Design, Synthesis and in Vitro Evaluation of Vinyl Ether Type Polymeric Prodrugs of Ibuprofen, Ketoprofen and Naproxen. *Int. J. Pharm.* **2008**, *356* (1–2), 167–173.
- (211) Shoba, G.; Joy, D.; Joseph, T.; Majeed, M.; Rajendran, R.; Srinivas, P. S. S. R. Influence of Piperine on the Pharmacokinetics of Curcumin in Animals and Human Volunteers. *Planta Med.* **1998**, *64* (04), 353–356.
- (212) Adams, B. K.; Ferstl, E. M.; Davis, M. C.; Herold, M.; Kurtkaya, S.; Camalier, R. F.; Hollingshead, M. G.; Kaur, G.; Sausville, E. A.; Rickles, F. R.; et al. Synthesis and Biological Evaluation of Novel Curcumin Analogs as Anti-Cancer and Anti-Angiogenesis Agents. *Bioorg. Med. Chem.* **2004**, *12* (14), 3871–3883.
- (213) Cao, Y.-K.; Li, H.-J.; Song, Z.-F.; Li, Y.; Huai, Q.-Y. Synthesis and Biological Evaluation of Novel Curcuminoid Derivatives. *Molecules* **2014**, *19* (10), 16349–16372.
- (214) Kuo, Y.-C.; Hsueh, C.-H. Neuronal Production from Induced Pluripotent Stem Cells in Self-Assembled Collagen-Hyaluronic Acid-Alginate Microgel Scaffolds with Grafted GRGDSP/Ln5-P4. *Mater. Sci. Eng. C* **2017**, *76* (Supplement C), 760–774.
- (215) Liu, Y.; Sun, Y.; Sun, L.; Rizwan-ur-Rehman; Wang, Y. In Vitro and in Vivo Study of Sodium Polyacrylate Grafted Alginate as Microcapsule Matrix for Live Probiotic Delivery. *J. Funct. Foods* **2016**, *24* (Supplement C), 429–437.
- (216) Yang, J.-S.; Xie, Y.-J.; He, W. Research Progress on Chemical Modification of Alginate: A Review. *Carbohydr. Polym.* **2011**, *84* (1), 33–39.
- (217) Galant, C.; Kjøniksen, A.-L.; Nguyen, G. T. M.; Knudsen, K. D.; Nyström, B. Altering Associations in Aqueous Solutions of a Hydrophobically Modified Alginate in the Presence of β -Cyclodextrin Monomers. *J. Phys. Chem. B* **2006**, *110* (1), 190–195.
- (218) Yang, L.; Zhang, B.; Wen, L.; Liang, Q.; Zhang, L.-M. Amphiphilic Cholesteryl Grafted Sodium Alginate Derivative: Synthesis and Self-Assembly in Aqueous Solution. *Carbohydr. Polym.* **2007**, *68* (2), 218–225.
- (219) Formo, K.; Cho, C. H.-H.; Vallier, L.; Strand, B. L. Culture of HESC-Derived Pancreatic Progenitors in Alginate-Based Scaffolds. *J. Biomed. Mater. Res. A* **2015**, *103* (12), 3717–3726.

- (220) Sandvig, I.; Karstensen, K.; Rokstad, A. M.; Aachmann, F. L.; Formo, K.; Sandvig, A.; Skjåk-Bræk, G.; Strand, B. L. RGD-Peptide Modified Alginate by a Chemoenzymatic Strategy for Tissue Engineering Applications. *J. Biomed. Mater. Res. A* **2014**, *103* (3), 896–906.
- (221) Zhang, J.; Wang, N.; Liu, W.; Zhao, X.; Lu, W. Intermolecular Hydrogen Bonding Strategy to Fabricate Mechanically Strong Hydrogels with High Elasticity and Fatigue Resistance. *Soft Matter* **2013**, *9* (27), 6331–6337.
- (222) Barcan, G. A.; Zhang, X.; Waymouth, R. M. Structurally Dynamic Hydrogels Derived from 1,2-Dithiolanes. *J. Am. Chem. Soc.* **2015**, *137* (17), 5650–5653.
- (223) Li, Y.-L.; Zhu, L.; Liu, Z.; Cheng, R.; Meng, F.; Cui, J.-H.; Ji, S.-J.; Zhong, Z. Reversibly Stabilized Multifunctional Dextran Nanoparticles Efficiently Deliver Doxorubicin into the Nuclei of Cancer Cells. *Angew. Chem.* **2009**, *121* (52), 10098–10102.
- (224) Jones, K. H.; Senft, J. A. An Improved Method to Determine Cell Viability by Simultaneous Staining with Fluorescein Diacetate-Propidium Iodide. *J. Histochem. Cytochem.* **1985**, *33* (1), 77–79.
- (225) Noverraz, F.; Montanari, E.; Pimenta, J.; Szabó, L.; Ortiz, D.; Gonelle-Gispert, C.; Bühler, L. H.; Gerber-Lemaire, S. Antifibrotic Effect of Ketoprofen-Grafted Alginate Microcapsules in the Transplantation of Insulin Producing Cells. *Bioconjug. Chem.* **2018**, *29* (6), 1932–1941.
- (226) Ligeour Caroline; Dupin Lucie; Marra Alberto; Vergoten Gérard; Meyer Albert; Dondoni Alessandro; Souteyrand Eliane; Vasseur Jean-Jacques; Chevolut Yann; Morvan François. Synthesis of Galactoclusters by Metal-Free Thiol “Click Chemistry” and Their Binding Affinities for Pseudomonas Aeruginosa Lectin LecA. *Eur. J. Org. Chem.* **2014**, *2014* (34), 7621–7630.
- (227) Tellers, D.; Colletti, S.; Dudkin, V.; Ikemoto, N.; Liao, H.; Parish, C.; Pei, T.; Shaw, A.; Truong, Q.; Wang, L.; et al. Novel Tetragalnac Containing Conjugates and Methods for Delivery of Oligonucleotides. WO2013166121 (A1), November 7, 2013.
- (228) Goswami, L. N.; Houston, Z. H.; Sarma, S. J.; Jalisatgi, S. S.; Hawthorne, M. F. Efficient Synthesis of Diverse Heterobifunctionalized Clickable Oligo(Ethylene Glycol) Linkers: Potential Applications in Bioconjugation and Targeted Drug Delivery. *Org. Biomol. Chem.* **2013**, *11* (7), 1116.
- (229) Benito-Alifonso David; Tremel Shirley; Hou Bo; Lockyear Harriet; Mantell Judith; Fermin David J.; Verkade Paul; Berry Monica; Galan M. Carmen. Lactose as a “Trojan Horse” for Quantum Dot Cell Transport. *Angew. Chem. Int. Ed.* **2013**, *53* (3), 810–814.
- (230) Guo, Y.; Nehlmeier, I.; Poole, E.; Sakonsinsiri, C.; Hondow, N.; Brown, A.; Li, Q.; Li, S.; Whitworth, J.; Li, Z.; et al. Dissecting Multivalent Lectin–Carbohydrate Recognition Using Polyvalent Multifunctional Glycan-Quantum Dots. *J. Am. Chem. Soc.* **2017**, *139* (34), 11833–11844.
- (231) Becht, J.-M.; Meyer, O.; Helmchen, G. Enantioselective Syntheses of (-)-(R)-Rolipram, (-)-(R)-Baclofen and Other GABA Analogues via Rhodium-Catalyzed Conjugate Addition of Arylboronic Acids. *Synthesis* **2003**, *2003* (18), 2805–2810.

References

- (232) Zhu, Z.-J.; Tang, R.; Yeh, Y.-C.; Miranda, O. R.; Rotello, V. M.; Vachet, R. W. Determination of the Intracellular Stability of Gold Nanoparticle Monolayers Using Mass Spectrometry. *Anal. Chem.* **2012**, *84* (10), 4321–4326.

8 CURRICULUM VITAE

François Noverraz

08.04.1987

Rue du Simplon, 07
1006 Lausanne, Switzerland
Telephone: +41786527767
E-mail: francois.noverraz@epfl.ch

EDUCATION

PhD study in organic chemistry and polymers functionalization École Polytechnique Fédérale de Lausanne (EPFL), Switzerland	2014-2018
Master in Molecular and Biological Chemistry École Polytechnique Fédérale de Lausanne (EPFL), Switzerland	2012-2014
Bachelor in Chemistry and Chemical Engineering École Polytechnique Fédérale de Lausanne (EPFL), Switzerland	2009-2012
Matura (High School Diploma), Option Biology and Chemistry College Sismondi (GE), Switzerland	2001-2007

PROFESSIONAL EXPERIENCE

PhD Student in the Group for Functionalized Biomaterials (EPFL; Gerber. S)	June 2014-September 2018
<ul style="list-style-type: none"> • Design and synthesis of bioactive molecules in collaboration with biologists. • Functionalization of alginate; preparation and characterization of hydrogels microspheres for cell immobilization. • Practical laboratory assistant for undergraduate chemistry and chemical engineering students. Supervision of Bachelor and Masters Projects. Assistant of Bachelor course "Organic functions and reactions I" and "Organic chemistry (for BIO, PHA)". <i>(Winner of the awards for best teaching assistant in 2016)</i> 	
Master Project, Organometallic Chemistry (University of Sydney; Master. T)	September 2013-Mars 2014
<ul style="list-style-type: none"> • Synthesis and investigation of bio-inspired catalysts for hydrogen production. 	
Bachelor Project, Organic Chemistry (EPFL; Gerber. S)	February 2013-June 2013
<ul style="list-style-type: none"> • Synthesis of targeting molecule with ligands that bind the surface of NPs with bio-orthogonal copper free click chemistry for cancer diagnostic and therapy. 	

COMPUTER PROGRAMS

Programming languages:	C, C++, MATLAB, HTML, BASH
Chemistry:	ChemDraw, MestRenova, topspin, VMD, Molden
Office:	Suite MS-Office, Latex

LANGUAGES

French	Mother tongue
English	Fluent

German Basic

Conferences

SSBE Annual Society meeting, Zurich, Switzerland, 27-28 August 2014. *Engineering Hydrogel Microspheres for Cell Therapy.*

Poster & Short talk

Swiss Summer School 2014 in Chemical Biology, Villars, Switzerland, 1-5 September 2014. *Engineering alginate-based hydrogels for cell microencapsulation.*

Poster

XXII International Conference on Bioencapsulation, 21st Bratislava International Conference on Macromolecules. Bratislava, Slovakia, September 17-19, 2014. *Engineering PEGylated alginate hydrogels for cell microencapsulation*

Poster. Award for Best poster

SSB+RM Conference, 20th anniversary, 21st Annual meeting, Lausanne, Switzerland, June 9-10, 2015. *Tuning the properties of alginate hydrogels for cell microencapsulation*

Talk & Poster

ESB European Conference on Biomaterial, Kraków, Poland, 30 August - 3 sept, 2015. *Functionalization of hydrogels for cells encapsulation*

Poster

SCS (swiss chemical society) Fall Meeting, Lausanne, Switzerland, September 4, 2015. *Development of functionalized hybrid hydrogels*

Poster

8th Training school on Microencapsulation, Cork, Ireland, 30 may - 2 June, 2016. *Functionalization of alginate hydrogels for cells microencapsulation.*

Poster

SCS (swiss chemical society) Fall Meeting, Zurich, Switzerland, September 15, 2016. *Development of functionalized hybrid hydrogels.*

Poster

25th International Conference on Bioencapsulation, Nantes, France, July 3-6, 2017. *Engineering pegylated alginate hydrogels for cell microencapsulation.*

Talk. Award for Best student contribution

SCS (swiss chemical society) Fall Meeting, Bern, Switzerland, August 21-22, 2017. *Improving the properties of alginate-based hydrogels by functionalization with bioactive ingredients.*

Poster

SCS (swiss chemical society) Fall Meeting, Lausanne, Switzerland, September 7, 2018. *Covalent conjugation of ketoprofen to alginate-based hydrogels reduces fibrosis in the transplantation of insulin producing cells*

Poster

ESB European Conference on Biomaterial, Maastricht, Netherlands, September 9-13, 2018. *Functionalization of alginate-based hydrogels with ketoprofen reduces fibrosis in transplantation of insulin producing cells.*

Poster

LITERATURE CONTRIBUTION

Antifibrotic Effect of Ketoprofen-Grafted Alginate Microcapsules in the Transplantation of Insulin Producing Cells.

Noverraz, F.; Montanari, E.; Pimenta, J.; Szabó, L.; Ortiz, D.; Gonelle-Gispert, C.; Bühler, L. H.; Gerber-Lemaire, S. *Bioconjugate Chem.* 2018, 29 (6), 1932–1941.

Beneficial effects of Human Mesenchymal Stromal Cells on Porcine Hepatocyte Viability and Albumin Secretion.

E. Montanari, J. Pimenta, L. Szabó, **F. Noverraz**, S. Passemaid, R. P. H. Meier, J. Meyer, J. Sidibe, A. Thomas, H.-J. Schuurman, S. Gerber-Lemaire, C. Gonelle-Gispert and L. H. Bühler. *Journal of Immunology Research*, p. Article ID 1078547, 2018.

Synthesis strategies to extend the variety of alginate-based hybrid hydrogels for cell microencapsulation.

S. Passemaid, L. Szabó, **F. R. P. Noverraz**, E. Montanari, C. Gonelle-Gispert, L. H. Bühler, C. Wandrey and S. Gerber-Lemaire. *Biomacromolecules*, vol. 18, num. 9, p. 2747-2755, 2017.

Contribution of polymeric materials to progress in xenotransplantation of microencapsulated cells - A review.

R. Mahou, S. Passemaid, M. Carvello, A. Petrelli, **F. Noverraz**, S. Gerber-Lemaire and C. Wandrey. *Xenotransplantation*, vol. 23, num. 3, p. 179-201, 2016.

Tuning the Properties of Hydrogel Microspheres by Adding Chemical Cross-linking Functionality to Sodium Alginate.

R. Mahou, F. Borcard, V. Crivelli, E. Montanari, S. Passemaid, **F. Noverraz**, S. Gerber-Lemaire, L. Bühler and C. Wandrey. *Chemistry of Materials*, vol. 27, p. 4380-4389, 2015.